CONFORMATIONS OF MOLECULES CONTAINING π SYSTEMS: MATRIX ISOLATION INFRARED AND *AB INITIO* STUDIES

By

BISHNU PRASAD KAR

Enrolment No: CHEM02200704014
Materials Chemistry Division, Chemistry Group,
Indira Gandhi Centre for Atomic Research, Kalpakkam

A thesis submitted to the
Board of Studies in Chemical Sciences
In partial fulfillment of requirements
For the Degree of

DOCTOR OF PHILOSOPHY
of
HOMI BHABHA NATIONAL INSTITUTE

September, 2012

Homi Bhabha National Institute

Recommendations of the Viva Voce Board

As members of the Viva Voce Board, we certify that we have read the dissertation prepared by **Bishnu Prasad Kar** entitled "**Conformations of Molecules Containing π Systems: Matrix Isolation Infrared and a*b initio* Studies**" and recommend that it may be accepted as fulfilling the dissertation requirement for the Degree of Doctor of Philosophy.

Date: 25/3/2013

Chairman- Dr. T. Gnanasekaran

Date: 25.3.2013

Convener- Dr. K. Sundararajan

Date: 25/3/13

External examiner- Dr. A. K. Mishra

A. Bharathi **Date:** 25.03.2013

Member 1- Dr. A. Bharathi

Date:

Member 2- Dr. V. Ganesan 25/3/2013

Final approval and acceptance of this dissertation is contingent upon the candidate's submission of the final copies of the dissertation to HBNI.

I hereby certify that I have read this dissertation prepared under my direction and recommend that it may be accepted as fulfilling the dissertation requirement.

Date: 25.03.2013

Place: Kalpakkam

STATEMENT BY AUTHOR

This dissertation has been submitted in partial fulfillment of requirements for an advanced degree at Homi Bhabha National Institute (HBNI) and is deposited in the Library to be made available to borrowers under rules of the HBNI.

Brief quotations from this dissertation are allowable without special permission, provided that accurate acknowledgement of source is made. Requests for permission for extended quotation from or reproduction of this manuscript in whole or in part may be granted by the Competent Authority of HBNI when in his or her judgment the proposed use of the material is in the interests of scholarship. In all other instances, however, permission must be obtained from the author.

Bishnu Prasad Kar

Bishnu Prasad Kar

DECLARATION

I, hereby declare that the investigation presented in the thesis has been carried out by me. The work is original and has not been submitted earlier as a whole or in part for a degree / diploma at this or any other Institution / University.

Bishnu Prasad Kar

Bishnu Prasad Kar

EPIGRAPH

“Almost all aspects of life are engineered at the molecular level, and without understanding molecules we can only have a very sketchy understanding of life itself”

…Francis Crick

DEDICATED

To My Family And
To The Well Wishers
Of Human Society

ACKNOWLEDGEMENT

First of all, I would like to express my sincere gratitude to my research supervisor *Dr. K. Sundararajan*. His valuable discussions and suggestions during my Ph.D. period, regarding the handling of different instruments, use of different computational tools and in data analysis, showed me the proper path for my thesis.

I have no words to express my gratefulness to my former research supervisor (September 2007-July2011) *Dr. K. S. Viswanathan,* without whom this dissertation would not have a reality. His proper guidance in the beginning, good teaching in course work, valuable discussions and suggestions during my working hours, and his scientific excitement, have inspired me a lot for science. I have enjoyed the work under his guidance.

I owe my sincere thanks to the doctoral committee members, *Dr. T. Gnanasekaran, Dr. A. Bharathi*, and *Dr. V. Ganesan* for their valuable suggestions and evaluating my work at each step.

This is my duty to thank *Sri. S. C. Chetal, Director, IGCAR* and *Dr. Baldev Raj, Former Director, IGCAR* for giving me permission to work in this institute and allowing me to stay in Kalpakkam with nice facilities during this period. Also, I express my thanks to *Dr. P. R. Vasudeva Rao, Director, Chemistry Group, Dr. K. V. G. Kutty, Head, Materials Chemistry Division* and *Dr. K. Sankaran, Head, Analytical Chemistry and Spectroscopy Section* for providing me all the facilities to work.

I am grateful for the financial support provided by the Department of Atomic Energy research fellowship scheme from Indira Gandhi Centre for Atomic Research for the duration of the work.

I wish to thank *Mr. N. Ramanathan* for his fruitful discussions in day-to-day work in laboratory in spite of his busy Ph.D. work. I also thank to *Dr Siuli Maji Gayen* and *Mr.*

Satendra Kumar for their help in using the Nd:YAG laser for photoirradiation.

My hearty thanks to all my lab members, Dr. S. Vijayalakshmi, *Mrs. Shyamala, Mrs. Saji, Mr. Shiva Kumar, Mrs. Usha Lakshmi, Mrs. Hemalatha, Mr. Sriram, Mr. Sekar, Ms. Annapoorani, Mrs. Uma Maheshwari* and *Mrs. Deivanayaki* for their helps and the spent pleasant moments with them in our laboratory. I also thank to each members of Chemistry Group for their support and help in various ways during the course of this work.

This is my pleasure to express my affectionateness thanks to *Madhu, Subhra, Prasana, Satya and his family* who have given me a family like environment in Kalpakkam. I would like to thank *Kalpataru, Karuna, Alok, Ashit, Kamalakanta, Taruna, Sunasira, Satyaprakash, Nilamadhaba, Girish, Sudhanshu, Pradeep, Saswat, Manas, Sulata, Prabhati, Maneesha, Sudipta, Trinadha, Rahul, Rajini, Kuheli, Nithila, Joyshankar, Varghese, Haribabu, Saravanakumar, Sorb* and *the all members of our enclave* who have helped me in various ways and gave me a pleasant stay in Kalpakkam. I also want to express my thanks to *Suranjan, Biranchi, Abhiram, Satyabrata, Sanatana, Nrusingha* and *Sada* who helped me in various ways. I would also like to thank to my friends, who are staying outside Kalpakkam, for their moral support to make this thesis successful.

Finally, and most importantly, my unexpressible thanks to my *father Sri Ganeswar Kar, mother Smt. Banabasisni Sarangi, brother Sri Madhusudan Kar and all relatives* for their encouragement and moral support to make this study fruitful.

CONTENTS

SYNOPSIS

Conformations of molecules have long been a topic of great interest, as molecular structures influence reactivity and properties. Many biological processes are determined by conformational changes, such as protein folding. For example, misfolding of proteins leads to a condition referred to as amyloidosis.

Conformations arise due to the different spatial orientations of atoms in a molecule, where one form can interconvert to another, through rotation around formal single bonds. Barriers for rotations around single bonds are relatively small for many molecules, such as 2.9 kcal/mol for ethane, compared with those for rotations around double bonds, which is ~65 kcal/mol for CHD=CHD. The large barriers for rotations around double bonds give rise to geometric isomers, such as trans and cis stilbene, which have, in fact, very different physical properties. For example, trans-stilbene is a solid and cis-stilbene is a liquid at room temperature. However, when a single bond is flanked between two double bonds, barrier for rotation around the single bond becomes high compared to an isolated single bond, due to conjugation. Conjugation arises, as is well known, due to interactions of p-orbitals across an intervening single bond. The systems, which involve interaction between a non-bonding p-orbital and a double bond, also come under this categories e.g. esters, amides, phenol and aniline. In these systems too the rotational barrier around the intervening single bond is large. In a similar manner, when an aromatic ring is in conjugation with another π-system, the aromatic ring may show ring rotation around the connecting single bond. Different conformations may arise due to this ring rotation.

Conjugation is also explained in terms of donor-acceptor concept, as an electron delocalization interaction between a filled ‘n’ or ‘π’ orbital and a vacant ‘π*’ orbital. This leads to partial double bond character of the connecting single bond, and a consequent large value for the rotational barrier around the single bond. Due to ease of delocalization of non-bonding orbitals, n→π* interactions are stronger compared to π→π* interactions and hence the barriers of rotation around the connecting single bonds are larger in the former type of interactions.

In the present work, five π systems were studied for their conformational preferences. Stilbene, which involves a π-system and three organic carbonates, which involve an n-π system, were studied using matrix isolation infrared spectroscopy and *ab initio* methods. The organic carbonates studied were dimethyl carbonate (DMC), diethyl carbonate (DEC) and diphenyl carbonate (DPC). Dimethoxy silanone (DMSi), a silicon analogue of dimethyl carbonate was studied for its conformations using *ab initio* computations, to understand the differences between carbon and silicon systems. A comparison of DMC, DMSi and trimethyl phosphate (TMP) was also done using natural bond orbital (NBO) analysis.

The motivation for the study of organic carbonates also stems from its many applications in the industry. In the present scenario of environmental concern, carbonates are specially useful as green reagents because their preparation and applications involve benign methodologies.

The detailed studies on the conformations of the above π systems are discussed in this thesis. A brief description of the eight chapters of this thesis is given below.

Chapter 1 – Introduction

This chapter gives an introduction of the conformations in π systems and conformational behaviours of some π systems drawn from the literature are discussed here. Details of earlier studies from our research group are also given in this chapter to justify the choice of the systems chosen in this study.

Chapter 2 – Experimental and Computational Procedures

Details of the experimental procedure and *ab initio* computational methods used in this work are described in this chapter.

Conformational behaviours of the systems mentioned above were studied using matrix isolation infrared spectroscopy. Ar and N_2 were used as matrix gases. A few experiments were also performed using Kr as the matrix. Single jet and double jet effusive sources were used to deposit the samples and matrix gases, on a KBr substrate maintained at ~10 K. Samples were also deposited using a heated effusive source and a pulsed supersonic jet source to alter the population of different conformers in matrix, to aid us in assigning features of the higher energy conformers. In a few experiments, a high pressure Xe lamp and an Nd-YAG laser were used to photoirradiate species isolated in the inert matrix, to study their photoisomerization behaviour. Where the sample had a low vapour pressure, such as stilbene and DPC, they were heated to appropriate temperatures to achieve the desired matrix to sample ratio. On the contrary, with DMC and DEC, which had relatively higher vapour pressures, a low temperature ethanol slush bath was used to cool the sample to the desired temperatures. After depositing the matrix, the infrared spectra of the matrix isolated samples were recorded using an FTIR, operated at a resolution of 1 cm^{-1}. After recording the infrared spectra of the matrix isolated species, the matrix was also annealed at elevated temperatures, such as 35 K.

Ab initio computations at B3LYP/6-31++G** level were performed, using Gaussian 94 package. In general, the structures of the different conformers were optimized, without imposing any geometrical constraints; however, in a few cases, optimization was performed by imposing some geometric constraints. Vibrational frequency calculations using analytical gradients were performed on the computed structures to ensure that the optimized structures did correspond to minima on the potential surface and also to assign the observed vibrational features in the experiments. Natural bond orbital (NBO) analysis was used to understand the role of delocalization interactions in the conformational preferences of molecules.

In addition to studying the conformations of the above mentioned, 1:1 complexes of DMC-H_2O and DEC-H_2O were also studied, as they presented interesting case studies of hydrogen-bonded complexes in these systems. Atoms-in-molecules (AIM) calculations were performed to understand the nature of interactions between the submolecules in complexes.

Chapter 3 – Studies on Non-planar Trans-stilbene

Matrix isolated infrared studies on non-planar trans-stilbene are discussed in this chapter. Cis-stilbene was trapped in N_2, Ar and Kr matrixes and then photoirradiated; vibrational spectra of the photoirradiated matrix showed evidence for the presence of the non-planar trans-isomer of stilbene, in the matrix. The vibrational spectrum of non-planar trans-stilbene was presented for the first time, as a result of this work. On annealing the matrix, after photoirradiation, the intensity of the non-planar trans vibrational features were decreased, while those of the planar trans isomer concomitantly increased. This observation indicated a conversion of the non-planar trans-isomer to the planar trans structure, indicating that the planar form is the more stable of these two structures, separated by only a small barrier. The assignment of experimental spectral features to the non-planar isomer were corroborated by computations at the B3LYP/6-31++G** level.

Chapter 4 – Studies on the conformations of dimethyl carbonate and its complexes with water

This chapter describes the matrix isolation infrared and *ab initio* studies on conformations of DMC ($(CH_3O)_2C=O$) and its (1:1) complexes with water. Infrared spectra of DMC trapped in inert gas matrixes (N_2 and Ar), using an effusive source at 298 and 423 K, showed evidences of both the ground state (cis-cis), and higher energy (cis-trans) conformers. Experiments were also performed using a supersonic jet source to deposit the matrix; conformational cooling observed in this expansion process further indicated the presence of the higher energy conformer. The structures and vibrational frequencies of these conformers were computed using *ab initio* methods. NBO analysis was performed to understand the role of the delocalization interactions in conformational preferences; vicinal interactions were found to be the dominating interactions here.

A 1:1 DMC-H_2O complex was identified in the matrix isolation experiments, where the carbonyl oxygen of DMC served as the proton acceptor for the hydrogen bonded complex. This observation was corroborated by *ab initio* computations. Our computations also indicated another minimum, corresponding to a methoxy bonded DMC-H_2O complex, which was less exothermic; however, this complex was not identified in our experiments. To study the nature of the intermolecular interaction in the DMC-H_2O complexes, atoms-in-molecules theory was performed on the computed complex structures.

Chapter 5 – Studies on the conformations of diethyl carbonate and its complexes with water

This chapter describes studies on conformations of DEC ($(C_2H_5O)_2C{=}O$) and its (1:1) water complexes. DEC was trapped in argon matrix at 12 K using an effusive nozzle source maintained at 298 and 423 K and a supersonic jet source. The experimental studies were supported by *ab initio* computations. The ground state conformer for DEC was found to have a "cc(tt)" geometry, where the 'c' refers to a cis orientation of the carbons attached to oxygen, while the 't' in parenthesis refers to the trans orientation of the terminal carbon. In addition to the ground state conformer, our computations also indicated the presence of conformers cc($tg^{\pm}$), cc($g^{\pm}g^{\mp}$) and cc($g^{\pm}g^{\pm}$), having relative energies 0.51, 0.98 and 1.00 kcal/mol respectively with respect to the ground state conformer.

Our computations indicated four minima on the potential surface; however, it was difficult to experimentally differentiate between these various conformers, as the most of the computed vibrational wavenumbers for all the conformers lie rather close to each other. Five features, which can be uniquely assigned to the higher energy conformers, decrease on annealing, and hence can be assigned to the three higher energy conformers cc(tg$^{\pm}$), cc(g$^{\pm}$g$^{\mp}$) and cc(g$^{\pm}$g$^{\pm}$). The higher energy conformers likely interconvert to the ground state, cc(tt) conformer during annealing. NBO analysis was also performed to understand the role of delocalization interactions and steric effect on conformational stability.

Similar to DMC, computations on DEC-H_2O (1:1) complexes, showed the possibility of formation of carbonyl and ethoxy complexes with the all four conformers of DEC. Ethoxy complexes were found to be less exothermic than the carbonyl complexes. However, we have corroborated our experimental vibrational frequencies only with the computed values that obtained for the water complexes of dominant ground state conformer [cc(tt)] of DEC. Only the carbonyl complex was observed in the matrix isolation experiments.

Chapter 6 – Studies on the conformations of diphenyl carbonate

This chapter describes the experimental and computational studies on the conformations of diphenyl carbonate ($(C_6H_5O)_2C{=}O$). DPC was trapped in N_2 matrix at 12 K using an effusive source heated at two different temperatures 303 and 473 K and also using a supersonic jet source. *Ab initio* computations were performed to corroborate the experimental result. Three conformers were indicated by our computations with cis-cis (anti), cis-cis (syn) and cis-trans structures, with relative energies of 0.00, 0.14 and 2.10 kcal/mol, respectively. Anti and syn conformers arise due to the rotation of phenyl rings. NBO analysis was performed to understand the role of delocalization interactions and steric effect on conformational stability. It was found that in DPC, both the effects together direct the molecule to have rotated structures for phenyl rings.

Chapter 7 – *Ab initio* study on the conformations of dimethoxy silanone and its comparison with dimethyl carbonate and trimethyl phosphate

Conformations of dimethoxy silanone ($(CH_3O)_2Si{=}O$) (DMSi) was studied using ab initio computations at the B3LYP/6-31++G** level of theory. Two conformers, cis-cis and cis-trans were indicated by our computations. The energy difference between the two conformers was found to be 1.04 kcal/mol. A comparison of the conformation of DMSi, DMC and TMP ($(CH_3O)_3P=O$) were also performed on the basis of natural bond orbital analysis to understand the effect of delocalization interactions on conformations in these molecules. Vicinal interactions were found to be dominating interactions in DMC and DMSi, whereas both geminal and vicinal interactions were found to participate towards molecular stability of TMP.

Chapter 8 – Summary and Conclusions

This chapter presents the conclusions drawn from the study of the above mentioned π systems with respect to their conformations. Non-planar trans-stilbene structure was found to be one of the conformers resulting from the rotation of the phenyl rings in the molecule. The same phenyl rotation also gives rise to the different conformations in DPC. In organic carbonates, the cis and trans orientation of alkyl and aryl groups arise due to the rotations around the RO–C bonds. Due to the partial double bond character of RO–C bond, conformation interconversions have somewhat large barriers. In DMSi, conformational preferences were found to be similar to those of DMC. A natural bond orbital analysis of DMC, DMSi and TMP showed a greater participation of *d* orbital of phosphorous in bonding, which resulted in strong geminal and vicinal delocalization interactions, and in turn, determined the conformational preferences in the phosphate.

LIST OF FIGURES

LIST OF TABLES

LIST OF ABBREVIATION

Symbol	**Abbreviation**
AIM	Atoms-in-Molecules
B3LYP	Becke-3-Parameter-Lee-Yang-Parr functional
BCP	Bond Critical Point
BLYP	Becke-Lee-Yang-Parr functional
BPA	Bisphenol A
BSSE	Basis Set Superposition Error
BVWN	Becke-88-Vosko-Wilk-Nusair functional
CCSD(T)	Coupled-Cluster methods with Single-, Double- and Triple-excitation operators
CP	Critical Point
DEC	Diethyl Carbonate
DEE	Diethoxyethane
DEM	Diethoxymethane
DFT	Density Functional Theory
DMC	Dimethyl Carbonate
DMDMSi	Dimethoxydimethylsilane
DME	Dimethoxyethane
DMM	Dimethoxymethane
DMMPSi	Dimethoxymethylphenylsilane
DMMSi	Dimethoxymethylsilane
DMP	Dimethoxypropane
DMSi	Dimethoxy Silanone
DPC	Diphenyl Carbonate
f.c.c.	Face centre cubic
FWHM	Full Width Half Maximum
h.c.p.	Hexagonal close packing
HF	Hartree-Fock
IUPAC	International Union of Pure and Applied Chemistry
L	Lewis
MO	Molecular Orbital
MP2	Møller-Plesset second order perturbation
MP3	Møller-Plesset third order perturbation
NAdO	Natural Atomic d Orbital
NAO	Natural Atomic Orbital
NBO	Natural Bond Orbital
NHO	Natural Hybrid Orbital
NL	Non-Lewis
NLMO	Natural Localized Molecular Orbital
NMB	Natural Minimal Basis

NPTS	Non-Planar Trans-Stilbene
PNAO	Pre-orthogonal Natural Atomic Orbital
QST2	Quasi-Synchronous Transit method with two geometry input
QST3	Quasi-Synchronous Transit method with three geometry input
RCP	Ring Critical Point
RY	Rydberg orbital
SCF	Self Consistent Field
TBP	Tributyl Phosphate
TEP	Triethyl Phosphate
TMM	Trimethoxymethane
TMMSi	Trimethoxymethylsialne
TMP	Trimethyl Phosphate
TMPhite	Trimethyl Phosphite
TS	Transition State
ZPE	Zero Point Energy

CHAPTER 1

INTRODUCTION

Study of molecular structures is an important aspect of chemistry, as it often provides the basis for understanding many chemical, biological and industrial processes. For example, studies on structure and reactivity of chlorophyll provide the basis for understanding light harvesting during photosynthesis[1]. Another example of the importance of molecular structure studies is the photoisomerization of retinal which is responsible for vision in humans and animals.[1,2] Molecules with high conjugation especially pigments emit light strongly in the visible regions e.g. β-carotene, natural dyes and synthetic dyes. The conjugated oligomers and polymers are used in preparing many devices such as field-effect transistors, light-emitting diodes, electrochromic devices and solar cells.[3] Several π systems have also been studied which act as fluorescent sensors for toxic cations e.g. Pb^{2+}, Hg^{2+}.[4,5] Nowadays the gap between chemistry and engineering is almost vanishing because of the emerging applications of such systems.

Conformational change in molecules leads to different chemical reactions and is responsible for many biological processes. Protein folding and unfolding at different environmental conditions occurs due to the conformational changes. Protein misfolding is the cause of amyloidosis diseases.[1] Conformations arise due to the different spatial orientations of atoms in a molecule, where one form can interconvert to another, through rotation around single bonds.[6] These stereoisomers are known as conformers, rotamers or conformational isomers.

Stability of conformational isomers is decided by two main factors: steric repulsions and delocalization interactions (stereoelectronic effect). In some cases intramolecular hydrogen bonding plays a role in stabilizing different conformations. In condensed systems, intermolecular interactions become important. Steric repulsions are generally considered to arise due to the electronic permutational antisymmetry imposed by the Pauli Exclusion Principle[7,8] and electrostatic repulsions[9]. Butane is the classic example of steric effect (spatial effect) where the anti form is the most preferred conformation.

Delocalization interactions arise due to the electron delocalization from a filled (bonding or non-bonding) orbital to a vacant (antibonding) orbital and lead to further lowering in energy of the system.[10] Conjugation and hyperconjugation are the two examples of delocalization interactions. Conjugation interactions involve π orbitals i.e. $n \rightarrow \pi^*$ and $\pi \rightarrow \pi^*$ interactions, whereas hyperconjugation involves the interactions among σ- and π-type orbitals. The $n \rightarrow \sigma^*$ hyperconjugative interaction is responsible for the conformational preferences in many molecules, such as 1,3-dioxanes[11-15], dialkoxymethanes[16-23] and dialkoxysilanes,[24-27] where the gauche conformer is found to be more stable than trans form. The above type of hyperconjugative interaction is well known as 'anomeric effect'. Lemieux first introduced anomeric effect[28] in 1958 to rationalize the relative stability of the axial conformer when compared to the equatorial conformer in acetylated derivatives of aldo–hexapyranoses even though axial form is sterically unfavorable. The generally accepted model for anomeric effect is based on molecular orbital theory approach, which involves the $n_X \rightarrow \sigma^*_{A\text{-}Y}$ delocalization, where n_X is the non bonding lone pair orbital of X and $\sigma^*_{A\text{-}Y}$ is the antibonding orbital of A-Y in an R-X-A-Y moiety. The delocalization is maximum when the n_X and $\sigma_{A\text{-}Y}$ are antiperiplanar to each other. Fig. 1.1 shows a typical $n_X \rightarrow \sigma^*_{A\text{-}Y}$ delocalization

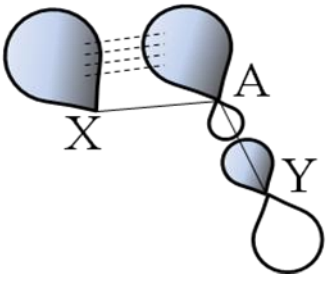

Fig. 1.1 – $n \rightarrow \sigma^*$, (anomeric) interaction.

(anomeric) interaction. In terms of valence bond theory, this is equivalent to a 'no-bond-double-bond resonance' and 'negative hyperconjugation'.[29]

Rotational barrier around a double bond is very high (65 kcal/mol, CHD=CHD) compared to a single bond (2.9 kcal/mol, ethane).[30] This leads to two stable geometrical isomers; cis and trans (Z and E) with respect to the double bond. Here double bond refers to C=C, C=N, N=N, C=S, C=O etc. where the atoms show sp^2 hybridization. However when a single bond separates two double bond, rotation can occur through the single bond and leads to two different conformations. But the barrier of rotation around such single bonds is comparatively higher (5.9 kcal/mol, 1,3-butadiene)[31] than an isolated single bond which is not adjacent to a double bond (3.6 kcal/mol, CH_3/H eclipsed barrier in butane),[30] due to conjugation. Conjugation involves the interaction of one p-orbital with another across an intervening σ-bond[6] e.g. $CH_2=CH–CH=CH_2$, $CH_2=CH–C\equiv N$ and $Cl–CH=CH_2$. This leads to partial double bond character of the connecting single bond, and a consequent large value for the rotational barrier around the single bond. In 1,3-butadiene, it is evidenced by shortening of the middle single bond and elongation of the terminal double bonds. Two conformers are found for butadiene due to the rotation around the middle single bond. The lower energy conformer of butadiene, the anti conformer (Fig.1.2) is planar in structure where the two double bonds are antiperiplanar to each other.[32] The higher energy conformer has a non-

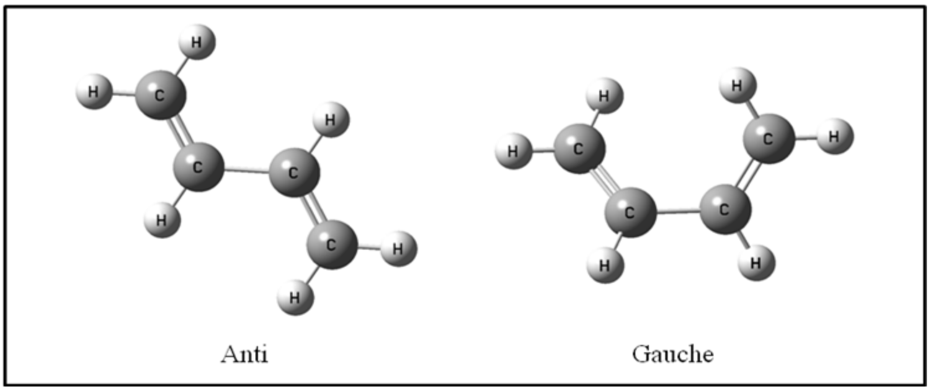

Fig. 1.2 – Conformations of 1,3-butadiene.

planar gauche structure (C-C-C-C dihedral angle is ~38°, Fig. 1.2) but not planar syn.[31-35] The steric interaction present between the two terminal hydrogen atoms leads the molecule to have the gauche form.

A phenyl ring in conjugation with a vinyl group also creates such a situation. Due to complete delocalization of π-electrons over the phenyl ring, phenyl group behaves as a single entity and can rotate along the single bond to have different conformations. Styrene is an example of such a system. The structure of styrene whether it is planar or non-planar is still debatable as exemplified by many experimental and theoretical studies.[30,36] While steric interaction plays the role to have non-planar gauche conformer (similar to gauche butadiene), strong π-electron delocalization of vinyl group with phenyl ring forces it to be in planar form. Similar instances were also observed in many molecules containing phenyl rings in conjugation with double bond, such as stilbene and azobenzene. These molecules are also known to have pedal motions in crystals, which facilitates phenyl ring rotation in molecules.[37,38] In many cases the phenyl rings take non-planar orientation with respect to the vinyl double bond due to strong steric interaction present in it, such as cis-stilbene which is known to be non-planar.[36]

Systems, such as acrolein and benzaldehyde, where a double bond or an aryl group is bonded with a carbonyl group through a single bond, show different conformers due to rotation around the single bond connecting the two. These molecules are found to have planar frameworks and exist in two conformational structures. In acrolein (propenal, CH_2=CH-CH=O), conformers arise due to the rotation around the C–C and the form in which O is anti to CH_2, is preferred over the other syn form by ~1.7 kcal/mol. The energy barrier for rotation in acrolein is 5.0–6.4 kcal/mol.[30,39] Benzaldehyde is also found to exist in planar structure as in case of acrolein and the rotational barrier is 7.6–7.9 kcal/mol.[30] Substitutions on benzene ring at different positions with different groups alter the rotational barrier in benzaldehyde.

For example, electron-donating group such as CH_3O and $(CH_3)_2N$ at para position increases the rotational barrier to 9.0-9.4 kcal/mol and 9.9-10.8 kcal/mol respectively as it would be expected from resonance considerations.[30] Furfural is another example where the rotational barrier is found to be higher, 10.9 kcal/mol.

When a hetero atom containing one or more lone pair of electrons (e.g. O, N, S etc.) is connected with a C=C through a single bond, the single bond acquires more double bond character compared to polyenes. This happens because $n \rightarrow \pi^*$ interactions are stronger than $\pi \rightarrow \pi^*$ interactions due to ease of delocalization of non-bonding orbital containing the lone pair of electrons. Similar to conjugated polyene systems, these molecules can also have two conformers with respect to rotation around the single bond. Shortening of the single bond and elongation of double bond can be noticed. A few molecules of such type are also known to show keto-enol and enamine-imine tautomers.[40]

A similar increase in bond strength also can be observed when the hetero atoms are connected to a phenyl ring e.g. phenol, thiophenol and aniline. Phenol is known to have planar structures due to the delocalization (resonance) of lone pair of electrons of oxygen with the phenyl ring.[41] The experimentally determined barrier height in phenol ranges from 3.36-3.56 kcal/mol.[42] Also in case of anisole, the same reason drives the methyl group carbon to be in the plane of phenyl ring.[43] p-dimethoxybenzene, due to the different orientation of methyl groups, shows the presence of two conformers both in vapor and liquid phase with the two methyl groups either syn or anti to each other.[44,45] Thiophenol is more stable in its planar form with a magnitude of the rotational barrier which falls within the experimental range of 0.80 ± 0.20 kcal/mol.[46,47] In case of aniline, even though $n \rightarrow \pi^*$ delocalization is observed, the molecule has a pyramidal structure due to highly directed sp^3 orbitals of nitrogen for bond formation.[48-54] However, in these cases rotation of phenyl ring is not totally restricted and can take the orientation according to the other group connected to the hetero atom to minimize the steric effect.

Shortening and strengthening of the connecting single bond takes place when one of the atom of a double bond is more electro negative compared to other as in the case of carboxylic acids, esters, amides, thioamides etc. (X-C=Y systems; X, Y=N, O, S). Rotational barrier depends on the ability of the hetero atom to donate the lone pair of electron and the ability of π^* orbital to accept the electrons which favors the $n \rightarrow \pi^*$ delocalization. According to natural bond orbital analysis, the interaction is more favored when overlap between the corresponding orbitals is more.[10] It has been found that amides (16-22 kcal/mol[55-57]) have high rotational barrier compared to esters (8-15 kcal/mol[58-61]) as nitrogen is a better electron donor compared to oxygen. However isomerization is found to be easier in amides relative to the corresponding thioamides.[57,62] The reason for this observation may be due to the lone pair of electron on nitrogen delocalizes better in the (thio)-carbonyl group. In *N*-phenylcarbamate, the rotational barrier around C(carbonyl)−N bond is ~12.5 kcal/mol which is less compared to that of an *N*-alkylcarbamate (~16 kcal/mol) and it is further lowered to 9 kcal/mol for *N*-(2-pyrimidyl)carbamates.[63] The *N*-aryl ring withdraws π-electron density from N, which reduces the delocalization of the lone pair of N with the carbonyl group and hence relatively small barriers are observed in these systems.

In case of carboxylic acids and esters (RCOOR'), the R' and carbonyl group can be in the same side of the single bond (cis conformer) or in opposite sides (trans conformer) this is due to restricted rotation around the X-C single bond. The cis conformer is more stable compared to trans form; as the size of R' increases, the later becomes more stable because the steric interaction with the carbonyl group is reduced.[64,65] *Ab initio* computations were carried out for cis and trans conformers of thioesters. The energy difference between trans and cis conformers are found to follow in the order methyl thiolformate < methyl thionoformate <

methyl formate.[66] The energy differences between trans and cis forms in methyl acetate and methyl thioacetate are calculated to be ~8 and ~5 kcal/mol respectively with energy barriers for the rotation ~13 and ~11 kcal/mol.[67] Amides are also found to be present in two different conformations. Energy difference between the two conformers in n-methylformamide is calculated to be 1.3 kcal/mol.[68] In few cases, hydrogen bonding has been shown to alter the equilibrium between different conformers of amides and carbamates.[69,70] Photoisomerization has also been reported for a few arylthioamides.[71,72]

When two hetero atoms are bonded to an atom with a double bond as in ureas (N-C(=O)-N), competitive conjugation can be observed in order to share the common π^* orbital for delocalization, which lowers the isomerization barrier. In ureas the free energy barrier for classical cis-trans isomerization is 18.5±1.6 kcal/mol and the whole body motion (urea flip) is 15.5±1.2 kcal/mol.[73] Here, cis-cis conformer is found to be the preferred geometry. Other examples of molecules where competitive conjugation may be observed are thioureas, carbonates and thiocarbonates.

Phosphates are important in biological and industrial field. As an extractant, tri-n-butyl phosphate (TBP) is used in nuclear industries for fuel reprocessing to extract U and Pu from the nuclear waste.[74] Dodecane is used as diluent, to alter the physical properties and the extracting efficiency of the phosphate. To understand the intermolecular interactions between the phosphates and diluents it is required first to understand the structure of phosphates. Therefore, matrix isolation infrared spectroscopy and *ab initio* study program was launched in our laboratory to understand the structure of organic phosphates. The first member of organic phosphates, trimethyl phosphate (TMP) was studied for its conformations.[75,76] *Ab initio* computations located three minima corresponding to C_3, C_1 and C_S symmetries, given in order of increasing energies. Effusive and supersonic jet experiments helped us to identify ground state C_3 ($G^{\pm}G^{\pm}G^{\pm}$) as well as higher energy conformer C_1 ($TG^{\pm}G^{\pm}$). ('G' and 'T' refers to gauche and trans orientation respectively.) Next member of phosphate series, triethyl phosphate (TEP) was studied using matrix isolation and *ab initio* methods to understand its conformational behaviour.[77] Earlier, semi-empirical method of calculations were used to study the conformations of TEP,[77] whereas in a later stage *ab initio* methods were used for the studies of TEP.[78] For the higher member of phosphates as the length of the alkyl chain increases then the number of conformers also increases which makes it challenging to study both by experimental and computational techniques.

Conformations in phosphates are decided by many factors, such as stereoelectronic effects, steric effects and hydrogen-bonding interactions etc. To understand the relative importance of these effects a set of model molecules were studied having backbone structure COCOC similar to that of phosphates COPOC. A number of acetals and ketals viz. Dimethoxymethane (DMM)[18], 1,1-dimethoxyethane (DME)[19], 2,2-dimethoxypropane (DMP)[20], Diethoxymethane (DEM)[21], 1,1-diethoxyethane (DEE)[22] and trimethoxymethane (TMM)[23] were studied for their conformations using matrix isolation infrared spectroscopy and *ab initio* methods. It was found that anomeric effect played a major role in deciding the conformations in these molecules.

The ground state conformers in DMM, DME and DMP were found to be $G^{\pm}G^{\mp}$ form, which is stabilized by two anomeric interactions. Matrix isolation infrared spectroscopy experiments and *ab initio* calculations at B3LYP/6-31++G** level of theory were used to identify the first higher energy conformers to be TG configuration. In DMM, the first higher energy conformer $TG^{\pm}$ was found to exist in two degenerate states whereas in DME this conformer was split into two different states TG^{-} and TG^{+} due to a lowering of symmetry. The TG^{-} conformer was found to be lower in energy due to less steric interaction than TG^{+}. The lost symmetry in DME, again picks up in DMP; as a result, a similar conformational behaviour was found in DMP as in case of DMM. Due to increase steric interaction in DMP, the relative energy of each conformer with respect to the ground state conformer is comparatively higher. In TMM, among the six possible conformers, $TG^{\pm}G^{\pm}$ was the ground state conformer and the other conformers were $G^{\pm}G^{\pm}G^{\pm}$, $TG^{+}G^{-}$, $TTG^{\pm}$, $CG^{+}G^{-}$, TTT with increasing order. Cyclic anomeric interactions played a major role in deciding the conformations in TMM. The ground state conformer $TG^{\pm}G^{\pm}$ were found to contain four anomeric interactions, among which three were in cyclic manner, whereas the first higher energy conformer, $G^{\pm}G^{\pm}G^{\pm}$ was found to possess only three anomeric interactions, involved in a cyclic fashion. The $TG^{+}G^{-}$ conformer was observed to have four anomeric interactions but no involvement of a cyclic interaction, which resulted in this conformer being a third higher energy conformer. Other three conformers $TTG^{\pm}$, $CG^{+}G^{-}$ and TTT were found to take fourth, fifth and sixth positions in the energy ladder as they posses 3, 2 and 0 anomeric interactions respectively.

In DEM and DEE, the anomeric carbon atoms (the carbon atom attached to oxygen in ethoxy group) were found to orient in gauche or trans positions due to anomeric interactions, whereas the terminal carbon atoms orient in trans or gauche due to steric interaction. In both the cases, $G^{\pm}G^{\mp}$(tt) was found to be the ground state conformer, where $G^{\pm}G^{\mp}$ represent the orientation of anomeric carbon atoms and ‘tt’ in parenthesis that for terminal carbon atoms. The first higher energy conformers were found to be $G^{+}G^{-}(g^{+}t)$ in DEM and for DEE it was TG^{-}(tt). Matrix isolation experiments and *ab initio* computations helped to identify the ground state as well as the first higher energy conformers in DEM and DEE with the other excited conformers $G^{+}G^{-}(g^{-}t)$ and $TG^{\pm}$(tt) for DEM. The relative energy difference between the conformers in acetals and ketals were rationalized on the basis of interplay between anomeric and steric effect. *Ab initio* calculations showed the presence of hydrogen-bonding in the higher energy conformers of DEE. The conformational study on acetals and ketals helped to resolve the conformations of TEP.[79] In TEP, due to the different orientation of the terminal carbon atoms for each position of anomeric carbon atoms, clusters of conformers were observed with respect to each conformer of TMP.

Further studies were also done on the conformations of methoxysilanes such as dimethoxymethylsilane (DMMSi)[24], dimethoxydimethylsilane (DMDMSi)[25], dimethoxymethylphenylsilane (DMMPSi)[26], trimethoxymethylsilane (TMMSi)[27] to understand the anomeric interaction in these compounds. In these compounds, anomeric effects do play a major role in deciding the conformers. In DMMSi, DMDMSi and DMMPSi $G^{\pm}G^{\mp}$ conformer was found to be the ground state conformer. Natural bond orbital (NBO) analysis was performed on the silanes (dimethoxysilane, DMMSi and DMDMSi) and the corresponding carbon analogous (DMM, DME and DMP) to understand and quantify the anomeric effect. It was found that the magnitude of anomeric effect in silicon systems was less compared to their corresponding carbon analogous[80] because of which the energy orderings of various conformers is found to be different in silane system. The ground state conformer of TMMSi was found to be $TG^{\pm}G^{\pm}$, similar to TMM but the energy ordering of conformers were different in both cases.

Trimethyl phosphite (TMPhite), which lacks the P=O group was found to show different conformational ordering from that of TMP.[81] $TG^{\pm}G^{\pm}$, $TG^{+}G^{-}$, $TTG^{\pm}$ and $G^{\pm}G^{\pm}G^{\pm}$ were the conformers of TMPhite with increasing order energies whereas in TMP it was $G^{\pm}G^{\pm}G^{\pm}$, $TG^{\pm}G^{\pm}$ and $TG^{+}G^{-}$. NBO analysis performed on these conformers showed that geminal interactions plays a major role in stabilizing the ground state $G^{\pm}G^{\pm}G^{\pm}$ conformer in TMP, which was almost absent in $G^{\pm}G^{\pm}G^{\pm}$ in TMPhite thus placing it as the highest energy conformer. The other conformers of TMPhite and the conformers of TMP were shown to posses both geminal and vicinal interactions. The d orbital of phosphorous was found to be responsible for geminal interactions in TMP and TMPhite.

This thesis work describes the matrix isolation infrared experiments and *ab initio* computations on the conformational study of molecules containing π systems. Five such molecules are studied here. They are Stilbene, a pure π- system and four n-π systems: Dimethyl carbonate (DMC), Diethyl carbonate (DEC), Diphenyl carbonate (DPC) and Dimethoxy silanone (DMSi).

The motivation to study stilbene molecule stems from the fact that stilbene and its derivatives are used in many industrial and biological applications. These compounds have multifunctional activities. The natural product trans-resveratrol, a derivative of stilbene, present in grapes and other food materials, shows cancer chemopreventive activity.[82,83] Stilbenes also show antioxidant properties,[83-86] due to which trans-resveratrol is believed to prevent cardio vascular diseases and certain type of cancer. In addition to its utility in living processes, stilbene and its derivatives also find industrial applications, such as in the production of optical brighteners, laser dyes, scintillators, light emitting diodes, optical switches and optical data storage.[87,88]

Nowadays environmental concern is a big issue, which makes it imperative for industries to develop biodegradable products and environmentally benign methodologies for chemical synthesis. In such a time, organic carbonates are the prototype examples of green reagents with versatile reactivity. Organic carbonates are biodegradable and nontoxic; thus, they could be considered as a possible “green solvents”. DMC replaces phosgene as a methoxycarbonylation agent in the formation of polycarbonates and carbamates and takes the role of dimethylsulphate and methylhalides for methylation.[89-92] DMC also finds applications as a blending agent and is also considered as an outstanding oxygenate for fuel additives in automobiles.[93] Its use increased since the mid-80s, when an efficient synthetic procedure for DMC was developed through a catalytic oxidative carbonylation of methanol with oxygen; a process developed by Eniche, Italy.[94] DMC and DEC are used to prepare the electrolyte solution along with other carbonates for Li and Li–ion batteries[95,96] and capacitor batteries.[97] DEC is also used as ethylating and ethoxycarbonylating reagent in organic synthesis and used as solvents of nitro-cotton, cellulose ether, synthetic resin and natural resin in the textile printing and dyeing industry. As like DMC, DEC can also be prepared in an environmental friendly way from ethanol and supercritical CO_2.[98]

DPC is used as an intermediate compound for the synthesis of Bisphenol A (BPA) polycarbonates in an environmental friendly and safety route without using poisonous chemical phosgene.[99] These polycarbonates are important engineering thermoplastics with excellent mechanical, optical, electrical, and heat resistance properties,[100] which make it very useful and versatile material in various applications. DPC has also versatile chemical properties and has been used both as a phenylating and a phenoxycarbonylating agent, which are very important in synthetic chemistry.[101] Dicarboxylic acids in reaction with diphenyl carbonate eliminate carbon dioxide and form diphenyl esters, which are the starting materials for the production of high molecular weight aromatic polyesters.[102,103] Synthesis of DPC in non-phosgene approaches has increased the use of it for the industrial applications.[99] A few of the methods are the transesterification of dimethyl carbonate (DMC) and phenol, the oxidative carbonylation of phenol and the transesterification of dialkyl oxalates and phenol.[89,99,103,104]

The purpose of studying the conformers of dimethyl carbonate (DMC), diethyl carbonate (DEC) and diphenyl carbonate (DPC) are twofold: one is the large applications mentioned above and the second important factor is that these compounds have a backbone structure COCOC and a C=O group very similar to phosphates COPOC and P=O and can be considered as another set of model compounds to understand the conformers of phosphates. Carbonates are also different from the corresponding dialkoxyalkanes, as the later does not have a centralised carbonyl group. *Ab initio* computation on dimethoxy silanone (DMSi) was studied to make a comparison between DMC, DMSi, and TMP in order to understand the conformational preferences in these molecules.

The infrared features of the matrix isolated species are of small line widths compared to solid, liquid and gas phase, which makes it ideal for the conformational studies. To identify the features due to higher energy conformers, depositions were performed using a heated nozzle and supersonic jet source. These experiments were performed to alter the population of different conformers in the gas phase before deposition. We also photoirradiated the samples using a broadband source and a monochromatic laser source to observe the photoisomerization. Details of these experimental methods are discussed in Chapter 2.

Ab initio calculations were used to corroborate the experimental results. Natural bond orbital (NBO) analysis helped us to understand the delocalization interactions operating in different conformers. Details of the computations are presented in chapter 2.

Along with the conformation studies, we have also studied the hydrogen-bonded complexes of DMC and DEC with water. This study was performed to assign the features due to the complexes and also to avoid the wrong assignments of the features due to these adducts as that of higher energy conformers.

Chapter 3 describes the studies on non-planar trans-stilbene, a conformer of trans-stilbene that arises due to phenyl ring rotation. This conformer was trapped in matrix on photoirradiation of cis-stilbene. Conformations of DMC and its complexes with water are presented in Chapter 4. This helps to understand the role of $n \rightarrow \pi^*$ delocalization on conformation. Chapter 5 discusses the experimental and computational results on the conformations of DEC and its complexes with water. Effect of phenyl ring rotation on the conformations of DPC is described in Chapter 6. *Ab initio* computation studies on conformations of DMSi and its comparison with DMC and TMP on the basis of NBO analysis are shown in Chapter 7. Summary and conclusions derived from these studies are presented in Chapter 8.

1.1 Scope of the present work

The goal of the thesis is to study of conformations of molecules containing π systems. All the systems were studied using matrix isolation infrared technique. *Ab initio* computations were also carried out for these systems to corroborate with the experimental results. Stilbene, a π-system was studied using matrix isolation infrared spectroscopy. A detailed vibrational analysis of non-planar trans-stilbene was presented in this study. DMC, DEC and DPC (n-π systems) were studied for their conformations. DMSi, silicon analogous of DMC is studied for its conformations using *ab initio* computations. NBO analysis was employed on carbonates to understand the role of delocalization interactions on the conformational preferences of these molecules. This work helps to understand the rotation of phenyl (aryl) group in a π-system. A comparison study on DMC, DMSi and TMP on the basis of NBO analysis helps to understand the different conformational behaviour in these molecules.

The summary of the work described in this thesis is as follows:

- Matrix isolation Infrared studies of non-planar trans-stilbene,
- Matrix isolation infrared and *ab initio* studies on the conformations of DMC, DEC, DPC.
- *Ab initio* studies on the conformations of DMSi.
- Matrix isolation infrared and *ab initio* studies on the H_2O complexes of DMC and DEC.

References

---

[1] M. M. Cox, D. L. Nelson, Lehninger Principles of Biochemistry, Fifth Edition, Freeman Publication, 2008.

[2] M. Jones Jr., Organic Chemistry, Third edition, W. W. Norton and company, New York, London, 2003.

[3] J. Roncali, Macromol. Rapid Commun., 2007, *28*, 1761.

[4] R. Satapathy, Y.-H. Wu, H.-C. Lin, Chem. Commun., 2012, *48*, 5668.

[5] R. Satapathy, Y.-H. Wu, H.-C. Lin, Org. Lett., 2012, *10*, 2564.

[6] IUPAC. Compendium of Chemical Terminology, 2nd ed. (the "Gold Book"). Compiled by A. D. McNaught and A. Wilkinson. Blackwell Scientific Publications, Oxford (1997). XML on-line corrected version: http://goldbook.iupac.org (2006-) created by M. Nic, J. Jirat, B. Kosata; updates compiled by A. Jenkins. ISBN 0-9678550-9-8. doi:10.1351/goldbook.

[7] V. F. Weisskopf, Science, 1975, *187*, 605.

[8] J. K. Badenhoop, F. Weinhold, J. Chem. Phys., 1997, *107*, 5406.

[9] V. Pophristic, L. Goodman, Nature, 2001, *411*, 565.

[10] F. Weinhold, C. Landis, Valency and Bonding- A natural bond orbital donor-acceptor perspective, Cambridge university press, 2005.

[11] W. F. Bailey, E. L. Eliel, J. Am. Chem. Soc., 1974, *96*, 1798.

[12] L. Nørskov-lauritsen, N. L. Allinger, J. Comp. Chem., 1984, *5*, 326.

[13] F. Perron, K. F. Albizati, Chem. Rev., 1989, *89*, 1617.

[14] J. E. Dubois, A. Cossé-Barbi, D. G. Watson, Tetrahedron Lett., 1989, *30*, 167.

[15] H. Senderowitz, L. Golender, B. Fuchs, Tetrahedron, 1994, *50*, 9707.

[16] E. S. Marcos, R. R. Pappalardo, J. L. Chiara, M. C. Domene, J. M. Martinez, R. M. Parrondo, J. Mol. Struct. Theochem, 1996, *371*, 245.

---

[17] G. D. Smith, R. L. Jaffe, D. Y. Yoon, Chem. Phys. Lett., 1998, *289*, 480.

[18] V. Venkatesan, K. Sundararajan, K. Sankaran, K. S. Viswanathan, Spectrochim. Acta Part A, 2002, *58*, 467.

[19] V. Venkatesan, K. Sundararajan, K. S. Viswanathan, J. Phys. Chem. A, 2002, *106*, 7707.

[20] V. Venkatesan, K. Sundararajan, K. S. Viswanathan, Spectrochim. Acta Part A, 2003, *59*, 1497.

[21] V. Venkatesan, K. Sundararajan, K. S. Viswanathan, J. Phys. Chem. A, 2003, *107*, 7727.

[22] V. Venkatesan, K. S. Viswanathan, J. Mol. Struct., 2011, *988*, 79.

[23] V. Venkatesan, K. S. Viswanathan, J. Mol. Struct., 2010, *973*, 89.

[24] V. Kavitha, K. Sankaran, K. S. Viswanathan, J. Mol. Struct., 2006, *791*, 165.

[25] V. Kavitha, K. S. Viswanathan, J. Phys. Chem. A, 2007, *111*, 1879.

[26] V. Kavitha, K. S. Viswanathan, J. Mol. Struct., 2009, *920*, 355.

[27] V. Kavitha, K. Sundararajan, K. S. Viswanathan, J. Phys. Chem. A, 2005, *109*, 9259.

[28] R. U. Lemieux, R. K. Kullnig, H. J. Bernstein, W. G. Schneider, J Am. Chem. Soc., 1958, *80*, 6098.

[29] R. S. Bitzer, A. G. H. Barbosa, C. O. da Silva, M. A. C. Nascimento, Carbohydr. Res., 2005, *340*, 2171.

[30] E. L. Eliel, S. H. Wilen, L. N. Mander, Stereochemistry of Organic Compounds, Wiley-Interscience Publication, Student Edition, Reprint-2008.

[31] M. A. Murcko, H. Castejon, K. B. Wiberg, J. Phys. Chem., 1996, *100*, 16162.

[32] J. E. Rice, B. Liu, T. J. Lee, C. M. Rohlfing, Chem. Phys. Lett., 1989, *161*, 277.

[33] G. R. De Mare, Y. N. Panchenko, J. V. Auwera, J. Phys. Chem. A, 1997, *101*, 3998.

[34] Y. N. Panchenko, G. R. De Maré, J. Struct. Chem., 2008, *49*, 235.

[35] P. Boopalachandran, N. Craig, P. Groner, J. Laane, J. Phys. Chem. A, 2011, *115*, 8920.

[36] C. H. Choi, M. Kertesz, J. Phys. Chem. A, 1997, *101*, 3823.

---

[37] J. Harada, K. Ogawa, J. Am. Chem. Soc., 2004, *126*, 3539.

[38] J. Harada, K. Ogawa, Chem. Soc. Rev., 2009, *38*, 2244.

[39] L. A. Carreira, J. Phys. Chem., 1976, *80*, 1149.

[40] F. A. Carey, Organic Chemistry, Seventh Edition, The McGraw-Hill companies, 2008.

[41] T. Bjorholm, J. P. Jacobsen, J. Mol. Struct., 1983, *96*, 315.

[42] W. Zierkiewicz, D. Michalska, P. Hobza, Chem. Phys. Lett., 2004, *386*, 95.

[43] L. I. Kruse, C. W. DeBrosse, C. H. Kruse, J. Am. Chem., Soc., 1985, *107*, 5435.

[44] P. J. Breen, E. R. Bernstein, H. V. Secor, J. I. Seeman, J. Am. Chem. Soc., 1989, *111*, 1958.

[45] H. Tylli, H. Konschin, B. Fagerström, J. Mol. Struct., 1985, *128*, 297.

[46] F. Remacle, E. S. Kryachko, J. Mol. Struct., 2004, *708*, 165.

[47] N. W. Larsen, L. Schulz, J. Mol. Struct., 2009, *920*, 30.

[48] M. Fukuyo, K. Hirotsu, T. Higuchi, Acta Crystallogr. Sec. B, 1982, *38*, 640.

[49] D. G. Lister, J. K. Tyler, J. H. Høg, N. W. Larsen, J. Mol. Struct., 1974, *23*, 253.

[50] N. W. Larsen, E. L. Hansen, F. M. Nicolaisen, Chem. Phys. Lett., 1976, *43*, 584.

[51] M. E. Vaschetto, B. A. Retamal, A. P. Monkman, J. Mol. Struct. Theochem, 1999, *468*, 209.

[52] Y. Wang, S. Saebø, C. U. Pittman Jr., J. Mol. Struct. Theochem, 1993, *281*, 91.

[53] P. M. Wojciechowski, W. Zierkiewicz, D. Michalska, J. Chem. Phys., 2003, *118*, 10900.

[54] M. A. Palafox, J. L. Núñez, M. Gil, J. Mol. Struct. Theochem, 2002, *593*, 101.

[55] G. Fischer, Chem. Soc. Rev., 2000, *29*, 119.

[56] J.-C. Micheau, J. Zhao, J. Phys. Org. Chem., 2007, *20*, 810.

[57] C. Dugave, L. Demange, Chem. Rev., 2003, *103*, 2475.

[58] J. F. Uebman, A. Greenberg, Biophys. Chem., 1974, *1*, 222.

[59] T. B. Grindley, Tetrahedron Lett., 1982, *23*, 1757.

---

[60] T. Zeegers-Huyskens, E. S. Kryachko, J. Phys. Chem. A, 2011, *115*, 12586.

[61] C. E. Blom, H. H. Gunthard, Chem. Phys. Lett., 1981, *84*, 267.

[62] D. Lauvergnat, P. C. Hiberty, J. Am. Chem. Soc., 1997, *119*, 9478.

[63] M. J. Deetz, C. C. Forbes, M. Jonas, J. P. Malerich, B. D. Smith, O. Wiest, J. Org. Chem., 2002, *67*, 3949.

[64] M. Oki, H. Nakanishi, Bul. Chem. Soc. Jpn., 1970, *43*, 2558.

[65] H. Nakanishi, H. Fujita, O. Yamamoto, Bul. Chem. Soc. Jpn., 1978, *51*, 214.

[66] R. Fausto, J. J. C. Teixeira-Dias, J. Mol. Struct. Theochem, 1987, *150*, 381.

[67] P. I. Nagy, F. R. Tejada, J. G. Sarver, Jr. W. S. Messer, J. Phys. Chem. A, 2004, *108*, 10173.

[68] Y. Kawashima, T. Usami, R. D. Suenram, G. Y. Golubiatnikov, E. Hirota, J Mol. Struct., 2010, *263*, 11.

[69] D. Marcovici-Mizrahi, H. E. Gottlieb, V. Marks, A. Nudelman, J. Org. Chem., 1996, *61*, 8402.

[70] A. L. Moraczewski, L. A. Banaszynski, A. M. From, C. E. White, B. D. Smith, J. Org. Chem., 1998, *63*, 7258.

[71] S. C. Sim, S. J. Lee, Bull. Korean Chem. Soc., 1988, *9*, 236.

[72] M. Sakamoto, T. Ishida, T. Fujita, S. Watanabe, J. Org. Chem., 1992, *57*, 2419.

[73] J. C. Williams, A. E. McDermott, J. Phys. Chem., 1993, *97*, 12393.

[74] H. A. C. Mckay, Science and technology of tri-n-butyl phosphate, Vol. 1, Ed. W. W. Schulz, J. D. Navratil, CRC Press, Boca Raton, 1984, chapter 1.

[75] V. Vidya, K. Sankaran, K. S. Viswanathan, Chem. Phys. Lett., 1996, *258*, 113.

[76] L. George, K. S. Viswanathan, S. Singh, J. Phys. Chem. A, 1997, *101*, 2459.

[77] V. Vidya, K. Sankaran, K. Sundararajan, K. S. Viswanathan, J. Mol. Struct., 1999, *476*, 97.

---

[78] K. Sankaran, V. Venkatesan, K. Sundararajan, K. S. Viswanathan, J. Indian Inst. Sci., 2005, *85*, 403.

[79] V. Venkatesan, Ph.D. Thesis, University of Madras, 2002.

[80] V. Kavitha, Ph.D. Thesis, University of Madras, 2007.

[81] N. Ramanathan, K. Sundararajan, B. P. Kar, K. S. Viswanathan, J. Phys. Chem. A, 2011, *115*, 10059.

[82] M. Jang, L. Cai, G. O. Udeani, K. V. Slowing, C. F. Thomas, C. W. W. Beecher, H. H. S. Fong, N. R. Farnsworth, A. D. Kinghorn, R. G. Mehta, R. C. Moon, J. M. Pezzuto, Science, 1997, *275*, 218.

[83] D. Donnez, P. Jeandet, C. Clement, E. Courot, Trends in Biotechnology, 2009, *27*, 706.

[84] L. Lv, X. H. Gu, J. Tang, C.-T. Ho, Food Chemistry, 2007, *104*, 1678.

[85] Z. Kerem, G. Regev-Shoshani, M. A. Flaishman, L. Sivan, J. Nat. Prod., 2003, *66*, 1270.

[86] J. Chong, A. Poutaraud, P. Hugueney, Plant science, 2009, *177***,** 143.

[87] C. H. Jeong, J. T. Lim, M. S. Kim, J. H. Lee, J. W. Bae, G. Y. Yeom, Organic electronics, 2007, *8*, 683.

[88] W.-G. Han, T. Lovell, T. Liu, L. Noodleman, Chemphyschem, 2002, *3*, 167.

[89] Y. Ono, Pure & App. Chem., 1996, *68*, 367.

[90] S. Memoli, M. Selva, P. Tundo, Chemosphere, 2001, *43*, 115.

[91] P. Tundo, Pure & App. Chem., 2001, *73*, 1117.

[92] P. Tundo, M. Selva, Acc. Chem. Res., 2002, *35*, 706.

[93] M. A. Pacheco, C. L. Marshall, Energy and Fuels, 1997, 11, 2.

[94] U. Romano, F. Rivetti, N. Di Muzio, Dimethyl Carbonate. U.S. Patent 4,318,862, 1979; Chem. Abstr. 1981, 95, 80141w. Rivetti, F.; Romano, U.; Delledonne, D. Dimethylcarbonate and its production technology. In Green Chemistry: Designing

---

chemistry for the Environment; Anastas, P., Williamson,T. C., Eds.; ACS Symposium Series 626; American Chemical Society: Washington, DC, 1996; pp 70.

[95] D. Aurbacha, Y. Talyosefa, B. Markovskya, E. Markevicha, E. Zinigrada, L. Asrafa, J. S. Gnanaraja, H.-J. Kimb, Electrochim. Acta, 2004, *50*, 247.

[96] Lithium Batteries: Science and Technology, edited by G.-A. Nazri and G. Pistoia. Kluwer Academic Publisher, Dordrecht, New York, London (2004).

[97] A. Jänes, E. Lust, Electrochem. Commun., 2005, *7*, 510.

[98] F. Gasc, S. Thiebaud-Roux, Z. Mouloungui, J. of Supercritical Fluids, 2009, *50*, 46.

[99] J. Gong a, X. Ma, S. Wang, App. Catal. A: Gen., 2007, *316*, 1.

[100] D. Freitag, U. Grico, P. R. Muller, in: H.F. Mark (Ed.), Polycarbonate in Encyclopedia of Polymer Science and Engineering, vol. 11, Wiley, New York, 1987.

[101] Chem. Eng. News, 2005, *83* (37), 15.

[102] Bayer Co., GB Patent, 1960, *958*,798.

[103] A. A. G. Shaikh, S. Sivaram, Chem. Rev., 1996, *96*, 951.

[104] Z. Weiqing, Z. Xinqiang, W. Yanji, Z. Jiyan, App. Catal. A: Gen., 2004, *260*, 19.

CHAPTER 2

EXPERIMENTAL AND COMPUTATIONAL PROCEDURES

2.1 Experiments

This section discusses the experimental procedures employed in this work and the computational methods adopted to corroborate the experimental results.

2.1.1 Matrix isolation infrared spectroscopy

Matrix isolation is a technique where the molecules of interest are trapped in solid inert gas matrixes at high dilution. Since solid inert gas matrixes are employed to trap the molecules, the experiments demand the use of cryogenic temperatures, typically 10-12 K. In a typical experiment, the molecule of interest is mixed with a rare gas, such as Ar or in some cases, N_2, at matrix to sample ratios of approximately 1000:1. This gas mixture is then effused through a nozzle and is allowed to deposit on a KBr substrate maintained at a low temperature (~10 K). The large matrix/analyte ratio ensures a high probability of isolation of the interested molecules in the inert gas solids. Under these conditions intermolecular interactions between the analyte molecules are considerably reduced. This technique was initially developed by G. C. Pimentel in the mid 1950s for the study of free radicals.[1] Reactive species isolated in such inert gas matrixes have long lifetimes for want of reaction partners and can be studied leisurely by spectroscopic techniques such as infrared, UV-visible, microwave, electron spin resonance etc. It turned out that the technique developed for the study of reactive species, also offered other advantages such as small line widths of spectral features, trapping of weakly bound complexes, such as hydrogen bonded and van der Waals complexes and not infrequently trapping of local minima in the case of adducts. All these features have made this technique a powerful tool for the study of conformations, weak complexes and reactions.

The principle of the matrix isolation and its hyphenation with various spectroscopic techniques, such as infrared, UV-visible and fluorescence spectroscopy have been described in several books.[2-4] Of the various spectroscopic methods, infrared spectroscopy is widely used in the study of matrix isolated species.

In matrix isolation experiments, the analyte molecules are isolated from each other, since they are present in a cage of inert matrix atoms. Consequently, the intermolecular interactions between the analyte molecules are largely minimized. While in principle, the analyte molecule can interact with the matrix atoms, these interactions are weak. Furthermore, since the molecules are immobilized in inert matrix at cryogenic temperatures, broadenings due to collision and Doppler effect are absent. The low temperature in the matrix also ensures that only low ro-vibronic and electronic levels of the analyte are populated which results in significant reduction of spectral congestion.

The success of the matrix isolation experiments depends largely on the choice of the matrix material. The matrix material should be chemically inert to prevent reactions between the analyte and matrix material. In addition to chemical inertness, a good matrix material must also be free from impurity, rigid at low temperature and transparent in the spectral region of interest. Also the substance should have enough vapor pressure at room temperature to deposit conveniently onto the cold substrate. The structure and characteristics of different matrix materials are discussed in several books.[5-7]

Inert gases and nitrogen meet the above criteria to use as matrix gases. In many cases gases like alkanes are also used for this purpose. In our experiments Ar, Kr, Xe and N_2 were used as matrix gases and these are also transparent in mid IR region. However a number of effects that can cause the spectrum of matrix isolated species to be complicated, do operate and these are briefly discussed in the following section.

2.1.2 Matrix effects

A proper interpretation of infrared spectra of matrix isolated species demands a better understanding of the various effects that the matrix can have on the vibrational features of the analyte. The most important among the various matrix effects is the perturbation of the vibrational potentials of analyte due to interactions. Under conditions of perfect isolation at any particular site, the guest molecule is subjected only to analyte-matrix interactions. These interactions can result in either in a shift in the frequency relative to isolated gas phase molecules, or splitting of the vibrational bands. The frequency shift, $\Delta\nu$, in a matrix with respect to the gas phase value arises from electrostatic ($\Delta\nu_{elec}$), inductive ($\Delta\nu_{ind}$), dispersive ($\Delta\nu_{dis}$) and repulsive interactions ($\Delta\nu_{rep}$) and is given by expression,

$$\Delta\nu = (\nu_{matrix} - \nu_{gas}) = \Delta\nu_{elec} + \Delta\nu_{ind} + \Delta\nu_{dis} + \Delta\nu_{rep} \qquad \ldots.\ (2.1)$$

where, ν_{matrix} and ν_{gas} are the frequencies of the vibrational mode in the matrix and gas phase respectively.[5] Thus matrix shift provides information regarding the interaction between the analyte and the matrix.

In inert gas matrixes, the long-range London dispersion forces and short range repulsive forces are the two dominant interactions. Pimentel and Charles have given a theoretical treatment of a matrix induced frequency shift.[8]

The frequency shift, $\Delta\nu$, in solutions arising from the perturbation due to solvent interactions is given by the Buckingham expression

$$\Delta\nu = (\nu_{solvent} - \nu_{gas}) = [B_e/hc\omega_e][U'' - (3aU'/\omega_e)] \qquad \ldots\ldots\ldots\ldots\ (2.2)$$

where $B_e = h/8\pi^2\mu c r_e^2$, is the rotational constant,

a = Anharmonicity constant,

U = Energy due to solute-solvent interaction,

$U' = \{\partial U/\partial r_{BC}\}$ and $U'' = \{\partial^2 U/\partial^2 r_{BC}\}$, r_{BC} refers to the fig. 2.1 $\ldots\ldots\ldots$ (2.3)

$c\omega_e$ = Harmonic oscillator frequency for normal vibrational, Q.[9]

This expression can be used to explain the frequency shift occurring in the matrix. Fig. 2.1 shows the interaction potential curves between the trapped molecule and matrix atoms when trapped in matrix cage. When R_{CM} is greater than R_1, i.e. when one of the atoms, C, of the trapped molecule is more distant from the matrix atom, M than R_e (equilibrium distance, Fig. 2.1), U′ and U″ are negative and since ‘a’ is also negative, the term Δν is negative (Eq. 2.2). Here the molecule experiences a loose cage effect inducing a negative frequency shift (red shift). When R_{CM} is less than R_e, U′ and U″ are positive and hence Δν is positive. The molecule experiences a tight cage effect, which induces a positive frequency shift (i.e. blue shift). It was reported that when poly atomic molecules are trapped in matrices, the high frequency stretching vibrations display negative shift as in a loose cage and the low frequency stretching, bending or rocking vibrations, give positive shifts as in a tight cage.[8]

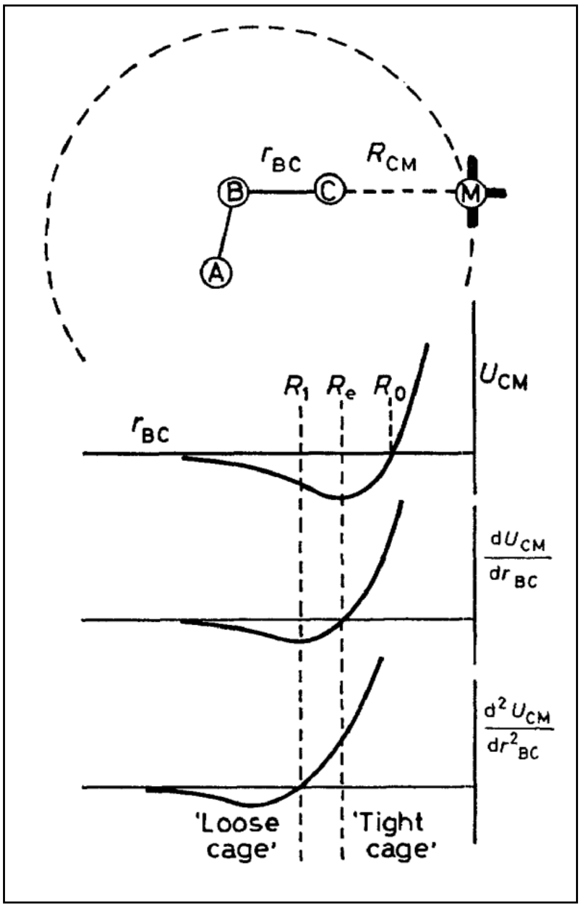

Fig. 2.1 – Dependence of U, U′ and U″ upon matrix cage size [Ref-8, with permission from IUPAC].

Due to these interactions, particularly in matrices with unsymmetrical trapping sites, such as nitrogen, the high frequency stretching modes will shift to lower frequency and low frequency bending modes will shift to higher frequency. Since nitrogen and noble gases are less reactive, these shifts are less. In other matrix materials such as carbon monoxide, carbon dioxide, sulfur hexafluoride and hydrocarbons, which are reactive, the shifts will be larger. While strongly interacting matrices like ethylene give substantial shifts; highly polar solutes such lithium fluoride gives a large shift even in noble gas matrixes.[10]

In addition to the shift in the vibrational features, other factors that are likely to contribute to multiple band structures for a particular vibration bonds in matrix are

1) Rotation or libration of the solute molecules in its trapping site,
2) Multiple trapping site effects,
3) Aggregation of the solute,
4) Lifting of degeneracy of the vibrational levels,
5) Inactive modes may also be induced.[11,12]

2.1.2.1 Rotation of analyte in matrix cage

Analyte species trapped in inert matrix cages at low temperatures are generally rotationally cold, as the matrix cage prevents rotational motion. However, rotations are less hindered in noble gas matrixes possessing a sufficiently large cavity. As a result, a number of small molecules, such as HX (X=F, Cl), H_2O, NH_3 and OH have been shown to rotate in noble gas matrixes. In general, rotation seems not to occur in matrixes with unsymmetrical matrix sites, although there are exceptions (e.g. H_2 in N_2 matrix). Rotational features can be identified by reversible intensity changes when the matrix temperature is cycled. This reversible intensity variation occurs due to the change in population of rotational energy levels as the temperature is varied. Confirmation that these small molecules rotate in noble gas matrixes has been provided by observation of the pure rotational transitions in the far infrared or Raman spectrum[13-16].

2.1.2.2 Multiple trapping site effects

It may also happen that the analytes may be trapped in different types of sites in the matrix. Different matrix sites perturb the vibrational potential differently and hence splitting in vibrational features occurs. Knowledge of these effects requires the knowledge of the geometrical structure of the cage of matrix atoms surrounding the trapped species. A brief discussion about the different sites is discussed below.

The common matrix materials, the noble gases, generally crystallize in cubic closed packed (face centre cubic f.c.c.) structure. A small amount of nitrogen or oxygen in solid argon can render hexagonal close packed (h.c.p.) structure more stable. In f.c.c. structure, each atom is surrounded by 12 equidistant nearest neighbors and its symmetry is found to be an octahedron, O_h. The h.c.p. structure is less stable compared to f.c.c. and it has also 12 equidistant nearest neighbor of symmetry D_{3h}.

The inert gases crystallize in f.c.c. structure at cryogenic temperatures when no impurity is present. The closed packed lattices can have three possible guest sites; substitutional, in which the guest molecule replaces one or more host species and two types of interstitial sites viz. tetrahedral and octahedral. The geometry of these holes is of importance to matrix studies in relation to the perturbation, which the trapped species will experience. A tetrahedral hole is in itself not tetrahedral in shape but is so named because a small guest atom trapped in such a hole would have four neighboring matrix spheres arranged at the corners of tetrahedron. For such grouping it can readily be shown by simple geometry that the radius of the small sphere that occupies the site is given by 0.225r, where r is the radius of the matrix sphere. Thus in order to occupy the tetrahedral site without disturbing the closed packed lattice, the radius of a trapped spherical species should be no larger than

0.225r. Additionally, there are tetrahedral holes from three spheres of top layer and one from the bottom; thus there is also one tetrahedral hole above each sphere of the bottom layer. In the crystal as a whole there is one tetrahedral hole above and one below every close-packed sphere.

Similarly an octahedral site is surrounded by six close-packed spheres situated on the corners of an octahedron. By simple geometry, it can be shown that the radius of an octahedral site is 0.414r. In a column of spheres, octahedral sites and spheres alternate, for f.c.c. lattices. Thus there is one octahedral site for every sphere in lattice, i.e. there are half as many octahedral sites in a closest-packed lattice as there are tetrahedral sites.

Vacancies in the crystal lattice may alter the existing site symmetry and crystal imperfections may provide further sites viz. dislocation sites. Generally solids grown by rapid condensation from vapor are unlikely to form perfect crystal, possibility of formation of grain boundaries and dislocation sites are quite high. Dislocation sites may well be larger but they are non-uniform. The most likely site is the substitutional site since it alone is large enough to accommodate a normal size diatomic guest. The octahedral interstitial sites are much smaller than the substitutional sites but could conceivably accommodate smaller diatomics where as tetrahedral interstitial sites must be too small to be seriously considered. Small molecules like H_2, HCl, can occupy interstitial sites, which have a diameter less than 2 Å in argon or nitrogen matrix. Larger guest molecules must occupy sites formed by removing two or more lattice molecules.

For solute molecules trapped in different sites, for example, in a substitutional site formed by removal of n or n+1 matrix atoms, each vibrational mode will exhibit more than one band since the interaction of the solute with the matrix environment will be different for different trapping sites. Multiple bands can, however arise from other causes; concentration studies and annealing studies are necessary to identify the effect due to multiple trapping sites. The relative intensity of multiplets due to different trapping sites is usually unaffected by solute concentration but can change on annealing at higher temperatures or by varying the rate of deposition.[17-20]

In addition to this, in a matrix, coupling may occur between certain internal vibrational modes of a molecule with low energy lattice vibrations of the matrix leading to splitting and broadening of spectral features. Sometimes a trapped impurity will disturb the host lattice symmetry and activate inactive modes leading to phonon bands.

2.1.2.3 Aggregation

True isolation is achieved only at a very high matrix/analyte (M/A) ratio, usually greater than 1000; at low M/A ratios molecular aggregates may be formed and trapped in addition to monomers. Molecular association will be greater for solutes capable of forming hydrogen bonds.[21,22] In contrast to liquids and solutions in which the absorption bands due to hydrogen-bonded multimer species are usually very broad, considerable narrowing occurs on condensation in matrixes. Multiple features due to self-association can be readily identified from their concentration dependence and from warm-up experiments in which monomers diffuse to form dimer and higher multimers.

It is important to consider here, how isolated the matrix-isoalted species is, since aggregation and chemical reaction lead to observable changes in the spectrum during annealing and diffusion. Similar interactions are bound to occur if two species are actually trapped in contact. It will effectively be the case if their respective cages overlap, so that one species forms part of the cage in which the other is trapped; for very reactive species non-nearest neighbor interactions may have to be taken into account as well.

The probability of these interactions will depend on the matrix to analyte ratio, on particular type of site adopted, the effective size of the cage and the intensity of the interaction between solutes. The probability of isolation is discussed in the following paragraphs.

For molecule such as carbon monoxide, which occupies a single substitutional site, the probability of interaction is simply the chance of finding another molecule occupying one of the 12 sites that form the cage. The chance for the absence of the second CO molecule is given by the formula $P = (1- r)^{12}$, where r is the reciprocal of the matrix ratio. For very small values of r the expression becomes, $P = 1-12r$. From this it is clear that a matrix ratio of 1000 is needed to ensure 99% isolation.

The cage occupied by a large trapped species will be large and will have a large probability of interaction. For example, a species with diameter three times that of a matrix atom will occupy a site produced by the loss of a matrix atom and its original 12 neighbors; such a species will have a cage containing 122 atoms, so the probability of isolation is given by $P = (1 - r)^{122}$. Here a matrix ratio of 10000 is needed to ensure 99% isolation.

A similar situation arises if the analyte is strongly interacting. For example atomic lithium, which can dimerise if trapped within next-nearest neighbor distance, interacts significantly if found even within about sixth-nearest neighbor distance. In such cases the probability of dimer or multimer formation will be greater and a matrix ratio of 10000 is needed to ensure 99% isolation.

In the above discussion the effect of diffusion during and after deposition are ignored. It is found experimentally, for example, that carbon monoxide forms dimers or higher aggregates to the extent of several percent at a matrix ratio of 1000 in argon, rather than the 1% expected on the basis of our analysis. As mentioned earlier, lithium atoms will dimerise completely even with matrix ratios of 10000 unless matrixes that rigidify at a very fast rate are used.[23,24]

It is also important that the matrix gas used must be free from impurities, even if these impurities do not interfere. The presence of, for instance, 1% of nitrogen in argon would result in some 12% of all sites having a cage containing at least one nitrogen molecule even if only single substitutional sites are considered.

Care must be taken to exclude traces of impurity, which might hetero-associate. Even if the interaction between solute molecules is weak, a group of two or more molecules will give rise to a frequency, which is slightly different from monomer. Solutes, which exhibit strong intermolecular interactions such as hydrogen bonding, may give very large shifts on aggregation. Aggregation can be eliminated by reducing the concentration of solute in the matrix. Matrix spectra should always be checked for concentration dependence to ensure that the bands are assigned to the correct species, i.e. the monomer, dimer or higher aggregate. Care has to be taken to check for possible impurity effects at low concentrations[25]. Impurities such as H_2O or N_2 become increasingly troublesome when deposition of a low concentration matrix over a long time period is attempted.

2.1.2.4 Lifting of degeneracy of vibrational levels

The symmetry of the site occupied by the molecule may also contribute to matrix effects. The perturbation of the molecule trapped in a particular site will be different for different vibrations and hence will have different frequency shifts. In case of degenerate vibrational modes, asymmetric sites can lead to a lifting of the degeneracy , resulting in the splitting of the vibrational features, such as that occurs in CO_2[26-28] and C_2H_2.[29,30]

Though both argon and nitrogen are commonly used as matrix materials, nitrogen often interacts strongly with solutes in low temperature matrixes.[10,31,32] Similarly, the presence of nitrogen as an impurity in argon matrixes leads to the appearance of additional bands for a wide range of solutes. This could be because the nitrogen lattice causes modes, which are degenerate in an argon matrix to be split in the presence of nitrogen.

2.1.3 Matrix isolation infrared setup

Main component of this set up involves: (a) Cryostat; (b) Vacuum system; (c) Sample introduction system and (d) Fourier transform infrared spectrometer. Fig. 2.2 shows a photograph of the matrix isolation setup used in this work. Experiments were performed using two different closed cycle helium compressor cooled cryostats; RD210 Model (Leybold AG) capable of going down to 12 K and RDK-408D2 Model (Sumitomo Heavy Industries Ltd.) which can attain a low temperature of 4 K. The cold finger of the cryostat was housed in a vacuum system. We used an Edwards Diffstak MK2 series diffusion pump, with a pumping speed of 280 l/s for air, to attain the necessary vacuum. The diffusion pump was backed by a rotary pump with a capacity of 300 l/min. The base vacuum obtained with the above vacuum system was better than 10^{-6} mbar, measured using a cold cathode gauge (Pfeiffer vacuum, Model TPG 261).

Vibrational spectra of matrix isolated species were recorded using a Bomem MB 100 FTIR spectrometer. The spectrometer was operated at a resolution of 1 cm^{-1} and typically 8 scans were coadded to obtain good signal-to-noise ratio. All spectra were recorded in the region of 4000 to 400 cm^{-1}. Once the sample and matrix were deposited at 12 K, a spectrum of the matrix isolated sample was recorded. After recording the spectrum, the temperature of the matrix was raised to temperatures, such as 30 to 35 K. The matrix was held at this temperature for about 15 minutes using the heater-temperature controller unit. The matrix was then cooled back to 12 K and the spectrum again recorded. This process called ‘annealing’ is generally done to remove the unstable sites in the matrix and also to encourage diffusion of precursor molecules to form adducts.

A high pressure Xe lamp (Hanovia L-5179-000, 1000W) and Nd-YAG laser (Quantel, Brilliant b) were used to photoirradiate the matrix isolated samples, in some of our experiments. A photo of the Xe lamp along with the power supply is shown in fig. 2.3.

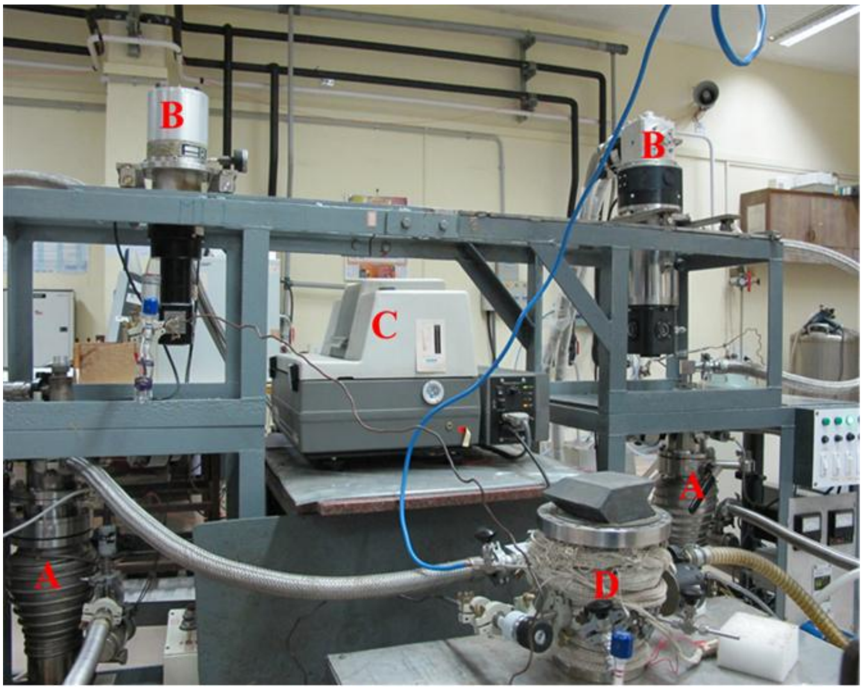

Fig. 2.2 – Photograph showing matrix isolation set up.
(A) Vacuum system, (B) Cryostat,
(C) FTIR Spectrometer, (D) Mixing Chamber.

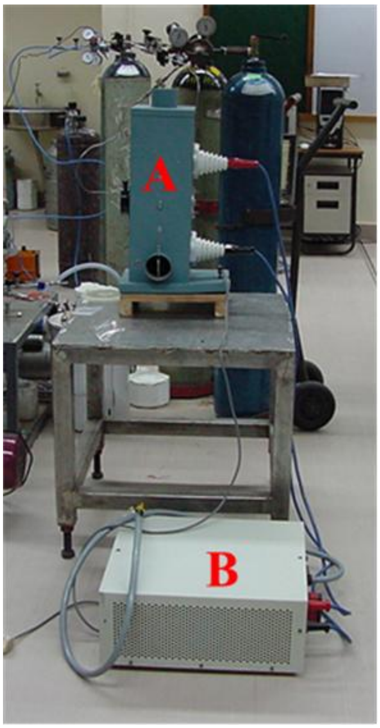

Fig. 2.3 – Photograph showing (A) Xe lamp and (B) Power supply.

These experiments were performed to study the photo isomerization behaviour of molecules. Photoirradiation was performed both during and after deposition of matrix gas.

2.1.3.1 Sample introduction system

A mixture of analyte and matrix was prepared in a stainless steel mixing chamber of one liter capacity, which was introduced to the vacuum system through a single effusive nozzle. In some cases, such as stilbene, which had low vapour pressure, deposition was carried out using a double jet nozzle system; through one nozzle, the matrix gas was allowed to effuse out, while the second nozzle was used to introduce the sample into the vacuum system. In the study of adducts, such as in studies on DMC-H_2O complex, sample deposition was carried out through a double jet nozzle to introduce DMC and H_2O separately into the vacuum system.

To identify the vibrational features for higher energy conformers sample deposition was performed through a hot nozzle source, where the nozzle was maintained at various elevated temperatures. Sample introduction to the vacuum chamber was also performed through a supersonic source. These experiments were performed to alter the population of conformers in gas phase before deposition. Details of the hot nozzle and supersonic jet source are discussed below and the pictures of the two are given in Figs. 2.4 and 2.5 respectively.

Hot nozzle source

Fig. 2.4 shows the photograph of a home-made hot nozzle source assembly. The main components of this assembly are the nozzle and sample holder. The nozzle was made using a 5 mm outer-diameter glass nozzle with a 1 mm orifice, which served as the effusive nozzle. A Nichrome wire of diameter 0.5 mm was coiled on the glass nozzle to heat it and on to which a Pt-resistance thermometer was mounted to measure the temperature of the nozzle. The length of the heated zone was 30 mm.

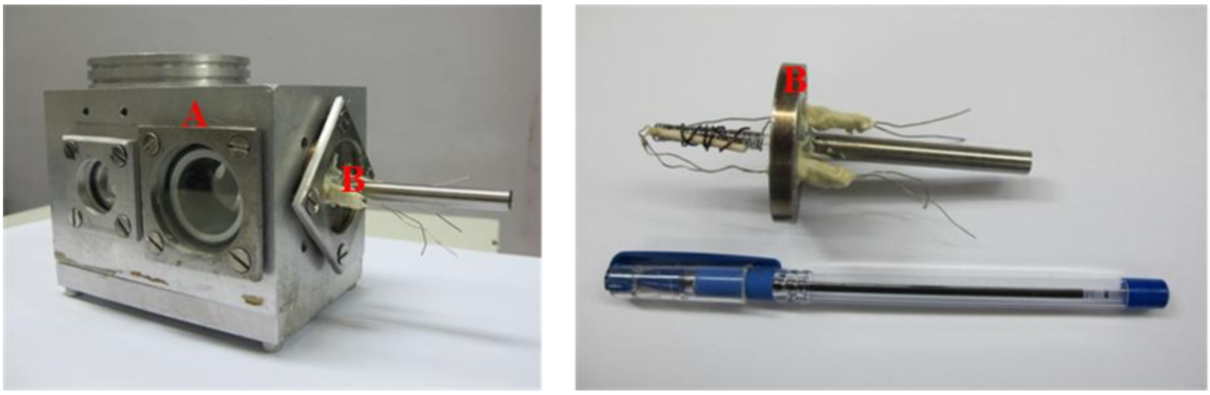

Fig. 2.4 – Photograph showing hot nozzle set up.

(A) Modified rotatable vacuum jacket, (B) Hot nozzle source assembly.

Fig. 2.5 – Photograph showing (A) Supersonic jet source and (B) Power supply.

The hot nozzle set assembly was mounted on a stainless steel flange and was coupled by means of Veeco type ultra-torr fitting. The typical distance of the hot nozzle tip from the cold KBr substrate was ~35 mm.

Before starting a deposition, the hot nozzle was heated to the required temperatures in a range of 298-473 K. The hot matrix/sample gas coming from the hot nozzle was allowed to deposit on the ~12 K KBr substrate at a rate of ~3 mmol/hour.

Supersonic source

Fig. 2.5 shows the photograph of the pulsed supersonic nozzle of 0.5 mm diameter (Parker Hanifin, USA) used in our experiment. The valve is capable of operating at pressure up to 85 atmospheres with speeds of 120 Hz and can be operated over a temperature range 277-398 K. The valve is driven by a controller, which enables the operation with pulse widths of microseconds. In our experiments we have employed a typical stagnation pressure of 1.3 atm. The valve was operated with a pulse width varying from 1 to 50 ms and repetition rate 0.1–0.4 Hz. At this deposition rate, the temperature of the cryotip did not rise.

2.1.4 Experimental procedure

The samples trans-stilbene (Sigma Aldrich, 96%), cis-stilbene (Sigma Aldrich, 96%), dimethyl carbonate (DMC) (Sigma Aldrich, anhydrous, ≥99%), diethyl carbonate (DEC) (Spectrochem, 99% purity), diphenyl carbonate (DPC) (Aldrich, 99% purity) were used for our study. Samples were loaded to glass bulbs connected to the system through high vacuum glass stopcocks, which were thoroughly degassed before use.

DMC and DEC are moisture sensitive; hence these were loaded in an argon atmosphere. The samples were subjected to several freeze-pump-thaw cycles before use. These samples are liquids of high vapor pressure; hence the samples were equilibrated at the required temperature, for about an hour, using an ethanol-liquid nitrogen slush bath, to obtain the desired vapor pressure over the sample. The temperature of the slush bath was measured using a platinum resistance thermometer. The desired matrix/sample ratios were thus obtained by controlling the vapour pressure over the sample.

A stainless steel mixing chamber of one liter capacity was used to prepare matrix/sample gas mixtures. The mixture was then allowed to deposit on the cold KBr substrate through one of the different nozzle systems described above. Speed of deposition was controlled by the help of a fine needle valve.

Trans-stilbene (solid) and cis-stilbene (liquid) have very low pressure and hence a double jet nozzle was used for deposition. The bulb containing sample was connected to one of the inlet of the double jet. The sample bulb and the deposition line were heated using a heater coil and the temperature was measured using a platinum resistance thermometer mounted on it. Matrix gas was allowed to effuse out through the second nozzle of the double jet. Concentration of sample in matrix was varied by changing the temperature of sample, thus altering its vapour pressure. For diphenyl carbonate (solid) a single jet nozzle system was used where the matrix gas was allowed to pass through the sample for deposition. Sample and the deposition line were heated to get the desired mixture of sample and matrix.

2.2 Computations

Ab initio computations were carried out using the Gaussian 94W[33] package operated in Pentium-4 and core-2-duo machines. Molecular properties such as structures, energies and frequencies obtained from the result were used to corroborate the experimental results. Detail treatments of *ab initio* calculations are given in various books.[34-40] AIM package[41] was used to examine the nature of the interactions between the precursors of the complexes, and NBO 3.1 was used to understand the delocalization interactions present in molecules under study. A brief discussion regarding the computations is given in the following sections.

2.2.1 Geometry optimization and frequency calculation

At the outset, a structure of the molecule corresponding to a minimum on the potential surface is obtained following geometry optimization. Geometry optimization begins at the guess molecular structure specified as input, and steps along the potential energy surface. The energy and gradient are first computed at the point on the potential surface corresponding to the initial geometry. This information is used to determine how far and in which direction the next step is taken to improve the geometry. At the minimum (or more generally a stationary point), forces will be zero. In the case of Gaussian program, the optimization was achieved when the forces, the root mean square of forces, the calculated displacement and the root mean square of the displacement for the subsequent step are below preset threshold values.

Optimization calculations were performed at various levels of theories using Hartree-Fock (HF), Moller-Plesset second order perturbation (MP2) and Density functional methods (BLYP and B3LYP) using a variety of basis functions. The experimental results were found to be in good agreement with our computations at the B3LYP/6-31++G** level of calculations, which has been used in this work. The B3LYP method uses the Becke three-parameter non-local exchange functional[42,43] with non-local correlation of Lee et al.[44] As mentioned above guess structures were used to start the optimization process, usually without imposing any symmetry constraints. In a few cases, though, such as in the case of non-planar trans-stilbene, constraints were imposed on the optimization. For complexes, optimized submolecule structures were used as starting geometries to compute the complex structures. Again no constraints were imposed, which therefore resulted in slight changes in the geometries of the precursors, during complex formation.

Vibrational frequency calculations were performed at the same level of theory used for geometry optimization. Analytical gradients used in the computations, though in a few cases a numerical method was also used. Vibrational frequency computations were done, first, to ensure that the computed structures did correspond to minima on the potential surface and also to assign the vibrational features observed in the experiments. The computed vibrational frequencies were scaled to bring them in agreement with experimental results. To arrive at the scaling factor the experimentally observed strongest feature was correlated with the computed strongest feature. The scaling factor that would bring the computed frequency in good agreement with that of experiment was used to scale all other vibrational frequencies. Zero point vibrational energies (ZPE) were also obtained from frequency calculations which were used to calculate ZPE corrected energies. The ZPE corrected relative energies were used to calculate the relative population at a particular temperature. The computed scaled frequencies were used to simulate vibrational spectra by the help of the SYNSPEC program.[45] The synthetic spectra were generated assuming a Lorentzian line profile with full width at half maximum (FWHM) of 1 cm^{-1}, which is the typical resolution of our instrument.

The transition state structures connecting different conformers were computed to obtain the barrier for interconversion. The QST2 and QST3[33,36] methods were used to calculate transition states. In QST2 method the two relevant minima were given as inputs, whereas a guess transition structure was included in input along with the two relevant minima for QST3 method. These procedures follow Synchronous Transit-Guided Quasi-Newton (STQN) methods[46,40] which use a linear synchronous transit or quadratic synchronous transit approach to get closer to the quadratic region of the transition state and then uses a quasi-Newton or eigenvector-following algorithm to complete the optimization.[41] The transition state structures obtained by these methods were subjected to frequency calculation to ensure that these were first-order saddle points. The ZPE corrected energy of the transition state was used to calculate the barrier for interconversion.

2.2.2 Stabilization energy calculation of complexes

The stabilization energy of the complex was computed using the method described below. The stabilization energy (ΔE) of a complex is given by

$$\Delta E = E_{AB} - (E_A + E_B) \qquad \ldots\ldots\ldots (2.4)$$

where, E_A, E_B and E_{AB} represent the energies for the monomers A, B and complex AB respectively. If the value of ΔE is negative, the complex is more stable relative to the precursors. In further discussions, only the magnitude of ΔE will be given and imply the negative sign by the use of the term stabilization. The stabilization energy of the complex corrected for zero point energy (ZPE) was also calculated.

When the energy of complex (E_{AB}) is computed, the basis functions used are those of both the monomer subunits. Whereas, for computing the energy of the individual precursors (i.e. E_A and E_B), the basis functions pertaining to only the corresponding precursor are used. As the number of basis functions used is larger in the computation of the complex, the energy obtained will be lower, as basically each monomer can use the basis functions of other. Stabilization energies thus derived from the calculated energies E_A, E_B and E_{AB} will be overestimated and the error is referred to as the basis set superposition error (BSSE).[47-51] Although the origin of BSSE is well understood, there is no easy way of correction for it. The best way to eliminate the BSSE is to increase the basis set until the stabilization energy is stable to the desired accuracy, which of course implies large computation times for even small systems. The commonly used method to correct for BSSE is by counterpoise correction proposed by Boys and Bernadi.[47] In this scheme, one calculates all quantities (energies of monomer E_A, E_B and the complex E_{AB}) in the same basis set spanned by the functions of the complex AB and the difference in energies is obtained as follows.

$$\Delta E = E_{AB}(AB) - \{E_A(AB) + E_B(AB)\} \qquad \ldots\ldots\ldots (2.5)$$

Where, E_A (AB) = Energy of the monomer A using the basis set AB

E_B (AB) = Energy of the monomer B using the basis set AB

E_{AB} (AB) = Energy of the complex AB using the basis set AB

In our studies, the stabilization energies of the complex corrected for the BSSE have also been included. Corrections of energies for ZPE and BSSE simultaneously were not included as these values are known to overcorrect the stabilization values.[52,53]

2.2.3 Atoms-in-molecules (AIM) methodology

Bader first proposed the atoms in molecules theory, which uses an analysis of the electron density topology.[54,41] The wave function corresponding to the optimized geometry of a molecule or complex are generated using the Gaussian package.[33] From the electron density plots, one obtains bond critical points, charge density ρ, Laplacian of charge density $\nabla^2\rho$, which is also the trace of the Hessian of ρ. The charge density, ρ(r), is a physical quantity which has a definite value at each point in space. It is a scalar field defined over three dimensional space. Each topological feature of ρ(r), where it is a maximum, a minimum, or a saddle point, has associated with it in a space called a critical point, where the first derivative of ρ(r) vanish. The sign of its second derivative or curvature at this point determines whether a function is maximum or minimum. The topological properties of such a scalar field are conveniently summarized in terms of the number and nature of its critical points. The rank of critical point, denoted by ω, is equal to the number of non-zero eigenvalues or non-zero curvature of ρ at the critical point. The signature denoted by σ, is the algebraic sum of the signs of the eigenvalues. The critical point (CP) is labeled by giving the duo values (ω, σ). For example, (3, -1) critical point means, three non-zero curvatures and one positive and two negative eigenvalues. A (3, -1) CP corresponds to a bond between two atoms, a (3, +1) CP to a ring, a (3, +3) CP to a cage and a (3, -3) CP corresponds to a maximum. The numbers of critical points of all types, which can coexist in a system with a finite number of nuclei, are governed by the Poincare-Hopf relationship.

$$n - b + r - c = 1 \qquad \ldots\ldots. (2.6)$$

where, n is the number of nuclei, b is the number of bond critical points, r is the number of ring critical points and c is the number of cage critical points.

The sum of three Hessians (λ_1, λ_2, λ_3) at a bond critical point, the quantity $\nabla^2\rho$, provides a useful characterization of the manner in which the electronic charge density is distributed in the inter nuclear region. If the value of charge density ρ ($<10^{-1}$ au) and the curvature of charge density are large, Laplacian of charge density may be positive or negative usually of the same order of magnitude as ρ then the interaction is of shared type, typical of covalent interaction. For the closed shell interactions, such as hydrogen bond complexes, van der Waals complexes and ionic systems, the charge density ρ ($\sim10^{-2}$ to 10^{-3} au) at the bond critical point is quite small and the laplacian of the charge density is positive.

2.2.4 Natural bond orbital (NBO) analysis

NBO analysis was performed to understand the role of different delocalization interactions towards the conformational preferences. NBO analysis is based on a method for transforming a given wave function into localized form, corresponding to the one-centre (lone pair) and two-centre (bond pair) elements of the Lewis structure picture. The NBOs are localized few-centred orbitals that describe the Lewis-like molecular bonding pattern of electron in optimally compact form. More precisely, NBOs are an orthonormal set of localized maximum occupancy orbitals whose leading N/2 members give the most accurate possible Lewis-like description of the total N-electron density. The NBOs are obtained as local block eigenfunctions of the one-electron density matrix, and are hence natural in the sense of Löwdin, having optimal convergence properties for describing the electron density. The set of highly occupancy NBOs, each taken double occupied is said to present the natural Lewis structure of the molecule. Delocalization effects appear as weak departures from this idealized localized picture.

NBO is symmetrically orthogonalized directed hybrid orbital derived through unitary transformation of natural atomic orbitals (NAO) centered on a particular atom. The various natural localized sets can be considered to be result from a sequence of transformations of the input atomic orbital basis set,

Input basis → NAOs → NHOs → NBOs → NLMOs

Each natural localized orbital forms a complete orthonormal set of one-electron functions for expanding the delocalized molecular orbitals (MOs) or forming matrix representations of one electron operators.

The optimal condensation of occupancy in the natural localized orbitals leads to partitioning into high- and low- occupancy types (reduction in dimensionality of orbitals having significant occupancy), as reflect in the orbital labeling. The small set of most highly occupied NAOs, having a close correspondence with the effective minimal basis set of semi-empirical quantum chemistry, is referred to as the natural minimal basis (NMB) set. The NMB functions are distinguished from the weakly occupied Rydberg functions that complete the span of the NAO space, but typically make little contribution to molecular properties. Similarly in the NBO space, the highly occupied NBOs of the natural Lewis structure can be distinguished from the non-Lewis antibond and Rydberg orbitals that complete the span of the NBO space. Each pair of the valence hybrids h_A, h_B in the natural hybrid orbital (NHO) basis give rise to a bond (σ_{AB}) and anti bond (σ^*_{AB}) in the NBO basis,

$$\sigma_{AB} = c_A h_A + c_B h_B$$

$$\sigma^*_{AB} = c_A h_A - c_B h_B$$

the former a Lewis (L) and the later a non-Lewis (NL) orbital. The antibonds typically play the primary role in delocalization from the idealized lewis structure.

The estimates of energy effects are based on second-order perturbation theory, or on the effect of deleting certain orbitals or matrix elements and recalculating the total energy to determine the associated vibrational energy lowering. This analysis is performed by

1) Deleting specified elements or block of elements from the NBO Fock matrix,

2) Diagonalizing this new Fock matrix to obtain a new density matrix, and
3) Passing this density matrix to the SCF routines for a single pass through the SCF energy evaluator.

The difference between this deletion energy and the original SCF energy provides useful measure of the energy contribution of the deleted terms. This way one can decompose the total energy into components associated with covalent and non-covalent contributions

$$E = E_{\sigma} - E_{\sigma^*}$$

where, σ and σ* are referred to filled and unfilled orbitals respectively. The filled orbital can be core orbital, lone pair, σ or π bond and the unfilled orbital can be σ or π antibond, Rydberg orbital etc. A schematic NBO perturbation diagram for 2-e stabilizing interaction (hyperconjugative interactions) is shown in Fig. 2.6. This figure depicts the interaction of a filled orbital σ of the formal Lewis structure with one of the unfilled antibonding orbitals σ* to give the second order energy lowering, $\Delta E^{(2)}_{\sigma\rightarrow\sigma^*}$. In SCF–MO theory this lowering in energy is given by the formula,

$$\Delta E^{(2)}_{\sigma\rightarrow\sigma^*} = q_{\sigma} < \sigma \mid F \mid \sigma^* >^2 / [\varepsilon_{\sigma^*} - \varepsilon_{\sigma}] \qquad \ldots\ldots.(2.7)$$

Where, q_{σ} is the donor orbital occupancy, F is the Fock operator and ε_{σ}**,** ε_{σ^*} are NBO orbital energies. The NBO perturbative framework permits one to apply qualitative concepts of valence theory to describe the non-covalent energy lowering. Since the non-covalent delocalization effect are associated with σ→σ* interactions between filled (donor) and unfilled (acceptor) orbitals, it is natural to describe them as being of “donor-acceptor”, “charge transfer”, or generalized “Lewis base-Lewis acid” type.[55]

NBO analysis was performed to understand the conformational preferences in molecules. The use of NBO has been shown to provide a detailed understanding of conformational preferences in several such systems.[56-59] NBO analysis was performed at

B3LYP/6-31++G** level of theory using NBO 3.1 version incorporated through Gaussian 94W. Deletion analysis was done using NBODEL option.

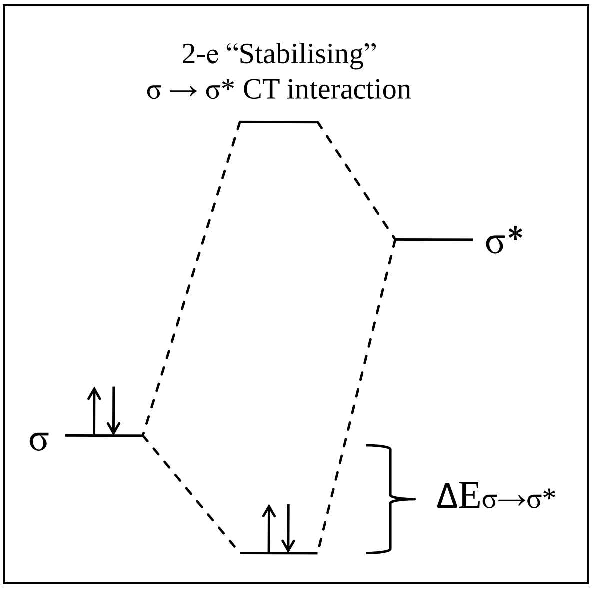

Fig. 2.6 – Schematic NBO perturbation diagram for

'2-e stabilizing' delocalization interaction.

2.2.5 Calculation of dipole moment

To compute the dipole moment of bulk molecules with different conformers in gas phase at a given temperature, we have used the formula

$$\mu^2 = \Sigma\, \mu_i^2 N_i, \qquad \ldots\ldots(2.8)$$

where, μ is the net dipole moment of the molecule in gas phase, μ_i is dipole moment of the conformer 'i' obtained from *ab initio* calculation and N_i is the computed mole fraction of conformer 'i' at that temperature.[60,61]

References

---

[1] E. Whittle, D. A. Dows, G. C. Pimentel, J. Chem. Phys., 1954, *22*, 1943.

[2] L. Andrews, M. Moskovits, Chemistry and Physics of Matrix-Isolated Species, Elsevier Science Publishers, B. V. Amsterdam, 1989.

[3] M. Moskovits, G. A. Ozin, Cryochemistry, John Wiley & Sons, New York, 1976.

[4] G. B. Sergeev, V. A. Batyuk, Cryochemistry, MIR Publishers, Moscow, 1981.

[5] H. E. Hallam, Vibrational Spectroscopy of Trapped Species, John Wiley and Sons, London, 1973.

[6] S. Cradock, A. J. Hinchliffe, Matrix Isolation: A tchnique for the study of reactive inorganic species, Cambridge University Press, Cambridge, 1975.

[7] A. J. Barnes, W. J. Orville-Thomas, A. Muller, R. Gaufres, Matrix Isolation Spectroscopy, D. Reidel Publishing Company, Holland, 1981.

[8] G. C. Pimentel, S. W. Charles, Pure and Appl. Chem., 1963, *7*, 111.

[9] S. D. Buckingham, Proc. Roy. Soc. (London) A, 1958, *248*, 169.

[10] A. J. Barnes, J. Mol. Struct., 1980, *60*, 343.

[11] J. A. Warren, G. R. Smith, W. A. Guillory, J. Chem. Phys., 1980, *72*, 4901.

[12] B. R. Carr, B. M. Chadwick, C. S. Edwards, D. A. Long, G. C. Wharton, J. Mol. Struct., 1980, *62*, 291.

[13] M. T. Bowera, G. I. Kerley, W. H. Flygare, J. Chem. Phys., 1966, *45*, 3399.

[14] D. W. Robinson, J Chem. Phys., 963, *39*, 3430.

[15] M. T. Bowers, W. H. Flygare, J. Chem. Phys., 1966, *44*, 1389.

[16] F. T. Prochaska, L. Andrews, J. Chem. Phys., 1977, *67*, 1139.

[17] B. Mile, Angew. Chem. Int. Ed., 1968, *7*, 507.

[18] G. L. Pollack, Rev. Mod. Phys., 1964, *36*, 748.

---

[19] C. J. Purnell, A. J. Barnes, S. Suzuki, D. F. Ball, W. J. Orville-Thomas, Chem. Phys., 1976, *12*, 77.

[20] B. I. Swanson, L. H. Jones, J. Chem. Phys., 1980, *73*, 986.

[21] D. Maillard, A. Schriver, J. P. Perchard, C. Girardet, J. chem. Phys., 1979, *71*, 505.

[22] D. Maillard, A. Schriver, J. P. Perchard, C. Girardet, J. chem. Phys., 1979, *71*, 517.

[23] L. Andrews, G. C. Pimentel, J. Chem. Phys., 1967, *47*, 2905.

[24] T. Welker, T. P. Martin, J. Chem. Phys., 1979, *70*, 5683.

[25] H. Dubost, L. Abouaf-Marguin, Chem. Phys. Lett., 1972, *17*, 269.

[26] L. H. Jones, B. I. Swanson, J. Chem. Phys., 1981, *74*, 3216.

[27] M. Dubs, H. H. Gunthard, Chem. Phys. Lett., 1979, *64*, 105.

[28] M. Poliakoff, J. J. turner, "Infrared laser photochemistry in matrixes" in "chemical and biological application of lasers", Ed. C. B. Moore, Academic Press, New York, 1980.

[29] K. Sundararajan, K. S. Viswanathan, J. Mol. Struct., 2006, *798*, 109.

[30] K. V. J. Jose, S. R. Gadre, K. Sundararajan, K. S. Viswanathan, J. Chem. Phys., 2007, *127*, 104501.

[31] A. J. Barnes, L. Le Gall, C. Madec, J. Lauransan, J. Mol. Struct., 1977, *38*, 109.

[32] B. Walsh, A. J. Barnes, S. Suzuki, W. J. Orville-Thomas, J. Mol. Spectrosc., 1978, *72*, 44.

[33] M. J. Frisch, G. W. Trucks, H. B. Schlegel, P. M. W. Gill, B. G. Johnson, M. A. Robb, J. R. Cheeseman, T. Keith, G. A. Peterson, J. A. Montgomery, K. Raghavachari, M. A. Al-Laham, V. G. Zakrzewski, J. V. Ortiz, J. B. Foresman, J. Cioslowski, B. B. Stefanov, A. Nanayakkara, M. Challacombe, C. Y. Peng, P. Y. Ayala, W. Chen, M. W. Wong, J. L. Andres, E. S. Replogle, R. Gomperts, R. L. Martin, D. J. Fox, J. S. Binkley, D. J. Defrees, J. Baker, J. P. Stewart, M. Head- Gordon, C. Gonzalez, J. A. Pople, GAUSSIAN 94, Revision D.1,Gaussian Inc., Pittsburgh, PA, 1995.

---

[34] E. Lewars, Computational Chemistry: Introduction to theory and applications of Molecular and Quantum Mechanics, Kluwer Academic Publishers, Boston, 2003.

[35] W. J. Hehre, L. Radom, P. V. R.; Schleyer J. Pople, A ab initio molecular orbital theory, John Wiley and Sons, New York, 1985.

[36] J. B. Foresman, A. Frisch, Exploring chemistry with electronic structure methods, Gaussian Inc., Pittsburgh, 1993.

[37] T. A. Clark, Handbook of Computational Chemistry: A practical guide to Chemical Structure and Energy Calculations, John Wiley & sons, New York, 1985.

[38] D. B. Cook, Ab initio valence calculations in chemistry, Butterwort, London, 1974.

[39] J. P. Lowe, Quantum Chemistry, Academic Press, New York, 1978.

[40] F. Jensen, Introduction to Computational Chemistry, Wiley Publication, Second edition, 2008.

[41] F. Biegle-Koning, R. F. W. Bader, W. -H. Tang, J. Comput. Chem. 96 (2000); 6796. AIM 2000, V.

[42] A. D. Becke, Phys. Rev. A, 1989, *38*, 3098.

[43] A. D. Becke, J. Chem. Phys., 1983, *98*, 5648.

[44] C. Lee, N. Yang, R. G. Parr, Phys. Rev. B, 1988, *37*, 785.

[45] The spectra were simulated using SYNSPEC made available by K. Irikura, National Institutes of Standards and Technology, Gaithesburg, MD, 20899, 1995.

[46] User's reference, Gaussian 94 Revision D.1 and higher, Gaussian Inc., 1996.

[47] S. F. Boys, F. Bernadi, Mol. Phys., 1970, *19*, 553.

[48] F. Jensen, Chem. Phys. Lett., 1996, *261*, 633.

[49] I. Mayer, P. R. Surján, Chem. Phys. Lett., 1992, *191*, 497.

[50] D. W. Schwenke, D. G. Truhlar, J. Chem. Phys., 1985, *82*, 2418.

[51] L. Turi, J. J. Dannenberg, J. Phys. Chem., 1993, *97*, 2488.

---

[52] L. Turi, J. J. Dannenberg, J. Phys. Chem., 1995, *99*, 639.

[53] N-B. Wong, Y-S. Cheung, D. Y. Wu, Y. Ren, X. Wang, A. M. Tian, W-K. Li, J. Mol. Struct., 2000, *507,* 153.

[54] R. F. W. Bader, Atoms in Molecules. A Quantum Theory, Clarendon Press, Oxford, 1994.

[55] F. Weinhold, C. Landis, Valency and Bonding: A natural bond orbital donor-acceptor perspective, Cambridge University press, 2005.

[56] V. Kavitha, Ph.D. Thesis, Madras University, 2007.

[57] S. Moon, Y. Kwon, J. Lee, J. Choo, J. Phys. Chem. A, 2001, *105*, 3221.

[58] H. Roohi, A. Ebrahimi, J. Mol. Struct. Theochem, 2005, *726*, 141.

[59] E. M. Sproviero, G. Burton, J. Phys. Chem. A, 2003, *107*, 5544.

[60] E. L. Eliel, S. H. Wilen, L. N. Mander, Stereochemistry of Organic Compounds, A Wiley-Interscience Publication, 2008.

[61] D. Labrenz, W. Schröer, J. Mol. Struct., 1991, *249,* 327.

CHAPTER 3

STUDIES OF NON-PLANAR TRANS-STILBENE

3.1 Introduction

Stilbene has been a molecule of interest, as it presents intriguing questions with respect to molecular structure and dynamics of isomerization. The structure of the ground state of stilbene and the dynamics involved in the cis-trans photoisomerization has been the subject of a number of experimental[1-6] and theoretical[7-9] studies, over many decades. The cis-isomer is known to be non-planar, with the two phenyl groups adopting an out-of-plane configuration, due to steric interactions. There is, however, considerable debate on whether the structure of the trans-isomer is planar or non-planar. Gas phase electron diffraction[10] and photoelectron spectroscopic studies[11] suggest the structure to be non-planar and that the phenyl groups are rotated by ~30° around C-phenyl bond. However, solid state X-ray diffraction studies[12,13] and gas phase studies in molecular beams[14] indicate the structure to be planar. In solution and melts, Raman spectroscopy indicates that the trans isomer appears to lose its planarity; a conclusion arrived at due to the observation of a strong Raman feature at 960 cm^{-1} [15] and a weaker feature at 760 cm^{-1}.[16] These features were observed to be weak in crystals, where the structure was shown to be planar. However, apart from these two vibrational features observed in the Raman spectrum, no other vibrational feature has been observed for this non-planar structure.

Theoretical calculations ranging from HF, MP2, MP3 and coupled cluster models have been used in a number of studies on this molecule, but have not led to an unambiguous resolution of this problem. Arenas et al.[17] have calculated the geometric parameters and the frequencies for trans- and cis-stilbene using a 3-21G basis and showed that the cis-stilbene is non planar with phenyl to ethylene torsional angles (i.e. the 10-1-12-14 and 12-14-16-25 dihedral angles in Fig. 3.1a) of 44.7°, whereas trans-stilbene was shown to have a value of 27.2° for these torsional angles (Fig. 3.1b). This geometry for trans-stilbene agreed fairly well with that observed in the electron diffraction study.[10] When a 6-31G* basis set was used, Choi and Kertesz[18] found that HF and MP2 methods showed trans-stilbene to be non-planar, while calculations at the BLYP, B3LYP and BVWN levels, indicated a planar structure for this isomer. Han et al.[19] concluded from their theoretical analysis that the phenyl groups of trans-stilbene can rotate freely up to about 30°. Kwasniewski et al.[20] have applied focal point analysis for a comparison of the planar and non-planar trans-stilbene. They estimated an energy difference of 0.46 kcal/mol between the planar and non-planar form, with the latter being lower in energy, at the CCSD(T)/6-31G** level. This difference almost vanished (0.02 kcal/mol) at the CCSD(T)/cc-pVDZ level, while the planar form was indicated to be more stable at the Møller-Plesset levels of theory in conjunction with Dunning's correlation consistent polarized valence basis sets. They eventually concluded that in the non-relativistic limit and within the frozen core approximation, trans-stilbene in vacuum has, as its minimum energy structure, a strictly planar form. Chowdary et al.[21] have performed computations on this problem at the MP2/6-31G**, and have shown that the zero-point-vibrational corrections are comparable to the barriers between the planar and non-planar form. Consequently, they argue, that the controversy that exists in experimental studies of the planar/non-planar enigma is as much caused by this "vibrational quasi-planarity". The above discussion highlights the ambiguity in our understanding of the structure of the ground state of trans-stilbene.

The issue of cis-trans photoisomerizm in stilbene has also been an area of intense study, as this system which leads to cis-trans isomerization through the rotation around the central ethylenic C=C bond, is a model system for the study of photoisomerization process. Orlandi and Siebrand[7] have reported that the second higher excited singlet state, S_2, has a potential which has a minimum corresponding to a perpendicular orientation of the two

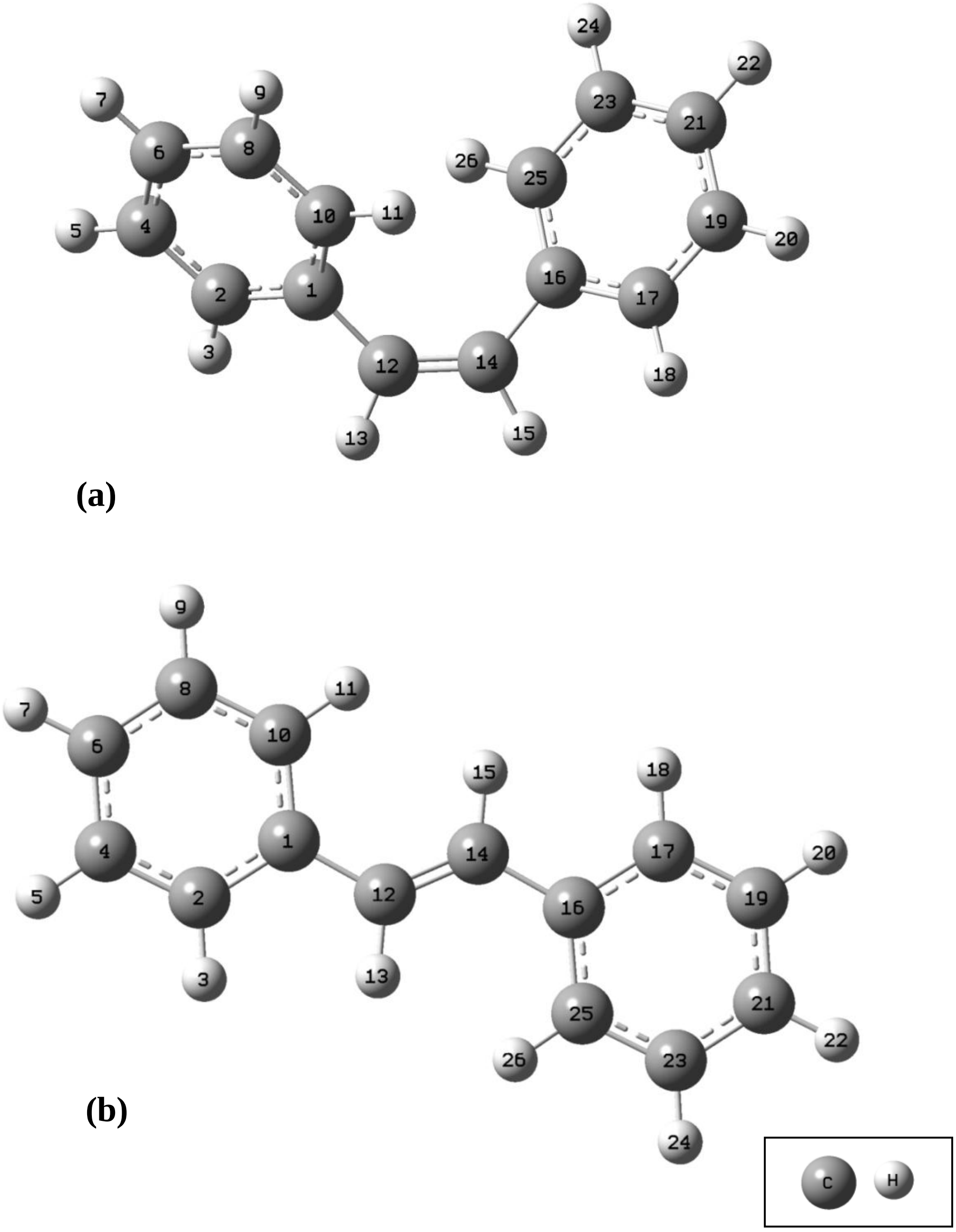

Fig. 3.1 – Computed structures at the B3LYP/6-31++G** level of (a) cis-stilbene and (b) trans-stilbene, showing the atom numbering.

phenyl groups (i.e. 1-12-14-16 dihedral angle in Fig. 3.1 is 90°); for the same orientation of the phenyl groups, the S_1 state shows a weak maximum, while the ground electronic state, S_0, displays a strong maximum. Waldeck[1] and later Tavan and Schulten[8] argued that the S_1 state actually involves a $\pi \rightarrow \pi^*$ state mixed with one or more higher energy doubly excited forms. From the minimum of the excited state, referred to as the "phantom state", the molecule returns to the ground electronic state at its maximum, from where it branches to the trans or the cis form. The mechanisms have been supported by Wan-Ge Han et al.[19] who described that the double excited state is a neutral form and not a zwitterionic species, by using spin unrestricted density functional theory (VWN Becke-Perdew potential method), including broken symmetry and spin-projection methods for their simulation. Levine and Martinez[9] have emphasized the role of conical intersection and charge transfer for the cis-trans photo isomerization about carbon double bonds. In a recent publication, Kovalenko[22] have experimentally shown the intermediacy of the phantom state in the cis-trans isomerization reaction, and have deduced, based on spectral shifts in different solvents, that this state is probably zwitterionic in nature.

The photoisomerization of cis-stilbene is therefore seen to proceed through the intermediacy of the phantom state and eventually the maximum in the ground state potential. From this maximum, a branching is observed to occur to the cis and trans forms. If as reported in some studies, a non-planar trans structure occurs as a weak minimum in the potential, close to the planar trans isomer, the branching from the maximum in the ground state potential can be expected to populate, at least to some extent, this weak minimum and which can likely be trapped in the matrix. Our earlier studies have shown that matrix isolation spectroscopy can trap weak local minima[23,24] and it was therefore thought interesting to examine if a non-planar trans structure can be observed in solid inert gas matrixes. Cis-stilbene was trapped in different matrixes, N_2, Ar, Kr and photoirradiated using a broad band source and, in some experiments, using the fourth harmonic of a Nd:YAG laser. The photoirradiation was conducted, both *during* and *after* deposition of the cis-stilbene in the matrix. The products of photoirradiation were studied using infrared spectroscopy. As a result of this study, we have been able, for the first time, to record the infrared spectrum of the non-planar form of trans-stilbene.

3.2 Experimental details

The experimental procedure followed has already been described in Chapter 2. Three different matrix gases, Ar, N_2 and Kr were used as matrix gases in this study. Trans-stilbene (Sigma Aldrich, 96%), cis-stilbene (Sigma Aldrich, 96%) were used without any further purification. Deposition was done using a double jet nozzle system; through one nozzle, the matrix gas was allowed to effuse out, while through the second nozzle, stilbene was introduced into the vacuum system. Due to the low vapor pressure of trans-stilbene, the sample and the deposition line were heated to temperatures ranging from 303 K to 343 K, while for cis-stilbene, which has a relatively higher vapor pressure, room temperature (~298 K) deposition was employed.

Photoirradiation of the sample was done using a 1000W Xe arc lamp (Hanovia L-5179-000). A few experiments were also done using the fourth harmonic (266 nm) of the Nd-YAG laser (Quantel, Brilliant b) for photoirradiation. Experiments were conducted where photoirradiation was performed both during and after deposition of the sample and matrix gas on the cold substrate.

Infrared spectra of matrix isolated species were recorded by using a BOMEM MB-100 FTIR spectrometer with a spectral resolution 1 cm^{-1}. After recording the IR spectra of the matrix isolated species, the matrix was annealed at various temperatures, and the IR spectra again recorded.

3.3 Computational details

Detailed computations at high levels of theory on the structure of stilbenes exist in the literature; we have, therefore, restricted our work to computing the vibrational features for the various isomers of stilbene, so as to enable us to assign the features in our experiments. *Ab initio* molecular orbital calculations were performed at the B3LYP/6-31++G** level. To compute the vibrational frequencies for cis-stilbene and planar trans-stilbene, the geometries of these isomers were first optimized, without imposing any symmetry constraints, followed by a vibrational frequency calculation, which yielded all-positive frequencies. For the non-planar trans-stilbene, based on the work of Choi and Kertesz,[18] we froze the phenyl-ethylene dihedral angle at 30^o, and then performed the geometry optimization, without imposing any further constraints. Frequency calculations were performed for this optimized geometry of the non-planar trans-stilbene, which yielded all frequencies to be positive.

3.4 Results

3.4.1 Experimental

Fig. 3.2 shows the infrared spectra of trans-stilbene (trace 'a') and cis-stilbene (trace 'b'), in a N_2 matrix. Trace 'c' is the spectra recorded after photoirradiation of cis-stilbene (before annealing), while trace 'd' corresponds to the spectra recorded after annealing the photoirradiated matrix at 32 K. The spectra span the region 1000-900 cm^{-1} (grid A), 800-650 cm^{-1} (grid B) and 550-510 cm^{-1} (grid C) which correspond to CH bending, wagging and ring deformation in stilbenes.

Cis-stilbene, which has an absorption maximum at 275 nm,[25] is known to undergo photoisomerization to yield trans-stilbene. When the matrix containing cis-stilbene was photoirradiated, not unexpectedly, we observed infrared features of trans-stilbene, in addition to those of cis-stilbene, as shown in Fig. 3.2. In addition to the peaks due to cis- and trans-stilbene, the matrix containing photoirradiated cis-stilbene, showed features at 525, 538, 739,

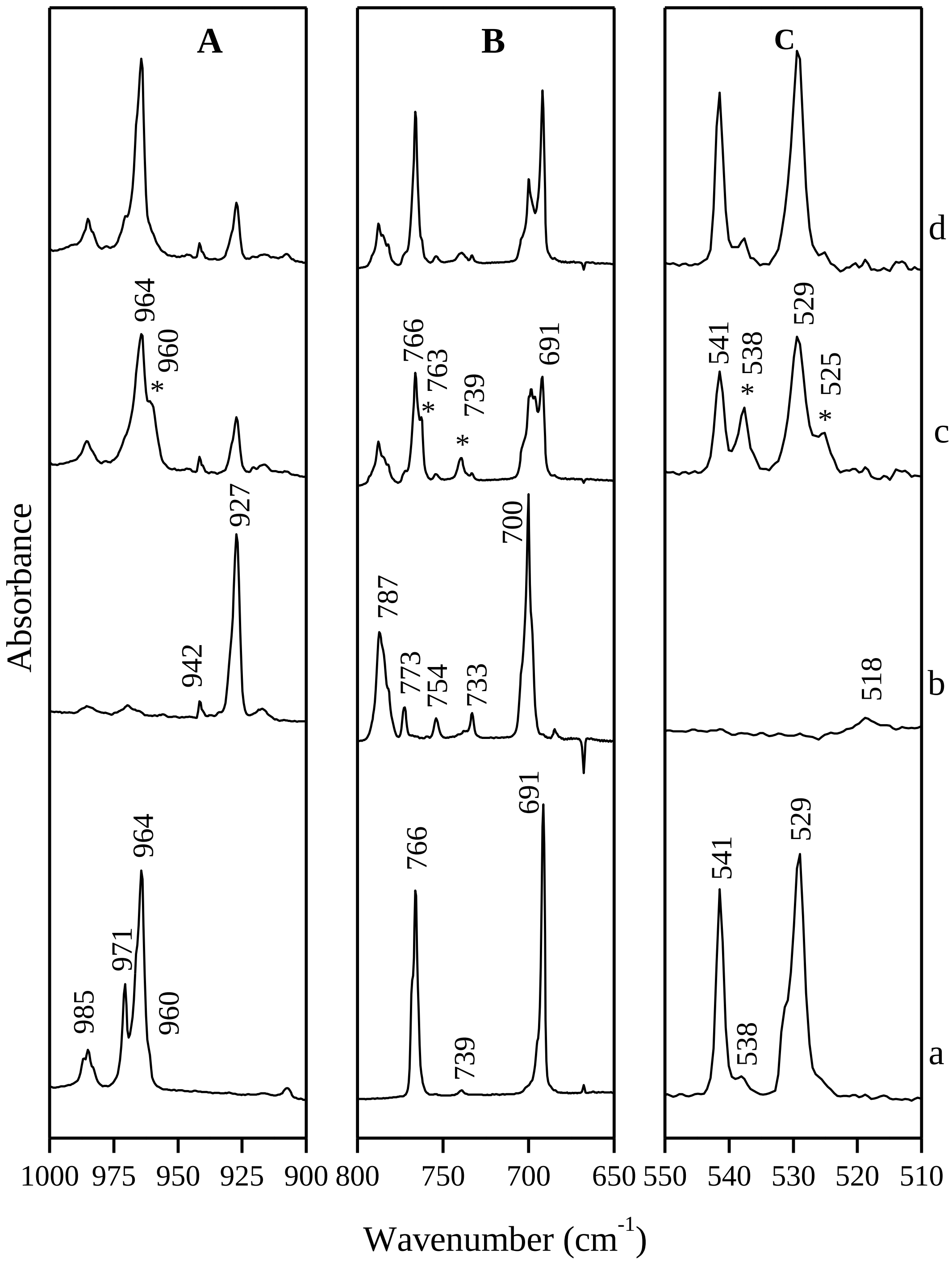

Fig. 3.2 – IR spectra of stilbenes in N_2 matrix at 12 K. (a) trans-stilbene (sample maintained at 343 K); (b) cis-stilbene (sample maintained at 298 K); (c) cis-stilbene after photoirradiation for 90 minutes; (d) Matrix corresponding to trace ‘c’ annealed at 32 K for 10 minutes.

763, 960 cm^{-1} which could not be assigned to either of these two isomers, and which we shall refer to as ‘extra features’. On annealing the matrix, these extra features decreased significantly in intensity. A corresponding increase in the intensity of the trans-stilbene features was observed. The increase in the intensity of the trans-stilbene features were confirmed by calculating the ratio of the peak intensity of the trans-stilbene with respect to a feature of cis-stilbene, used as a reference. For example, the ratio of the features at 964 cm^{-1} (of trans-stilbene) and 927 cm^{-1} (of cis-stilbene) increased from a value of 2.4 in the pre-annealed matrix to 3.5 in the annealed matrix, thereby implying that during the process of annealing, the trans isomer was being produced.

It must be noted that the features at 538, 739, and 960 cm^{-1} which are produced during photoirradiation of cis-stilbene are also observed in the spectrum of trans-stilbene (unirradiated) but with a significantly smaller intensity.

The extra features observed in the photoirradiation experiments, may be due, either, to matrix site effects or to new products produced in the photoirradiation process. Experiments were performed in various matrixes to confirm the presence or not, of matrix site effects. Figs. 3.3 and 3.4 represent the experiments performed using Ar and Kr as matrix gases respectively. Traces ‘a’, ‘b’ and ‘c’ in both the figures show the spectra of trans-stilbene, cis-stilbene and photoirradiated cis-stilbene in the corresponding matrixes. The spectra recorded after annealing the matrixes corresponds to spectra in trace ‘c’ are shown in trace ‘d’. The annealing temperature was 35 and 50 K for Ar and Kr matrixes respectively. The spectral regions showed in different grids follows the same trend as in Fig. 3.2. From the Figs. 3.2, 3.3 and 3.4 it can be clearly observed that the extra features occurred in all the matrixes, N_2, Ar and Kr, which makes it highly unlikely that these features are due to matrix site effects. We therefore rule out matrix site effects as a possible cause for the extra features mentioned above.

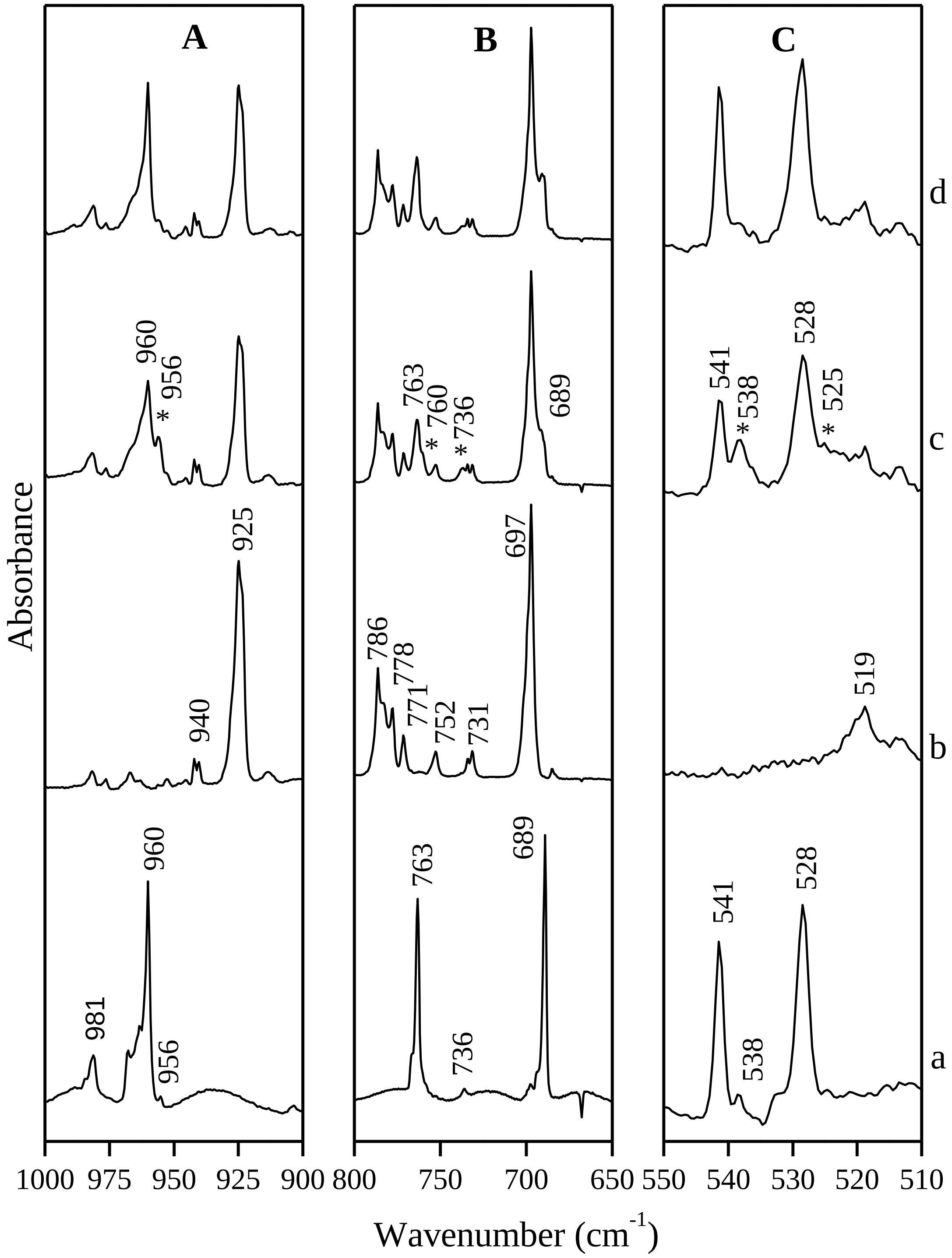

Fig. 3.3 – IR spectra of stilbenes in Ar matrix at 12. K (a) trans-stilbene (sample maintained at 343 K); (b) cis-stilbene (sample maintained at 298 K); (c) cis-stilbene after photoirradiation for 90 minutes; (d) Matrix corresponding to trace ‘c’ annealed at 35 K for 10 minutes.

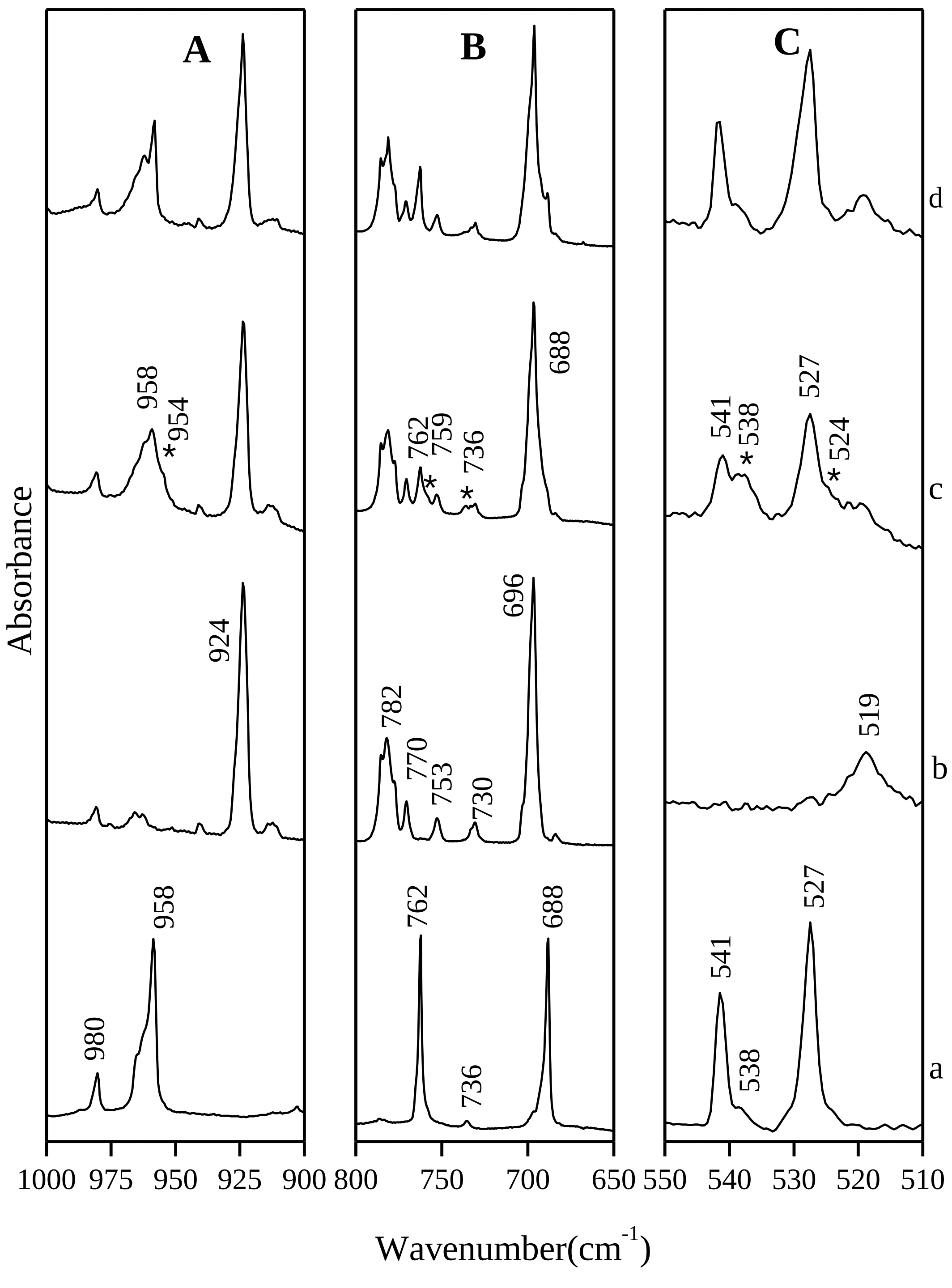

Fig. 3.4 – IR spectra of stilbenes in Kr matrix at 12 K. (a) trans-stilbene (sample maintained at 343 K); (b) cis-stilbene (sample maintained at 298 K); (c) cis-stilbene after photoirradiation for 90 minutes; (d) Matrix corresponding to trace ‘c’ annealed at 50 K for 10 minutes.

We considered the possibility that the extra features may be due to a photodecomposition product of cis-stilbene. A possible product, though minor (~5%),[22] produced during photoirradiation of cis-stilbene is 4a,4b-dihydrophenanthrene.[26,27] The spectrum of this compound reported by Rodier et al.[28] does not match with the extra features that we observed. Furthermore, the computed vibrational frequencies for this compound by Zhou et al.[29] at the HF/4-21G level and our own at the B3LYP/6-31++G** level, do not agree with the frequencies of the extra features referred above. Dihydrophenanthrene as a candidate responsible for the extra features is therefore ruled out.

We also found that quinoline could be present in commercial cis-stilbene (purity 96%), as an impurity. To rule out possibility that quinoline or photoproducts of quinoline were responsible for the extra features, we recorded the spectrum of quinoline and photoirradiated quinoline, under conditions identical to that employed in the photoirradiation of cis-stilbene. These experiments too, did not yield any of the extra features referred to above. We therefore conclusively ruled out the possibility that any impurity in cis-stilbene was responsible for the extra features referred to above.

The extra features are therefore likely to be due to reaction products produced in the photoirradiation process, and as we will show below, is the result of a photoisomerization reaction.

Since cis-stilbene is known to have a strong $S_0 \rightarrow S_1$ absorption near the 260 nm wavelength,[4] experiments were also performed using the 266 nm output of the Nd:YAG laser. Identical results were obtained with the laser as with the broad band source.

3.4.2 Computational

As mentioned earlier, all calculations were done at the B3LYP/6-31++G** level of theory. For the purpose of assigning the experimental features, the computed vibrational frequencies at this level were used, after appropriate scaling. To compute the scaling factor, the strongest experimental feature of trans-stilbene at 691 cm^{-1}, was correlated to the strongest computed feature for this isomer in this region, which was at 703 cm^{-1}. The factor, 0.9829, that brought this computed feature in agreement with experiment was then used as the scaling factor to scale the computed features for all the isomers of stilbene. The scaled features in combination with experimental results are shown in Table 3.1. Our B3LYP level calculations were generally in agreement with those reported by Choi and Kertesz,[18] where the level of theory used was BLYP/6-31++G**, with a C_2 symmetry imposed on the geometric framework. It may be noted that the frequencies reported by Choi and Kertesz[18] are unscaled.

The optimized structures of the cis- and planar trans-stilbene are shown in Fig. 3.1 and some selected geometrical parameters are given in Table 3.2.

3.5 Discussion

At the outset, the features in traces ‘a’ and ‘b’ of Fig. 3.2 agree well with the features reported for trans and cis-stilbene respectively.[17,18] These features also agree well with our computed and scaled infrared features for these isomers at the B3LYP/6-31++G**, shown in Table 3.1. In trace ‘c’, which is the spectrum recorded after photoirradiation of cis-stilbene, extra features were observed in addition to the features of the cis- and trans-stilbene.

Choi and Kertesz[18] computed the vibrational frequencies, at the BLYP/6-31++G** level theory, for the non-planar trans-stilbene, by freezing the dihedral angles that correspond to the orientation of the phenyl groups with respect to the ethylenic plane (i.e. 10-1-12-14 dihedral) at 30^{o} and imposing a C_2 symmetry on the geometry. They showed that the non-planar trans-stilbene features are slightly red shifted with respect to the planar trans-stilbene features, as does our own computations. Table 3.1 shows the computed frequencies of Choi and Kertesz, together with our own computed frequencies and also the frequencies observed in our matrix isolation experiments. It can be seen that the extra features observed in the

Table 3.1 – Experimental and computed vibrational wavenumbers for the various isomers of stilbene.

Isomer	Experimental Wavenumbers (cm^{-1})			Computed Wavenumbers (cm^{-1})		
	N_2	Ar	Kr	This work[a]	Choi and Kertesz[b]	
Cis	-[c]	-	-	695(15)[d]	683	Puckering
	700	697	697	697(74)	686	Ring C-H opb
	733	731	730	731(9)	721	XCY[e] def, CH wag, antisym def
	754	752	753	752(3)	740	Ring deformation, ring torsion
	773	771	770	770(6)	757	Puckering, ring CH opb, C-X opb
	787	786	782	785(65)	773	C-H wag, ring CH opb, puckering
	927	925	924	926(20)	904	Ring C-H opb
Planar trans	529	528	527	540(20)	535	Anti sym def
	541	541	541	546(22)	546	C-X opb
	691	689	688	691(82)	681	Puckering
	766	763	762	771(65)	761	Puckering, ring C-H opb
	964	960	959	975(18)	953	C-X torsion, CH wag
	985	981	980	991(20)	970	Ring CH opb, CX torsion
Non-planar trans	525	525	524	527(14)	518	C-X opb
	538	538	538	535(16)	530	Anti sym def
	-	-	-	690(13)	678	Puckering
	696	693	693	694(54)	682	Puckering
	739	736	735	739(20)	724	Puckering, ring CH opb
	763	760	759	758(55)	744	Puckering, ring CH opb
	960	956	954	969(30)	951	CX torsion, CH wag

[a] Computed using B3LYP/6-31++G** level of theory and scaled by 0.9829.

[b] Ref. 18, computed using BLYP/6-31++G** level of theory; frequencies are unscaled.

[c] Not discerned in experiments as it occurs between two strong features of cis and trans-stilbene.

[d] Infrared intensities (km/mol) are shown in parenthesis.

[e] X=Phenyl ring, Y=Ethylene double bond.

Table 3.2 – Selected structural parameters, bond distances (Å), bond angles (°) and torsional angles[a] (°) of the various isomers of stilbene.

Parameters	Cis-stilbene	Planar Trans-stilbene	Non-planar trans-stilbene
C1-C12	1.477	1.467	1.470
C12-C14	1.351	1.350	1.349
C14-C16	1.477	1.467	1.470
C1-C12-C14	130.7	127.2	125.7
C12-C14-C16	130.8	127.1	125.7
C10-C1-C12	123.0	123.7	122.4
C2-C1-C12	118.9	118.6	119.5
C14-C16-C17	118.9	118.7	119.5
C14-C16-C25	123.0	123.6	122.4
C1-C12-C14-C16	-7.0	-180.0	178.8
H13-C12-C14-H15	-4.6	180.0	-173.0
C10-C1-C12-C14	-35.7	0.0	30.0
C25-C16-C14-C12	-35.0	0.0	30.0

[a] Torsional angles of the fragment ABCD, denotes the angle between ABC and BCD planes.

photoirradiation experiments agree well with the computed features for the non-planar trans-stilbene.

Choi and Kertesz[18] have assigned their calculated feature at 724 cm^{-1} with the observed Raman band[17] at 734 cm^{-1} and considered it as a clear evidence for the existence of non-planar trans-stilbene. The same feature was found at 739 cm^{-1} in both our calculation and experiments.

In order to obtain the vibrational spectrum of the non-planar trans-stilbene, the spectra of cis- and trans-stilbene spectra were subtracted from the photoirradiated cis-stilbene spectra, after scaling the intensity of cis- and trans-stilbene spectra, so as to eliminate the features of these isomers. The subtracted spectrum, which represents the spectrum of non-planar trans-stilbene, is shown in Fig. 3.5b. The subtraction process helps in discerning the feature at 696 cm$^{-1,}$ which was merged into the strong features of the cis- and planar-trans form near 700 cm^{-1}. The computed spectrum of non-planar trans-stilbene is also shown in Fig. 3.5a for comparison, which agrees well with the subtracted spectrum shown in Fig. 3.5b. When calculating the spectra for the non-planar trans-stilbene (Fig. 3.5a), computed frequencies scaled by 0.9829 were used.

It can be seen that the features of the planar and non-planar trans-stilbene occur only slightly shifted from each other. In order to resolve the features of these two structures, a curve fitting routine, implemented through Origin 6.1 was used to decompose the spectral features in the regions 985-945, 780-755, 750-725 and 550-515 cm^{-1}. The curves were fitted to Lorentzian profiles and iterated to obtain a minimum in the χ^2 value. The fitted curves were interpolated using B-spline for smoothing. The non-planar trans-stilbene feature which appeared overlapped with those of the planar trans isomer can be clearly discerned in this spectral decomposition procedure, which is shown in Fig. 3.6.

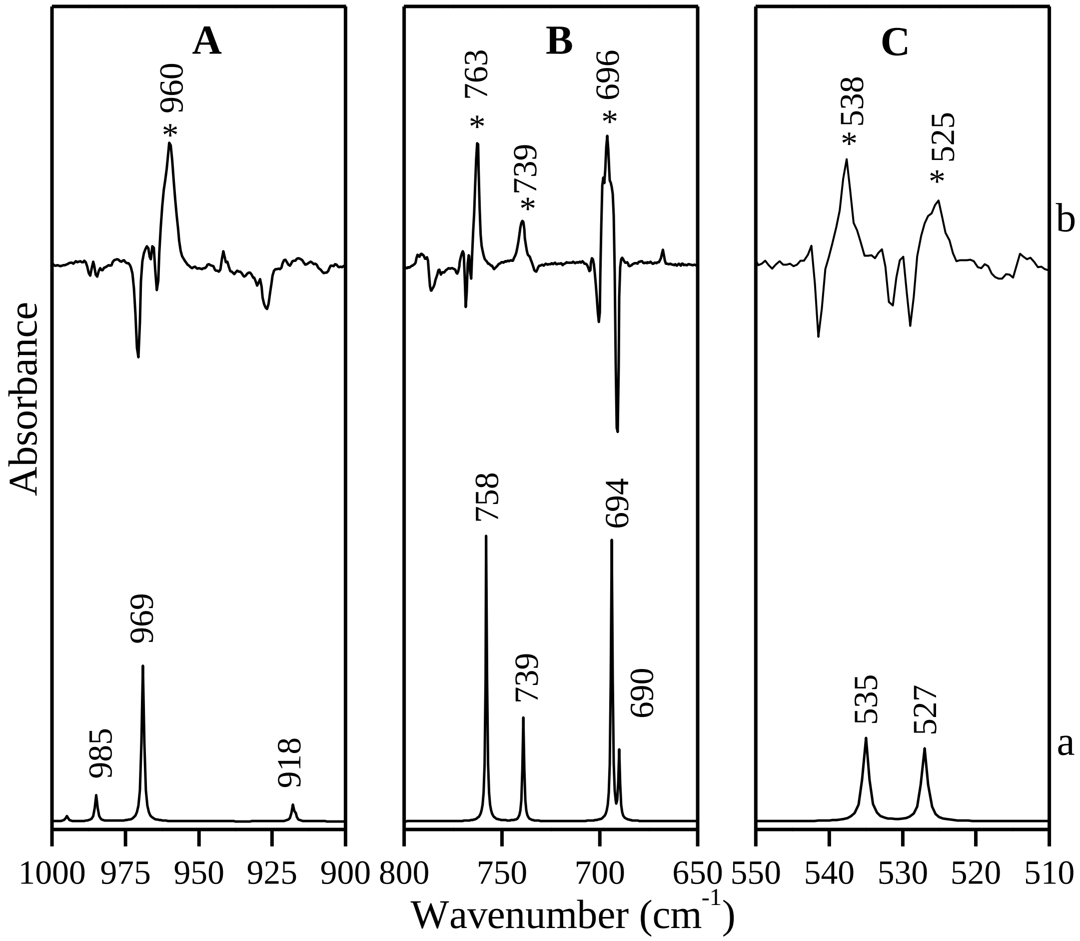

Fig. 3.5 – (a) Computed spectra for non-planar trans-stilbene and (b) Spectra of non-planar trans-stilbene in a N_2 matrix, obtained after subtracting the features of cis- and trans-stilbene from the spectra of photoirradiated cis-stilbene (See text for details).

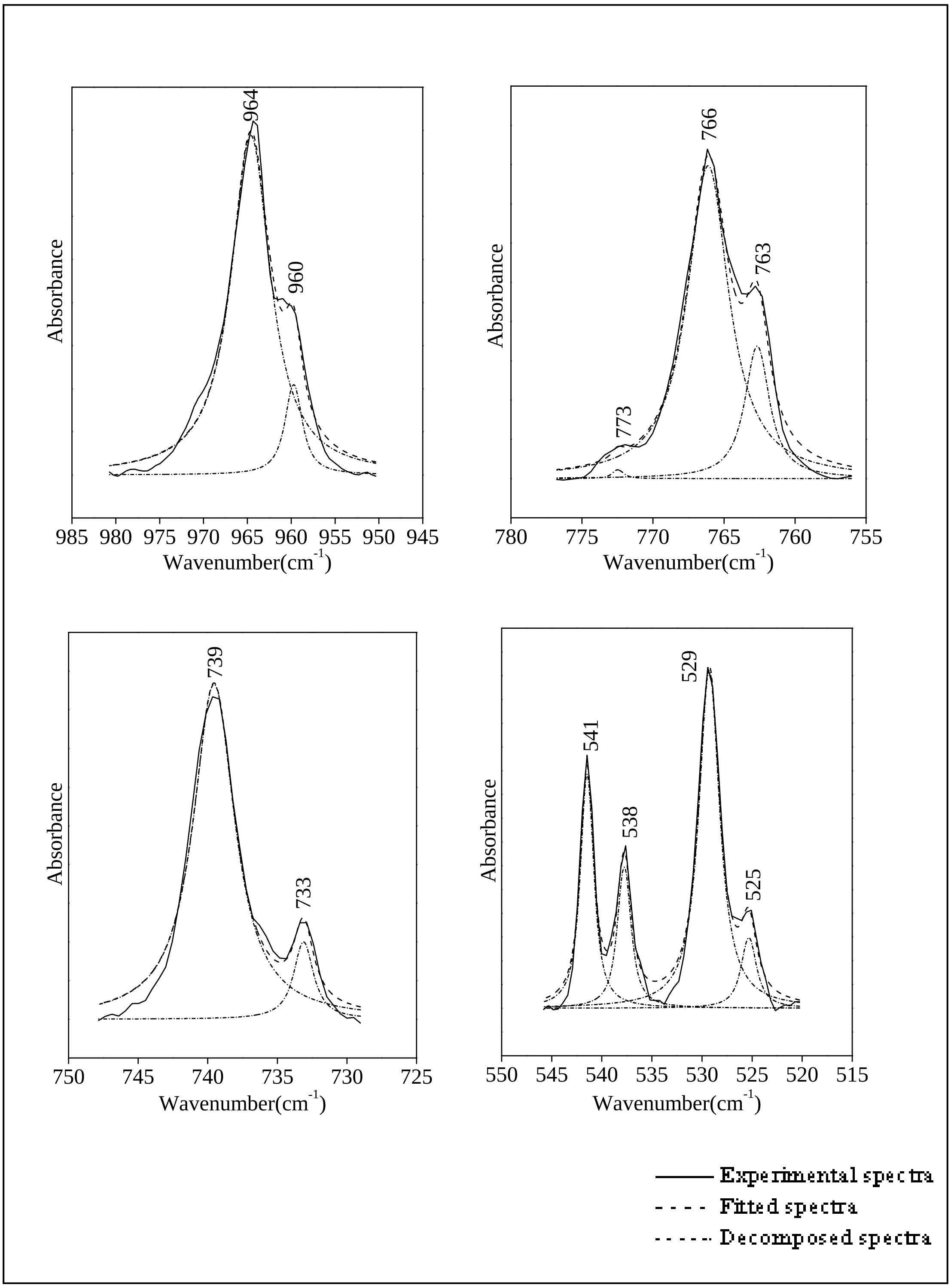

Fig. 3.6 – Spectral decomposition of the features in the region 985-945, 780-755, 750-725 and 550-515 cm^{-1} by fitting to Lorentzian profiles. (See text for details).

The features assigned to non-planar trans-stilbene reduced significantly on annealing the matrix at 32 K, with a concomitant increase in the intensity of the features due to planar trans-stilbene. The conversion of the non-planar form to the planar form indicates a very small barrier between these two structures. Furthermore, the conversion of the non-planar form to the planar form also indicates that the planar form is lower in energy than the non-planar form.

To summarize, cis-stilbene on photoirradiation undergoes excitation from S_o to S_1 state, where the 1-12-14-16 dihedral angle adopts a perpendicular orientation, following a rotation about the ethylenic C-C bond. Through the intermediacy of the phantom state, the molecule eventually returns, non-radiatively, to the maximum of the ground state potential. From here on, the molecule branches to either cis-, planar trans- or to the shallow non-planar trans orientation of stilbene. Even though, the non-planar form is separated from the planar-trans structure by only a small barrier, the matrix cage helps in trapping the shallow local minimum. The trapped non-planar form relaxes to the planar form on annealing the matrixes.

It must be emphasized that earlier structural determinations of trans-stilbene, performed in the gas phase and in crystals yielded either a non-planar or a planar trans structure. Experiments using melts have shown both forms;[15] however, the identification of the non-planar structure in this experiment rested on the assignment of just one feature at 960 cm^{-1}. Our matrix isolation experiments yielded both forms of the trans-stilbene and we have also been able to obtain a detailed vibrational spectrum of the non-planar structure. Clearly, the matrix has had a role to play in trapping both forms of trans-stilbene.

3.6 Conclusion

For the first time, we have trapped the non-planar trans-stilbene isomer in inert gas matrixes and recorded its infrared spectra. The non-planar structure was obtained following the photo irradiation of cis-stilbene and trapping the products in solid inert gas matrixes at temperature near 10 K. Earlier studies had identified only one mode for the non-planar trans-stilbene and the identification of this isomer rested on the observation of just the one mode at 960 cm^{-1}. This work therefore represents the first report of the vibrational spectrum for this structure. The almost quantitative loss of the non-planar trans conformer, on annealing, with a corresponding increase in the intensity features of the planar trans-stilbene indicates the planar trans form to be lower in energy than the non-planar structure.

References

---

[1] D. H. Waldeck, Chem. Rev., 1991, *91*,415.

[2] J. S. Baskin, L. Banares, S. Pedersen, A. H. Zewail, J. Phys. Chem., 1996, *100*, 11920.

[3] H. P. Lehmann, J. Phys. Chem., 1969, *73*, 20.

[4] M. Sumitani, K. Yoshihara, Bull. Chem. Soc. Jpn., 1982, *55*, 85.

[5] J. A. Syage, W. R. Lambert, P. M. Felker, A. H. Zewail, R. M. Hochstrasser, Chem. Phys. Lett., 1982, *88*, 266.

[6] D. Riedel, M. Cranney, M. Martin, R. Guillory, G. Dujardin, M. Dubois, P. Sonnet, J. Am. Chem. Soc., 2009, *131*, 5414.

[7] G. Orlandi, W. Siebrand, Chem. Phys. Lett., 1975, *30*, 352.

[8] P. Tavan, K. Schulten, Chem. Phys. Lett., 1978, *56*, 200.

[9] B. G. Levine, T. J. Martinez, Ann. Rev. Phys. Chem., 2007, *58*, 613.

[10] M. Traetteberg, E. B. Frantsen, F. C. Mijlhoff, A. Hoekstra, J. Mol. Struct., 1975, *26*, 57.

[11] T. Kobayashi, H. Suzuki, K. Ogawa, Bull. Chem. Soc. Jpn., 1982, *55*, 1734.

[12] A. Hoekstra, P. Meertens, Aafje Vos, Acta Cryst. B, 1975, *31*, 2813.

[13] J. A. Bouwstra, A. Schouten, J. Kroon, Acta. Cryst. C, 1984, *40*, 428.

[14] W.-Y. Chiang, J. Lanne, J. Chem. Phys., 1995, *100*, 8755.

[15] M. Edelson, A. Bree, Chem. Phys. Lett., 1976, *41*, 562.

[16] A. Bree, M. Edelson, Chem. Phys., 1980, *51*, 77.

[17] J. F. Arenas, I. L. Tocon, J. C. Otero, J. I. Marcos, J. Phys. Chem., 1995, *99*, 11392.

[18] C. H. Choi, M. Kertesz, J. Phys. Chem. A, 1997, *101*, 3823.

[19] W.-G. Han, T. Lovell, T. Liu, L. Noodleman, Chemphyschem, 2002, *3*, 167.

[20] S. P. Kwasniewski, L. Claes, J. P. Francois, M. S. Deleuze, J. Chem. Phys., 2003, *118*, 7823.

[21] P. D. Chowdary, T. J. Martinez, M. Gruebele, Chem. Phys. Lett., 2007, *440*, 7.

---

[22] S. A. Kovalenko, A. L. Dobryakov, I. Ioffe, N. P. Ernsting, Chem. Phys. Letts., 2010, *493*, 255.

[23] K. Sundararajan, K. S. Viswanathan, J. Mol. Struct., 2006, *798*, 109.

[24] K. V. J. Jose, S. R. Gadre, K. Sundararajan, K. S. Viswanathan, J. Chem. Phys., 2007, *127*, 104501.

[25] M. Traetteberg, E. B. Frantsen, J. Mol. Struct., 1975, *26*, 69.

[26] K. A. Muszkat, E. Fischer, J. Chem. Soc. (B), 1967, 662.

[27] H. Petek, K. Yoshihara, Y. Fujwara, Z. Lin, J. H. Penn, J. H. Frederick, J. Phys. Chem., 1990, *94*, 7539.

[28] J-M. Rodier, X. Ci, A. B. Myers, Chem. Phys. Lett., 1991, *183*, 55.

[29] X. Zhou, R. Liu, Chem. Phys. Lett., 1992, *191*, 477.

CHAPTER 4

STUDIES ON THE CONFORMATIONS OF DIMETHYL CARBONATE AND ITS COMPLEXES WITH WATER

4.1 Introduction

As described in Chapter 1, carbonates have been studied here to understand their conformational behaviour. Dimethyl carbonate (DMC), the first member of dialkyl carbonates, provides an interesting case study for understanding conformational preferences in molecules containing the methoxy groups, such as esters. In such molecules, the various conformations essentially arise due to the hindered rotation around the (O=C)−O moiety. In the case of DMC, the possible conformations are ‘cis-cis’, ‘cis-trans’ and ‘near-trans-near-trans’, as shown in Fig. 4.1.

Conformations of dimethyl carbonate have been experimentally studied by different groups. Collingwood et al.[1] have studied the infrared spectra of DMC in the gas phase and in solvents such as CS_2 and CCl_4. They have assigned all the observed features to the cis-cis conformer. A gas phase electron diffraction study supported this conclusion and showed that DMC has a cis-cis structure with a planar heavy-atom geometry corresponding to a C_{2v} symmetry.[2] On the other hand by a comparison of the IR spectra of the liquid and the crystalline phase of DMC, Katon et al.[3,4] reported the presence of a cis-trans conformer in the liquid phase, with an enthalpy difference of 2.6 ± 0.5 kcal/mol between the ground state cis-cis and the cis-trans conformers. This observation was supported by Labrenz and Schröer,[5] who on the basis of semi-empirical and *ab initio* calculations, together with dielectric measurements in gas and liquid phases, deduced the presence of cis-cis and cis-trans conformers. Furthermore, their calculations also showed that the trans-trans conformer was a saddle point with one imaginary frequency. Molecular dynamics simulation by Okada,[6] showed that in liquid DMC at 353 K, the cis-cis conformer had a 68% population. However,

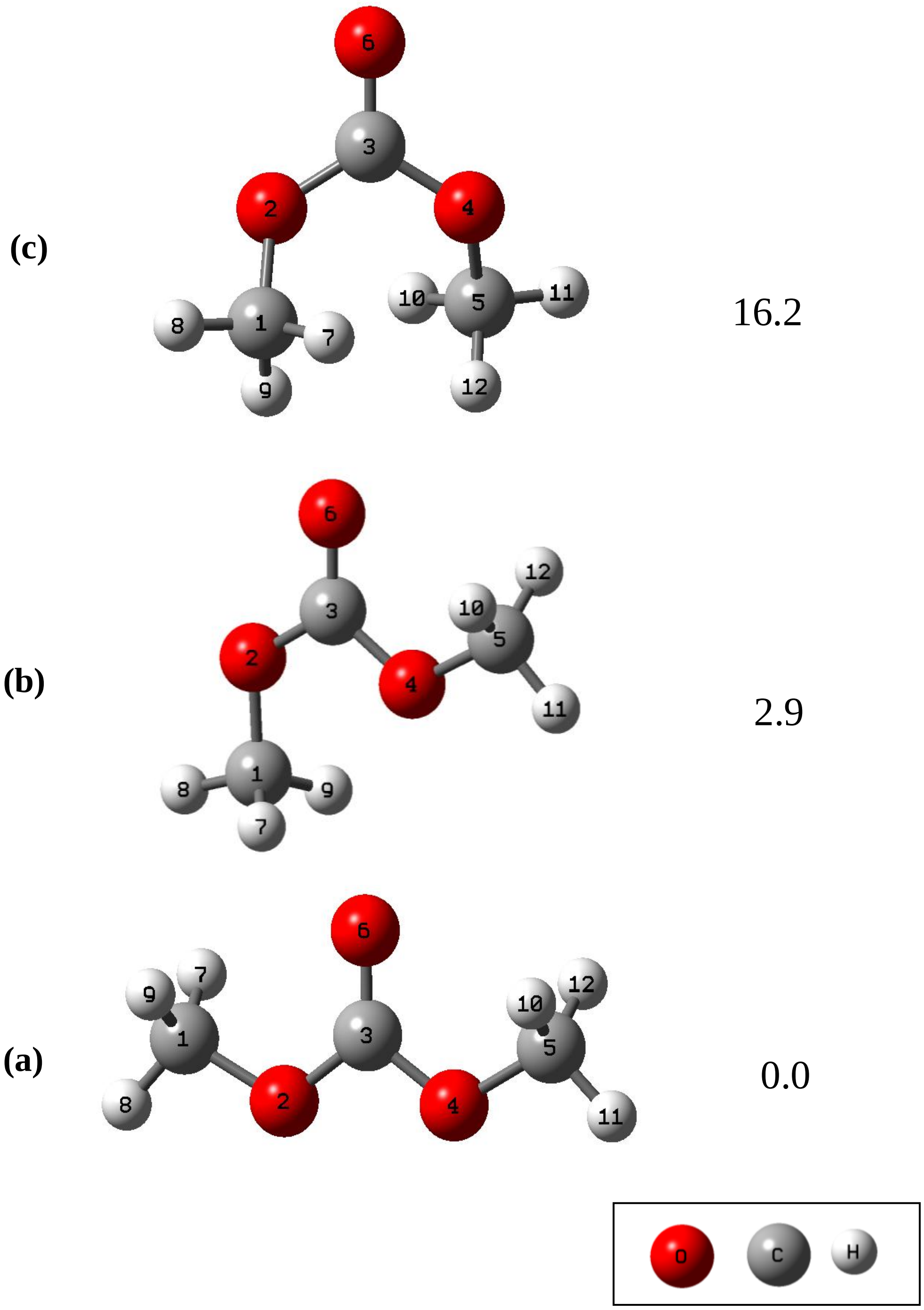

Fig. 4.1 – Computed structures at B3LYP/6-31++G** level of the different conformers of DMC (a) cis-cis; (b) cis-trans; (c) near-trans-near-trans. The energy, in kcal/mol, of each conformer relative to the ground state conformer, is given against each structure.

using dispersive X-ray scattering and molecular dynamics, Gontrani et al.[7] concluded that population of the cis-cis conformer was almost 99%. Gillespie et al. have pointed out that molecular compactness, which arises due to the 1,4 interaction places cis-cis as the lowest energy conformer.[8]

Bohets and van der Veken[9] recorded the infrared and Raman spectra of the vapor, amorphous and the crystalline solid of DMC. They also performed *ab initio* calculations at the DFT and MP2 level using the 6-31G** basis set. Using their experimental and computational results, they deduced the presence of both ground state cis-cis conformer and higher energy cis-trans conformer in DMC. However in their experiments, they could observe only a few features corresponding to the cis-trans structure, which were not clearly resolved from the strong features of the ground state cis-cis conformer. Their computations also indicated the presence of yet another minimum, with a near-trans-near-trans structure, located at an energy of 16.4 kcal/mol relative to the ground state conformer, which was not detected in their experiments. Recently Bernad et al. have recorded the IR spectra of carbonic acid trapped in inert gas matrixes at ~6 K and have reported the presence of both cis-cis and cis-trans conformer.[10]

In an effort to clearly delineate the different conformers of DMC and also to understand the reasons for the conformational preferences in this molecule, we have studied this molecule using matrix isolation infrared spectroscopy and *ab initio* computations. 1:1 hydrogen bonded complexes of DMC-H_2O were also studied, using the above experimental and computational facilities.

4.2 Experimental details

Details of the experimental procedure followed are given in chapter 2. DMC, (Sigma Aldrich, anhydrous, ≥99%) was used without further purification. However the sample was subjected to several freeze-pump-thaw cycles before preparation of the sample-matrix gas mixtures. The sample to matrix ratios was varied from 0.25:1000 to 4:1000, using standard manometric procedures. Ar and N_2 were used as matrix gases.

Experiments were also performed by maintaining the effusive source at different nozzle temperatures, viz. 298 (room temperature), 373 and 423 K. These experiments were performed in order to alter the population of the higher energy conformer relative to the ground state conformer, to enable us to unequivocally identify the features of the higher energy structure. We also performed experiments using a pulsed supersonic jet nozzle to deposit the sample mixture. The pulsed valve was operated with a pulse width of 3 ms at a repetition rate of 0.25 Hz in all the experiments and with stagnation pressure of typically 1.3 atm. At this deposition rate, the temperature of the cryotip did not rise.

On annealing the matrix, new features were observed which was likely due to DMC-H_2O adduct as water is a ubiquitous impurity in matrix experiments. However, there is a possibility that these new features may be due to higher clusters of DMC and/or due to conformers of DMC that were not initially deposited in the matrix but were produced by interconversion during annealing. To understand the phenomena, we deliberately studied DMC-H_2O complex by codepositing the two monomers. For this purpose, the concentrations of DMC and water were varied independently, over the range 0.25:1000 to 0.75:1000 for DMC and 1.0:1000 to 1.3:1000 for H_2O. These experiments were performed using a double jet nozzle; through one nozzle the matrix gas and DMC were allowed to stream out, while through the second nozzle H_2O was admitted to the vacuum system. The matrix was then annealed for 15 min at 35 K to encourage complex formation.

4.3 Computational details

We have performed *ab initio* calculations at the B3LYP level using 6-31++G** and 6-311++G** basis sets. However, relatively good agreements of experimental vibrational features were found with those obtained from the computation with the former level of basis set and hence results at this level are discussed here.

The structures of the conformers and barrier for conformer interconversion were calculated using the above level of theories. Vibrational frequency calculations were carried out using analytical gradients on the optimized geometries. To calculate the scaling factor the experimentally observed strongest feature at 1293.6 cm^{-1} was correlated with the strongest computed feature for the ground state conformer in this region, occurring at 1321.9 cm^{-1}. A scaling factor of 0.9786 was required to bring the two values in agreement. This scaling factor was used to scale other features of the ground and higher energy conformers. To understand the role of delocalization interactions in determining conformational preferences, Natural Bond Orbital (NBO) analysis were performed at B3LYP/6-31++G** level of theory.

The structures of the DMC-H_2O complexes were optimized and vibrational frequency calculations were performed on the optimized geometries. The same scaling factor used for assigning the features of the various conformers of DMC, was employed for assigning the infrared features of the DMC submolecule in the DMC-H_2O complexes. To assign the O-H stretching features of the H_2O submolecule in the complex, a scaling factor of 0.9484 was used, which was arrived at by correlating the experimental feature of the antisymmetric stretch of monomer H_2O at 3727.1 cm^{-1}, with the computed feature for this mode at 3929.9 cm^{-1}. For the bending modes of H_2O, the same scaling factor as that used for the DMC modes was used, as the bending mode of H_2O falls in the same spectral region as the modes of DMC considered in this study. The matrix is known to perturb the modes in the different spectral regions differently; and hence to account for these systematic differences, we have used a variable scaling factor.[11,12]

Stabilization energies, corrected separately for zero point energy (ZPE) and basis set superposition errors (BSSE) were calculated for the complexes. The nature of the interaction between DMC and water was studied using the atoms-in-molecules (AIM) theory by Bader.[13] A few calculations on structure and frequencies of DMC conformers and DMC-H_2O complexes were also performed at MP2/6-31++G** level of theory.

We will first present our results on the conformations of DMC; in a subsequent section we will discuss our results on the DMC-H_2O hydrogen bonded complex.

4.4 Results - Conformations of DMC

4.4.1 Experimental

Fig. 4.2 shows the IR spectra of DMC in a N_2 matrix at 12 K, over the spectral region 2000 to 600 cm^{-1}. The regions, marked ‘I’ and ‘II’ in this figure, are shown in an expanded scale in Fig. 4.3, as grids A (1830-1770 cm^{-1}), B (1290-1080 cm^{-1}) and C (1040-1000 cm^{-1}), to enable easy identification of spectral features, due to the different conformers. Traces ‘b’ to ‘d’ in Fig. 4.3 show the infrared spectra of DMC, deposited using different deposition conditions. Traces ‘b’ and ‘c’ show the spectrum obtained using the effusive nozzle maintained at room temperature and 423 K respectively. The spectra obtained using a supersonic jet source is shown in trace ‘d’. The spectral regions shown in Fig. 4.3 correspond to the C=O stretching, O−C−O stretching, H_3C−O stretching and CH_3 rocking modes of DMC. For all these experiments the typical sample to matrix ratio was maintained at 0.5:1000. Trace ‘a’ in Fig. 4.3 represents the computed IR spectra of the two conformers of DMC at 423 K. The computed intensities of the various modes of the two conformers were weighted by their relative populations at 423 K to simulate a spectrum at the elevated temperature.

A few experiments were also performed with higher sample to matrix ratios (i.e. 4:1000), in an effort to observe some of the weak features of DMC, particularly in the region 500-800 cm^{-1}, the spectra for which are shown in Fig. 4.4.

Features corresponding to the C-H stretching and deformation modes are not clearly

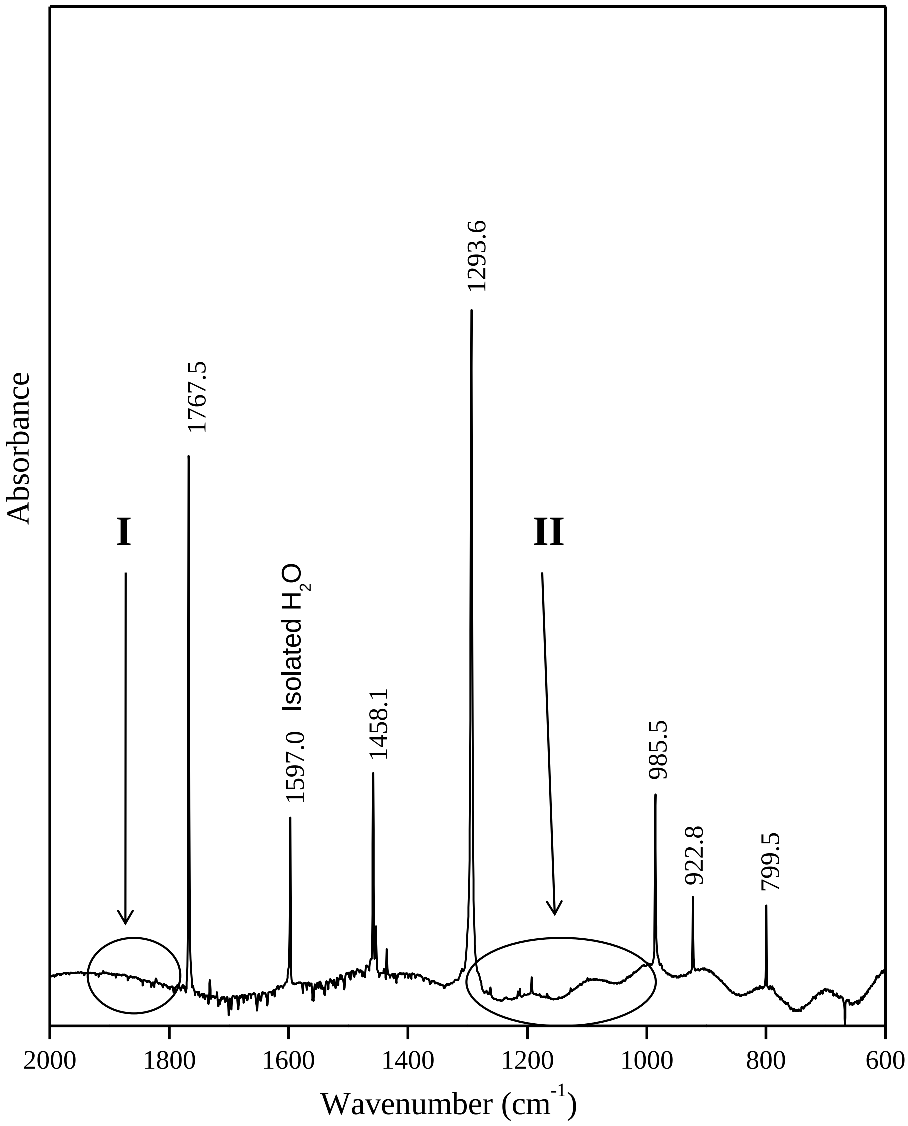

Fig. 4.2 – IR spectra of DMC in a N_2 matrix at 12 K, over the region 2000-600 cm^{-1}. The regions marked ‘I’ and ‘II’ have been expanded in Fig. 4.3.

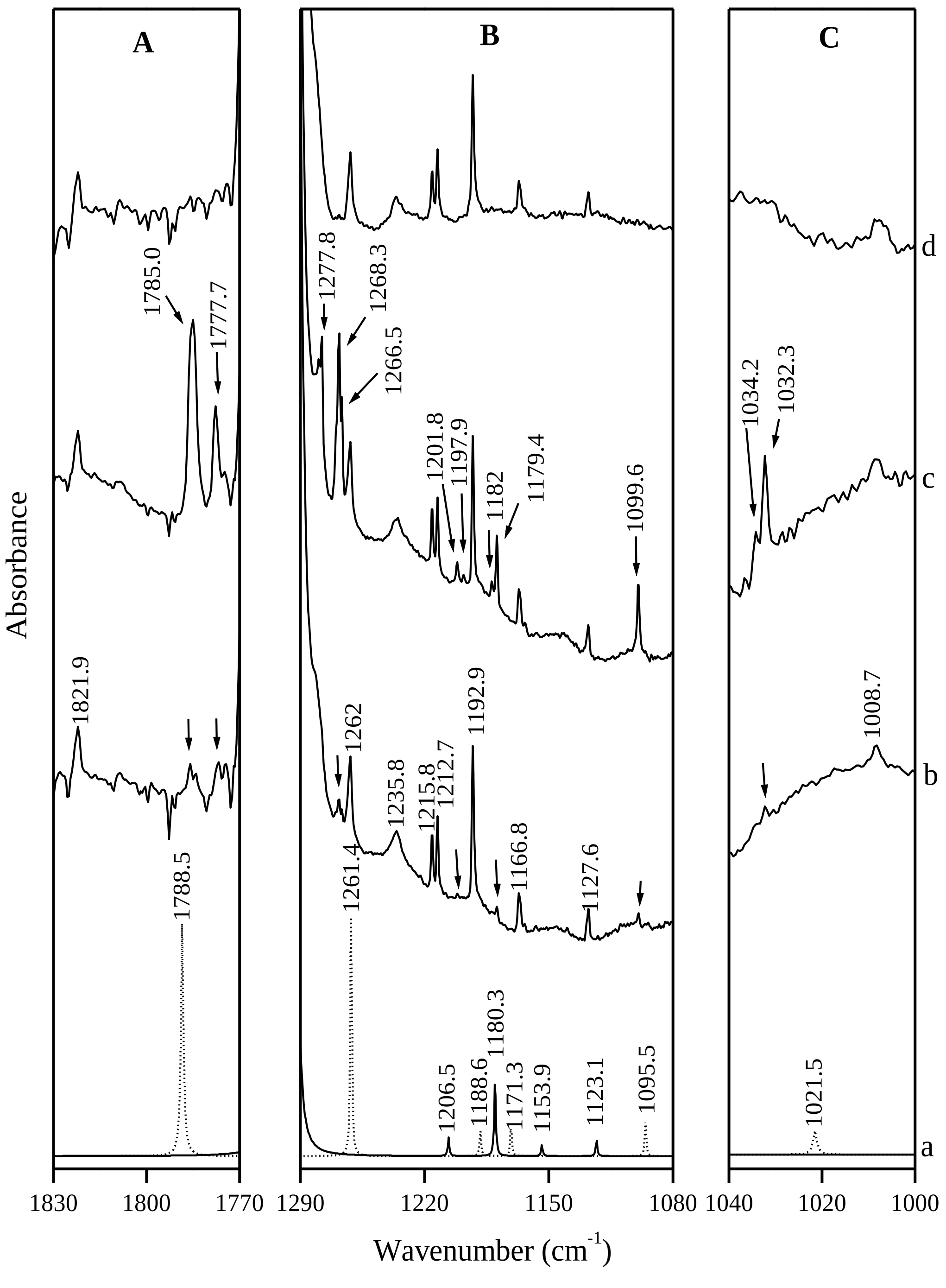

Fig. 4.3 – IR spectra of DMC (Grid A: 1830-1770 cm^{-1}, Grid B: 1290-1080 cm^{-1} and Grid C: 1040-1000 cm^{-1}) (a) computed spectra at 423 K (solid line for cis-cis and dotted line for cis-trans conformer), (b) and (c) matrix isolation spectra recorded using an effusive nozzle at 298 K and 423 K respectively, and (d) matrix isolation spectra recorded using a supersonic jet source. Matrix-isolation spectra were recorded in a N_2 matrix at 12 K using sample to matrix ratio of 0.5:1000.

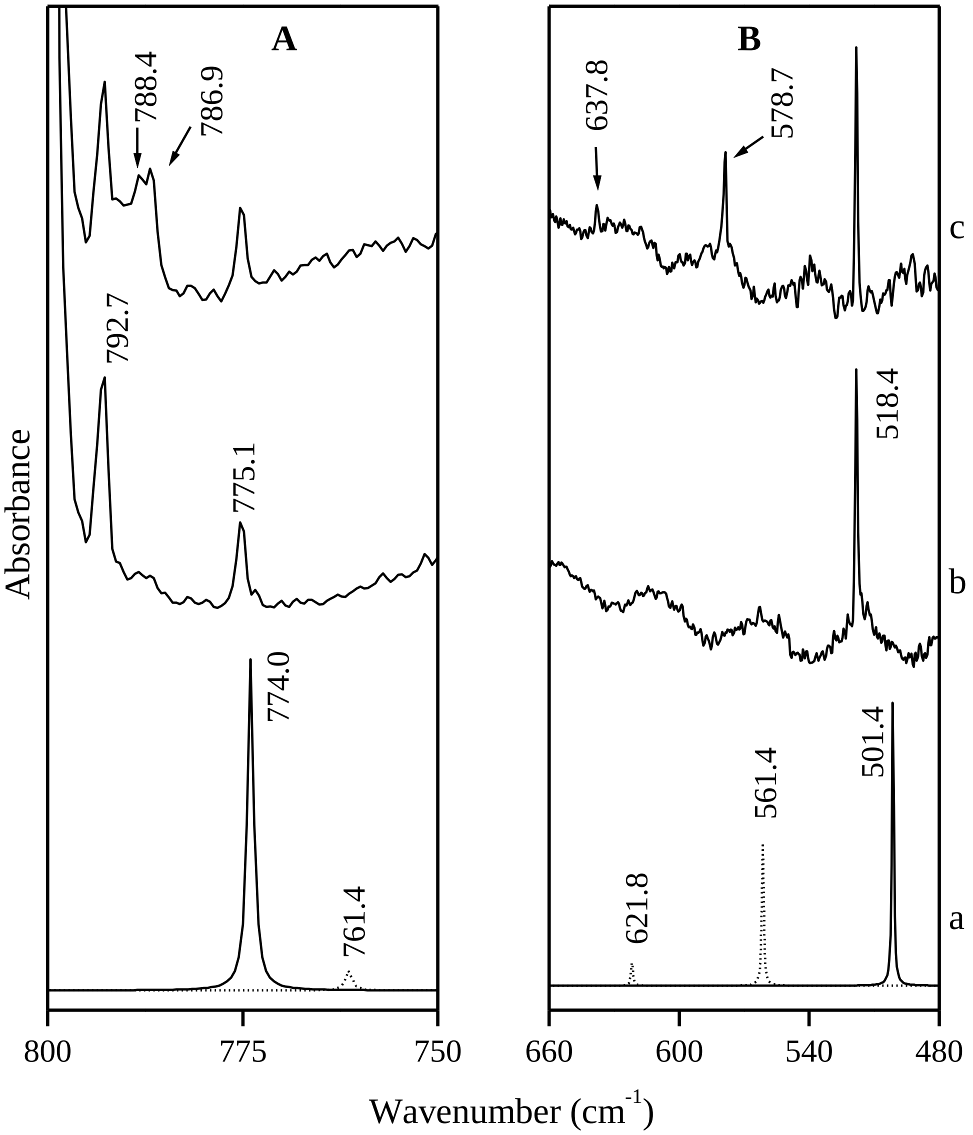

Fig. 4.4 – IR spectra of DMC (Grid A: 800-750 cm^{-1} and Grid B: 660-480 cm^{-1}) in N_2 matrix at 12 K, at a sample to matrix ratio 4:1000. (a) Computed spectra at 443 K (solid line for cis-cis and dotted line for cis-trans conformer); (b) and (c) matrix isolation spectra recorded using an effusive nozzle at 298 K and 443 K respectively.

resolved for the various conformers and hence we will not present a discussion for these modes.

4.4.2 Computational

Our computations indicated a conformation with a cis-cis structure (Fig 4.1a) to be the global minimum. Lying above this structure, were two minima corresponding to a cis-trans (Fig. 4.1b) and near-trans-near-trans structure (Fig. 4.1c), located respectively at energies of 2.9 and 16.2 kcal/mol above the cis-cis structure. The important structural parameters for these conformers are given in Table 4.1. The structure of the transition state connecting the ground state conformers to the first higher energy cis-trans structure was also computed, the energy of which is shown in Table 4.2. Using the computed energies of the transition state, the barrier for conformer interconversion from the cis-trans to the cis-cis structure was computed to be 6.4 kcal/mol. Table 4.2 shows the relative energies, corrected for zero point energy, and dipole moments of the various conformers of DMC. The experimental and calculated frequencies are compared in Table 4.3.

4.5 Discussions – Conformations of DMC

4.5.1 Vibrational assignments

It can be seen from Fig. 4.2 and Table 4.3 that the computed features of the ground state cis-cis conformer correlate well with the strong features observed in the matrix isolated spectra of DMC, which is in agreement with the findings of Bohets and van der Veken.[9] In addition to the features of the ground state conformer, experiments were performed to identify the presence of higher energy conformers of DMC. When the effusive nozzle was heated to 423 K, it was observed that a number of features gained in intensity, which are labeled with arrows in Fig. 4.3. The temperature dependence of these features presents a strong case for these features to be assigned to higher energy conformers. It can be noted that these new features are not due to any decomposition product of DMC, as it is stable up to

Table 4.1 – Important structural parameters, bond lengths (Å), bond angles (°) and torsional angles[a] (°), of the conformers of DMC, computed at the B3LYP/6-31++G level.**

Parameters	**Cis-cis**	**Cis-trans**	**Near-trans-near-trans**
O2-C3	1.340	1.341	1.358
C3-O4	1.340	1.352	1.358
C3-O6	1.215	1.208	1.202
C1-O2-C3	115.1	120.1	120.7
O2-C3-O4	108.2	112.3	116.9
O2-C3-O6	125.9	122.6	121.5
O4-C3-O6	125.9	125.1	121.5
C3-O4-C5	115.1	115.1	120.7
C1-O2-C3-O6	-0.0	-180.0	-141.5
C1-O2-C3-O4	179.9	0.0	38.5
C5-O4-C3-O6	-0.0	0.0	-141.4
C5-O4-C3-O2	-180.0	-180.0	38.6

[a] Torsional angle ABCD implies the angle between two planes ABC and BCD.

Table 4.2 – Relative energies (kcal/mol), and dipole moment (D) of the different conformers and transition state of DMC, computed at different levels of theories.

Conformer	**Relative energy[a] (kcal/mol)**			**Dipole moment (D)**		
	B3LYP/6-31++G**	**B3LYP/6-311++G****	**MP2/6-31++G****	**B3LYP/6-31++G****	**B3LYP/6-311++G****	**MP2/6-31++G****
Cis-cis	0.0	0.0	0.0	0.33	0.27	0.24
Cis-trans	2.9	2.9	3.1	3.84	3.79	4.16
Near-trans-near-trans	16.2	16.1	16.6	5.43	5.33	5.92
TS1[b]	9.3	9.1	9.8	2.68	2.63	2.90

[a] Energies corrected for ZPE.

[b] Transition state connecting cis-cis and cis-trans conformer of DMC.

Table 4.3 – Experimental and calculated (B3LYP/6-31++G theory) vibrational wavenumbers (cm^{-1}) of cis-cis and cis-trans conformers of DMC.**

Cis-cis		Cis-trans		Mode assignment[a]
Exp	**Calc**	**Exp**	**Calc**	
518.4[b]	501.4(2)[c]	578.7[d]	561.4(17)	ν_9 CO_2 def
695.5[b]	677.1(0.1)	637.8[d]	621.8(3)	ν_{23} O=CO_2 rock
799.5	774.0(28)	786.9[d]	761.4(29)	ν_{28} CO_3 out-of-plane def
		788.4[d]		
922.8	909.4(28)	-[e]	849.1(2)	ν_8 CO_2 sym stretch
985.5	975.9(72)	1032.3	1021.5(46)	ν_{22} CH_3-O stretch
		1034.2		
1008.7	-			
1127.6	1123.1(2)	1099.6	1095.5(74)	ν_7 CO_2 sym stretch
-	1149.9(0)	-	1145.9(1)	ν_{13} CH_3 rock
1166.8	1153.9(1)	-	1152.8(1)	ν_{27} CH_3 rock
1192.9	1180.3(11)	1179.4	1171.3(69)	ν_{21} CH_3 rock
		1182.0		
1212.7	1206.5(2)	1197.9	1188.6(57)	ν_6 CH_3 rock
1215.8		1201.8		
1235.8	-			
1262	-			
1293.6	1293.6(831)	1266.5	1261.4(547)	ν_{20} CO_2 antisym stretch
		1268.3		
		1277.8		
1435.5	1438.2(9)	-	1439.0(7)	ν_5 CH_3 sym def
-	1457.2(0)	-	1455.3(9)	ν_{12} CH_3 antisym def
1453.8	1457.7(17)	-	1462.9(8)	ν_{26} CH_3 antisym def
1458.1	1458.9(87)	-	1462.8(41)	ν_{19} CH_3 sym. def.
-	1470.8(0.4)	-	1468.6(21)	ν_4 CH_3 antisym def
1470.1	1471.5(10)	-	1472.4(17)	ν_{18} CH_3 antisym def
1767.5	1757.5(341)	1777.7	1788.5(511)	ν_3 C=O stretch
		1785.0		
1821.9	-			$\nu_5 + \nu_{24}$[f]

[a] Assignments taken from ref. 9.

[b] Features seen when experiments were performed with sample to matrix ratio of 4:1000.

[c] IR intensities (km/mol) are given in parentheses.

[d] Features seen when experiments were performed with sample to matrix ratio of 4:1000 and the nozzle temperature was maintained at 443K.

[e] Experimental features were not observed.

[f] ν_{24} = C-O-C antisym. def.

623 K.[14] We also performed experiments using a supersonic jet source to look for conformational cooling. In this experiment, the population of the higher energy conformer can be expected to deplete in the expansion process. It can be seen from Fig. 4.3 that all the features marked with an arrow, were found to occur with significantly reduced intensities in Fig. 4.3d, further supporting the assignment of these labeled features to higher energy cis-trans conformer of DMC.

Based on the energy difference between the cis-cis and the cis-trans conformer, which was computed to be 2.9 kcal/mol at the B3LYP/6-31++G** (Table 4.2) and the statistical weights of 1 and 2 respectively for the two conformers, the populations of the two conformers were computed at room temperature (298 K) and 423 K, which were the temperatures adopted in recording the spectra shown in Figs. 4.3b and 4.3c, respectively. The population of the higher energy cis-trans conformer increased from 1.5% at 298 K to 6.0% at 423 K; a 4-fold increase. This population increase supports the assignment of the features labeled with arrows, in Fig. 4.3c, (whose intensities increased with increase in temperature), to the cis-trans structure, as discussed below and presented in Figs. 4.3, 4.4 and Table 4.3.

The features at 1785.0 and 1777.7 cm^{-1}, which occurred to the blue of the strong feature of the ground state conformer at 1767.5 cm^{-1} were assigned to the ν_3 C=O stretch of the higher energy cis-trans conformer, which is in agreement with our computations. Likewise, the features at 1268.3 and 1266.5 cm^{-1} can be assigned to the ν_{20} O-C-O antisymmetric stretch in the cis-trans conformer. It should be mentioned that Bohets and van der Veken[9] in their experiment could not observe any feature corresponding to ν_3 and ν_{20} modes for the higher energy conformer. It must be mentioned that a feature at 1277.8 cm^{-1} observed in our hot nozzle experiment, could not be assigned to any of the conformers.

Likewise features due to the ν_6 CH_3 rocking mode at 1201.8 and 1197.9 cm^{-1}, and ν_{21} CH_3 rocking mode at 1182.0 and 1179.4 cm^{-1}, not observed in earlier studies, were clearly observed in our spectra.

It should be mentioned that many features for the cis-cis and cis-trans conformer DMC in Ar matrix display site splitting, which was why we chose to present the spectra recorded in a N_2 matrix. However, the spectra related to hot nozzle experiments in Ar matrix are shown in Fig. 4.5. Traces 'a', 'b' and 'c' in this figure corresponds to experiments performed using an effusive nozzle kept at temperatures 298, 423 and 473 K respectively. Grid A, B and C show the spectral region 1820-1780 cm^{-1}, 1275-1075 cm^{-1} and 1040-1000 cm^{-1} respectively. The features shown with arrows are found to increase with increase in temperature and hence can be assigned to cis-trans conformer.

Bohets and van der Veken have also attempted to observe the features of the higher energy conformer in their work, but they could assign only a few features corresponding to the higher energy conformer.[9] For example, they observed a weak shoulder near the 1760 cm^{-1} feature in the spectrum of amorphous DMC, which they assigned to the carbonyl stretching of the higher energy conformer. The same feature could not be observed in their gas phase sample, presumably due to the broad features of the cis-cis conformer. Likewise one of the strongest features of the cis-trans conformer in our calculation corresponds to the O-C-O antisymmetric stretch was not observed in their spectrum. However, the line widths in our matrix isolated spectra being small, we were able to identify many of the features of the higher energy cis-trans conformer. Our work therefore presents a detailed assignment of the infrared features of the cis-trans conformer of DMC.

While many of the features not seen in the earlier work have been observed in our experiments, a few features corresponding to the higher energy conformer reported by Bohets and van der Veken,[9] such as those at 578, 636 and 859 cm^{-1}, were not observed in our work. These were features with low intensities, as indicated by our computations. In an effort to observe these features, we performed hot nozzle experiments at 443 K with sample to

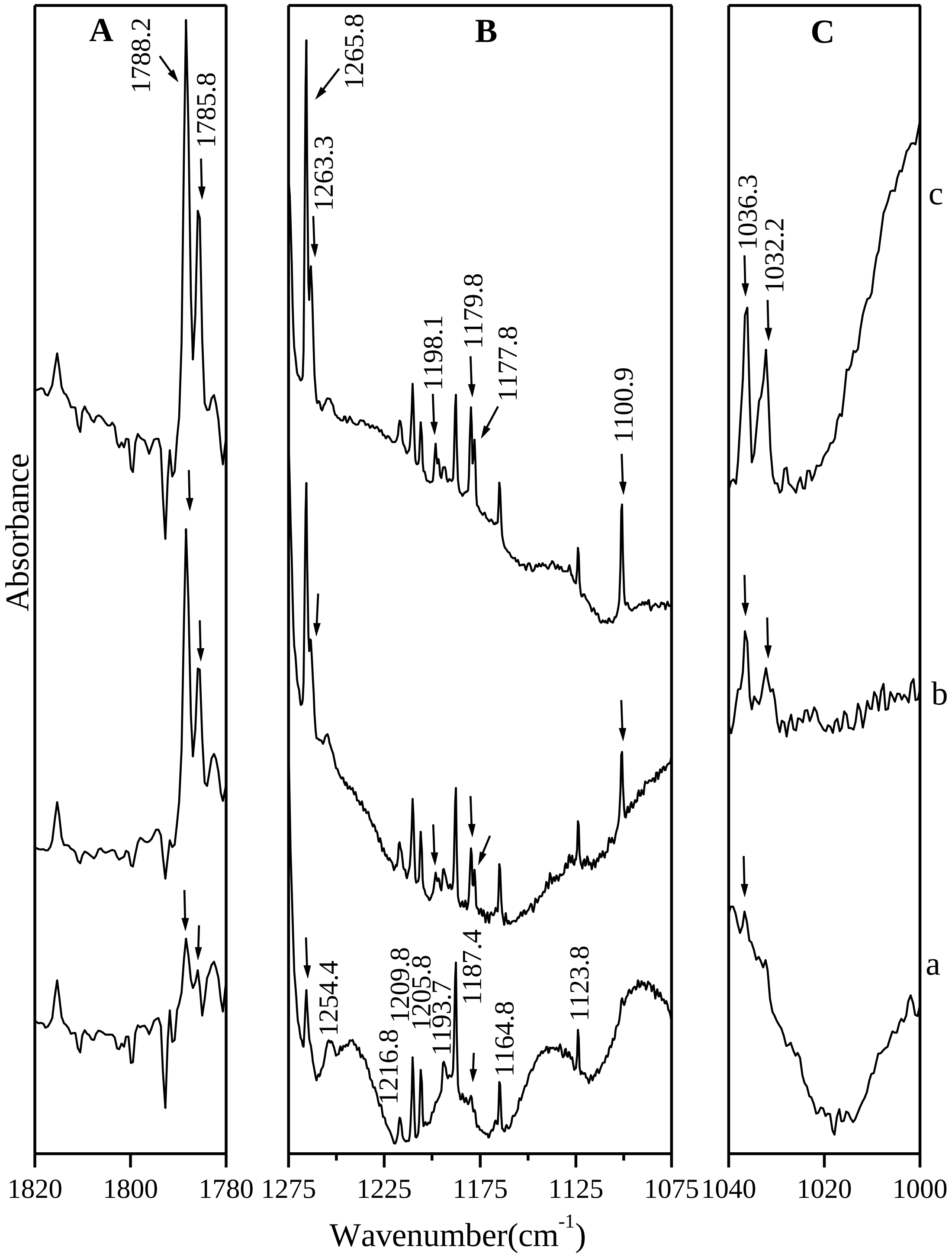

Fig. 4.5 – IR spectra of DMC in Ar matrix at 12 K with a sample to matrix ratio of 0.5:1000 (Grid A: 1820-1780 cm^{-1}, Grid B: 1275-1075 cm^{-1} and Grid C: 1040-1000 cm^{-1}). (a), (b) and (c) are matrix isolation spectra recorded using an effusive nozzle at 298, 373 and 423 K respectively.

matrix ratios as high as 4:1000, which is shown in Fig. 4.4 (trace ‘c’). This experiment clearly reveals the low intensity features at 578.7 and 637.8 cm^{-1}. Based on our computations these features could be assigned to the ν_9 and ν_{23} modes of the cis-trans conformer of DMC. Similarly, the feature corresponding to the ν_{28} mode of the higher energy conformer was observed as matrix site split features at 786.9 and 788.4 cm^{-1} which was not observed by Bohets and van der Veken.[9] The features at 792.7 and 775.1 cm^{-1} shown in Fig. 4.4 (Grid A) were observed only at higher sample to matrix ratios. These features are probably due to higher clusters of DMC.

Figs. 4.2, 4.3, 4.4 and Table 4.3 present all the features assignable to both the ground state cis-cis and higher energy cis-trans conformers.

The energy difference between the two conformers was estimated from our experimental data by examining the variation of the intensities of the features assigned to the two conformers as a function of temperature. From the plot of the logarithm of the intensity ratio, $\ln(I_{1127.6}/I_{1009.6})$, against (1/T), the enthalpy difference between the two conformers was estimated to be of 3.4 kcal/mol. This experimentally determined value is in reasonable agreement with the computed value of 2.9 kcal/mol.

4.5.2 Natural bond orbital analysis

Natural bond orbital analysis on the three conformers was performed. The important delocalization interactions of different conformers along with the second order perturbation energies (E_2) are listed in Table 4.4. It was found that the dominant interactions involve the lone pair of electrons on O2 and O4, and the π^* orbital of the C=O group. While this interaction is important in all the conformers, it is marginally stronger in the cis-cis conformer compared with the cis-trans, and significantly weaker in the near-trans-near-trans structure, as indicated by the second order perturbation energies, E_2, of 49.2 kcal/mol, 47.5 kcal/mol and 31.4 kcal/mol, respectively for the cis-cis, cis-trans and near-trans-near-trans

Table 4.4 – Second order perturbation energies E_2 (kcal/mol) of different delocalization interactions in different conformers of DMC.

Donor orbital	Acceptor orbital	Second order perturbation energy (E_2)		
		Cis-cis	**Cis-trans**	**Near-trans-near-trans**
n^1O2	σ*C3-O4	2.33	8.29	8.83
n^1O2	σ*C3-O6	10.87	0.80	0.90
n^1O2	π*C3-O6	-[a]	-	1.59
n^2O2	σ*C3-O4	-	-	2.38
n^2O2	σ*C3-O6	-	-	2.85
n^2O2	π*C3-O6	49.23	47.47	31.40
n^1O4	σ*C1-O2	-	0.91	-
n^1O4	σ*O2-C3	2.32	2.32	8.83
n^1O4	σ*C3-O6	10.85	9.57	0.89
n^1O4	π*C3-O6	-	-	1.60
n^2O4	σ*O2-C3	-	-	2.39
n^2O4	σ*C3-O6	-	-	2.89
n^2O4	π*C3-O6	49.16	45.53	31.27
n^1O6	Ry*(1)C3	17.34	15.70	17.16
n^1O6	σ*O2-C3	2.47	2.39	2.20
n^1O6	σ*C3-O4	2.47	2.45	2.20
n^2O6	σ*O2-C3	29.72	29.66	31.86
n^2O6	σ*C3-O4	29.75	32.09	31.86
Cr(1)O6	Ry*(1)C3	6.88	6.20	6.92

[a] Values are less than threshold value 0.5 kcal/mol.

structures. The next strongest delocalization interaction involves the lone pair on O6 into the σ* orbital of O2-C3 and C3-O4. This interaction is almost nearly as strong in all the three conformers ($E_2 \approx 30$ kcal/mol) and therefore probably does not contribute to a particular preference for any of the conformations. The interaction involving the lone pair on O2 and the σ* of C3-O6 is another strong hyperconjugative delocalization that is operative in DMC. This interaction is strong in the cis-cis ($E_2 = 10.9$ kcal/mol) but significantly weaker in the cis-trans ($E_2 = 0.8$ kcal/mol) and the near-trans-near-trans conformers ($E_2 = 0.9$ kcal/mol), due to the altered orientation of the terminal methyl group in the different conformers. Consistent with this observation, the lone pair on O4 to σ* of C3-O6 interaction are nearly equally strong in the cis-cis ($E_2 = 10.9$ kcal/mol) and cis-trans ($E_2 = 9.6$ kcal/mol) since the methyl groups on O4 have the same orientation in both conformers. This interaction is again weak in the near-trans-near-trans structure ($E_2 = 0.9$ kcal/mol).

Table 4.5 shows the increase in energy when each of the interactions mentioned above were selectively suppressed. The deletion energies were the largest for the deletion of the lp(O2)→π*(C3-O6) and lp(O4)→ π*(C3-O6) interactions, followed by lp(O6)→σ*(O2-C3) and lp(O6)→σ*(C3-O4) delocalizations and the lp(O2)→σ*(C3-O6) and lp(O4)→σ*(C3-O6) interactions. It should be mentioned that all these interactions involve the C=O group and belong to the vicinal type of delocalization interactions, which appear to be important in DMC, while the geminal type interactions, such as σ(C3-O4)→σ*(O2-C3), play an insignificant role in conformational preferences in DMC. The importance of the interactions involving the π* orbital is also evidenced by the significant occupancy (~0.3e) of this orbital, obtained from NBO calculation. Electron occupancies of other orbitals involved in the above delocalization interactions are given in Table 4.6. It is clear from this exercise that the delocalization of the lone pair on the methoxy oxygens (O2 and O4) to the π* orbital of the carbonyl group leads to the strongest stabilization, particularly in the cis-cis and cis-trans

Table 4.5 – Interactions deleted, deletion energies, changes in energies for different conformers of DMC.

Conformer	Interaction deleted		Deletion energy (Hartree)	Change in energy (kcal/mol)	Relative change in deletion energy (%)
Cis-cis	1	n^{2}O2→ π*C3-O6 n^{2}O4→ π*C3-O6	-343.403844930	142.7	0.0662
	2	n^{2}O6→ σ*O2-C3 n^{2}O6→ σ*C3-O4	-343.494838883	85.6	0.0397
	3	n^{1}O2→ σ*C3-O6 n^{1}O4→ σ*C3-O6	-343.572011655	37.1	0.0172
	4	n^{1}O2→ σ*C3-O4 n^{1}O4→ σ*O2-C3	-343.619285569	7.5	0.0035
Cis-trans	1	n^{2}O2→ π*C3-O6 n^{2}O4→ π*C3-O6	-343.404190043	139.5	0.0647
	2	n^{2}O6→ σ*O2-C3 n^{2}O6→ σ*C3-O4	-343.490178689	85.5	0.0397
	3	n^{1}O2→ σ*C3-O6 n^{1}O4→ σ*C3-O6	-343.598503993	17.6	0.0081
	4	n^{1}O2→ σ*C3-O4 n^{1}O4→ σ*O2-C3	-343.602474305	15.1	0.0070
Near-trans-near-trans	1	n^{2}O2→ π*C3-O6 n^{2}O4→ π*C3-O6	-343.456364760	93.0	0.0431
	2	n^{2}O6→ σ*O2-C3 n^{2}O6→ σ*C3-O4	-343.475317257	81.1	0.0376
	3	n^{1}O2→ σ*C3-O6 n^{1}O4→ σ*C3-O6	-343.598281457	4.0	0.0018
	4	n^{1}O2→ σ*C3-O4 n^{1}O4→ σ*O2-C3	-343.564866016	24.9	0.0115

Table 4.6 – Electron occupancies of some important NBOs in different conformers of DMC.

NBOs	Occupancy		
	Cis-cis	Cis-trans	Near-trans-near-trans
n^1O2	1.96063	1.95868	1.95535
n^2O2	1.81158	1.81467	1.84181
n^1O4	1.96070	1.96131	1.95533
n^2O4	1.81176	1.82033	1.84198
n^1O6	1.97453	1.97568	1.97593
n^2O6	1.83315	1.82345	1.82562
σO2-C3	1.99087	1.98985	1.99223
σC3-O4	1.99085	1.99335	1.99223
σC3-O6	1.99752	1.99488	1.99391
πC3-O6	1.99566	1.99653	1.99266
σ*O2-C3	0.09667	0.09444	0.11419
σ*C3-O4	0.09679	0.11354	0.11418
σ*C3-O6	0.03434	0.02414	0.02403
π*C3-O6	0.33279	0.32098	0.26200

conformers.

It must be noted that in DMC, the interactions involving the lp(O2)→σ*(C3-O4) and lp(O4)→σ*(C3-O2) are less important compared to the interactions involving the C=O, whereas in dimethoxymethane (DMM), which lacks the C=O group, the interactions involving the methoxy oxygen, play a significant role in the conformational preferences.

For a quantitative evaluation of the relative importance of the geminal and vicinal interactions, we performed an analysis where we systematically deleted the relevant interactions. Table 4.7 shows the increase in energy following such deletions. The increase in energy when all geminal interactions were collectively deleted was compared with that obtained when all vicinal interactions were deleted. This table also shows the increase in energy due to deletion of all delocalization interactions. Fig. 4.6 shows a correlation diagram depicting the increase in energy for geminal and vicinal deletions with respect to each conformer. It can be seen that the vicinal deletion causes a significantly larger increase in energy compared with that obtained when geminal interactions were deleted, indicating that the vicinal interactions are significantly more important in stabilizing the various conformers than geminal interactions. Furthermore, when vicinal interactions were deleted, even the order of conformational preferences was found to be altered. For example, when the vicinal interactions were suppressed, the cis-cis conformer turned out to be the highest in energy, which indicates that this interaction plays a key role in the conformational preference in DMC. It is relevant to note that in some molecules such as trimethyl phosphite, we observed that the geminal interactions, rather than the vicinal, played a key role in conformational preferences.[15]

4.5.3 Comparison of DMC with Dimethoxymethane (DMM) and Methylformate

DMC differs from DMM in that the former has a carbonyl group, which allows for DMC to achieve a planar cis-cis structure, whereas DMM adopts a non-planar G^+G^-

Table 4.7 – Energies of different conformers after deletion of all geminal, all vicinal and all delocalization interactions.

Conformer	Interactions deleted	Deletion energy (Hartree)	Change in energy (kcal/mol)	Relative change in deletion energy (%)
Cis-cis	Geminal	-343.537650732	58.7	0.027
	Vicinal	-342.884758087	468.4	0.218
	All	-342.783541550	531.9	0.247
Cis-trans	Geminal	-343.529766651	60.7	0.028
	Vicinal	-342.906869525	451.6	0.210
	All	-342.793944521	522.4	0.243
Near-trans-near-trans	Geminal	-343.507739648	60.8	0.028
	Vicinal	-342.905191886	438.9	0.204
	All	-342.800574054	504.5	0.234

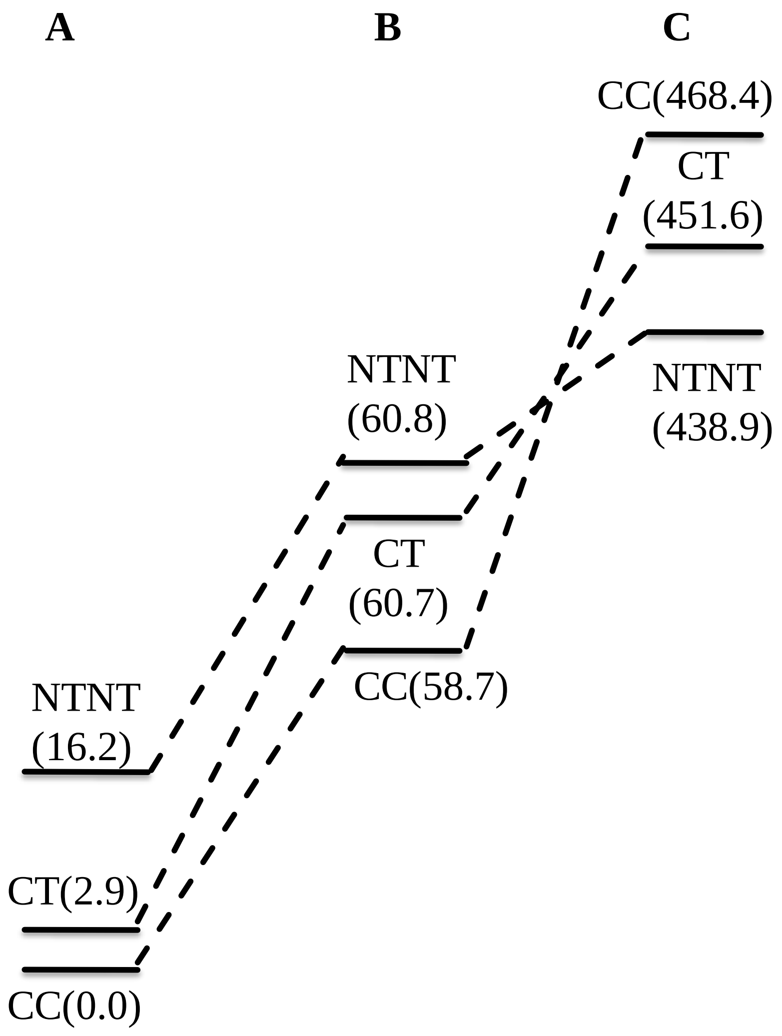

Fig. 4.6 – Correlation diagram showing the increase in energy for the different conformers of DMC, following deletion of various interactions. Deletion energy (kcal/mol) shown in parentheses are relative to the energy of each conformer with all interactions present. (A) No delocalization interactions deleted; (B) all geminal interactions deleted; (C) all vicinal interactions deleted. (Energy levels are not shown to scale.)

configuration,[16] in their respective ground state conformations. Furthermore, the cis-cis structure in DMC, the lowest energy conformer closely resembles the anti-anti (trans-trans in ref. – 16) conformation of DMM, which is its highest energy form. The role of the carbonyl group, and the associated n→π* delocalization is clearly evident from this comparison.

In methylformate, presence of one methoxy group in conjugation with carbonyl group, makes one n→π* delocalization interaction possible, whereas two such interactions are found due to presence of two methoxy groups in DMC. This may lead to a competition between the two interactions in DMC to share the π* orbital of carbonyl group, resulting a relatively low rotational barrier for trans to cis (or vice versa) conversion of methyl group. To compare the rotational barrier in both the molecules, we have carried out calculations on methylformate at B3LYP/6-31++G** level. Several groups have performed calculations on the rotational barrier of methylformate but not at the above mentioned level,[17-19] The computations showed that the rotational barrier of trans to cis conversion in methylformate to be 8.3 kcal/mol, which is higher in comparison with DMC, where the barrier of cis-trans to cis-cis conversion is 6.4 kcal/mol. This type of competitive conjugation was also reported in case of ureas in comparison with corresponding amides.[20,21]

4.5.4 Dipole moment

The computed dipole moments of the different conformers of DMC are given in Table 4.2. The dipole moment of the cis-cis conformer is the lowest at 0.33 D, with the cis-trans and near-trans-near-trans forms having higher values of 3.84 D and 5.43 D, respectively. Using the individual dipole moments of each conformer, the dipole moment of bulk DMC was computed at 328, 350, 412 and 480 K, weighted for their relative populations, at each of the temperatures. Since the near-trans-near-trans conformer has negligible population at all these temperatures, this conformer was not considered in the above calculation. The above temperatures were chosen, as experimental dipole moments of DMC have been reported at these temperatures by Labrenz and Schröer,[5] which are 0.86, 0.89, 0.94 and 1.00 D, respectively. Our computed dipole moments at the above temperatures turned out to be 0.67, 0.74, 0.96 and 1.18 D for DMC, which is in fair agreement with the experimental values. The bulk dipole moment of DMC at room temperature (298 K) was also calculated and it was found to be 0.57 D.

4.6 Results - DMC-H_2O complex

4.6.1 Experimental

Figs. 4.7 and 4.8 show the IR spectra of the DMC-H_2O complex in a N_2 matrix at 12 K, over the spectral region which corresponds to the vibrational features of DMC, while Fig. 4.9 shows the IR features over the region that correspond to features of the H_2O submolecule. It may be noted that the features assigned to DMC-H_2O complex were observed even when no H_2O was deliberately added, as H_2O is a ubiquitous impurity in matrix isolation experiments. However, the fact the features assigned to the DMC-H_2O complex were found to increase in intensity, when the concentration of either of the two reagents were increased, indicates that these features are due to the DMC-H_2O complex. The features due to the complex are clearly shifted and resolved from the features of the precursor molecules and are marked with arrows, in these figures. These features were observed even at low concentrations of DMC and H_2O in the matrix, which suggests that these are due to 1:1 complexes. The infrared features of the complex are also listed in Table 4.8, together with the assignments.

4.6.2 Computational

Structures of the DMC-H_2O complex were computed at the B3LYP/6-31++G** level. The optimized structures of the DMC and H_2O submolecules at the same level of theory were used as starting geometries for obtaining the structures of the complex. Two minima were located on the DMC-H_2O potential energy surface, corresponding to two proton acceptor

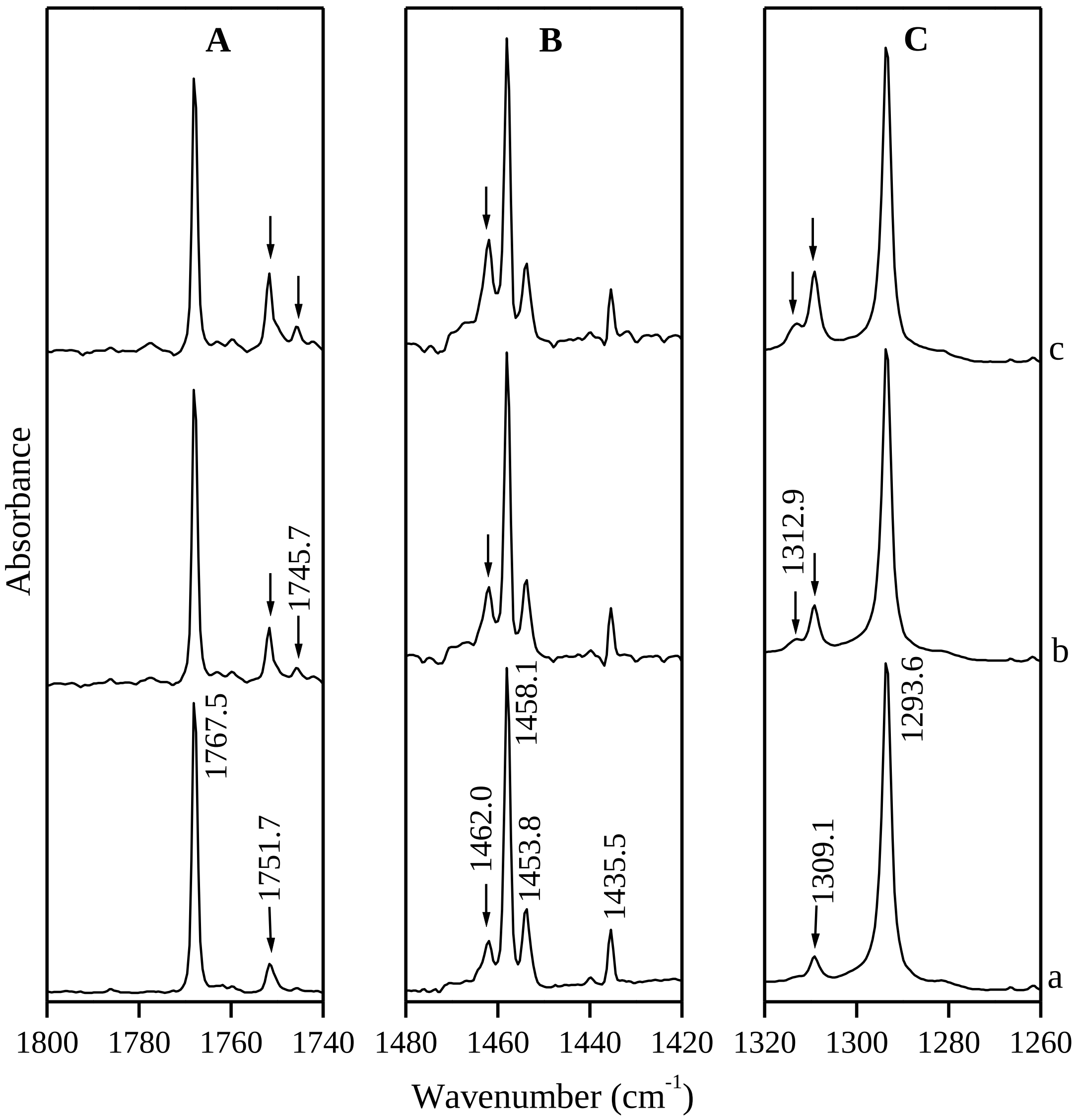

Fig. 4.7 – IR spectra of DMC-H_2O complex (Grid A: 1800-1740 cm^{-1}, Grid B: 1480-1420 cm^{-1}, Grid C: 1320-1260 cm^{-1}), in N_2 matrix at 12 K recorded after annealing the matrix at 30 K for 15 minutes; (a) DMC:H_2O:N_2 (0.5:0:1000); (b) DMC:H_2O:N_2 (0.5:1:1000); (c) DMC:H_2O:N_2 (0.5:1.3:1000). (Ratio 0:1000 of H_2O to N_2 implies no water is added deliberately to the matrix. See text for details.)

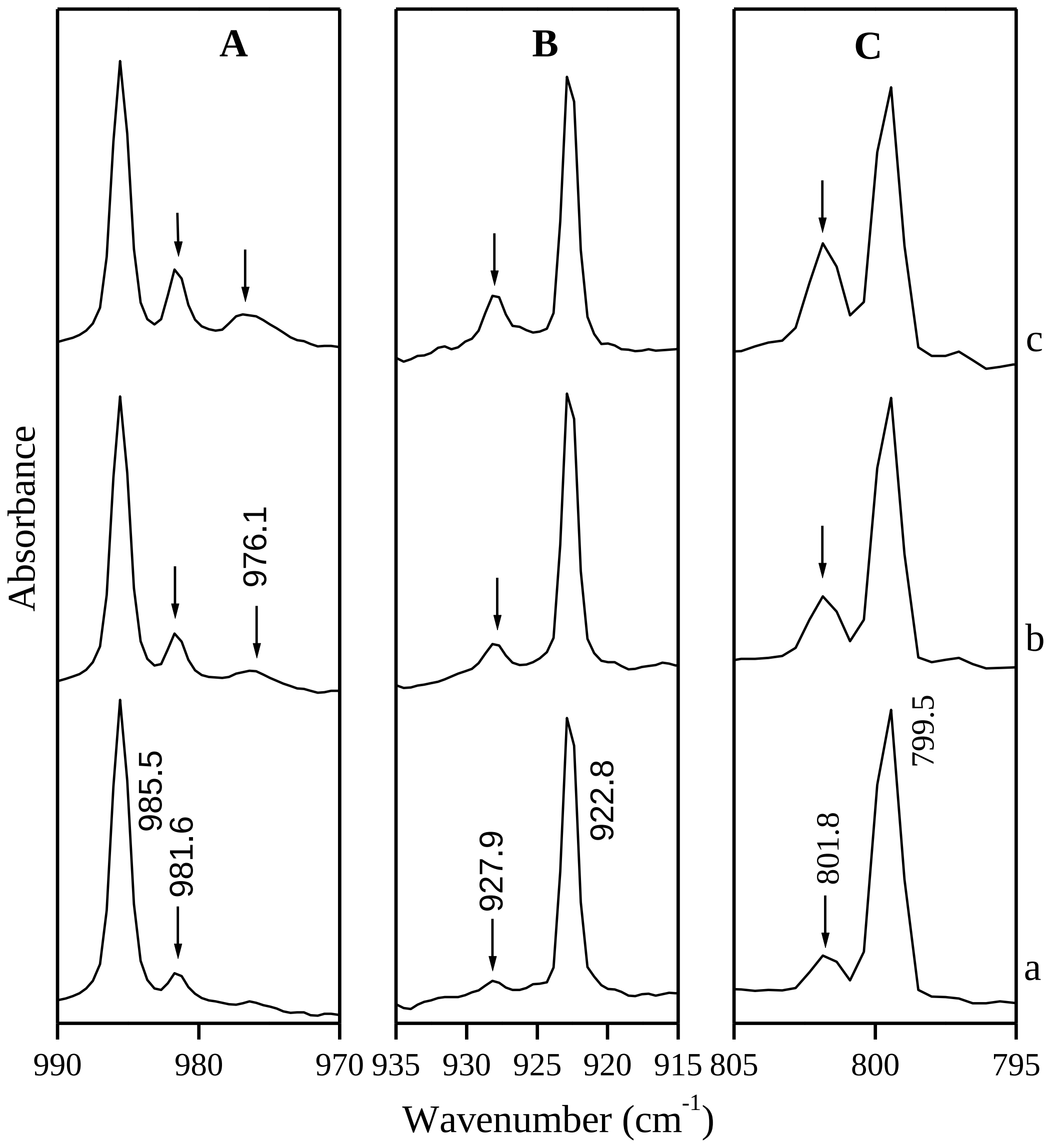

Fig. 4.8 – IR spectra of DMC-H_2O complex (Grid A: 990-970 cm^{-1}, Grid B: 935-915 cm^{-1}, Grid C: 805-795 cm^{-1}), in N_2 matrix at 12 K recorded after annealing the matrix at 30 K for 15 minutes; (a) DMC:H_2O:N_2 (0.5:0:1000); (b) DMC:H_2O:N_2 (0.5:1:1000); (c) DMC:H_2O:N_2 (0.5:1.3:1000). (Ratio 0:1000 of H_2O to N_2 implies no water is added deliberately to the matrix. See text for details.)

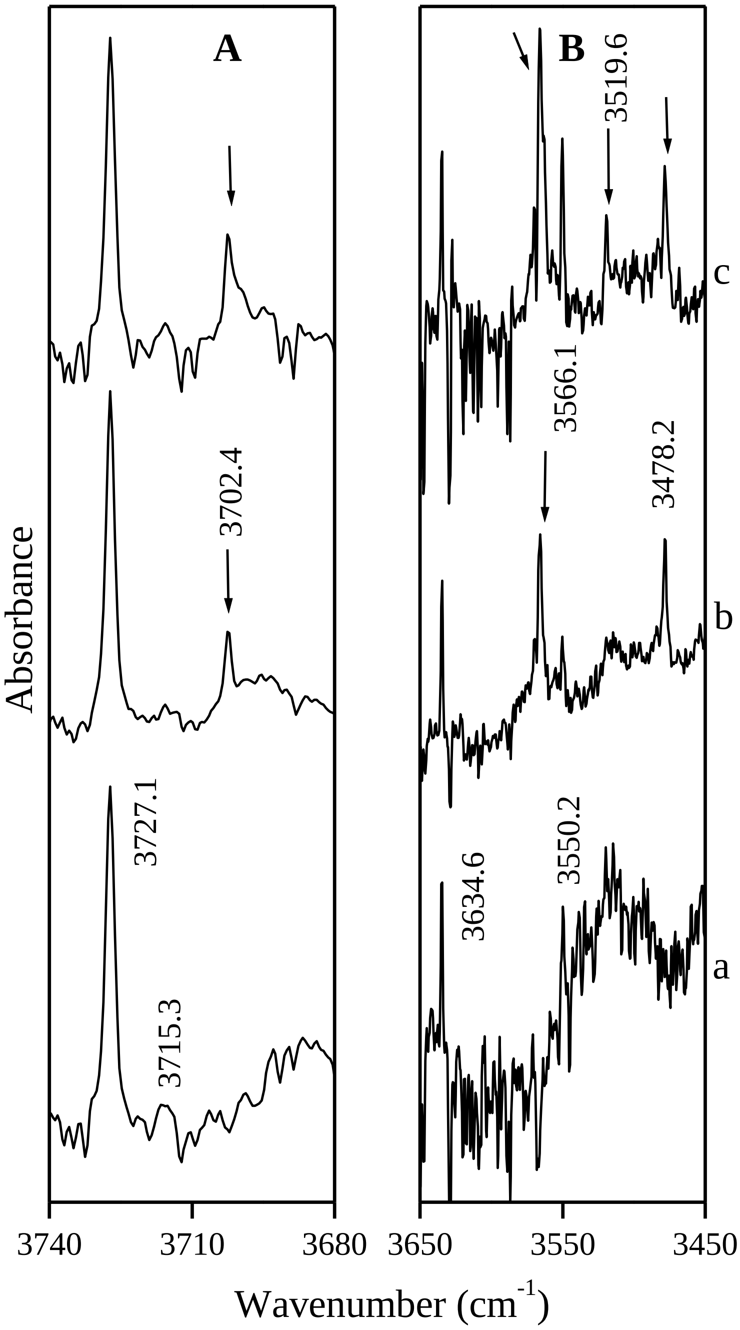

Fig. 4.9 – IR spectra of DMC-H_2O complex (Grid A: 3740-3680 cm^{-1}, Grid B: 3650-3450 cm^{-1}), in N_2 matrix at 12 K recorded after annealing the matrix at 30 K for 15 minutes; (a) DMC:H_2O:N_2 (0:1:1000); (b) DMC:H_2O:N_2 (0.25:1:1000); (c) DMC:H_2O:N_2 (0.5:1:1000).

Table 4.8 – Experimental and calculated (B3LYP/6-31++G theory) vibrational wavenumbers (cm^{-1}) of the DMC(cis-cis)-H_2O (1:1) complex.**

Experiment			**Calculation**[a]					**Modes**
DMC	**Complex**	**Δν**[b]	**Cis-cis**	**Complex 1 (Carbonyl)**	**Δν**	**Complex 2 (Methoxy)**	**Δν**	**DMC**[c]
799.5	801.8	2.3	774.0(28)[d]	774.4(30)	0.4	770.8(29)	-3.2	ν_{28} CO_3 out-of-plane def
922.8	927.9	5.1	909.4(28)	914.3(20)	4.9	910.0(39)	0.6	ν_8 CO_2 sym stretch
985.5	976.1	-9.4						ν_{22} CH_3-O stretch
	981.6	-3.9	975.9(72)	964.6(79)	-11.3	965.6(75)	-10.3	
1293.6	1309.1	15.5	1293.6(831)	1316.0(765)	22.4	1283.0(792)	-10.6	ν_{20} CO_2 antisym stretch
	1312.9	19.3						
1435.5	-	-	1438.2(9)	1439.1(17)	0.9	1439.4(9)	1.2	ν_5 CH_3 sym def
1453.8	-	-	1457.7(16)	1463.8(34)	6.1	1456.9(7)	-0.8	ν_{26} CH_3 antisym def
1458.1	1462.0	3.9	1458.9(87)	1465.4(90)	6.5	1458.4(77)	-0.5	ν_{19} CH_3 sym def
1767.5	1745.7	-21.8						ν_3 C=O stretch
	1751.7	-15.8	1757.5(341)	1732.5(421)	-25.0	1770.2(367)	12.7	
Water	**Complex**	**Δν**	**Water**	**Complex 1 (Carbonyl)**	**Δν**	**Complex 2 (Methoxy)**	**Δν**	**Water**
1597.0	-	-	1566.5(87)	1594.0(85)	27.5	1587.4(86)	21.9	ν_2 Bending
3634.6	3566.1	-68.5	3611.3(5)	3508.8(355)	-102.5	3561.2(190)	-50.1	ν_1 Sym Stretch
3727.1	3702.4	-24.7	3727.1(53)	3695.7(110)	-31.4	3703.0(130)	-24.1	ν_3 Antisym Stretch

[a] Scaled with a factor 0.9786 for the vibrational modes of DMC and the bending mode of water; OH stretching modes of water were scaled with 0.9484 (See text for details).

[b] $\Delta\nu = \nu(\text{complex}) - \nu(\text{monomer})$.

[c] Assignments performed in ref. 9.

[d] IR intensities (km/mol) are in parenthesis.

sites on the DMC molecule. Complex 1 (Fig. 4.10a) represents the structure of the complex where the carbonyl oxygen on DMC served as the proton acceptor, whereas in complex 2 (Fig. 4.10b), the methoxy oxygen was the proton acceptor. Stabilization energies for both the complexes calculated at different levels of theories are shown in Table 4.9. The ZPE and BSSE corrected interaction energies are also shown in the same table. Complex 1 corresponded to the global minimum with BSSE corrected stabilization energy of 5.6 kcal/mol, while complex 2 was less exothermic with a stabilization energy of 3.8 kcal/mol.

The hydrogen bonded distances in the two complexes also show a correlation with the strength of the complexes. The distance between the hydrogen (H13) of H_2O and the carbonyl oxygen (O6) of DMC was computed to be 1.928 Å in complex 1, which is the stronger of the two hydrogen bonded complexes. The corresponding distance between the hydrogen (H13) of H_2O and the methoxy oxygen (O2) of DMC in complex 2 was found to be 2.014 Å. Furthermore, we also observed secondary interactions between the O14 of H_2O and H10 and H12 of DMC in complex 1 as indicated by our AIM calculation, which will be discussed in the next section. The bond distances between O14-H10 and O14-H12 in complex 1 are 2.847 and 2.843 Å respectively.

The infrared frequencies of both the complexes were computed and scaled as indicated earlier and are shown in Table 4.8.

The higher energy cis-trans conformer had only a small population at room temperature and hence was not considered in the assignment of the experimental features of the DMC- H_2O complex.

4.7 Discussions – DMC-H_2O complex

4.7.1 Vibrational assignments

Our computations indicated that two types of complexes can be formed; the global minimum being the carbonyl complex, while the methoxy complex corresponded to a local

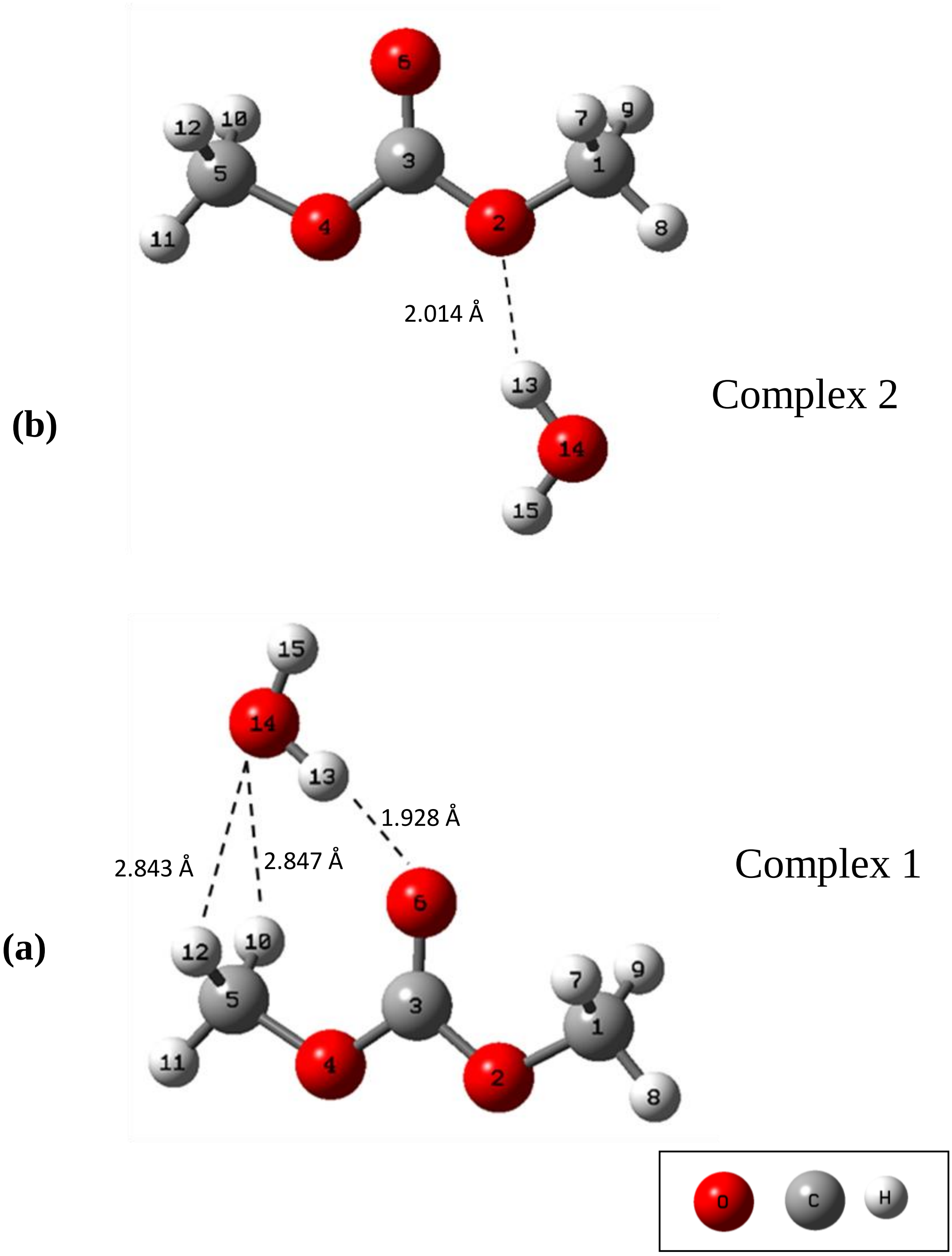

Fig. 4.10 – Computed structures of DMC-H_2O (1:1) complex, at the B3LYP/6-31++G** level. (a) Complex 1: H-bond at the carbonyl oxygen of DMC (b) Complex 2: H-bond at the methoxy oxygen of DMC.

Table 4.9 – Raw[a]/ZPE[b] corrected/BSSE[c] corrected interaction energies (ΔE) in kcal/mol for the DMC-H_2O (1:1) complexes.

Complex	**B3LYP/6-31++G****			**B3LYP/6-311++G****			**MP2/6-31++G****		
	Raw	**ZPE corrected**	**BSSE corrected**	**Raw**	**ZPE corrected**	**BSSE corrected**	**Raw**	**ZPE corrected**	**BSSE corrected**
Complex 1	-6.0	-4.3	-5.6	-5.8	-4.2	-5.5	-6.8	-5.2	-5.5
Complex 2	-4.3	-2.9	-3.8	-4.3	-3.0	-3.9	-5.7	-4.3	-3.9

[a] Raw interaction energies refer to energies not corrected for either ZPE or BSSE.
[b] Zero point energy.
[c] Basis set superposition error.

minimum. Our previous work on the complexes of C_2H_2-MeOH[22,23] and C_2H_2-C_2H_4[11] have shown that the matrix allows for the trapping and identification of both global and local minima; hence when assigning the experimental features of the complex, we considered the possibility that both complexes may be produced in our matrix when DMC and H_2O were codeposited. We present below the assignments of the various modes in the DMC-H_2O complexes.

4.7.1.1. Features of the DMC submolecule in the DMC-H_2O complex

4.7.1.1.1. C=O stretch (ν_3)

This mode provides the best indicator to differentiate between complexes 1 and 2. The carbonyl complex of DMC-H_2O displays a red shift for the C=O stretch relative to that in uncomplexed DMC, while the methoxy complex show a blue shift for the same mode. In our experiments, we observed a strong feature of the DMC-H_2O complex at 1751.7 cm^{-1} (Fig. 4.7, Grid A) which is shifted to the red of the C=O stretching feature of uncomplexed DMC occurring at 1767.5 cm^{-1}, indicating the formation of the carbonyl complex. The experimentally observed shift is consistent with the computed red shift of 25 cm^{-1}. We also observed a red shifted feature at 1745.7 cm^{-1}, which is probably due to the matrix site effect. No feature to the blue was observed, indicating that the methoxy complex was not formed in the matrix.

4.7.1.1.2. CH_3 symmetric deformation (ν_{19})

In the co-depositing experiments, this mode was observed at 1462.0 cm^{-1} in the complex (Fig. 4.7, Grid B), which is blue shifted from the feature in uncomplexed DMC by 3.9 cm^{-1}. This shift agrees well with our computations for complex 1, which indicated this feature to be blue shifted by 6.5 cm^{-1}.

4.7.1.1.3. O-C-O antisymmetric stretch (ν_{20})

Experimentally, this mode in monomer DMC occurs at 1293.6 cm^{-1}, new features were observed as doublet at 1309.1 and 1312.9 cm^{-1}, a red shift of 17.4 cm^{-1}. The experimental value agrees well with the computed value at 1316.0 cm^{-1}, a red shift of 22.4 cm^{-1} for the carbonyl complex.

4.7.1.1.4. CH_3-O stretch (ν_{22})

This mode is computed to occur in the complex, red shifted from the feature of the uncomplexed DMC submolecule. Experimentally, a feature was observed at 981.6 cm^{-1} (Fig. 4.8, Grid A), which could be attributed to the DMC-H_2O complex based on its concentration dependence and its occurrence to the red of the ν_{22} feature of the DMC submolecule. This feature is therefore assigned to this mode in complex 1. The red shifted feature at 976.1 cm^{-1} may be due to the site splitting as observed in case of ν_3 and ν_{20} mode.

4.7.1.1.5. CO_2 symmetric stretch (ν_8)

This mode in the complex is observed at 927.9 cm^{-1} (Fig. 4.8, Grid B) and occurs blue shifted by 5.1 cm^{-1} from the corresponding feature of the DMC submolecule. This shift compares well with the computed shift of 4.9 cm^{-1} for this mode of complex 1.

4.7.1.1.6. CO_3 out-of-plane deformation (ν_{28})

Corresponding to this mode, a feature is observed at 801.8 cm^{-1} (Fig. 4.8, Grid C) in experiments where DMC and H_2O were codeposited, which is blue shifted from the same mode of uncomplexed DMC and is assigned to complex 1. Computations also indicate this complex to be blue shifted.

4.7.1.2. Features of the H_2O submolecule in the DMC-H_2O complex

4.7.1.2.1. H_2O symmetric stretch (ν_1)

The experimental feature for this mode is observed at 3566.1 cm^{-1} (Fig. 4.9, Grid B), a red shift of 68.5 cm^{-1} from the same mode of uncomplexed H_2O. This feature was computed to have a red shift of 102.5 cm^{-1}. Interestingly Complex 2 is computed to show a red shift of 50.1 cm^{-1} for this mode, which seemingly agrees well with the experimentally observed shift.

However, an examination of the features of the DMC submolecule has already ruled out the formation of complex 2 and hence the red shifted feature of H_2O cannot be attributed to the methoxy complex. The experimentally observed feature must therefore be due to the carbonyl DMC-H_2O complex. As can be seen from the table 4.8, the calculated shift for the symmetric stretching frequency is more than the experimental shift. To address this problem we then optimized the H_2O and DMC-H_2O complex 1, at MP2/6-31++G** level and calculated the frequency using numerical method. After appropriate scaling the corresponding shift in this mode was found to be 76.3 cm^{-1} which agrees well with the experimental shift.

In the figure 4.9 we also observed features at 3519.6 and 3478.2 cm^{-1} which may be due to DMC-$(H_2O)_n$ (n>1) complexes.

4.7.1.2.2 H_2O antisymmetric stretch (ν_3)

The ν_3 mode of the H_2O submolecule in the DMC-H_2O complex was observed at 3702.4 cm^{-1} (Fig. 4.9, Grid A), with a red shift of 24.7 cm^{-1} from the feature of uncomplexed H_2O. This shift compares well with the computed shift of 31.4 cm^{-1} for complex 1.

4.7.1.2.3 H_2O bending (ν_2)

The computed shift for the bending mode in H_2O was 27.5 cm^{-1}; however an examination of this region of the experimental infrared spectrum did not reveal a feature that could be assigned to this mode for the DMC-H_2O complex. It is likely that this feature is probably masked by the features due to the water dimer.

The features at 3715.3, 3550.1 cm^{-1} shown in Fig. 4.9, which are also found in experiments where water alone was deposited, are due to the water dimers.[24]

4.7.2 AIM analysis

An examination of the charge density topology was performed using the atoms–in-molecules (AIM) theory of Bader. (3, -1) bond critical points (BCP) and (3, +1) ring critical points (RCP) that could be associated with complexes 1 and 2 were located. The electron density ($\rho(r_c)$) and Laplacian of electron density ($\nabla^2\rho(r_c)$) were computed for the critical points and the values are shown in Table 4.10. The $\rho(r_c)$ and $\nabla^2\rho(r_c)$ values for HOH···O bond critical points in both the complexes were found to be in the order of 10^{-2} au, but the magnitude of values being larger in complex 1 than complex 2. In complex 1, a secondary interaction was also present between O14 of H_2O and methyl group of DMC. The secondary interactions are mentioned as BCP2 and RCP in Table 4.10. We had observed similar secondary interaction in the trimethylphosphate-H_2O complexes.[25]

4.8 Conclusion

Clearly resolved features for carbonyl stretching, O-C-O antisymmetric stretching and other vibrational features of higher energy cis-trans conformer of DMC were observed in our experiments; which were not resolved in earlier studies. Spectra of DMC recorded in solid N_2 allowed us to present a detailed vibrational spectrum of the higher energy cis-trans conformer of DMC. NBO analysis on the optimized geometries clearly indicated that vicinal interactions involving the C=O group, play a significant role in the conformational preferences of DMC. $n\rightarrow\pi^*$ and $n\rightarrow\sigma^*$ delocalization interactions involving the C=O group are the major delocalization interactions found in these conformations, which directs the molecular framework to adopt a planar cis-cis structure.

For the first time, we trapped the 1:1 complex of DMC-H_2O in inert gas matrix and recorded its IR spectra. The IR spectra of the matrix isolated DMC-H_2O complex, together with *ab initio* computations, indicate that the global minimum is a carbonyl bound hydrogen-bonded complex, where the carbonyl oxygen on DMC serves as a proton acceptor. A local minimum where the methoxy oxygen was the proton acceptor was also indicated by the computations; however no experimental evidence was found in the matrix for this complex.

Table 4.10 – Properties of different critical points present in DMC–H_2O complexes as a result of AIM analysis.

Complex	**Critical point**	**$\rho(r_c)$**	**$\nabla^2\rho(r_c)$**
Complex 1	BCP 1	0.02419	-0.01884
	BCP 2	0.00496	-0.00588
	RCP	0.00496	-0.00596
Complex 2	BCP	0.02054	-0.01588

References

---

[1] B. Collingwood, H. Lee, J. K. Wilmshurst, Aust. J. Chem., 1966, *19*, 1637.

[2] F. C. Mijlhoff, J. Mol. Struct., 1977, *36*, 334.

[3] J. E. Katon, M. D. Cohen, Can. J. Chem., 1974, *52*, 1994.

[4] J. E. Katon, M. D. Cohen, Can. J. Chem., 1975, *53*, 1378.

[5] D. Labrenz, , W. Schröer J. Mol. Struct., 1991, *249*, 327.

[6] O. Okada, Mol. Phys.,1998, *93*, 153.

[7] L. Gontrani, O. Russina, F. C. Marincola, R. Caminiti, J. Chem. Phys., 2009, *131*, 244503.

[8] R. J. Gillespie, E. A. Robinson, J. Pilme, Chem. Eur. J., 2010, *16*, 3663.

[9] H. Bohets, B. J. van der Veken., Phys. Chem. Chem. Phys., 1999, *1*, 1817.

[10] L. Bernad, M. Seidl, I. Kohl, K. R. Liedl, E. Mayer, O. Galvez, H. Grothe, T. Loerting, Angew. Chem. Int. Ed., 2011, *50*, 1939.

[11] K. Sundararajan, K. Sankaran, K. S. Viswanathan, A. D. Kulkarni, S. R. Gadre, J. Phys. Chem. A, 2002, *106*, 1504.

[12] G. C. Pimentel, S. W. Charles, Pure and Appl. Chem., 1963, *7*, 111.

[13] R. F. W. Bader, Atoms in Molecules. A Quantum Theory, Clarendon Press. Oxford, 1994.

[14] A. S. Gordon, W. P. Norris, J. Phys. Chem., 1965 *69*, 3013.

[15] N. Ramanathan, K. Sundararajan, B. P. Kar, K. S. Viswanathan, J. Phys. Chem A., 2011, *115*, 10059.

[16] V. Venkatesan, K. Sundararajan, K. Sankaran, K. S. Viswanathan, Spectrochim. Acta Part A, 2002, *58*, 467.

[17] K. B. Wiberg, K. E. Laidig, J. Am. Chem. Soc., 1987, *109*, 5935.

[18] T. Uchimaru, S. Tsuzuki, M. Sugie, A. Sekiya, Chem. Phys. Lett., 2003, *373*, 182.

[19] D. Cain, D. M. Pawar, M. S. Stewart, H. Billings Jr., E. A. Noe, J. Org. Chem., 2001, *66*, 6092.

---

[20] J. C. Williams, A. E. McDermott, J. Phys. Chem., 1993, *97*, 12393.

[21] C. Dugave, L. Demange, Chem. Rev., 2003, *103*, 2475.

[22] K. Sundararajan, K. S. Viswanathan, J. Mol. Struct., 2006, *798*, 109.

[23] K. V. J. Jose, S. R. Gadre, K. Sundararajan, K. S. Viswanathan, J. Chem. Phys., 2007, *127*, 104501.

[24] R. M. Bentwood, A. J. Barnes, W. J. Orville-Thomas, J. Mol. Spectrosc., 1980, *84*, 391.

[25] K. Sankaran, V. Vidya, K. S. Viswanathan, L. George, S. Singh, J. Phys. Chem. A, 1998, *102*, 2944.

CHAPTER 5

STUDIES ON CONFORMATION OF DIETHYL CARBONATE AND ITS COMPLEXES WITH WATER

5.1 Introduction

Studies on diethyl carbonate (DEC) is described in this chapter, which addresses the problem of conformational orientations in long alkyl chain organic carbonates. There have been a few reports on the conformations of DEC. Chia et al. have measured the dipole moment and molar Kerr constant of DEC in carbon tetrachloride solution at 25° C and reported the presence of eight planar and a number of non-planar conformers.[1] Labrenz and Schröer performed dielectric measurements and further carried out quantum mechanical calculations[2] on the conformations of DEC and concluded that DEC predominantly exists in gauche-gauche and gauche-trans conformers. Wang et al. have assigned the IR and Raman bands of DEC to the cis-cis and trans-trans conformers.[3] To the best of our knowledge this is the only vibrational assignment reported in literature and there is no detail study on the conformations of DEC have been reported using matrix isolation infrared technique and *ab initio* computations.

5.2 Experimental details

Diethyl carbonate, (Spectrochem, 99% purity) was used without any further purification, except subjecting it to several freeze-pump-thaw cycles, before use. The sample to matrix ratios was varied from 0.05:1000 to 5:1000. The vapor pressure data reported by Kozlova et al.[4] was used to prepare the matrix-sample mixture of desired ratio. Ar and N_2 were used as matrix gases. Details of experimental procedure are discussed in chapter 2.

Experiments were performed by maintaining the effusive source at two different nozzle temperatures, viz. 298 and 423 K. A supersonic jet source was also used to deposit the matrix mixture. A sample to matrix ratios of 1:1000 (DEC:Ar) gave broad features in the supersonic jet deposition; hence a smaller sample to matrix ratio (0.05:1000) was used in these experiments. In supersonic jet experiments, the matrix was deposited for ~2 h to obtain a good signal. However in supersonic jet experiment in N_2 matrix we have used a sample to matrix ratio 0.5:1000.

Infrared spectrum, over the region 4000 to 400 cm^{-1}, of DEC in the vapor phase was recorded using a 10 cm path length gas cell. IR spectra of the liquid DEC (neat) were also recorded over the same spectral region, where the liquid sample was sandwiched between two KBr windows.

On annealing the matrix, new features were observed which was likely due to DEC-H_2O adduct. However, the possibility could not excluded that these new features may be due to conformers of DEC that were not initially deposited in the matrix but were produced by interconversion during annealing and/or due to higher clusters of DEC. To resolve these issues we deliberately codeposited H_2O with DEC with a view to studying the DEC-H_2O complex. The concentration of DEC and water were varied independently over the range 0:1000 to 2:1000 for DEC and 0:1000 to 1.5:1000 for water. The matrix was then annealed at different temperatures to ease the complex formation.

5.3 Computational details

Ab initio calculations were performed at the B3LYP/6-31++G** level of theory. Geometry optimization was performed to arrive at the structures of various conformers and their vibrational frequencies. Transition state structures were also computed to calculate the barriers for conformer interconversion among the conformers. Natural Bond Orbital (NBO) analysis were performed at B3LYP/6-31++G** level of theory.

The structures of the 1:1 DEC-H_2O complexes were optimized and vibrational frequency calculations were performed on the optimized geometries. Atoms-in-molecules (AIM) calculations were performed to examine the 1:1 DEC-H_2O complexes. Stabilization energies, corrected separately for zero point energy (ZPE) and basis set superposition errors (BSSE) were calculated for the complexes.

The results and discussions on the conformations of DEC will be discussed first and in a subsequent section the DEC-H_2O hydrogen bonded complex will be presented.

5.4 Results – Conformations of DEC

5.4.1 Experimental

Figs. 5.1 and 5.2 show the IR spectra of DEC recorded under different conditions. Fig. 5.1 spans the region 1800-1700 cm^{-1} (Grid A), 1500-1350 cm^{-1} (Grid B), 1350-1200 cm^{-1} (Grid C) whereas Fig. 5.2 covers the region 1200-760 cm^{-1}. In both the figures, trace ‘a’ and ‘b’ show the IR spectra of DEC isolated in N_2 and Ar matrices, respectively. In these experiments, the sample to matrix ratio of 1:1000 was maintained and deposited using an effusive source kept at 298 K. We have also carried out experiments using a hot nozzle and a supersonic jet source.

For comparison, the infrared spectra of DEC recorded in gas and liquid phases are also shown in both Figs. 5.1 and 5.2 (trace ‘c’ and ‘d’ respectively).

Figs. 5.3 and 5.4 show the IR spectra of matrix isolated DEC in Ar matrix, at different experimental conditions, over the same spectral region as in Figs 5.1 and 5.2 respectively. Traces ‘a’ and ‘b’ in both these figures (Figs. 5.3 and 5.4) show the IR spectra corresponds to the experiments, where an effusive nozzle source maintained at two different temperatures 298 and 423 K respectively, was used for deposition. IR spectrum recorded for supersonic jet experiment with sample to matrix ratio 0.05:1000 is shown in trace ‘c’. Trace ‘d’ corresponds to the spectra recorded after annealing the matrix of trace ‘a’ at 35 K for 15 minutes. Figs. 5.5 and 5.6 show the spectra of DEC in N_2 matrix, the experimental conditions were similar to Ar matrix. However, an annealing temperature of 30 K was used for N_2 matrix and the sample to matrix ratio of 0.5:1000 was maintained for the supersonic jet experiments.

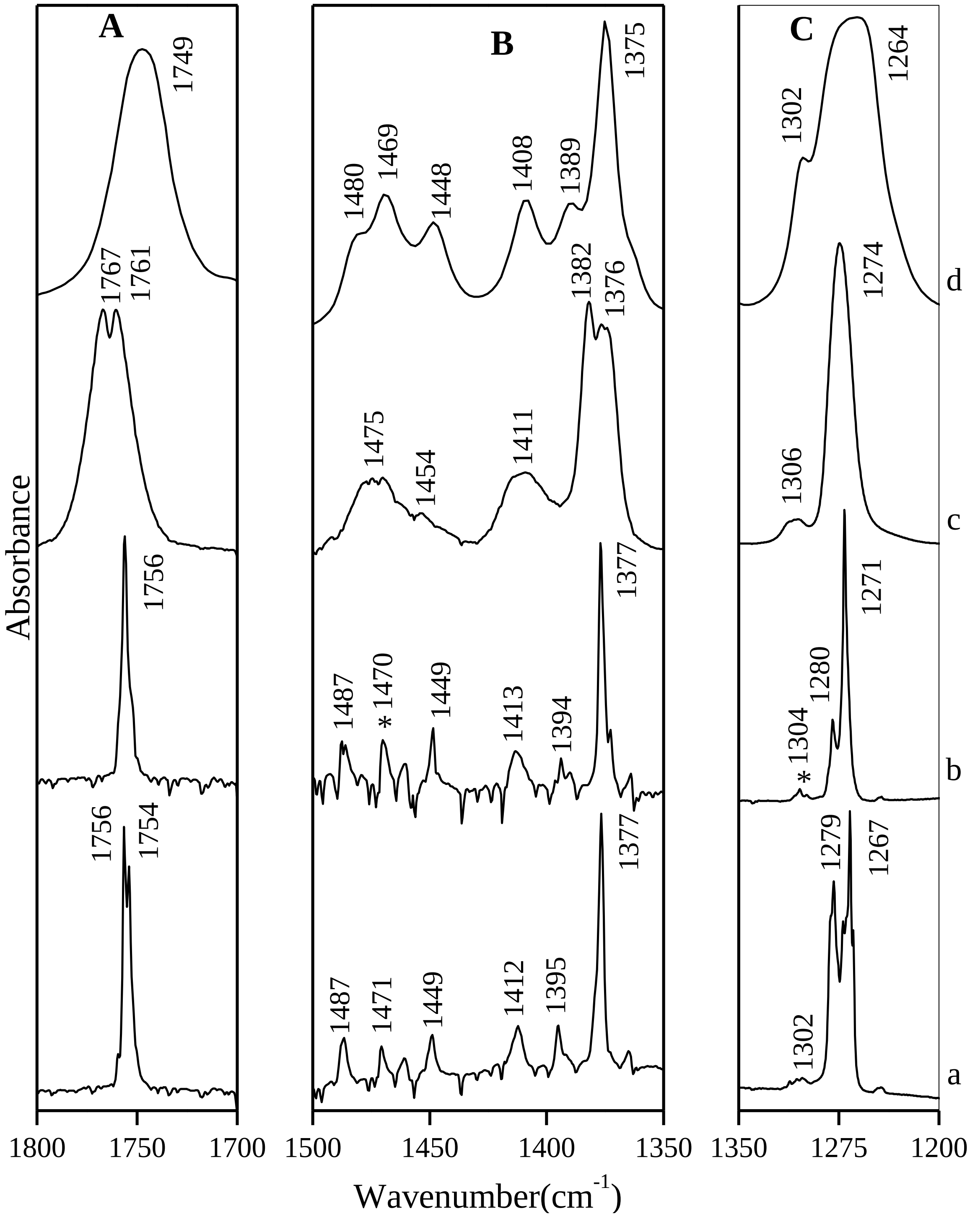

Fig. 5.1 – IR spectra of DEC (Grid A: 1800-1700 cm^{-1}, Grid B: 1500-1350 cm^{-1} and Grid C: 1350-1200 cm^{-1}). (a) in N_2 matrix at 12 K; (b) in Ar matrix at 12 K; (c) gas phase; (d) liquid phase.

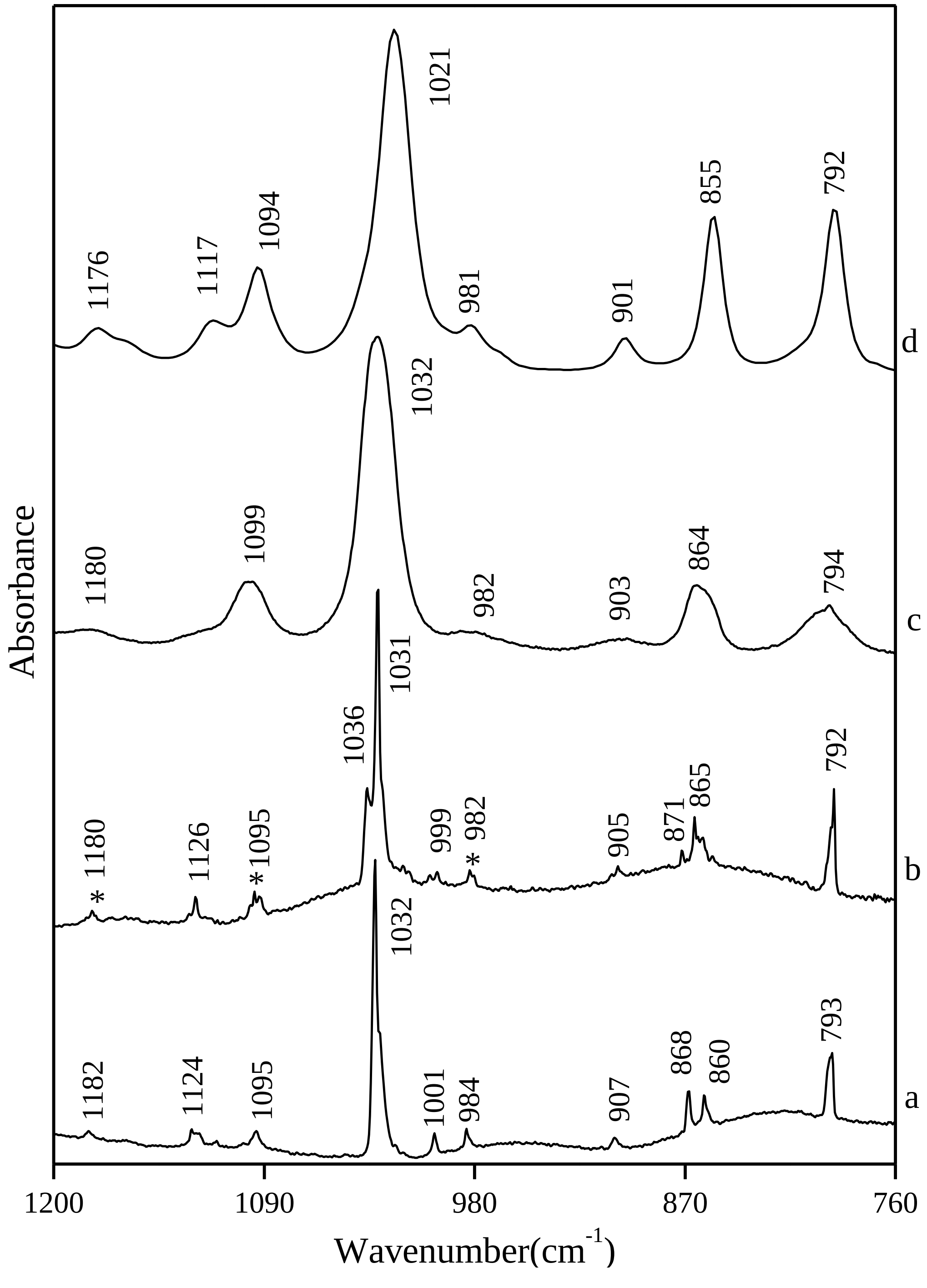

Fig. 5.2 – IR spectra of DEC (1200-760 cm^{-1}). (a) in N_2 matrix at 12 K; (b) in Ar matrix at 12 K; (c) gas phase; (d) liquid phase.

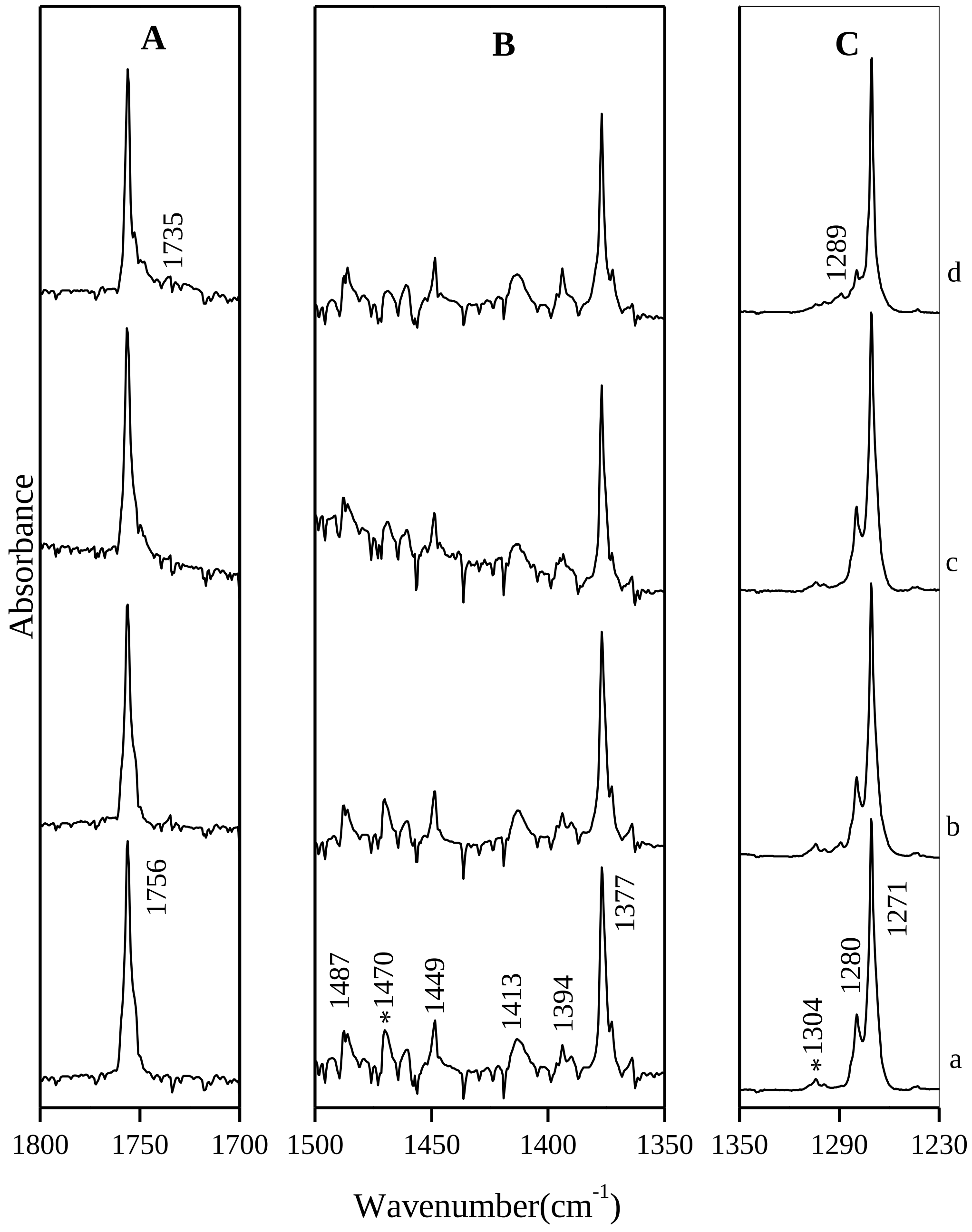

Fig. 5.3 – IR spectra of DEC in Ar matrix at 12 K under different experimental conditions (Grid A: 1800-1700 cm^{-1}, Grid B: 1500-1350 cm^{-1} and Grid C: 1350-1230 cm^{-1}). (a) Using an effusive nozzle source maintained at 298 K and (b) at 423 K; (c) Using a supersonic pulsed jet; (d) same as '(a)' after annealing at 35 K for 15 minutes. Traces (a), (b), (d) represent experiments with DEC:Ar at 1:1000 and (c) with ratio 0.05:1000.

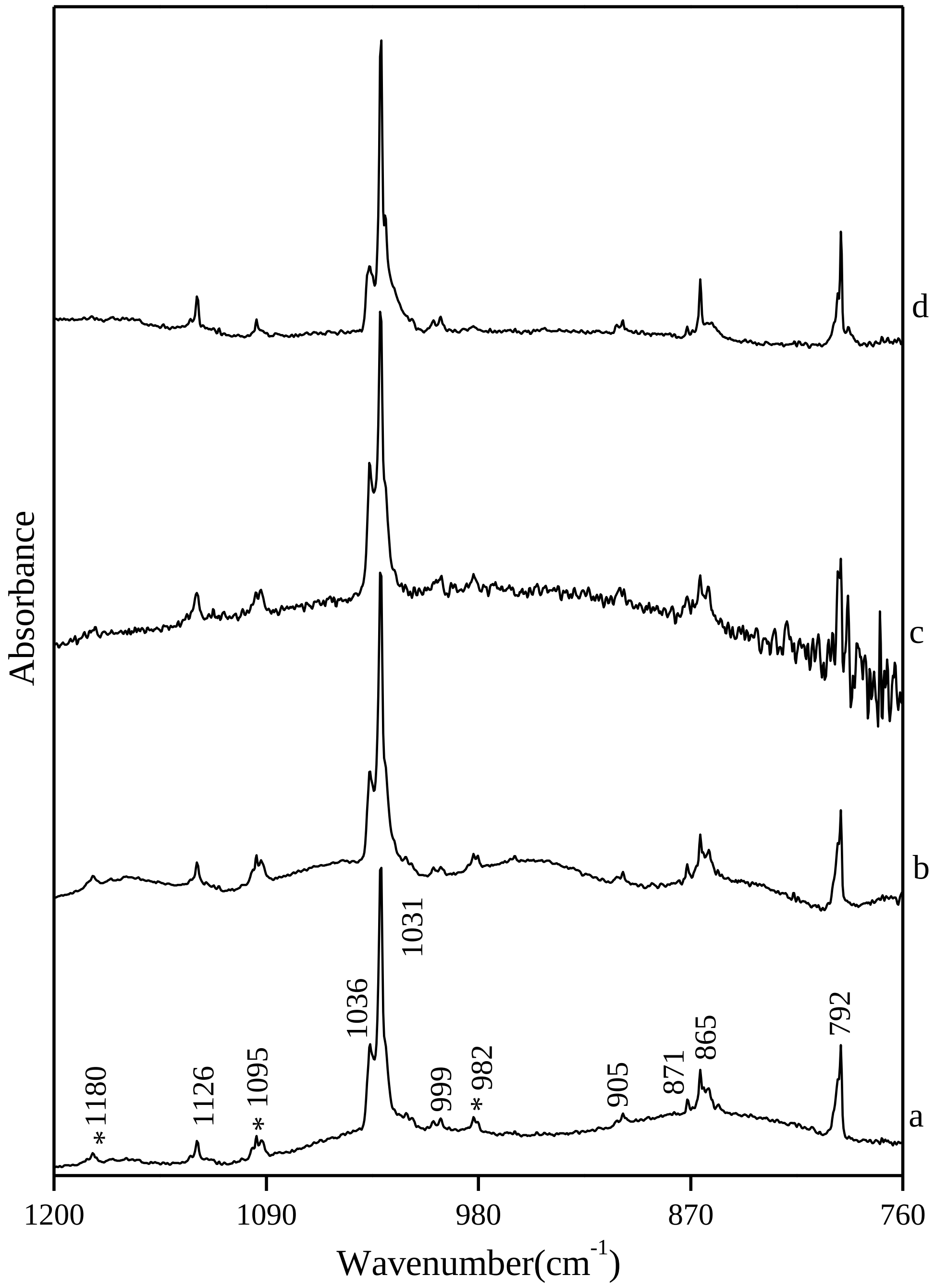

Fig. 5.4 – IR spectra of DEC in Ar matrix at 12 K under different experimental conditions (1200-760 cm^{-1}). (a) Using an effusive nozzle source maintained at 298 K and (b) at 423 K; (c) Using a supersonic pulsed jet; (d) same as '(a)' after annealing at 35 K for 15 minutes. Traces (a), (b), (d) represent experiments with DEC:Ar at 1:1000 and (c) with ratio 0.05:1000.

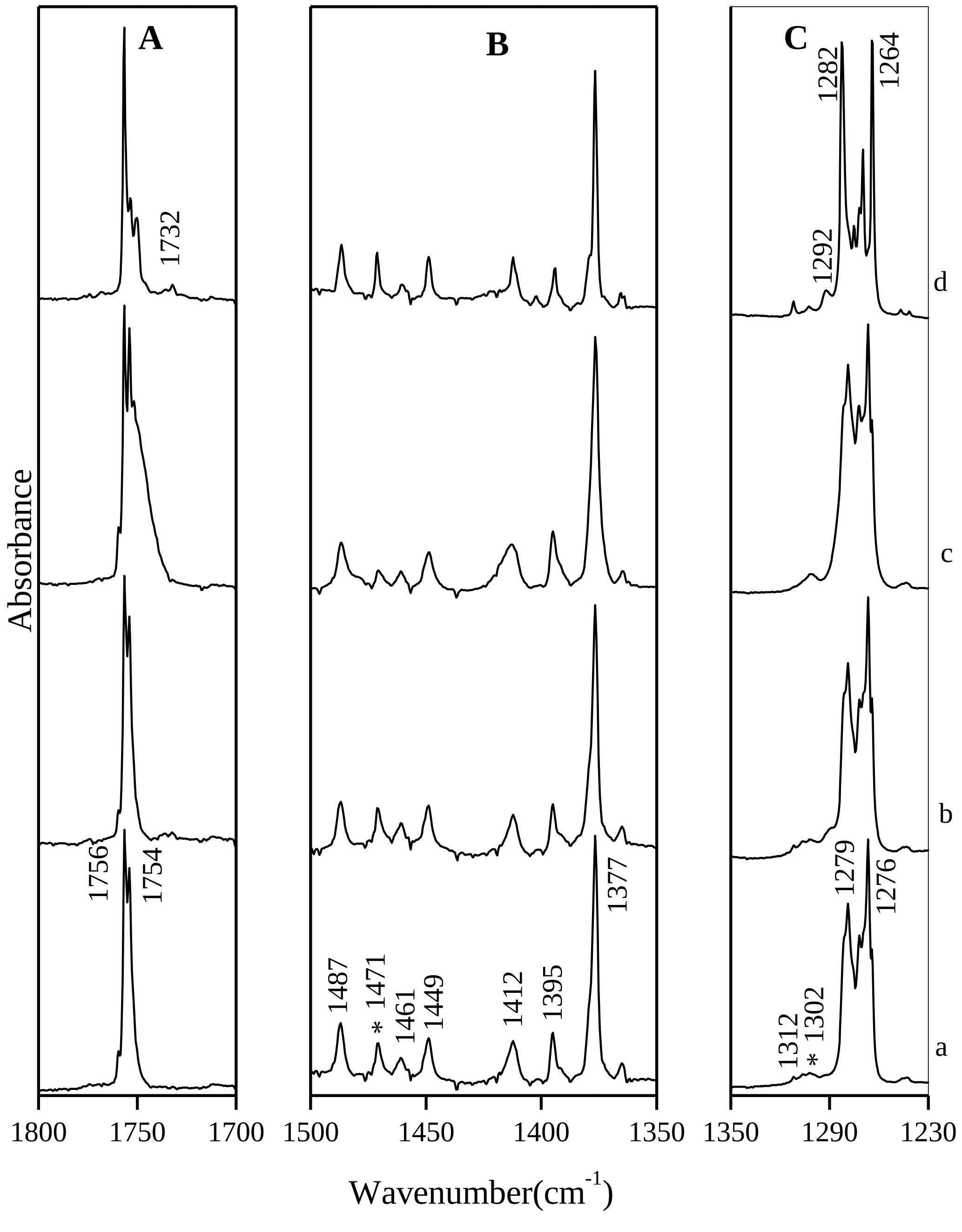

Fig. 5.5 – IR spectra of DEC in N_2 matrix at 12 K under different experimental conditions (Grid A: 1800-1700 cm^{-1}, Grid B: 1500-1350 cm^{-1} and Grid C: 1350-1230 cm^{-1}). (a) Using an effusive nozzle source maintained at 298 K and (b) at 423 K; (c) Using a supersonic pulsed jet; (d) same as '(a)' after annealing at 35 K for 15 minutes. Traces (a), (b), (d) represent experiments with DEC:N_2 at 1:1000 and (c) with ratio 0.5:1000.

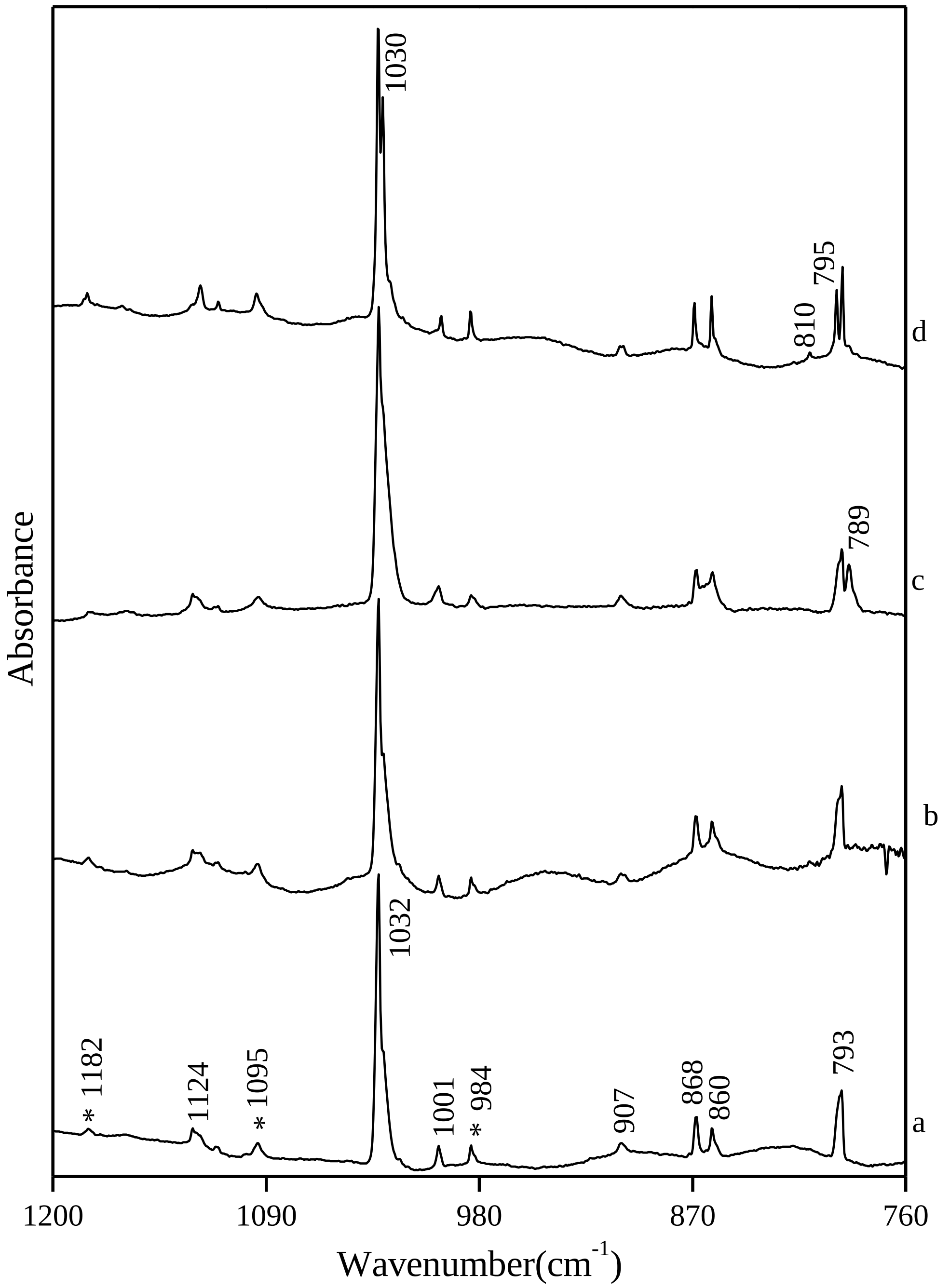

Fig. 5.6 – IR spectra of DEC in N_2 matrix at 12 K under different experimental conditions (1200-760 cm^{-1}). (a) Using an effusive nozzle source maintained at 298 K and (b) at 423 K; (c) Using a supersonic pulsed jet; (d) same as '(a)' after annealing at 35 K for 15 minutes. Traces (a), (b), (d) represent experiments with DEC:N_2 at 1:1000 and (c) with ratio 0.5:1000.

Features corresponding to the C-H stretching are not clearly resolved for the various conformers and hence we will not present the discussions for these modes in Ar and N_2 matrices.

5.4.2 Computational

DEC is the second member in the dialkyl carbonate family after DMC. The replacement of the methyl groups in DMC with ethyl groups in DEC increases the conformational possibilities. The conformations of DEC can be considered as an extension of those of DMC (Chapter 4) and a correlation can be sought between the conformational landscapes of the two molecules. In our earlier study on the conformation of DMC (Chapter 4), we had shown that the cis-cis (cc) conformer, to be the ground state, where both the methyl groups are oriented cis with respect to the carbonyl group. The other conformers occurring in increasing order of energy are cis-trans (ct) and near-trans-near-trans (ntnt). Based on our earlier work on TEP[5] and DEM,[6] in DEC too, the carbon atoms of the ethyl group attached to the oxygen atoms (referred to as anomeric carbon atoms) can adopt a cis and trans orientations. For each orientation (i.e. cis or trans) of the anomeric carbon, the terminal carbons can then take on various orientations. For example, for a cis orientation of the anomeric carbon, the terminal carbon atom can be oriented trans or gauche.

To identify each of the possible conformers of DEC, we have followed the same notations as in our earlier work.[6] For example, the ground state of DMC being cis-cis, the conformations of DEC correlating with this conformations of DMC can be written as cc(xy), where ‘c’ stands for cis. ‘x’ and ‘y’, which denote the orientation of the terminal carbon atoms, can be ‘t’, ‘g^+’ or ‘g^-’ to indicate trans or gauche orientation. Likewise, conformations of DEC correlating with the cis-trans structure of DMC are denoted as ct(xy), Further, if both the terminal carbon atoms are oriented in same side of the molecular plane, they are denoted by the same superscript sign g^+g^+ or g^-g^- (or $g^\pm g^\pm$); if they are oriented on opposite sides of the plane, they are denoted as g^+g^- or g^-g^+ (or $g^\pm g^\mp$).

As mentioned earlier, all the geometry optimizations were performed at B3LYP/6-31++G** level. At this level of calculation, we obtained four minima corresponding to a cluster of conformers that arises from the cis-cis orientation of the anomeric carbon: cc(tt), cc($tg^\pm$), cc($g^\pm g^\mp$), cc($g^\pm g^\pm$). Similarly, five minima, ct(tt), ct($g^\pm t$), ct($tg^\pm$), ct($g^\pm g^\mp$) and ct($g^\pm g^\pm$), were identified corresponding to a cluster of conformers that arises from the cis-trans orientation of the anomeric carbon. The relative energy (kcal/mol), zero point energy (Hartree) dipole moments (D) and degeneracy of the various conformers are given in Table 5.1. Some selected geometrical parameters of the conformers are given in Table 5.2. The computed structures of the conformers are shown in Fig. 5.7.

A correlation diagram between the conformations of DMC and DEC is shown in Fig. 5.8. As in our earlier studies, it is clear that the conformational landscapes is decided by the anomeric carbons, while the conformations resulting from the orientation of the terminal carbon atoms provide a fine structure in the conformational ordering. For example, all the conformations of DEC resulting from the 'cc' orientation of the anomeric carbons, form a cluster of low lying conformations, followed by the conformations resulting from the 'ct' orientation of the anomeric carbons. In each cluster, the lowest energy conformer, was one where the terminal carbons were oriented trans. Hence, the lowest energy conformer in the 'cc' cluster was cc(tt), while the lowest in the 'ct' cluster was ct(tt). The higher energy conformers in a given cluster are produced as the terminal carbon atom is progressively oriented gauche. Hence, the higher energy conformers for the cc cluster turns out to be cc($tg^\pm$), cc($g^\pm g^\mp$) and cc($g^\pm g^\pm$) in the order of increasing energy. Likewise, in the 'ct' cluster, the higher energy conformers were computed to be ct($g^\pm t$), ct($tg^\pm$), ct($g^\pm g^\mp$) and ct($g^\pm g^\pm$). The relative energies of each conformer are shown in Fig. 5.8. From the above observation it can

Table 5.1 – Relative energies (kcal/mol), zero point energies (ZPE) (Hartree), dipole moment (D) and degeneracy of different conformers of DEC at B3LYP/6-31++G level of calculations.**

Conformer	Relative energy[a]	ZPE (Hartree)[b]	Dipole moment (D)	Degeneracy
cc(tt)	0.00	0.151725	0.64	1
cc(tg$^{\pm}$)	0.51	0.151965	0.48	4
cc(g$^{\pm}$g$^{\mp}$)	0.98	0.152147	0.23	2
cc(g$^{\pm}$g$^{\pm}$)	1.00	0.152153	0.46	2
ct(tt)	2.86	0.151681	4.01	2
ct(g$^{\pm}$t)	3.23	0.151842	3.78	4
ct(tg$^{\pm}$)	3.73	0.151858	4.13	4
ct(g$^{\pm}$g$^{\mp}$)	4.06	0.152018	3.88	4
ct(g$^{\pm}$g$^{\pm}$)	4.14	0.152036	3.90	4
TS1[c]	0.80	0.151816	0.60	-
TS2[d]	1.24	0.151948	0.39	-
TS3[e]	1.26	0.151964	0.52	-
TS4[f]	8.96	0.151102	2.83	-

[a] ZPE corrected values.
[b] Unscaled value.
[c] Transition state connecting to cc(tt) and cc(tg$^{\pm}$).
[d] Transition state connecting to cc(tg$^{\pm}$) and cc(g$^{\pm}$g$^{\mp}$).
[e] Transition state connecting to cc(tg$^{\pm}$) and cc(g$^{\pm}$g$^{\pm}$).
[f] Transition state connecting to cc(tt) and ct(tt).

Table 5.2 – Important structural parameters of different conformers[a] of DEC. Bond length (Å), bond angles (°) and torsional angles[b] (°).

Parameters	**cc(tt)**	**cc(tg$^{\pm}$)**	**cc(g$^{\pm}$g$^{\mp}$)**	**cc(g$^{\pm}$g$^{\pm}$)**
C1-C2	1.516	1.516	1.520	1.520
C2-O3	1.450	1.450	1.451	1.452
O5-C6	1.450	1.451	1.451	1.452
C6-C7	1.516	1.520	1.521	1.520
C1-C2-O3	107.4	107.3	111.4	111.4
O5-C6-C7	107.4	111.4	111.4	111.4
C1-C2-O3-C4	-180.0	179.5	87.0	-86.8
C4-O5-C6-C7	-179.9	86.2	85.9	86.4

[a] The conformers with anomeric carbon atoms at cis positions.

[b] Torsional angle ABCD implies the angle between two planes ABC and BCD.

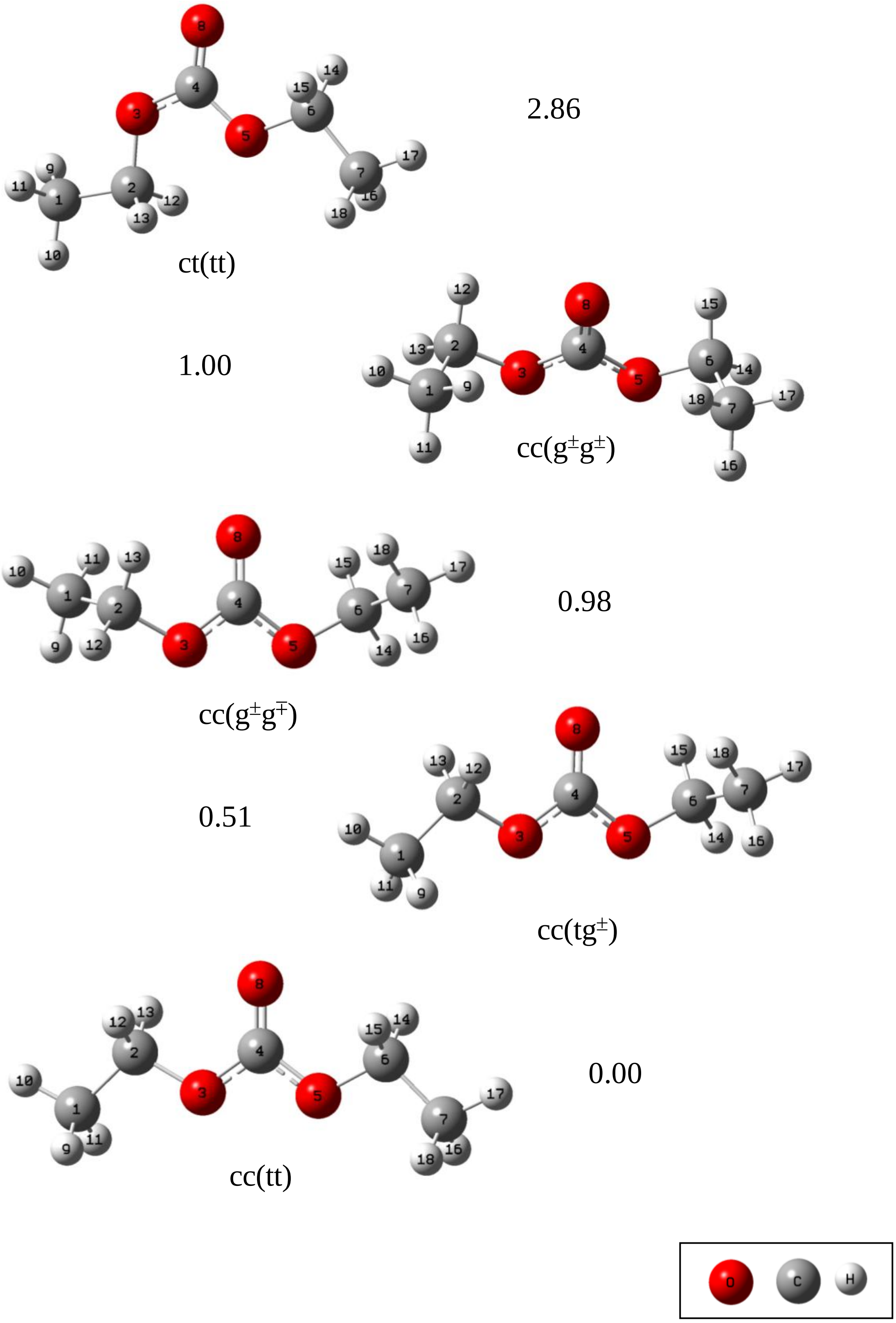

Fig. 5.7 – Computed structures at the B3LYP/6-31++G** level of different conformers of DEC. Relative energies (kcal/mol) are mentioned against each structure.

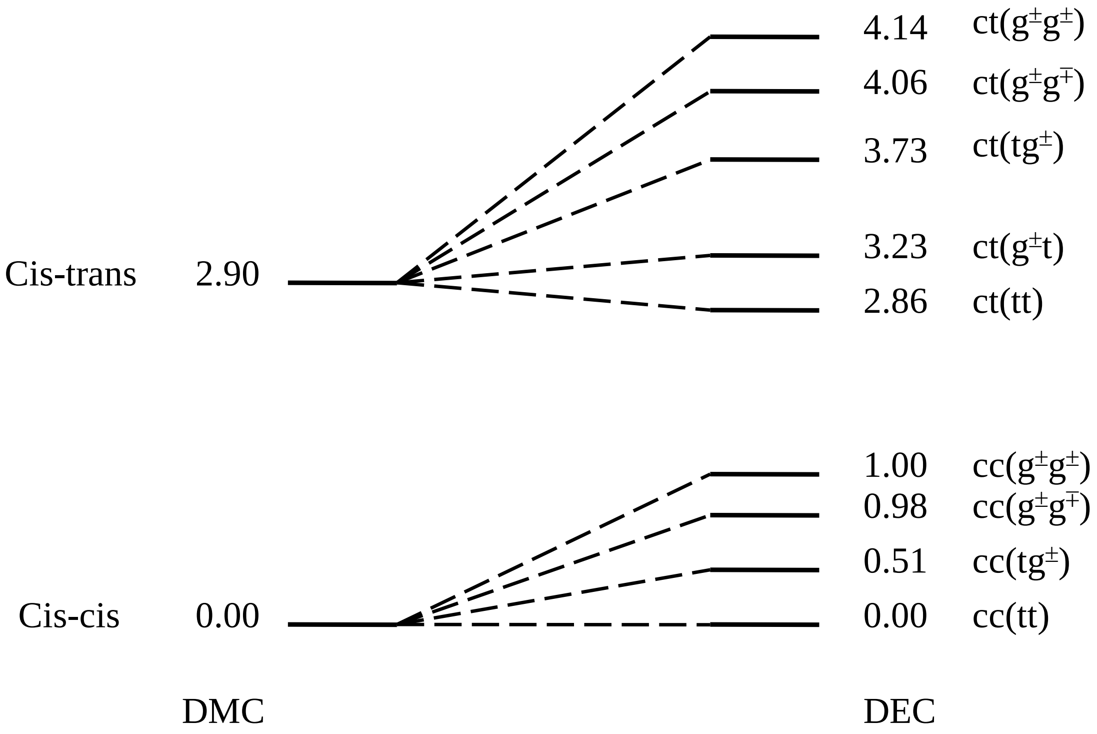

Fig. 5.8 – Diagram showing the correlation between the conformers of DMC and DEC. Energies (kcal/mol) of each conformer relative to the ground state conformer are also shown in the figure.

be pointed out that, trans position is the most preferred orientation for the terminal carbon atoms. Earlier studies on the conformations of DEM,[6] DEE[7] and TEP,[5] also revealed similar trends.

The energy difference between cis-cis and cis-trans conformer of DMC, which was 2.90 kcal/mol, is also approximately maintained between the conformers cc(tt) and ct(tt) of DEC (2.86 kcal/mol). It can be therefore be surmised from the above observation that the next higher cluster of conformers of DEC, would be those correlating with the near-trans-near-trans conformer of DMC, with the lowest energy conformer in this cluster being ntnt(tt). Since we did not observe the conformers of DMC corresponding to the 'ntnt' geometry, it is unlikely that conformers of DEC correlating with the 'ntnt' cluster would be experimentally observed. In this work, we have therefore restricted our study of the conformers of DEC correlating with the cis-cis and cis-trans orientation of the anomeric carbons.

The barrier for conformer interconversion from cc(tg$^{\pm}$) to cc(tt) was computed to be very small (0.29 kcal/mol). Likewise, the barriers for interconversion of cc(g$^{\pm}$g$^{\mp}$) and cc(g$^{\pm}$g$^{\pm}$) to cc(tg$^{\pm}$) were calculated to be 0.26 kcal/mol each.

To assign the experimental features corroborating with the computations, the computed values were appropriately scaled. To obtain the scaling factor, the experimentally observed feature with the highest intensity, occurring at 1271 cm^{-1}, was correlated with the calculated infrared feature of the ground state conformer, cc(tt), at 1301 cm^{-1}, which was computed to have the highest infrared intensity. The factor, 0.9769, that would bring the two frequencies in agreement was thus arrived at, and used to scale the other computed frequencies.

5.5 Discussion – Conformations of DEC

5.5.1 Vibrational assignments

Our calculations indicate that cc(tt) is the lowest energy conformer, while the conformers cc(tg$^{\pm}$), cc(g$^{\pm}$g$^{\mp}$) and cc(g$^{\pm}$g$^{\pm}$) lie at 0.51, 0.98 and 1.0 kcal/mol respectively above the ground state conformer. The lowest energy conformer in the cis-trans cluster, i.e. ‘ct(tt)’, occurs at an energy of 2.86 kcal/mol above the ground state conformer, while all the other conformers in this cluster occur at energies higher than 3 kcal/mol, as shown in Table 5.1. At room temperature (298 K), contributions of cc(tt), cc(tg$^{\pm}$), cc(g$^{\pm}$g$^{\mp}$) and cc(g$^{\pm}$g$^{\pm}$) conformers to the total population was calculated to be 28.6%, 48.4%, 11.0% and 10.6% respectively. The higher energy conformers cis-trans cluster have negligible population (~1.4%) to be of any experimental significance. It may be noted that the cc(tg$^{\pm}$) conformer has the highest population amongst all the conformers, due to its higher conformational degeneracy.

The scaled computed frequencies of the different conformers of the cis-cis cluster, whose intensities are computed to be greater than 5 km/mol, are listed in Table 5.3. From this table it can be seen that most of the strong features of *all* the conformers belonging to the cis-cis cluster have very close vibrational frequencies, making it difficult to unambiguously differentiate features belonging to the ground state, cc(tt), and the higher energy conformers of the ‘cc’ cluster, if at all these higher energy conformers were trapped in the matrix. The spectral features observed at 1756, 1487, 1449, 1413, 1394, 1377, 1280, 1271, 1126, 1036, 1031, 905, 871, 865 and 792 cm^{-1} in an Ar matrix, labeled in traces ‘b’ of Figs. 5.1 and 5.2, are all assigned to the members of cis-cis cluster, as shown in Table 5.3. We also observed similar features in N$_2$ matrix with slight shifts in the features (trace ‘a’, Figs. 5.1 and 5.2). The doublets observed at 1280 and 1271 cm^{-1}, 1036 and 1031 cm^{-1}, 871 and 865 cm^{-1} in Ar matrix are probably due to matrix site split features. The features observed at 999 and 1001 cm^{-1} in Ar and N$_2$ matrices respectively are probably the features that can be uniquely assigned to the ground cc(tt) conformer; however, the intensity of these feature are very small, as indicated by our computations, to be of much use in identifying the ground state conformer.

Table 5.3 – Experimental and calculated wavenumbers of DEC.

Calculated[a]				Experimental		Approximate Assignment of Vibrational Modes
cc(tt)	cc(tg$^{\pm}$)	cc(g$^{\pm}$g$^{\mp}$)	cc(g$^{\pm}$g$^{\pm}$)	Ar	N$_2$	
–[b]	398(5)	415(7)	437(2)	–	–	skeletal def
768(24)[c]	769(24)	769(23)	768(23)	792	793	skeleton out-of plane def
797(1)	793(2)	780(7)	782(8)	–	–	CH$_2$ Waging
851(28)	846(26)	843(25)	842(24)	865, 871	860, 864	C-C str + C$_{eth}$-O str
891(7)	887(7)	883(6)	883(7)	905	907	C$_{eth}$-O str+ O-C$_{car}$ str
–	969(14)	952(10)	952(10)	982	984	C-C str + O-C$_{car}$ str
988(10)	–	–	–	999	1001	
1019(153)	1014(133)	1006(126)	1006(118)	1031, 1036	1032	C-C-O antisym str
–	–	1078(0.3)	1079(15)	–	–	
1104(1)	1083(25)	1089(51)	1087(45)	1095	1095	C-C-O sym str
1116(8)	1109(6)	–	–	1126	1124	
1120(5)	1116(3)	1115(2)	1116(2)	–	–	O-C-O sym str
1154(7)	1153(4)	1165(4)	1165(4)	–	–	CH Rock
–	1174(9)	1179(4)	1180(5)	1180	1182	
1271(1060)	1269(952)	1266(827)	1265(803)	1271, 1280	1276,1279	O-C-O antisym str
–	1301(54)	1302(128)	1301(140)	1304	1302	CH$_2$ def
–	–	1304(13)	1303(4)	–	–	
1376(80)	1375(67)	1375(63)	1375(55)	1377	1377	CH def
1397(15)	1392(15)	1390(0.1)	1391(22)	1394	1395	
1408(16)	1405(19)	1400(30)	1399(23)	1413	1412	
1455(0.0)	1456(7)	1456(20)	1456(19)	–	–	
1456(14)	1457(10)	1456(1)	1461(4)	1449	1449	
1467(4)	1461(13)	1463(17)	1463(14)	–	–	
1468(2)	1475(16)	1475(8)	1475(10)	1470	1471	
–	–	1476(26)	1476(25)	–	–	
1487(15)	1489(8)	–	–	1487	1487	
1745(347)	1745(324)	1745(301)	1744(302)	1756	1754,1756	C=O stretch

[a] Computed at B3LYP/6-31++G** level and scaled with a factor 0.9769; computed wavenumbers with intensities ≥5 km/mol are listed here; a few wavenumbers with intensities ≤ 5 km/mol are also listed here for the sake of completion of the table.

[b] The features are not observed in computation or experiment.

[c] Intensities (km/mol) in parenthesis.

Apart from the major features belonging to the cc cluster, a few features, with very small intensities were observed in Ar matrix at 1470, 1304, 1180, 1095 and 982 cm^{-1}, marked with asterisks in the spectra (trace ‘b’ of Figs 5.1 and 5.2). These features may be either due to (1) higher energy conformers or (2) matrix site split features. When the experiment was carried out in N_2 matrix we found similar features (trace ‘a’ of Figs. 5.1 and 5.2) as observed in Ar matrix, which makes it less likely that these asterisk-marked features observed in Ar matrix are due to matrix site split features. These features observed in both the matrices may be due to higher energy conformers as the experimentally observed frequencies of these features in Ar and N_2 matrices agreed well with the scaled computed value for the higher energy cis-cis clusters (Table 5.3).

It was observed by many groups that a barrier of up to energy ~2.5 kcal/mol can be surmounted in the matrix on annealing.[8] For DEC the energy barriers for conformer interconversion from higher to lower energy conformers are ~0.3 kcal/mol and can therefore be expected to convert to the lower energy structure during annealing. It should be mentioned that on annealing the DEC in Ar and N_2 the features marked with asterisks behaved differently in these matrices. In Ar matrix some of the features decreased in intensity (Figs. 5.3d and 5.4d) whereas in N_2 matrix there is no change in intensity (Figs. 5.5d and 5.6d) , indicating that the matrix does play a role in stabilizing the conformers. At present we do not have an explanation for the different behaviour in these matrices. However, such a behaviour has been observed with TMP in Ar, N_2, Xe and Kr matrices (not reported). Interestingly, these new features appeared as a broad spectrum in the gas and liquid phase at room temperature of DEC, presented in traces ‘c’ and ‘d’ of Figs. 5.1 and 5.2.

To further clarify that the new features were indeed due to higher energy conformers of cis-cis cluster we have carried out hot nozzle and supersonic jet experiments. In the effusive hot nozzle the sample was heated at higher temperature, 423 K, to increase the populations of higher energy conformers in gas phase prior to deposition. At 423 K, the populations of the conformers cc(tt), cc($tg^{\pm}$), cc($g^{\pm}g^{\mp}$) and cc($g^{\pm}g^{\pm}$) were calculated to be 21.4%, 46.6%, 13.4% and 13.1% respectively, while all the other conformers together contribute to ~5.5%. While the hot nozzle experiments is expected to increase the population of the higher energy conformers, experimentally, in Ar (Figs 5.3b and 5.4b) and N_2 (Figs. 5.5b and 5.6b) matrixes, we have not observed any change in the IR spectra because the change in population of higher energy cluster were only a few percent.

We have also performed supersonic jet experiments to observe conformational cooling which are shown in Figs. 5.3c and 5.4c for Ar matrix and in Figs. 5.5c and 5.6c for N_2 matrix. In these experiments too we have not observed any appreciable conformational cooling.

To summarize the observations:

1) New features were observed both in Ar and N_2 matrices indicating that these features are not due to matrix site split features but may be due to higher energy conformers.
2) These new features observed in Ar and N_2 matrices corroborated well with the scaled computed value for the higher energy cis-cis clusters (Table 5.3).
3) On annealing the matrices, new features decreased in intensity in Ar matrix whereas there was no change in intensity in N_2 matrix, showing that the matrix probably plays a role in stabilizing the conformers.

However, effusive hot nozzle and supersonic jet experiments did not gave a conclusive indication for the higher energy conformers because the populations increase for the higher energy forms are small. It is also likely that the higher energy conformers could get interconverted to the ground state conformer cc(tt), as the barriers for conformer interconversion is rather low (~0.3 kcal/mol). Recent work on the conformations of trimethyl phosphite has shown a similar interconversion during deposition,[9] where the barrier for conformational interconversion was 0.7 kcal/mol. Fausto et al. also observed such interconversions for a number of compounds, such as dimethyl sulphite,[10,11] methylcyano acetate[12,13] and 1,3-butanediol.[14]

Based on the above facts we assign the five features observed in Ar and N_2 matrices to higher energy conformers of cis-cis cluster.

5.5.2 Dipole moment

The dipole moments of the various DEC conformers computed using B3LYP/6-31++G** level of theory are given in Table 5.1. The dipole moments of the members of lower cluster are close to each other and range from 0.46 to 0.64 D where as in case of higher energy cluster, it varies from 3.78 to 4.13 D. The net dipole moment of DEC at room temperature (298 K), weighted for populations of each conformer, was computed to be 0.69 D. Labrenz and Schröer have reported the experimental gas phase values, as well as calculated dipole moments of DEC over the temperature range 353 to 477 K.[2] MP2 and MP4 methods, with a 6-31G* basis set, were used in their calculations, but they considered only two conformers gg and gt to calculate the dipole moments of DEC. In our calculations of dipole moments, contributions from all the conformers arising from the ‘cc’ and ‘ct’ clusters of DEC, were taken into consideration. The calculated dipole moments obtained in our calculation for the above range of temperature are given in Table 5.4 along with the experimental and calculated dipole moments reported by Labrenz and Schröer. While our computations indicate significant increase in the dipole moment over the temperature range 353 to 477 K, the experimental dipole moments[2] were found to be constant for the same temperature range. Further experiments are required to resolve this issue.

5.5.3 Comparison of conformations of DEC with Diethoxymethane (DEM)

In DEM, the carbonyl group of DEC, is replaced by a methylene ($-CH_2-$) group.[6] The $n \rightarrow \pi^*$ interaction in DEC directs the anomeric carbon atoms to a cis or trans orientation,

Table 5.4 – Dipole moments (D) of DEC at different temperatures.

Temperature (K)	**Experimental[a] (Gas Phase)**	**Calculated[a]**		**Calculated[b] B3LYP/6-31++G****
		MP2/6-31G*	**MP4/6-31G***	
353	1.06	0.94	0.96	0.83
382	1.06	1.02	1.04	0.98
413	1.06	1.12	1.14	1.02
477	1.07	1.30	1.33	1.21

[a] Ref. 2.
[b] This work.

whereas n→σ* interaction in DEM leads them to have gauche or trans orientation. A similar observation have also made in case of DMC and DMM comparison (Chapter 4). However, as described earlier, the terminal carbon atoms in DEC and DEM can orient to a trans or gauche position, leading to further clusters of conformations. In both the cases, the conformations where the terminal carbon atoms adopt a trans orientation are lower in energy compared to the gauche orientation. It has been observed that the energy difference between the ground state conformer and the first higher energy conformer (cc(tg$^{\pm}$)) of DEC is 0.51 kcal/mol, whereas in DEM this difference is 1.25 kcal/mol.[6]

DEC has a planar C-O-C-O-C frame work, while DEM does not; as a result some of the conformers which are degenerate in DEC split in DEM. For example, the cc(tg$^{\pm}$) conformer in DEC is four-fold degenerate; however, in DEM, the tg^{+} and tg^{-} structures are non-degenerate leading to non-equivalent conformers, g^{+}g^{-}(tg^{+}) and g^{+}g^{-}(tg^{-}), each of which is of course is doubly degenerate. This sort of degeneracy results in fewer distinguishable conformers in DEC compared with DEM. As a result, four conformers for the cis-cis cluster and five for cis-trans cluster are observed in DEC, whereas in DEM, six and nine conformers can be enumerated for the g$^{\pm}$g$^{\mp}$ and tg$^{\pm}$ clusters respectively. Also, in DEC the cluster of conformers due to cis-cis and cis-trans orientations of anomeric carbon atoms are clearly separated in energy, whereas in the case of DEM, cluster of conformers arising from the g$^{\pm}$g$^{\mp}$ and tg$^{\pm}$ orientations of anomeric carbon atoms are not clearly separated. In fact, the tg$^{\pm}$(tt) structure stands third in energy in the conformation ladder.[6]

5.5.4 Natural bond orbital analysis

Natural bond orbital analysis was performed for the different conformers of DEC to study the different delocalization interactions present in them. The major delocalization interactions responsible for the conformational stability in DMC (Chapter 4) were also present in DEC. These delocalizations involve the lone pairs on oxygen and double bond of the carbonyl group and are responsible for the cis and trans orientations of anomeric carbon atoms in both DMC and DEC.

To examine, if vicinal and geminal interactions have any role to play in deciding the conformational preferences involving the terminal carbon atoms in DEC, we have systematically deleted these delocalization interactions for all the members of the cis-cis cluster. The effect of deletion of all delocalization interactions was also examined by deleting all acceptor orbitals. The deletion energies, changes in energies and relative change in deletion energy (%) for specific deletions, in the different conformers of cis-cis cluster in DEC, are listed in Table 5.5.

Relative change in deletion energies (%) from Table 5.5 show that all geminal interactions contribute almost equally for the stabilization of each of the conformers. Similar observations are also made following the deletion of all vicinal and all delocalization interactions. This clearly reveals that delocalization interactions are not responsible in deciding the conformational preferences involving the orientation of the terminal carbon atoms in DEC, and it is the steric interactions which are responsible. A similar NBO analysis on DEM also indicated a similar behaviour; namely, that while delocalization interactions play an important role in deciding the conformational preferences of the anomeric carbon, they have little role to play in the orientation of the terminal carbon atoms.

5.6 Results – DEC-H_2O complex

In this study, we also studied the DEC-H_2O complex, the reasons for which have been indicated earlier.

5.6.1 – Experimental

Fig. 5.9 spans the two IR spectral regions of DEC 1785-1715 cm^{-1} (Grid A) and 1325-1250 cm^{-1} (Grid B) whereas Fig. 5.10 shows the OH stretching region of H_2O 3800 – 3500 cm^{-1} in an Ar matrix. Traces 'a' and 'b' in the Fig. 5.9 shows the spectra with DEC:H_2O:Ar

Table 5.5 – Energies of different conformers of DEC after deletion of all geminal, all vicinal and all delocalization interactions.

Conformer	Interactions deleted	Deletion energy (Hartree)	Change in energy		Relative change in deletion energy (%)
			Hartree	kcal/mol	
cc(tt)	Geminal	-422.157865828	0.118963	74.6	0.028
	Vicinal	-421.442752057	0.834077	523.4	0.198
	All	-421.301785837	0.975043	611.8	0.232
cc(tg$^{\pm}$)	Geminal	-422.154937983	0.121381	76.2	0.029
	Vicinal	-421.442398187	0.833921	523.3	0.198
	All	-421.294097772	0.982221	616.4	0.234
cc(g$^{\pm}$g$^{\mp}$)	Geminal	-422.152369835	0.123352	77.4	0.029
	Vicinal	-421.442465366	0.833256	522.9	0.198
	All	-421.286643860	0.989078	620.6	0.235
cc(g$^{\pm}$g$^{\pm}$)	Geminal	-422.151748119	0.123897	77.7	0.029
	Vicinal	-421.443367712	0.832277	522.3	0.198
	All	-421.287122181	0.988523	620.3	0.235

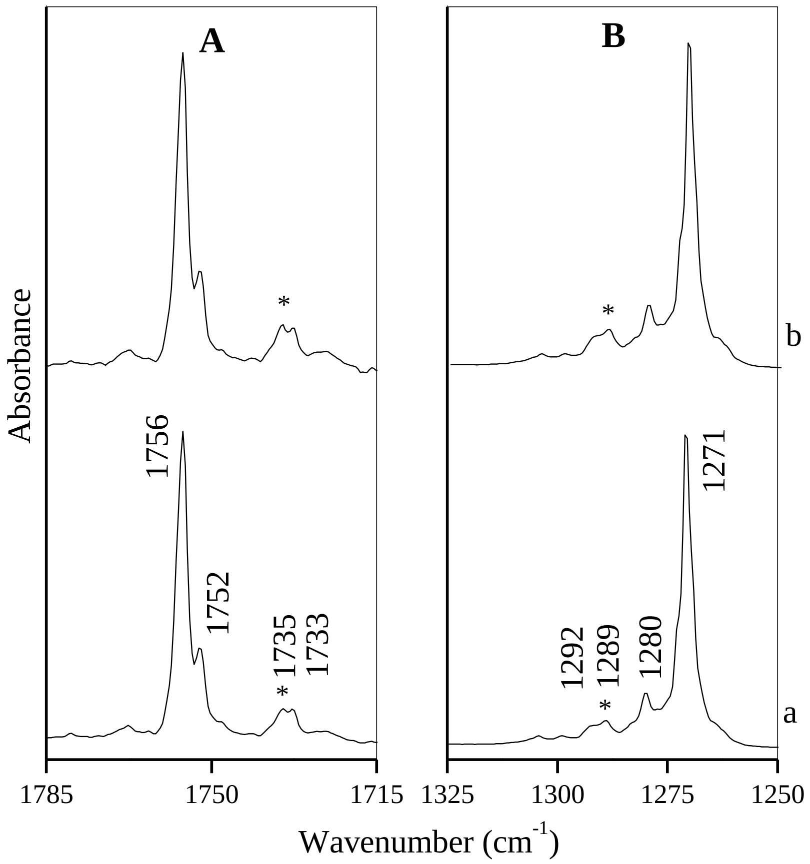

Fig. 5.9 – IR spectra of DEC-H_2O complex (Grid A: 1785-1715 cm^{-1}, Grid B: 1325-1250 cm^{-1}), in Ar matrix at 12 K recorded after annealing the matrix at 35 K for 15 minutes; (a) DEC:H_2O:Ar (1:0:1000); (b) DEC:H_2O:Ar (1:1.5:1000). (Ratio 0:1000 of H_2O to Ar implies no water is added deliberately to the matrix. See text for details.)

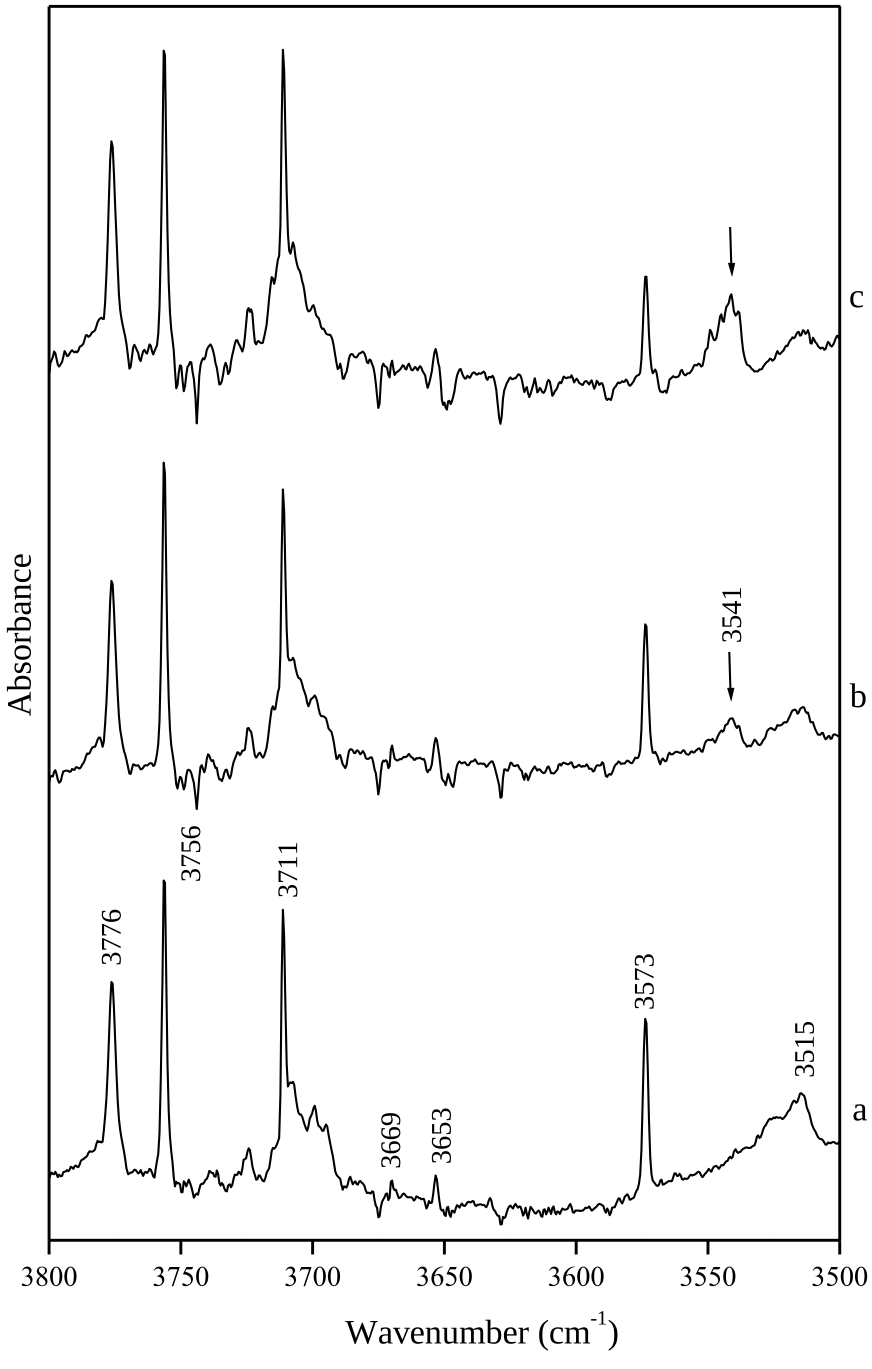

Fig. 5.10 – IR spectra of DEC-H_2O complex in Ar matrix at 12 K recorded after annealing the matrix at 35 K for 15 minutes, covers the spectral region 3800 – 3500 cm^{-1}; (a) DEC:H_2O:Ar (0:1.5:1000); (b) DEC:H_2O:Ar (0.5:1.5:1000); (c) DEC:H_2O:Ar (1:1.5:1000).

ratios 1:0:1000 and 1:1.5:1000 respectively. Whereas in Fig. 5.10, traces ‘a’, ‘b’ and ‘c’ shows the spectra with DEC:H_2O:Ar ratios 0:1.5:1000, 0.5:1.5:1000 and 1:1.5:1000 respectively. All the spectra shown here were annealed at 35 K. We have also carried out experiments in N_2 matrix. Figs. 5.11 and 5.12 shows the experiments performed in N_2 matrix. On annealing the matrix, new features were observed at 1735, 1733, 1292, 1289 and 3541 cm^{-1} in Ar matrix and 1732, 1292, 3704 and 3555 cm^{-1} in N_2 matrix. It should be mentioned that without adding water to the matrix (marked asterisks in trace ‘a’ Figs. 5.9 and 5.11) these features were observed, the assignments of which is the motivation for this study. When the water concentration is increased by adding deliberate additions, these new features were found to increase in intensity clearly showing that these features could be due to DEC-H_2O adducts as shown in respective figures. In the experiments where no water was deliberately added, the DEC-H_2O adducts were formed, as trace levels of water cannot be avoided in the matrix.

5.6.2 – Computational

As described before, all the calculations for DEC-H_2O complexes were performed at B3LYP/6-31++G** level of theory. DEC has two sites of attack; carbonyl and ethoxy oxygen. Water can form hydrogen-bonded complexes with these two sites. As discussed earlier DEC has four conformers in the cis-cis cluster and computations were performed for the DEC-H_2O complexes for all the four conformers. Figs. 5.13 and 5.14 show the computed structures for the 1:1 DEC-H_2O carbonyl and ethoxy complexes. Due to symmetric nature of the cc(tt), cc($g^{\pm}g^{\mp}$) and cc($g^{\pm}g^{\pm}$), attack of H_2O in the carbonyl oxygen, either towards O5 or O3 are degenerate (complex-1, 3 and 4 in Fig. 5.13), whereas for the complex with cc($tg^{\pm}$) conformer (complex-2a and complex-2b) they are non-degenerate. Similar observations were found for the ethoxy complexes. Interaction energies for the carbonyl and ethoxy complexes of all the four conformers are given in Table 5.6 along with the degeneracy.

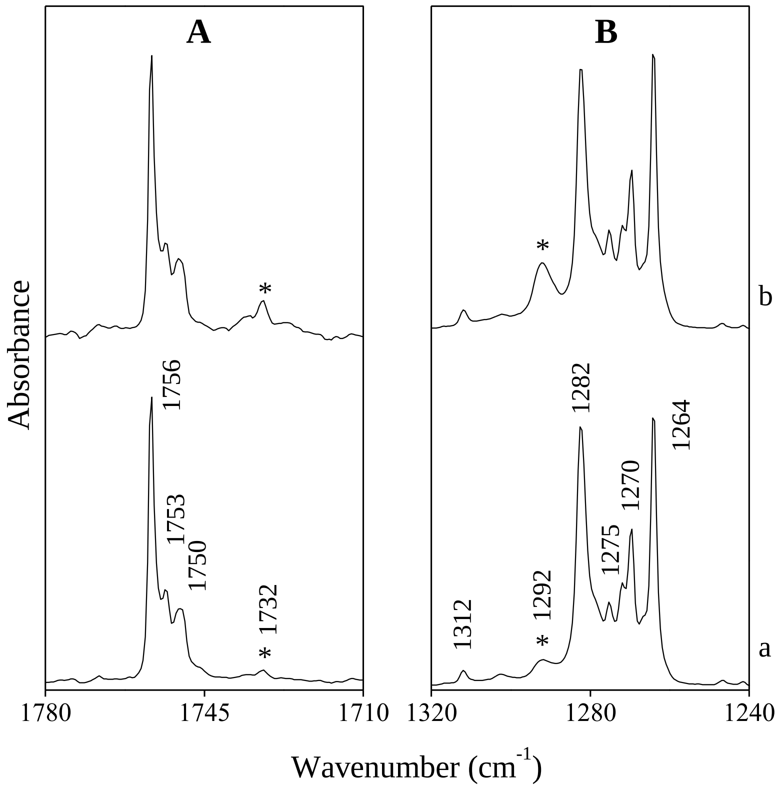

Fig. 5.11 – IR spectra of DEC-H_2O complex (Grid A: 1780-1710 cm^{-1}, Grid B: 1320-1240 cm^{-1}), in N_2 matrix at 12 K recorded after annealing the matrix at 30 K for 15 minutes; (a) DEC:H_2O:N_2 (1:0:1000); (b) DEC:H_2O:N_2 (1:1.5:1000). (Ratio 0:1000 of H_2O to N_2 implies no water is added deliberately to the matrix. See text for details.)

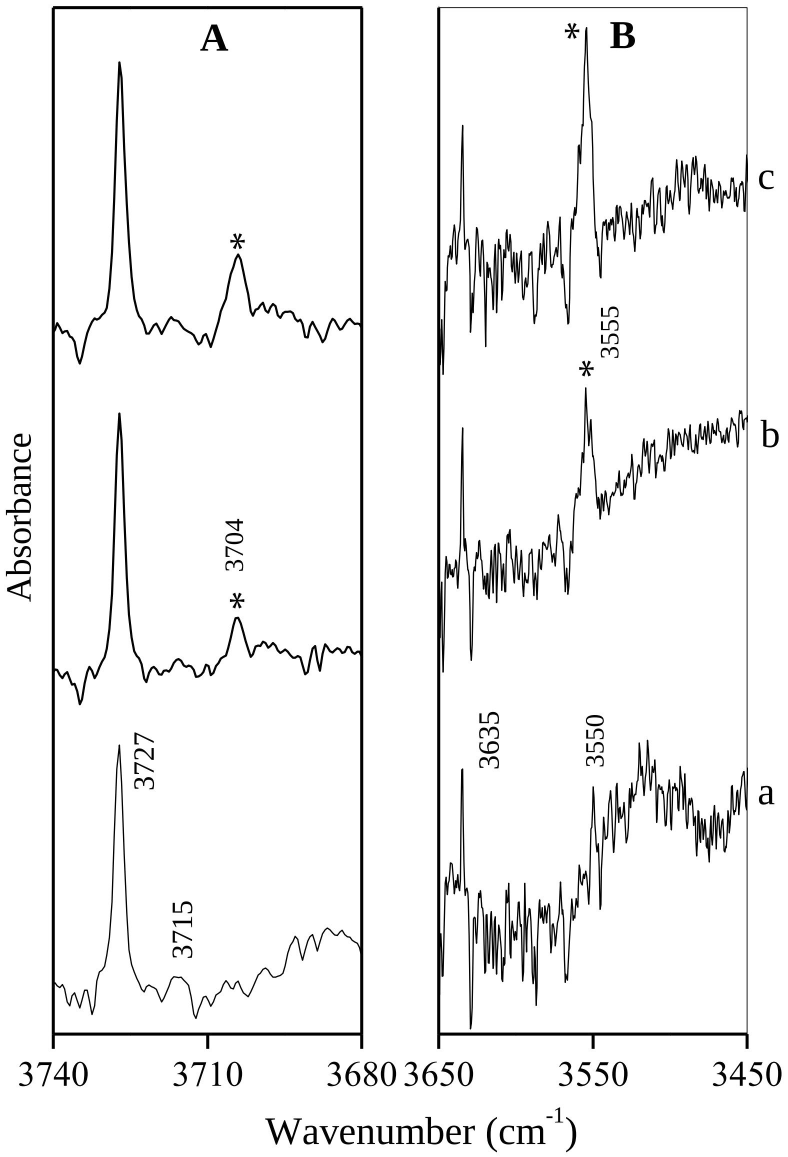

Fig. 5.12 – IR spectra of DEC- H_2O complex (Grid A: 3740-3680 cm^{-1}, Grid B: 3650-3450 cm^{-1}), in N_2 matrix at 12 K recorded after annealing the matrix at 30 K for 15 minutes; (a) DEC:H_2O:N_2 (0:1:1000); (b) DEC:H_2O:N_2 (1:1:1000); (c) DEC:H_2O:N_2 (2:1:1000).

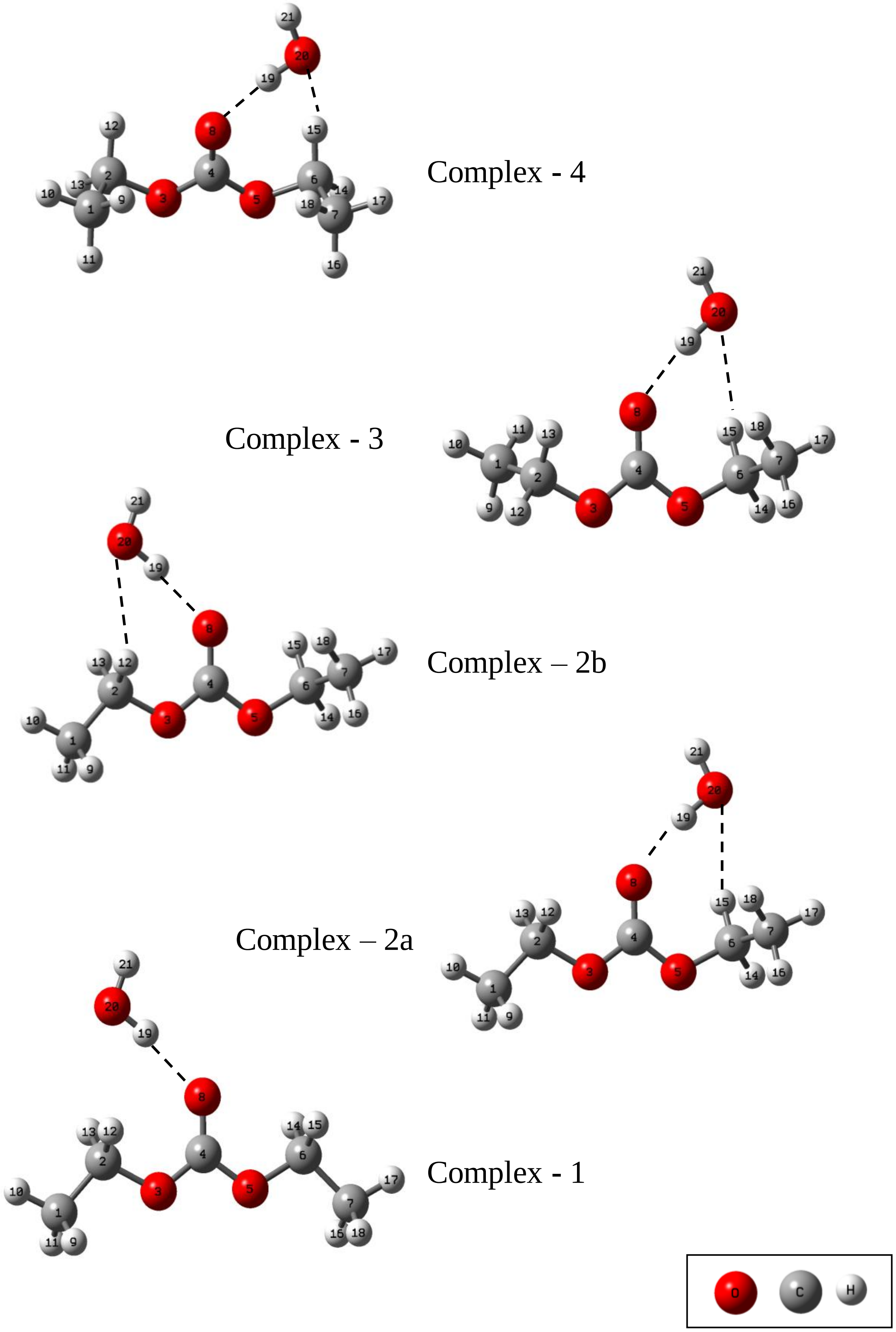

Complex - 4

Complex - 3

Complex – 2b

Complex – 2a

Complex - 1

Fig. 5.13 – Computed structures at B3LYP/6-31++G** level of DEC-H_2O carbonyl complexes for all the members of cis-cis clusters.

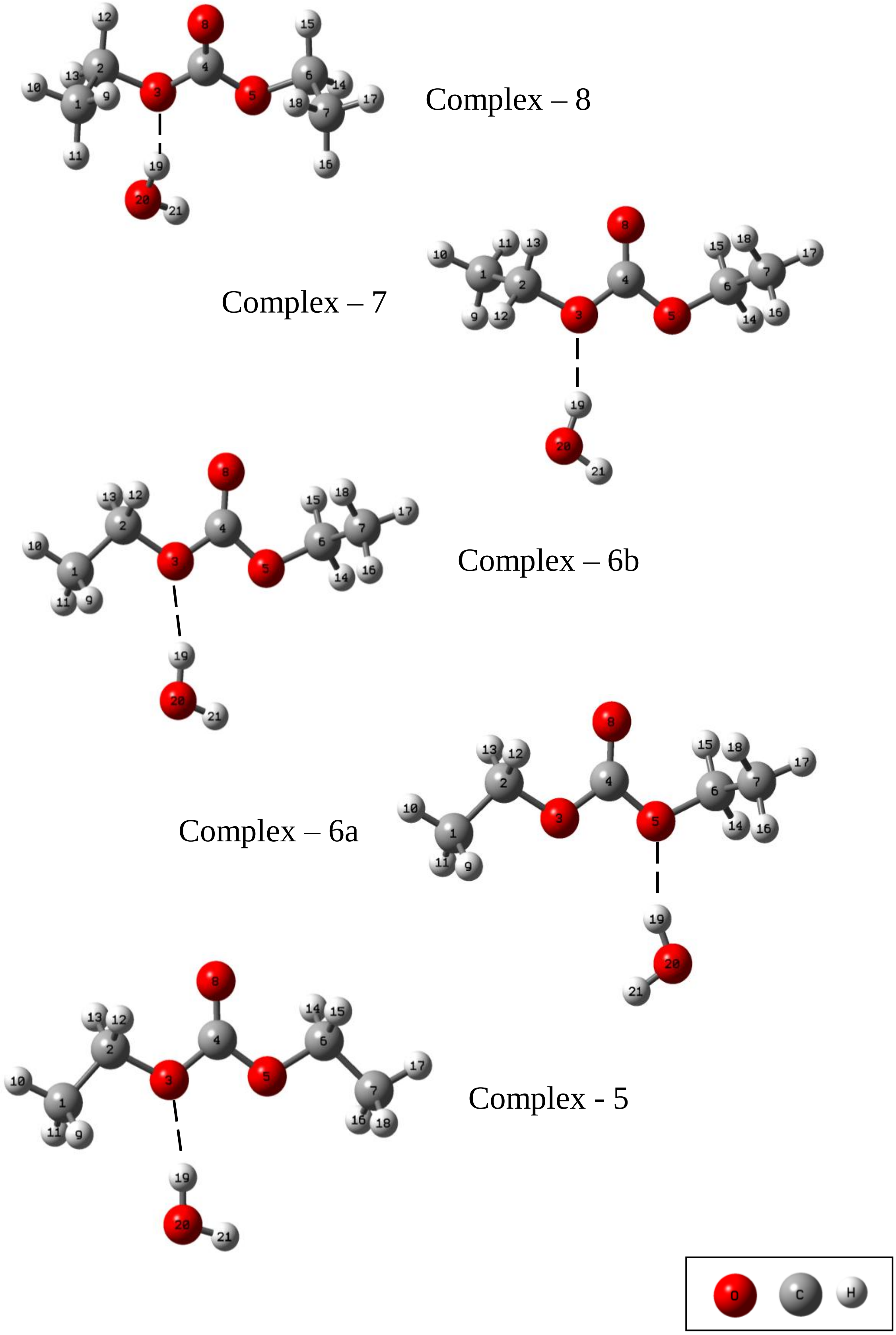

Complex – 8

Complex – 7

Complex – 6b

Complex – 6a

Complex - 5

Fig. 5.14 – Computed structures at B3LYP/6-31++G** level of DEC-H_2O ethoxy complexes for all the members of cis-cis clusters.

Table 5.6 – Raw[a]/ZPE[b] corrected/BSSE[c] corrected interaction energies (ΔE) in kcal/mol for the DEC-H_2O (1:1) complexes computed at the B3LYP/6-31++G level of theory.**

Complex type	Complexes	Raw	ZPE	BSSE	Degeneracy
Carbonyl complexes	Complex 1	-6.19	-4.38	-5.79	2
	Complex 2a	-6.01	-4.31	-5.64	4
	Complex 2b	-6.15	-4.37	-5.74	4
	Complex 3	-5.96	-4.23	-5.61	4
	Complex 4	-5.96	-4.28	-5.60	4
Ethoxy complexes	Complex 5	-4.46	-3.03	-3.86	2
	Complex 6a	-4.48	-3.11	-3.86	4
	Complex 6b	-4.59	-3.12	-4.03	4
	Complex 7	-4.59	-3.22	-4.05	4
	Complex 8	-4.58	-3.23	-4.03	4

[a] Raw interaction energies refer to energies not corrected for either ZPE or BSSE.
[b] Zero point energy.
[c] Basis set superposition error.

As the assignment of the higher energy conformers of DEC was considered tentative, we have studied only the dominant ground state conformer, cc(tt), for the formation of the water complex and the assignment of vibrational frequencies. Table 5.7 gives the experimental and calculated vibrational frequencies for the 1:1 carbonyl and ethoxy complexes of DEC[cc(tt)]-H_2O. We have used the same scaling factor for the DEC-H_2O complex in the DEC region as that used for DEC. The scaled vibrational frequencies of carbonyl and ethoxy complexes, with intensities greater than 10 km/mol are given in the same table. To scale the calculated OH stretching frequencies of H_2O, we followed the same method which has been used for DMC-H_2O complex in Chapter 4, and the scaling factor 0.9484 was used to scale the calculated vibrational modes to corroborate the experimental results obtained from a N_2 matrix. The bending mode of H_2O is scaled separately with a factor 0.9975. This scaling factor was obtained when the monomer feature of water in N_2 matrix at 1597 cm^{-1} was correlated with that of computed feature at 1601 cm^{-1}. We have also computed the vibrational frequencies of the water complexes with other conformers of cis-cis clusters which are listed in Tables 5.8 and 5.9.

5.7 Discussion – DEC-H_2O complex

5.7.1 Vibrational assignments

As discussed above, each conformers of cis-cis cluster of DEC can form two types of complexes where hydrogen of water is either attached to carbonyl or ethoxy oxygens. Interaction energies shown in Table 5.6, indicate the carbonyl complexes are stronger than the corresponding ethoxy complexes. The BSSE corrected stabilization energies of carbonyl (Complex-1) and ethoxy (Complex-5) water complexes of cc(tt) conformer are -5.79 and -3.86 kcal/mol respectively. We looked for both types of complexes in our experiments as it is known that matrix isolation experiments could trap both global and local minima.[15-17] The details of the assignment of vibrational frequencies are discussed below.

Table 5.7 – Experimental and calculated (B3LYP/6-31++G theory) vibrational wavenumbers (cm^{-1}) of the DEC(cc(tt))-H_2O (1:1) complexes.**

Experiment			Calculation[a]					Approximate Assignment of Vibrational Modes
DEC in Ar	**Complex in Ar**	**Δν[b]**	**cc(tt)**	**Complex 1 (Carbonyl)**	**Δν**	**Complex 5 (Ethoxy)**	**Δν**	
-	-	-	-	-	-	451(97)[c]	-	skeletal def
-	-	-	-	541(93)	-	-	-	OH out of plane bending
792	-	-	768(24)	770(25)	2	766(27)	-2	skeleton out-of plane def
865, 871	-	-	851(28)	846(37)	-5	845(36)	-6	C-C str + C_{eth}-O str
	-	-	-	-	-	892(12)	-	C_{eth}-O str+ O-C_{car} str
999	-	-	988(10)	-	-	987(14)	-1	C-C str + O-C_{car} str
1031, 1036	-	-	1019(153)	1012(151)	-7	1012(159)	-7	C-C-O antisym str
	-	-	-	-	-	1118(15)	-	C-C str+ O-C-O sym str
1271	1289	18	1271(1060)	1290(964)	19	1260(999)	-11	O-C-O antisym str
	1292	21						
1377	-	-	1376(80)	1382(97)	6	1377(63)	1	CH def
1394	-	-	1397(15)	1399(19)	2	-	-	
1413	-	-	1408(16)	1417(55)	9	1417(55)	9	
1487	-	-	1487(15)	1483(20)	-4	1487(13)	0	
1756	1733	-23	1745(347)	1720(433)	-25	1760(374)	15	C=O str
	1735	-21						
Water in N_2	**Complex in N_2**	**Δν**	**Water**	**Complex 1 (Carbonyl)**	**Δν**	**Complex 5 (Ethoxy)**	**Δν**	**Water**
1597	-	-	1601(87)	1631(93)	30	1629(107)	28	ν_2 Bending
3635	3555	-80	3611(5)	3500(390)	-111	3565(186)	-46	ν_1 Sym Stretch
3727	3704	-23	3727(53)	3695(107)	-32	3699(109)	-28	ν_3 Antisym Stretch

[a] Computed wavenumbers over the DEC region are scaled with 0.9769 to compare with Ar matrix results; computed wavenumbers with intensities ≥10 km/mol are listed here; the water region computed values are compared with N_2 matrix results; bending mode of water is scaled with a value 0.9975 and the OH stretching modes of water were scaled with 0.9484 (See text for details).

[b] $\Delta\nu = \nu(\text{complex}) - \nu(\text{monomer})$.

[b] Intensities (km/mol) in parenthesis.

Table 5.8 – Computed wavenumbers of DEC-H_2O 1:1 carbonyl complexes[a].

Complex 1	Complex 2a	Complex 2b	Complex 3	Complex 4	Approximate Assignment of Vibrational Modes
Vibrational region of DEC					
541(93)[b]	543(97)	540(91)	541(97)	543(97)	OH out of plane bending
770(25)	769(25)	770(25)	769(25)	768(25)	skeleton out-of plane def
846(37)	841(34)	841(35)	837(33)	837(32)	C-C str + C_{eth}-O str
-	972(18)	973(13)	-	-	C-C str + O-C_{car} str
1012(151)	1008(125)	1007(134)	1000(127)	999(117)	C-C-O antisym str
-	1084(25)	1083(21)	1079(0.3)	1081(14)	C-C-O sym str
-	-	-	1088(43)	1086(38)	
-	1177(6)	1175(10)	1182(4)	1183(4)	CH Rock
1290(964)	1286(691)	1288(701)	1281(500)	1281(501)	O-C-O antisym str
-	1300(235)	1304(212)	1301(133)	1301(169)	CH_2 def
-	-	-	1303(247)	1303(187)	
1382(97)	1380(103)	1381(80)	1379(91)	1379(78)	CH def
-	1393(16)	1395(22)	1391(1)	1391(22)	
1399(19)	-	-	1402(34)	1401(56)	
1417(55)	1408(44)	1414(48)	-	-	
1456(9)	1455(10)	1491(9)	1455(12)	1456(12)	
1468(6)	1466(2)	1463(17)	1461(10)	1463(11)	
-	1479(34)	1476(23)	1447(9)	1476(14)	
1483(20)	1488(12)	1484(14)	1481(47)	1483(44)	
1720(433)	1720(405)	1718(405)	1719(377)	1719(378)	C=O str
Vibrational region of H_2O					
1631(93)[c]	1625(93)	1630(92)	1624(92)	1624(90)	ν_2 Bending
3500(390)	3502(375)	3501(381)	3502(363)	3503(364)	ν_1 Sym Stretch
3695(107)	3696(109)	3695(107)	3696(107)	3696(109)	ν_3 Antisym Stretch

[a] Computed wavenumbers over the DEC region are scaled with 0.9769 to compare with Ar matrix results; computed wavenumbers with intensities ≥10 km/mol are listed here; a few wavenumbers with intensities ≤ 10 km/mol are also listed here for the sake of completion of the table; the water region computed values are compared with N_2 matrix results; bending mode of water is scaled with a value 0.9975 and the OH stretching modes of water were scaled with 0.9484. (See text for details).

[b] Intensities (km/mol) in parenthesis.

Table 5.9 – Calculated wavenumbers of DEC-H_2O 1:1 ethoxy complexes[a].

Complex 5	Complex 6a	Complex 6b	Complex 7	Complex 8	Approximate Assignment of Vibrational Modes
Vibrational region of DEC					
451(97)[b]	461(97)	446(99)	460(99)	462(97)	skeletal def
766(27)	766(26)	766(27)	765(25)	764(25)	skeleton out-of plane def
845(36)	841(33)	840(34)	838(32)	837(31)	C-C str + C_{eth}-O str
892(12)	888(19)	888(12)	884(11)	884(11)	C_{eth}-O str+ O-C_{car} str
-	968(19)	968(21)	953(13)	953(14)	C-C str + O-C_{car} str
987(14)	-	-	-	-	
1012(159)	1009(139)	1008(138)	1000(133)	1000(124)	C-C-O antisym str
-	-	1082(24)	1078(0.7)	1079(16)	C-C-O sym str
-	1085(23)	-	1089(48)	1087(42)	
1118(15)	1110(5)	1112(7)	1110(2)	1110(2)	C-C str+ O-C-O sym str
1260(999)	1261(929)	1258(901)	1256(829)	1256(817)	O-C-O antisym str
-	1304(35)	1301(49)	1302(93)	1300(90)	CH_2 def
1377(63)	1377(54)	1377(54)	1376(52)	1375(46)	CH def
-	1395(12)	1393(15)	1392(0.4)	1392(22)	
1399(15)	1405(12)	1405(6)	1400(20)	1398(10)	
1457(4)	1458(11)	1456(10)	1456(15)	1457(15)	
1467(9)	1463(13)	1462(10)	1464(13)	1464(12)	
-	1475(15)	1475(15)	1476(26)	1476(23)	
1487(13)	1488(7)	1487(6)	-	-	
1760(374)	1758(353)	1759(349)	1757(330)	1757(331)	C=O str
Vibrational region of H_2O					
1630(107)	1623(86)	1630(105)	1624(85)	1624(81)	ν_2 Bending
3565(186)	3552(224)	3565(189)	3552(231)	3552(233)	ν_1 Sym Stretch
3699(109)	3699(122)	3698(115)	3699(126)	3698(127)	ν_3 Antisym Stretch

[a] Computed wavenumbers over the DEC region are scaled with 0.9769 to compare with Ar matrix results; computed wavenumbers with intensities ≥10 km/mol are listed here; a few wavenumbers with intensities ≤ 10 km/mol are also listed here for the sake of completion of the table; the water region computed values are compared with N_2 matrix results; bending mode of water is scaled with a value 0.9975 and the OH stretching modes of water were scaled with 0.9484. (See text for details).

[b] Intensities (km/mol) in parenthesis.

5.7.1.1 – C=O stretch

The C=O stretch of the DEC submolecule in the complex is observed as a doublet at 1735 and 1733 cm^{-1} in Ar matrix, and at 1732 cm^{-1} in N_2 matrix, a red shift of 21 and 23 cm^{-1} in Ar and 24 cm^{-1} in N_2 matrices. These values agree well with the scaled computed value of 1720 cm^{-1}, a red shift of 25 cm^{-1} for the complex-1 (Table 5.7). In Ar matrix, the feature appears as doublet may be due to matrix site effect.

Table 5.7 also shows the calculated frequencies for the C=O stretching mode for the ethoxy complex at 1760 cm^{-1}, a blue shift of 15 cm^{-1} from the monomer features. However, we did not observe any new feature in our experiment both in Ar and N_2 matrices. This implies that complex-5 is not formed in our experiments.

5.7.1.2 – O-C-O stretch

Experimentally we observed new features as a doublet at 1292 and 1289 cm^{-1} in Ar and 1292 cm^{-1} feature in N_2. matrix, a blue shift of 21 and 18 cm^{-1} in Ar and ~19 cm^{-1} in N_2 from the DEC submolecule. The experimentally observed shift agrees well with the computed value (Table 5.7), for the complex-1 at 1290 cm^{-1} for this mode, a blue shift of 19 cm^{-1}. For the complex-5 the computed value at 1260 cm^{-1} a red shift of ~11 cm^{-1} (Table 5.7). We could not discern any new feature for the complex-5 in this mode.

5.7.1.3 – H_2O symmetric stretch (ν_1)

The monomer features of ν_1 mode of H_2O were observed at 3669.0 and 3653.0 cm^{-1} in Ar matrix[18] and 3635 cm^{-1} in N_2 matrix.[19] The O-H symmetric stretch for the ν_1 mode of H_2O in the DEC-H_2O complex was observed at 3541 and 3555 cm^{-1}, a red shift from the ν_1 stretch in the uncomplexed H_2O by ~118 cm^{-1} & 80 cm^{-1} in Ar and N_2 matrices respectively. The experimental frequencies agrees well with the computed red shifts of ~111 cm^{-1} for the complex-1 of cc(tt) conformer of as shown in Table 5.7.

The perturbation in the ν_1 mode of H_2O for the ethoxy oxygen bound complex

(complex-5) was computed to be a red shift of 46 cm^{-1}, which is considerably smaller than the carbonyl oxygen bound complex. Experimentally we could not discern any feature corresponding to this mode in the complex.

5.7.1.4 – H_2O antisymmetric stretch (ν_3)

The ν_3 mode of H_2O was computed to be red shifted by 32 cm^{-1} in the complex-1. The perturbation in this mode could not be discerned experimentally in Ar matrix because they were probably masked by the features due to ro-vibrational transitions of monomer H_2O and the self-associated complexes of H_2O. In N_2 matrix we observed a new feature at 3704 cm^{-1}, a red shift of 23 cm^{-1} which agrees well with the computed shift for the complex-1. This feature was assigned to the ν_3 mode of water in complex-1.

The bending mode ν_2 of water in the complex is computed to be blue shifted by about 30 cm^{-1} in the complex-1 and 28 cm^{-1} for the complex-5, relative to the uncomplexed H_2O. Experimentally we could not discern any new feature for this mode in Ar and N_2 matrices. As we have mentioned in the introduction the new features observed on annealing the Ar and N_2 matrices were due to DEC-H_2O complexes and not the higher clusters or to the higher energy conformers of DEC.

5.7.2 – AIM analysis

Atoms-in-molecules (AIM) theory calculations were used to find out the electronic charge density topology for the DEC-H_2O carbonyl and ethoxy complexes. We located (3, -1) bond critical points (BCP) and (3, +1) ring critical points (RCP) that could be associated with different complexes. The electron density ($\rho(r_c)$) and Laplacian of electron density ($\nabla^2\rho(r_c)$) computed for the critical points are shown in Table 5.10. The $\rho(r_c)$ and $\nabla^2\rho(r_c)$ values for HO−H···O bond critical points (BCP1, Table 5.10) in both types of complexes were found to be in the order of 10^{-2} au, the magnitude of the values were found to be larger in carbonyl complexes than ethoxy complexes. As shown in Table 5.10, we also observed secondary

Table 5.10 – Properties of different critical points in DEC-H_2O complexes computed using AIM analysis.

Complex types	**Complexes**	**Critical point**	**$\rho(r_c)$**	**$\nabla^2\rho(r_c)$**
Carbonyl complexes	Complex 1	BCP1	0.02468	0.07672
	Complex 2a	BCP1 BCP2 RCP	0.02511 0.00685 0.00634	0.07953 0.02835 0.03103
	Complex 2b	BCP1 BCP2 RCP	0.02466 0.00498 0.00498	0.07676 0.02394 0.02409
	Complex 3	BCP1 BCP2 RCP	0.02498 0.00692 0.00637	0.07905 0.02868 0.03122
	Complex 4	BCP1 BCP2 RCP	0.02496 0.00727 0.00653	0.07897 0.02925 0.03174
Ethoxy complexes	Complex 5	BCP1	0.01967	0.05773
	Complex 6a	BCP1	0.02154	0.06450
	Complex 6b	BCP1	0.01962	0.05764
	Complex 7	BCP1	0.02143	0.06411
	Complex 8	BCP1	0.02153	0.06430

interactions (BCP2 and RCP) in complexes 2a, 2b, 3 and 4, between O14 of H_2O and H-atoms of ethyl groups. A similar interaction was also observed in case of carbonyl complex of DMC-H_2O described in Chapter 4.

5.8. Conclusion

We have studied the infrared spectra of DEC in an Ar and N_2 matrix. The infrared features observed were assigned primarily to the lowest energy cc(tt) structure. Five features of relatively low intensity were also observed, which are probably due to the higher energy conformers of cis-cis cluster of DEC in the matrix. These higher energy conformers, with cc(tg$^{\pm}$), cc(g$^{\pm}$g$^{\mp}$) and cc(g$^{\pm}$g$^{\pm}$) structures, probably interconvert to the cc(tt) form during deposition in the low temperature matrix and hence have small intensities. The computed frequencies obtained at B3LYP/6-31++G** level of theory were used to corroborate the experimental results. We have also computed energies and structures of the other possible higher energy conformers, belonging to the cis-trans and near-trans-near-trans clusters; however they have not been observed experimentally due to their negligible populations. This work in combination with the studies on the conformations of DEM, DEE and TEP show that the preferred orientation for the terminal carbon atom in an ethoxy chain is trans, in all these compounds. Natural bond orbital analysis reveals that while the delocalization interactions direct the orientation of the anomeric carbon atoms, these interactions do not play any role on the orientation of the terminal carbon atoms in DEC, rather it is the steric effect which decides the conformational preferences of the non-anomeric carbon atoms.

DEC-H_2O, 1:1 complexes were also studied in inert gas matrixes. From the two possible types of water complexes of cc(tt) conformer, carbonyl and ethoxy complexes, the former complex was trapped in Ar and N_2 matrixes and the IR spectra was recorded. The features of complexes were assigned based on the *ab initio* computations performed at B3LYP/6-31++G** level of theory.

References

---

[1] L. H. L. Chia, K. J. Kwan, H. H. Huang, Aust. J. Chem., 1981, *34*, 349.

[2] D. Labrenz, W. Schröer, J. Mol. Struct., 1991, *249*, 327.

[3] J. Wang, Y. Wu, X. Xuan, H. Wang, Spectrochim. Acta Part A, 2002, *58*, 2097.

[4] S. A. Kozlova, V. N. Emel'yanenko, M. Georgieva, S. P. Verevkin, Y. Chernyak, B. Schäffner, A. Börner, J. Chem. Thermodynamics, 2008, *40*, 1136.

[5] K. Sankaran, V. Venkatesan, K. Sundararajan, K. S. Viswanathan, J. Indian Inst. Sci., 2005, *85*, 403.

[6] V. Venkatesan, K. Sundararajan, K. S. Viswanathan, J. Phys. Chem. A, 2003, *107*, 7727.

[7] V. Venkatesan, K. S. Viswanathan, J. Mol. Struct., 2011, *988*, 79.

[8] A. J. Barnes, Matrix isolation spectroscopy, Ed. A. J. Barnes, W. J. Orville-Thomas, A. Müller, R. Gaufrès, D. Reidel, Publishing Company, Holland, 1981, Chapter 23.

[9] N. Ramanathan, K. Sundararajan, B. P. Kar, K. S. Viswanathan, J. Phys. Chem. A, 2011, *115*, 10059.

[10] A. Borba, A. G. Zavaglia, P. N. N. L. Simoes, R. Fausto, J. Phys. Chem. A, 2005, *109*, 3578.

[11] A. Borba, A. G. Zavaglia, R. Fausto, J. Mol. Struct., 2006, *794*, 196.

[12] I. D. Reva, S. V. Ilievab, R. Fausto, Phys. Chem. Chem. Phys., 2001, *3*, 4235.

[13] I. D. Reva, S. G. Stepanian, L. Adamowicz, R. Fausto, Chem. Phys. Lett., 2003, *374*, 631.

[14] M. T. S. Rosado, A. J. L. Jesus, I. D. Reva, R. Fausto, J. S. Redinha, J. Phys. Chem. A, 2009, *113*, 7499.

[15] K. Sundararajan, K. S. Viswanathan, J. Mol. Struct., 2006, *798*, 109-116.

[16] K. V. J. Jose, S. R. Gadre, K. Sundararajan, K. S. Viswanathan, J. Chem. Phys., 2007, *127*, 104510.

---

[17] K. Sundararajan, K. Sankaran, K. S. Viswanathan, A. D. Kulkarni, S. R. Gadre, J. Phys. Chem. A, 2002, *106*, 1504.

[18] J. Szczepanski, S. Ekern, M. vala, J. Phys. Chem., 1995, *99*, 8002.

[19] R. M. Bentwood, A. J. Barnes, W. J. Orville-Thomas, J. Mol. Spectrosc., 1980, *84*, 391.

CHAPTER 6

STUDIES ON THE CONFORMATIONS OF DIPHENYL CARBONATE

6.1 Introduction

Study of DPC conformations has been a topic of great interest, as the conformations of this molecule is believed to influence the structure and mobility of polycarbonates in the crystalline polymer.[1] The glassy state of DPC and polycarbonates are expected to have a nearly random mixture of 'syn/anti' conformers, which arise due to the phenyl rings rotation.[2] Change in polymer conformations due to the diphenyl carbonate moiety is responsible for the irregular behaviour of thermal crystallization of polycarbonates.[3] A few groups have reported the conformations of DPC in order to understand the physical properties of polycarbonates. They have reported that the three conformations of DPC are cis-cis (anti), cis-cis (syn) and cis-trans, which are shown in Fig. 6.1. Based on the study of the dipole moment and molar Kerr constant of DPC in carbon tetrachloride solution, Chia et al. have proposed that a mixture of conformers with cis-cis and cis-trans configurations exist, with a phenyl ring rotation of angle (φ) where the range of angles vary from 0° <φ <90°. They have concluded that the angle φ need not have the same value in each conformation.[4] King and Codella have studied the IR spectra of DPC in methylene chloride solution at different temperatures 298, 213 and 183 K. However, they could not make any conclusion on the conformational behaviour of DPC.[5] IR spectra of DPC in CCl_4 solution near the 1200 cm^{-1} region has been studied by Schmidt et al.[6] and the features at 1240 and 1227 cm^{-1} have been assigned for the cis-cis and cis-trans conformers respectively. They have not considered the band corresponding to carbonyl stretching for their analysis as it has been reported that the assignment of this band may be complicated due to Fermi resonance.[7] In a later work, on the basis of *ab initio* calculation at B3LYP/6-31G* level of theory and experimental results of IR

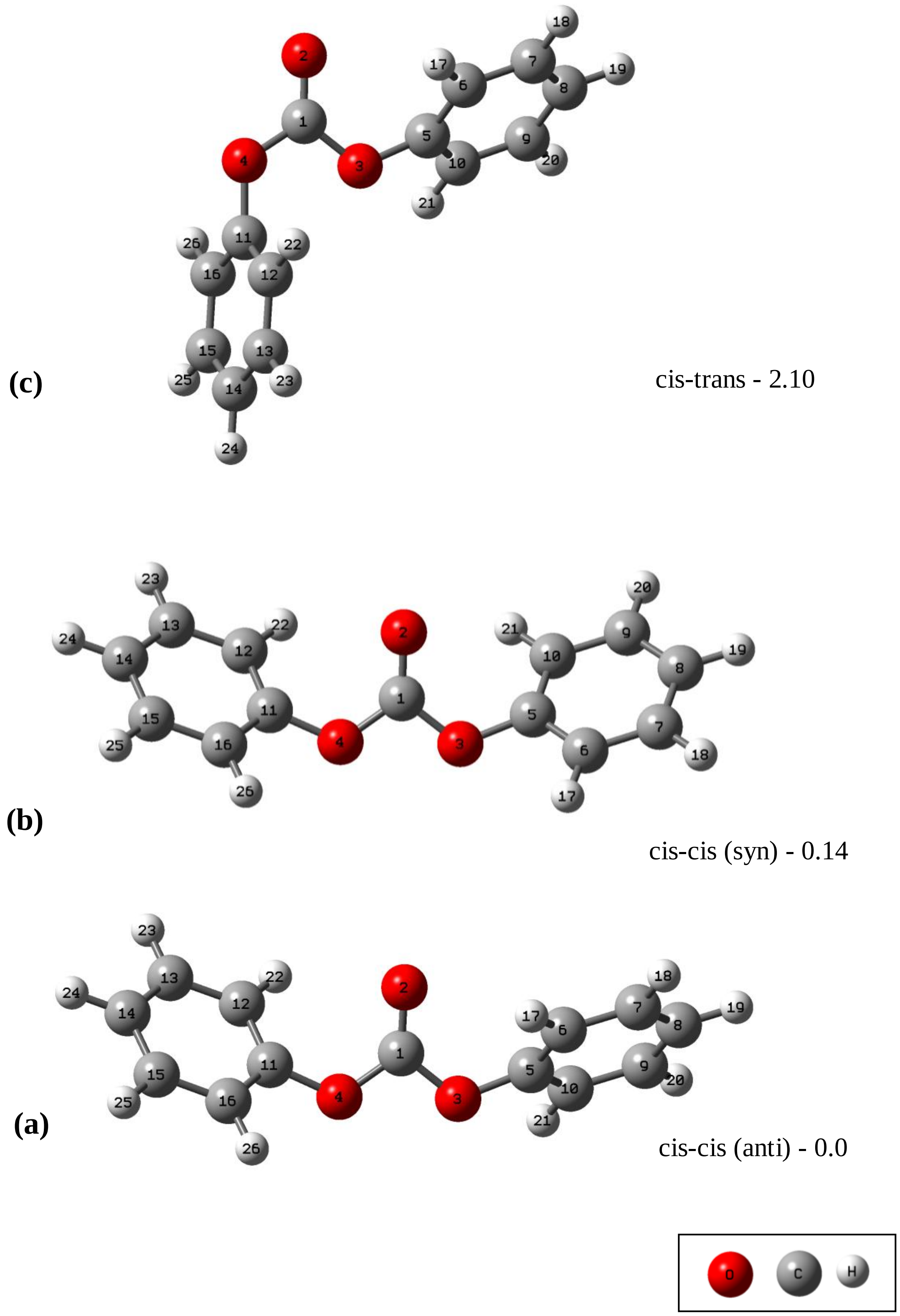

Fig. 6.1 – Computed structures at B3LYP/6-31++G** level of different conformers of DPC (a) cis-cis (anti); (b) cis-cis (syn); (c) cis-trans. The relative energy (kcal/mol) of each conformer relative to the ground state conformer is given against each structure.

and Raman spectroscopy study of DPC in CCl_4 and $CDCl_3$, Dybal et al. have shown that cis-trans conformer is energetically preferred in these solutions.[1] Using spectra in the 1300-1200 cm^{-1} region, they have shown that "the high-frequency component in the infrared spectra and the low-frequency component in the Raman spectra can be assigned to the cis-trans conformational structure", which contradicts the work reported by Schmidt et al.[6]

Several groups have carried out theoretical calculations on conformations of DPC. Erman et al.[8] have presumed the structure of DPC to be cis-cis and pointed out that the potential energy surface of DPC is dominated by two opposing effects: (i) steric interactions between the carbonyl oxygen and an ortho CH group of phenyl, which oppose coplanarity of the phenyl rings and carbonate group, and (ii) electron delocalization favoring the planar configuration. Laskowski et al.[9] have performed the *ab initio* calculation on the conformations of DPC at SCF level using STO-3G, 4-31G and 6-31G* basis sets and pointed out that cis-cis form is the ground state conformer with the cis-trans form being the next higher energy structure located at an energy of 2.75 kcal/mol above the ground state conformer. The calculation performed using polarization basis sets (6-31G*) agreed well with the experimental values. Bicerano and Clark[10] performed AM1 calculation and have shown that two nearly degenerate structures arise from the cis-cis conformation of DPC; one, where the two phenyl rings are rotated to one side of the carbonyl group, while in the second conformer, the phenyl rings are rotated opposite to each other. Sun et al. using all-atom force field calculations have obtained results similar to that reported by Laskowski et al.[11] The cis-cis configuration exists in two possible rotated conformers as discussed above with phenyl ring rotations amounting to ~60º. In later work[12] they have performed *ab initio* calculations using HF/6-31G*, MP2/6-31G* and DFT(ACM)/DZVP level of theories on methyl phenyl carbonate. According to these calculations the phenyl ring in the methyl phenyl carbonate has been found to be rotated at angles corresponding to 63.5º, 59.1º and 59.2º respectively, which yield different structures. Blender has also emphasized on the competition between electron delocalization and steric repulsion interactions which make the phenyl rings to be rotated at different angles.[2] On the basis of HF/6-31G** level of calculation, he has reported the two conformers 'syn' and 'anti' for the cis-cis configuration where the two phenyl rings are twisted on the same or opposite sides. He has also proposed the glassy state of DPC is a mixture of 'syn' and 'anti' conformers. Using HF/6-311G** and B3LYP/6-311G** levels of calculation Meyer et al. has found similar informations regarding the conformations of DPC.[13] However, so far, to best of our knowledge, no detailed studies on IR spectra in combination with *ab initio* calculations have been performed to discuss the molecular conformations of DPC.

In this work, diphenyl carbonate (DPC) was studied for its conformations using matrix isolation infrared spectroscopy and *ab initio* computations.

6.2 Experimental details

Diphenyl carbonate, (Aldrich, 99% purity) was used without further purification for our experiments. DPC has low vapor pressure at room temperature, and hence the sample and the deposition line had to be heated over the temperature range 298-308 K to obtain acceptable concentrations of the compound in the matrix. Matrix gas, Ar or N_2, swept over the heated sample carried the DPC to the cold KBr substrate.

Experiments were performed by maintaining the effusive source at two different nozzle temperatures, 303 K and 473 K. A pulsed supersonic jet source was also used to deposit the sample mixture with stagnation pressure varied over a range 300 - 1000 torr. In these experiments the pulse width and pulse repetition rate were kept at 50 msec and 0.1 Hz respectively. The sample and the transfer line were heated over the temperature range 343 - 373 K during these experiments.

6.3 Computational details

The structure and vibrational frequencies of different conformers were calculated at the B3LYP/6-31++G** level of theory. Natural Bond Orbital analysis was also performed at the same level of theory to find out the delocalization interactions involved in different conformations.

6.4 Results

6.4.1 Experimental

Figs. 6.2 and 6.3 show the IR spectra of DPC isolated in a N_2 matrix at 12 K over the mid-IR region. Fig. 6.2 shows Grid A (1820- 1740 cm^{-1}), Grid B (1630-1450 cm^{-1}) and Grid C (1340-1150 cm^{-1}) whereas Fig. 6.3 shows Grid A (1030-990 cm^{-1}), Grid B (900-670 cm^{-1}) and Grid C (550-480 cm^{-1}). The spectral regions shown in the two figures correspond to the C=O stretching, O−C−O stretching, C−O stretching, CH deformation and ring deformation modes of DPC. In both the figures traces ‘b’ and ‘c’ represent the IR spectra using effusive source at two different nozzle temperatures 303 and 473 K respectively. Trace ‘a’ in both figures, represent the computed IR spectra of DPC at 473K. The infrared spectrum of DPC in Ar matrix is complicated due to the appearance of multiple site split features and we have therefore presented only our experiments using the N_2 matrix.

We have also carried out experiments using supersonic jet source. In these experiments we were able to deposit only a small amount of DPC and observed features due to phenol and carbon dioxide. The high stagnant pressure and heating, probably leads to the hydrolysis of DPC and gives the above products.[14,15] As a result, supersonic jet experiment did not provide any new information regarding the conformations of DPC and hence it is not discussed.

6.4.2 Computational

Three conformations of DPC, cis-cis (anti), cis-cis (syn) and cis-trans were found to

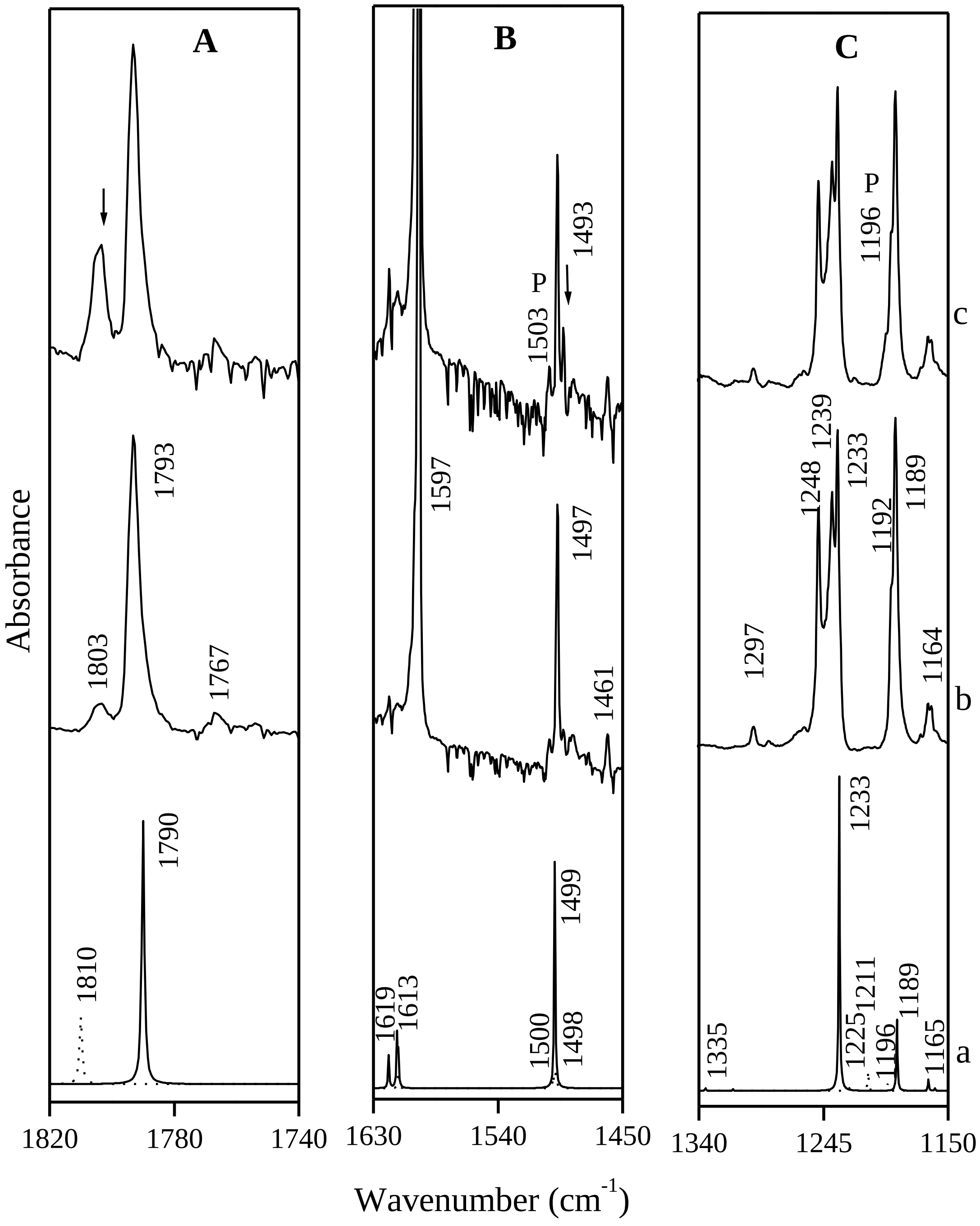

Fig. 6.2 – IR spectra of DPC in N_2 matrix at 12 K (Grid A: 1820-1740 cm^{-1}, Grid B: 1630-1450 cm^{-1} and Grid C: 1340-1150 cm^{-1}) (a) simulated spectra at 473 K (solid line for cis-cis (anti) and dotted line for cis-trans conformer) (see text for detail); (b) and (c) MI spectra recorded using an effusive nozzle at 303 K and 473 K respectively.

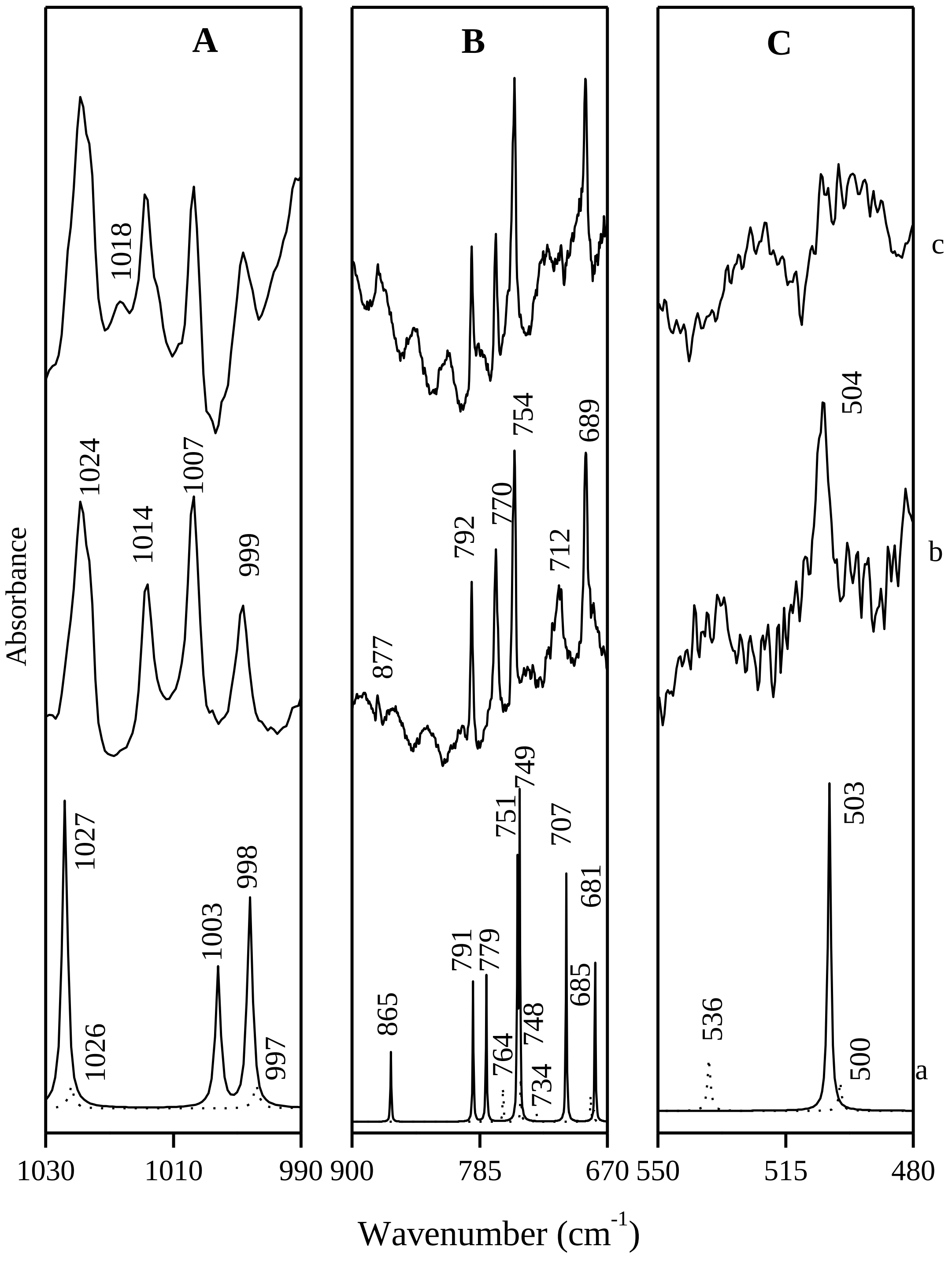

Fig. 6.3 – IR spectra of DPC in N_2 matrix at 12 K (Grid A: 1030-990 cm^{-1}, Grid B: 900-670 cm^{-1} and Grid C: 550-480 cm^{-1}) (a) simulated spectra at 473 K (solid line for cis-cis (anti) and dotted line for cis-trans conformer) (see text for detail); (b) and (c) MI spectra recorded using an effusive nozzle at 303 K and 473 K respectively.

be minima on the potential energy surface at B3LYP/6-31++G** level. The structures of conformers are shown in Fig. 6.1. The relative energies corrected for zero point energy (kcal/mol), zero point energies (Hartree), dipole moments and degeneracies of different conformers and transition states are given in Table 6.1. Table 6.2 shows the important geometrical parameters of the optimized structures. It is clear from Table 6.1 and Fig. 6.1 that cis-cis (anti) form is the ground state conformer of DPC. Here the two phenyl rings are not coplanar with the carbonate group; rather they are rotated to opposite sides with respect to the carbonate (-OCOO-) group (Fig. 6.1a, Table 6.2) at angles of 52.5° and 55.0°, respectively. The second conformer, cis-cis (syn), lies 0.14 kcal/mol (Table 6.1) above the ground state conformer. Here both the phenyl rings are rotated at an angle 55.1° and 55.8° respectively, but on the same side with respect to the plane containing the carbonate group, as shown in Fig. 6.1b and Table 6.2. The calculated structural parameters (except the phenyl ring rotation angle) for both the conformers of cis-cis configuration of DPC are nearly the same and agree well with the reported crystal structure data.[16]

In order to understand the rotational flexibility of the phenyl rings in the molecule, energies of the various structures, where the phenyl group was progressively rotated, was calculated. For this purpose, the dihedral angles H17-C6-C5-O3 and H22-C12-C11-O4 of anti conformer were frozen at a particular value and other geometrical parameters were allowed to optimize such that the phenyl rings were rotated to the opposite sides of the carbonyl group with same angle. The dihedral angles were varied over the range 0^{o} to 90^{o}, in steps of 10^{o}. In syn form, the dihedral angles varied are H21-C10-C5-C3 and H22-C12-C11-O4, and both are rotated to one side with same angle.

Table 6.3 shows the energies of the above optimized geometries, relative to the corresponding conformers. Two barriers are observed in both the case, one at 0° and other at 90° for phenyl rings rotation. For anti form, the minimum energy geometries correspond to

Table 6.1 – Relative energies (kcal/mol), zero point energies (ZPE) (Hartree), dipole moment (D) and degeneracy of different conformers of DPC at B3LYP/6-31++G level of calculations.**

Conformer	**Relative energy**[a]	**ZPE (Hartree)**[b]	**Dipole moment (D)**	**Degeneracy**
Cis-cis (anti)	0.00	0.199515	0.20	1
Cis-cis (syn)	0.14	0.199479	0.24	1
Cis-trans	2.10	0.199294	3.65	2
TS1[c]	6.21	0.199024	2.27	-
TS2[d]	6.53	0.198994	2.39	-
TS3[e]	0.17	0.199378	0.23	-

[a] ZPE corrected values.
[b] Unscaled value.
[c] Transition state connecting to cis-cis and cis-trans.
[d] Transition state connecting to cis-cis and cis-trans.
[e] Transition state connecting to cis-cis (anti) and cis-cis (syn).

Table 6.2 – Important structural parameters of different conformers of DPC. Bond length (Å), bond angles (°) and torsional angles[a] (°).

Parameters	cis-cis (anti)	cis-cis (syn)	cis-trans	TS1	TS2	TS3
C1-O2	1.205	1.205	1.202	1.201	1.201	1.205
C1-O3	1.351	1.351	1.356	1.349	1.349	1.352
C1-O4	1.351	1.351	1.352	1.364	1.365	1.350
O3-C5	1.402	1.402	1.403	1.406	1.406	1.406
O4-C11	1.403	1.402	1.405	1.393	1.393	1.402
C1-O3-C5	119.7	119.5	119.9	120.4	120.7	117.4
C1-O4-C11	119.4	119.4	122.1	119.8	119.9	120.1
O2-C1-O3	127.1	127.1	126.9	127.1	127.1	126.6
O2-C1-O4	127.0	127.1	122.0	124.5	124.5	127.4
O2-C1-O3-C5	0.8	-0.5	1.4	-0.1	0.1	-0.8
C1-O3-C5-C6	52.5	-55.1	52.6	50.8	50.1	97.5
C1-O3-C5-C10	-131.9	129.3	-131.7	-133.6	-134.2	-86.7
O2-C1-O4-C11	0.9	0.7	-179.2	92.5	-93.1	0.9
C1-O4-C11-C12	55.0	55.8	84.9	168.0	19.0	49.6
C1-O4-C11-C16	-129.4	-128.6	-100.1	-13.1	-162.4	-134.8
O4-C1-O3-C5	-179.1	179.8	-178.8	-177.1	176.7	179.4
O3-C1-O4-C11	-179.1	-179.6	1.0	-90.4	90.2	-179.4

[a] Torsional angle ABCD implies the angle between two planes ABC and BCD.

Table 6.3 – Relative energies and number of negative wavenumbers of different frozen geometries of DPC at B3LYP/6-31++G level of theory.**

Dihedral angle of phenyl rotation	Anti		Syn	
	Relative energy[a] (kcal/mol)	No. of negative wavenumbers	Relative energy[b] (kcal/mol)	No. of negative wavenumbers
0	1.02	2	0.86	2
10	0.97	2	0.79	2
20	0.74	1	0.63	2
30	0.46	2	0.38	0
40	0.18	0	0.16	0
50	0.02	0	0.02	0
60	0.03	0	0.02	0
70	0.21	2	0.11	0
80	0.38	2	0.25	2
90	0.70	2	0.30	2

[a] Relative energies correspond to cis-cis (anti) conformer, not corrected for ZPE.
[b] Relative energies correspond to cis-cis (syn) conformer, not corrected for ZPE.

phenyl dihedral angle of 40º-60º. The potential energy surface is also flat in this region. Hence, the rotational flexibility of the phenyl rings with a dihedral angle of 40º-60º corresponds to a minimum, which agrees well with the earlier force field calculation.[3] In a similar manner, a larger rotational flexibility 30º-70º is observed for the syn geometry, which is shown in Table 6.3. However, at room temperature (298 K), the phenyl rings could rotate freely from 20° to 90° and overcome the smaller barrier at 90°. A similar study was carried out to correlate the phenyl ring rotation in trans-stilbene where phenyl rings could rotate freely from 0° (planar geometry) to 30°.[17]

The next higher energy conformer is the cis-trans form (Fig. 6.1c), which lies at 2.10 kcal/mol above the ground state conformer. The phenyl ring is oriented in cis position to the carbonyl group and it is rotated at an angle of 52.6° in a similar manner as in the case of anti and syn form, whereas the phenyl ring which is oriented in trans position is almost perpendicular to the plane containing carbonate group, which probably reduces the steric interaction between the two phenyl rings. The dihedral angles presented in Table 6.2 for cis-trans conformer shows, C1-O4-C11-C16 (-100.1°) is greater than C1-O4-C11-C12 (84.9°) probably reduces the steric repulsion between the phenyl hydrogens H26 and H21.

The barriers of conformer interconversion between different conformations of DPC were computed using the methods described in Chapter 2. The transition state connecting the cis-cis (anti) and cis-cis (syn) conformers lies 0.17 kcal/mol above the ground state conformer. This shows that the conformer inter conversion from cis-cis (syn) to cis-cis (anti) faces a negligible barrier of 0.03 kcal/mol which agrees well with the HF/6-31G* level calculations carried out by Sun et al.[11,12] The structure of the transition state is given in Fig. 6.4a, where the dihedral angle H17-C6-C5-O3 is 90°. Similarly, interconversion barriers from cis-trans to cis-cis (anti) were calculated; two first order saddle points were optimized with a

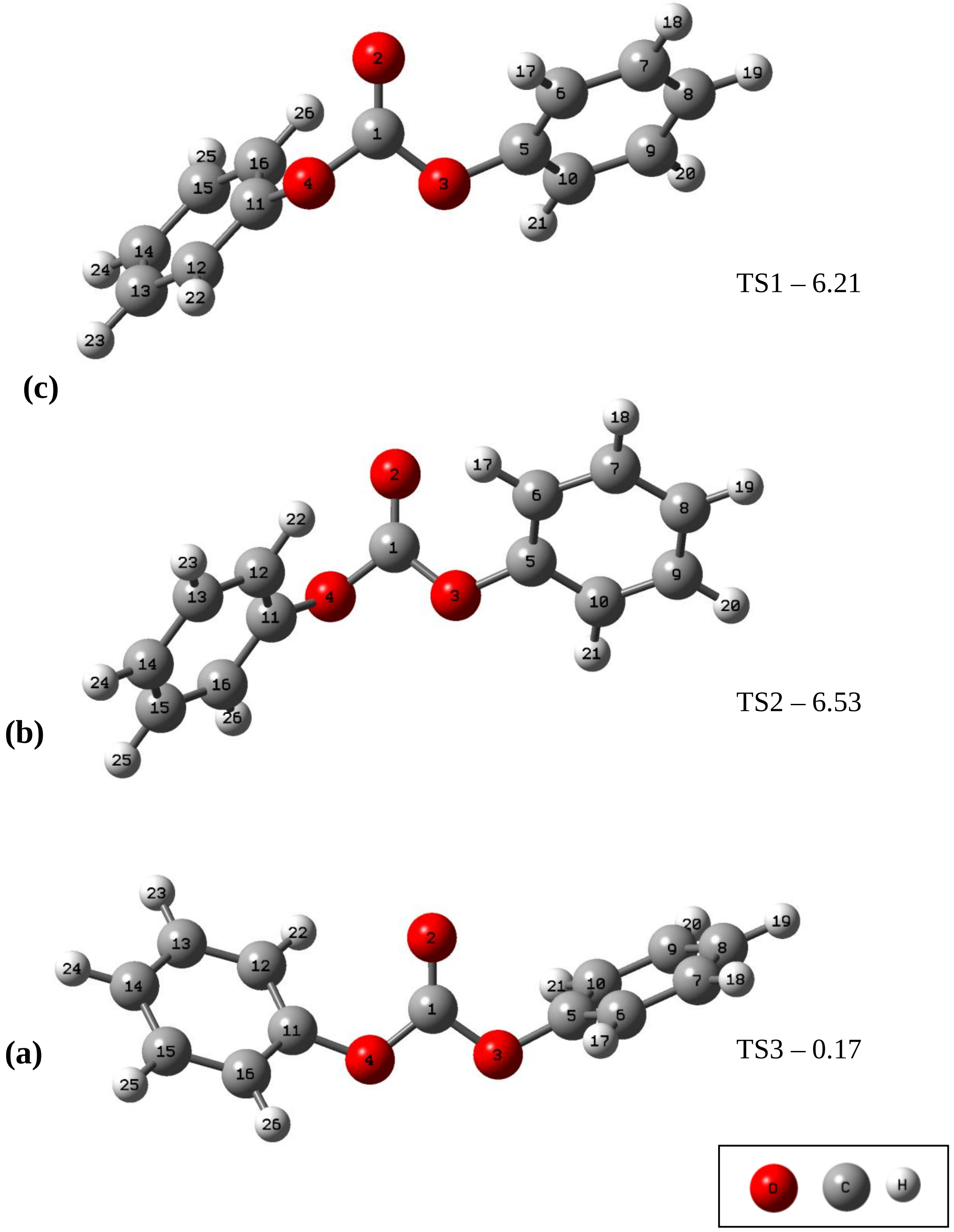

Fig. 6.4 – Computed structures at B3LYP/6-31++G** level of the different transition states connecting to the conformers of DPC (a) TS1; (b) TS2; (c) TS3. TS1 connects the conformers cis-cis (anti) and cis-cis (syn), whereas TS2 and TS3 connect the conformers cis-cis (anti) and cis-trans. The relative energy (kcal/mol) of each structure relative to the ground state conformer is given against each structure.

barrier height of 4.43 and 4.11 kcal/mol. Figs. 6.4b and 6.4c, gives the transition state structures.

Calculated vibrational frequencies were scaled with a scaling factor of 0.9817. The scaling factor was obtained when the highest intensity feature occurring at 1233 cm^{-1} in experiment was correlated with the highest intensity computed feature at 1256 cm^{-1} of the ground state conformer. The scaled computed vibrational frequencies are shown in Table 6.4. The vibrational frequencies for the cis-cis (anti) and cis-cis (syn) are nearly the same. Hence the simulated spectrum of the ground state cis-cis (anti) conformer shown in trace ‘a’ is weighted for the sum of cis-cis (anti) and cis-cis (syn) conformer populations at 473 K. Simulated spectrum of cis-trans conformer is weighted for its population at 473 K.

6.5 Discussion

6.5.1 Vibrational assignments

The spectral features observed at 1793, 1497, 1297, 1248, 1239, 1233, 1192, 1189, 1164, 1024, 1007, 999, 877, 792, 770, 754, 712, 689, 504 cm^{-1} shown in trace ‘b’ of Figs. 6.2 and 6.3 are essentially due to the ground state cis-cis (anti) conformer of DPC. Features observed at 1248, 1239 and 1233 cm^{-1}; 1192 and 1189 cm^{-1} of DPC in N_2 matrix may be due to matrix site split features because similar spectral features with different shapes were observed in Ar matrix (not shown). The scaled computed frequencies for the cis-cis (anti) conformer agree well with the experimental observed spectra obtained using an effusive nozzle source heated at 303 K which are shown in Table 6.4, Figs. 6.2 and 6.3. Table 6.4 shows the calculated vibrational frequencies of features with intensities ≥10 km/mol, which were observed experimentally.

It should be mentioned that the calculated frequencies of cis-cis (syn) conformer occur very close to that of ground state cis-cis (anti) structure and hence it becomes rather difficult to discern unambiguously the features due to these two structures (Table 6.4). The

Table 6.4 – Experimental and calculated wavenumbers of different conformations of diphenyl carbonate.

Calculated[a]		Exp. cis-cis (anti)	Calculated[a] cis-trans	Exp. cis-trans	Approximate assignment of vibrational modes
Cis-cis (anti)	Cis-cis (syn)				
503(13)[b]	504(19)	504	500(10)[b]	-	Ring Puckering
530(5)	530(4)	-[c]	536(18)	-	
681(25)	681(43)	689	682(16)	-	
707(39)	708(11)	712	685(36)	-	
749(50)	744(24)	754	734(12)	-	CH opb
751(39)	754(94)		748(60)		CO_3 Out of Plane Def
779(23)	778(4)	770	764(47)	-	CH opb+ CO_3 Dancing + COC bend
791(22)	791(26)	792	816(3)	-	Ring Def
865(11)	866(11)	877	857(9)	-	Ring def + OCO bend
997(4)	997(15)	999	986(24)	-	Ring def + OCO sym str
998(15)	997(4)		997(14)	-	Ring def
1003(10)	1003(11)	1007	999(0.2)	-	Ring def + OCO sym str
-	-	1014	-	-	
1027(22)	1027(21)	1024	1026(14)	-	Ring def
1081(7)	1081(16)	-	1081(9)	-	
1160(14)	1160(16)	1164	1161(2)	-	CH ipb
1165(64)	1165(65)		1164(11)		
1170(0.3)	1170(0.2)	-	1168(18)	-	
1189(405)	1189(411)	1189, 1192	1196(374)	-	O-C_{ring} str
1233(1789)	1232(1759)	1233, 1239, 1248	1211(968)	-	OCO asym str
1245(0.5)	1245(0.5)	-	1225(201)	-	COC asym str
1314(10)	1314(2)	1297	1314(4)	-	CH ipb + Ring Str
1335(15)	1334(16)	-	1334(5)	-	
-	-	1461, 1486		-	
1499(110)	1499(112)	1497	1498(82)	1493 ?	CH ipb + Ring Str
1502(4)	1502(3)	-	1500(50)	-	
1612(15)	1612(35)	Coinciding with water features	1612(32)	-	
1613(25)	1612(4)		1612(38)		
1618(1)	1618(13)		1616(4)		
1619(16)	1619(7)		1619(8)		
1790(257)	1791(262)	1793	1810(570)	1803 ?	C=O str

[a] Computed at B3LYP/6-31++G** level and then scaled with 0.9817 (N_2 matrix); computed wavenumbers with intensities ≥10 km/mol are listed here; a few wavenumbers with intensities <10 km/mol are also listed here for the sake of completion of the table.

[b] Intensities (km/mol) in parenthesis.

[c] The features are not observed in computation or experiment.

relative energy of cis-cis (syn) with respect to the ground state conformer is only 0.14 kcal/mol and it may be expected that this conformer could be significantly populated. In fact, the population of this conformer is almost equal to that of the cis-cis (anti) at room temperature. However, it should be noted that the interconversion from syn to anti is almost a barrier less transition (0.03 kcal/mol) and it is therefore very likely that this inter conversion is facile during deposition and we may be observing only the cis-cis (anti) structure in the matrix. A similar observation was reported for trimethyl phosphite with a rotational barrier < 0.7 kcal/mol.[18]

The next higher energy conformer is cis-trans form, which lies 2.10 kcal/mol above the ground state conformer. At the temperature of the experiments (303 K), contributions of cis-cis (anti), cis-cis (syn) and cis-trans conformer to the total population was computed to be 53.9%, 42.8% and 3.3% respectively. At an elevated temperature 473 K, the populations of the respective conformers would be 48.2%, 41.5% and 10.3%. This calculation shows an almost threefold increase in population for the cis-trans conformer, whereas no significant change in population could be observed for the other conformers. Hence, to trap the cis-trans conformer in matrix, experiments were carried out at an elevated temperature. The resulting IR spectrum is shown in trace 'c' of Figs. 6.2 and 6.3. Five features at 1803, 1503, 1493, 1196 and 1018 cm^{-1} were found to gain intensity when experiments were performed at 473 K. The features at 1503 and 1196 cm^{-1} were assigned to phenol,[19] a hydrolysis product of DPC.[14,15] Feature at 1018 cm^{-1} does not show any temperature dependence and hence was ruled out as a possible feature of the higher energy conformer. The experimental features at 1803 and 1493 cm^{-1} were close to the computed frequencies at 1810 and 1498 cm^{-1} respectively. However, the features which were computed to have large intensities and occurring at 1211 and 1225 cm^{-1}, for the cis-trans conformer were not observed experimentally. Hence we refrain from assigning the features at 1803 and 1493 cm^{-1} for the cis-trans conformer. These two features may be due to some decomposition products or some other adducts formed in the process of deposition. Hence, we conclude that only the ground state cis-cis (anti) conformer was trapped in the matrix.

We also tried to populate the higher energy conformer by photoirradiating the sample. For this purpose, photoirradiations were performed in both after and during deposition methods, using the fourth harmonic wavelength (266 nm) light of the Nd-YAG laser (Quantel, Brilliant b). When laser light was irradiated onto DPC we found it decomposes to phenoxyl radical and carbon monoxide which agrees well with earlier observation by Spanget-Larsen et al.[20]

6.5.2 Comparison of DPC with DMC

In DPC phenyl groups replaces the methyl groups of DMC (Chapter 4). The rotation of the phenyl ring leads to additional conformers viz. cis-cis (anti) and cis-cis (syn). Both the molecules possess higher energy conformer cis-trans. The energy difference between cis-cis and cis-trans in DMC is 2.90 kcal/mol whereas in DPC it is 2.10 kcal/mol between cis-cis (anti) and cis-trans structure. Although, the second higher energy conformer, near-trans-near-trans is optimized to be a minimum in DMC, no such conformer was obtained for DPC, probably due to the steric repulsion among the large phenyl groups.

The barrier for conformer interconversion from cis-trans to cis-cis form was found to be 6.44 kcal/mol for DMC where as in DPC it is 4.11 kcal/mol. Decrease in barrier in DPC can be explained as the phenyl ring withdraws π-electron density from $O_{phenoxy}$ due to formation of different resonance structures and hence there is less π-electron density available for delocalization with carbonyl group. As a result, the corresponding C-OPh bond weakens and has more of a single bond character which facilitates rotation. Weakening of the bond can be explained as C-OPh bond elongates to 1.351 Å in DPC from 1.340 Å in DMC. A similar decrease in rotational barrier around C-N bond has been observed in case of N-aryl carbamates.[21,22]

6.5.3 Natural bond orbital analysis

Natural bond orbital analysis was performed on the different conformers of DPC to understand the role of delocalization interactions towards conformational preferences. The major delocalizations were found to be between the lone pairs of oxygens and the C=O group of DPC which are responsible for the cis and trans orientations of the phenyl groups as observed in case of DMC (Chapter 4) and DEC (Chapter 5). We have also observed delocalizations correspond to the phenyl rings. Each phenyl ring shows six $\pi \rightarrow \pi^*$ interactions which create an overall electron delocalization in the ring. Each interaction participates in complementary cyclic bi-directional donor-acceptor interactions making the phenyl rings as a unit group.[23]

Other important interactions involved in DPC are delocalizations of lone pair of phenoxy oxygens to the phenyl rings ($n \rightarrow \pi^*$). In cis-cis (anti) and cis-cis (syn) conformers, where the phenyl rings are rotated ~55° from the plane of the carbonate (-O(C=O)O-) group, the second order perturbation energies (E_2) corresponding to these interactions are 9.1 and 10.0 kcal/mol respectively. When the phenyl rings of DPC lie in the same plane of the carbonate group (The above planar geometry is obtained by freezing the phenyl ring rotation at 0° and then optimizing for all other geometrical parameters) the $n \rightarrow \pi^*$ interaction is maximum and the E2 value was found to be 22.4 kcal/mol. The $n \rightarrow \pi^*$ interaction is almost negligible ($E_2 < 0.5$ kcal/mol) when the phenyl rings are in the perpendicular orientations with respect to the carbonate group. (Here the phenyl rings rotations were frozen at 90° and then optimized for all other geometrical parameters.)

All vicinal and geminal interactions were deleted separately for each conformer of DPC to understand their role of importance in conformational preferences. All possible delocalization interactions were also deleted for each conformer. The deletion energy, change in energy and relative change in energy are tabulated in Table 6.5. As in the case of DMC and DEC, vicinal interactions were found to be dominating interactions in DPC. It has to be pointed out that geminal interactions do play significant role in deciding the conformational preferences e.g. trimethyl phosphite.[18] From the Table 6.5 it is clear that the change in energy due to deletion of all vicinal interactions is more for cis-cis when compared to cis-trans conformer and shows its importance in conformational preferences.

A comparative study was also performed for deletion of all delocalization interactions for cis-cis (anti), cis-cis (syn) conformers and a geometry where the two phenyl rings and the carbonate group are in one plane (planar geometry). The results are shown in Table 6.5. When NBO calculations are performed for the planar geometry, the phenyl rotation angles are frozen at 0° and optimized for all other geometrical parameters and the change in energy due to deletion of all delocalization interactions is found to be more for the frozen planar geometry whereas it is almost same for both cis-cis (anti) and cis-cis (syn) conformer. This clearly shows that delocalization interactions stabilize more for the planar geometry and this should be the ground state conformer when compared to the other two forms but actually, this is not the case. In fact, cis-cis (anti) and cis-cis (syn) forms are the preferred optimized structures of DPC as discussed in previous sections and the energy of the planar conformer is 1.02 kcal/mol higher relative to the cis-cis (anti) conformer (Table 6.3). Hence, from the above discussion it implies that apart from the stabilizing $n \rightarrow \pi^*$ delocalization interaction, steric interaction also plays a major role in stabilizing the conformers in DPC.

It has been reported[2,8] that there are steric repulsions between ortho hydrogens (one of the two ortho hydrogens of each phenyl group) of phenyl rings and the carbonyl oxygen which forces the phenyl rings to have rotated geometries. However, NBO analysis shows, for the planar geometry, an $n \rightarrow \sigma^*$ delocalization interaction (E_2=1.7 kcal/mol) is present between the lone pair of carbonyl oxygen and the σ^* orbital of C-H at the ortho position of

Table 6.5 – Energies of different conformers of DPC after deletion of all geminal, all vicinal and all delocalization interactions.

Conformer	Interactions deleted	Deletion energy (Hartree)	Change in energy		Relative change in deletion energy (%)
			Hartree	kcal/mol	
Cis-cis (anti)	Geminal	-726.629363219	0.495143	310.7	0.068
	Vicinal	-725.398406550	1.726100	1083.1	0.238
	All	-724.946075003	2.178431	1367.0	0.301
Cis-cis (syn)	Geminal	-726.629273865	0.495048	310.6	0.068
	Vicinal	-725.399235965	1.725085	1082.5	0.238
	All	-724.947095640	2.177226	1366.2	0.301
Cis-trans	Geminal	-726.625745550	0.495341	310.8	0.068
	Vicinal	-725.420372723	1.700714	1067.2	0.235
	All	-724.955521033	2.165566	1358.9	0.300
Cis-cis (0^{o}) Frozen geometry	Geminal	-726.625029665	0.497935	312.4	0.068
	Vicinal	-725.391621000	1.731344	1086.4	0.239
	All	-724.931842416	2.191122	1375.0	0.303

phenyl ring. Furthermore, deletion of these two possible interactions results in 9.1 kcal/mol increase in energy for the planar geometry. This indicates that there is an attractive and not a repulsive interaction between the oxygen and hydrogens. To probe further, AIM analysis were performed on the planar geometry to look for the (3-1) bond critical point between the ortho hydrogen and carbonyl oxygen. The result showed BCPs between the ortho hydrogens and the carbonyl oxygen, which explains the H-bond formation. The electronic charge density ($\rho(r_c)$) and Laplacian of electronic charge density ($\nabla^2\rho(r_c)$) of the two critical points are almost similar and the values are nearly 0.0183 and 0.0667 respectively. Hence, the steric repulsion may not be between the ortho hydrogens and carbonyl oxygen but may be between the ortho carbon atom of the phenyl ring and the carbonyl group, which forces the ortho carbon atom to orient in the gauche position.

To find out the reasons of steric interaction we compared the geometrical parameters of planar geometry with that of cis-cis (anti) conformer. For the planar geometry the atomic distances O2C6, O2C12, C1C6 and C1C12 are 2.856, 2.856, 2.991and 2.991 Å respectively. These atomic distances are smaller than the sum of van der Waals radii of the corresponding atoms and this could be the cause of steric interaction. The steric interaction decreases as the phenyl ring rotates and the atomic distances between the carbons and oxygens increase. In cis-cis (anti) conformer these atomic distances increases to 2.970, 2.988, 3.000 and 3.007 Å respectively.

From the above discussion it clearly shows that both delocalization and steric interactions play an important role in stabilizing the cis-cis (anti) and cis-cis (syn) conformers of DPC.

6.6 Conclusion

Infrared spectra of DPC isolated in N_2 matrix were recorded and the vibrational frequencies were assigned to the ground state cis-cis (anti) conformer. Heated nozzle and supersonic jet experiments could not help us to trap the higher energy conformers of DPC as the heating resulted in the hydrolysis of DPC to form phenol and carbon dioxide. Vibrational assignments were made based on the *ab initio* calculations performed using B3LYP/6-31++G** level of theory. Two more conformers, cis-cis (syn) and cis-trans were also indicated in our computation. Natural bond orbital analysis shows vicinal interactions are the dominating interactions in DPC similar to DMC and DEC. When phenyl ring takes the cis orientation, in planar geometry, an attractive interaction was observed between the ortho hydrogen of phenyl ring and carbonyl oxygen rather the steric repulsion explained before by different groups. The steric repulsion between an ortho carbon atom of phenyl ring and the carbonyl group may contribute to the steric forces that responsible for the rotated geometry of phenyl rings at cis position with respect to carbonyl group in DPC.

References

---

[1] J. Dybal, P. Schmidt, J. Baldrian, J. Kratochvil, Macromolecules, 1998, *31*, 6611.

[2] J. T. Bendler, Comp. and Theor. Polymer Science, 1998, *8*, 83.

[3] P. R. Sundararajan, Can. J. Chem., 1985, *63*, 103.

[4] L. H. L. Chia, K. J. Kwan, H. H. Huang, Aust. J. Chem., 1981, *34*, 349.

[5] J. A. King Jr., P. J. Codella, Macromolecules, 1990, *23*, 345.

[6] P. Schmidt, J. Dybal, E. Turska, A. Kulczycki, Polymer, 1991, *32*, 1862.

[7] G. Guiheneuf, C. Laurence, Spectrochim. Acta (A), 1978, *34*, 15.

[8] B. Erman, D. C. Marvin, P. A. Irvine, P. J. Flory, Macromolecules, 1982, *15*, 664.

[9] B. C. Laskowski, D. Y. Yoon, D. McLean, R. L. Jaffe, Macromolecules, 1988, *21*, 1629.

[10] J. Bicerano, H. A. Clark, Macromolecules, 1988, *21*, 585.

[11] H. Sun, S. J. Mumby, J. R. Maple, A. T. Hagler, J. Am. Chem. Soc., 1994, *116*, 2978.

[12] H. Sun, S. J. Mumby, J. R. Maple, A. T. Hagler, J. Phys. Chem., 1995, *99*, 5873.

[13] H. Meyer, O. Hann, F. Muller-Plathe, J. Phys. Chem. B, 1999, *103*, 10591.

[14] C. M. Comisar, S. E. Hunter, A. Walton, P. E. Savage, Ind. Eng. Chem. Res., 2008, *47*, 577.

[15] A. G. Strikovsky, D. Kasper, M. Grün, B. S. Green, J. Hradil, G. Wulff, J. Am. Chem. Soc., 2000**,** *122*, 6295.

[16] J. A. King Jr., G. L. Bryant Jr., Acta Crystallogr., 1993, *C49*, 550.

[17] W.-G. Han, T. Lovell, T. Liu, L. Noodleman, Chemphyschem, 2002, *3*, 167.

[18] N. Ramanathan, K. Sundararajan, B. P. Kar, K. S. Viswanathan, J. Phys. Chem. A, 2011, *115*, 10059.

[19] K. Sundararajan, N. Ramanathan, J Mol. Struct., 2009, *920*, 369.

[20] J. Spanget-Larsen, M. Gil, A. Gorski, D. M. Blake, J. Waluk, J. G. Radziszewski, J. Am. Chem. Soc., 2001, *123*, 11253.

---

[21] M. J. Deetz, C. C. Forbes, M. Jonas, J. P. Malerich, B. D. Smith, O. Wiest, J. Org. Chem., 2002, *67*, 3949.

[22] C. Dugave, L. Demange, Chem. Rev., 2003, *103*, 2475.

[23] F. Weinhold, C. Landis, Valency and Bonding: A natural bond orbital donor-acceptor perspective, Cambridge University press, 2005.

CHAPTER 7

AB INITIO STUDY ON THE CONFORMATIONS OF DIMETHOXY SILANONE AND ITS COMPARISON WITH DIMETHYL CARBONATE AND TRIMETHYL PHOSPHATE

7.1 Introduction

This chapter describes *ab initio* computations on the various conformers of dimethoxy silanone (DMSi, $(CH_3O)_2Si{=}O$) and compares the computed results of DMSi with dimethyl carbonate (DMC, $(CH_3O)_2C{=}O$) and trimethyl phosphate (TMP, $(CH_3O)_3P{=}O$).

It is well known that the silicon shows similar chemical properties as C and P. Silicon can form multiple bonds like carbon, though multiple bonds involving Si was not observed experimentally, till 1981, when, tetramesityldisilene, a stable compound containing a silicon-silicon double bond was synthesized by West et al.[1] After that many such molecules containing silicon-silicon multiple bond have been synthesized.[2,3]

Silicon shows penta and hexa co-ordinate bonds due to the participation of ‘d’ orbital in bonding, whereas carbon does not exhibit these higher co-ordination numbers.[4] In addition, Si-X (X=O, N) shows partial double bond character in many compounds. Ma and Inagaki have shown in disilaoxirane (ring systems) molecule that oxygen atoms tend to form dative π bonds to the silicon atoms.[5]

Molecules containing multiple bonds between silicon and oxygen (e.g. silanones and silanoic acids) are very rare. The high polarity of Si=O bond drives these molecules to undergo oligomerization, which makes them unstable at room temperature[6]. These molecules were formed and studied only in cryogenic matrixes.[7-9] In recent times a few molecules containing Si=O bonds have been synthesized.[10,11]

Khabashesku et al.[9] have found DMSi as one of the product in their experiment while studying the vacuum pyrolysis of 3,3-dimethoxy-6-oxa-3-silabicyclo[3.1.0]hexane. DMSi thus produced were trapped in an Ar matrix and studied using infrared spectroscopy. Vibrational assignments were made by comparing the experimental and *ab initio* computations of DMSi using B3LYP method with 6-31G* and 6-311G** basis sets. It should be mentioned that so far to our knowledge there is no complete conformational analysis of DMSi was carried out.

We have carried out conformational analysis of DMSi using B3LYP/6-31++G** level of theory. Natural bond orbital (NBO) analysis was performed to understand the role of different delocalization interactions on conformational stability and to find out the participation of d orbital in bonding in the molecule. Computational studies on DMC and TMP, performed at B3LYP/6-31++G** level of theory, were used to compare with those of DMSi.

7.2 Computational details

All the *ab initio* calculations for DMSi were performed at B3LYP/6-31++G** level of theory as it would be easy to compare with the computed results of DMC and TMP obtained with the same level of theory earlier. Guess geometries for different conformers of DMSi were allowed to optimize without applying any symmetrical constraints. Vibrational frequency calculations were carried out using analytical gradients on the optimized geometries to find out whether these optimized geometries are minima or not and to assist us to compare with the experimental results obtained earlier.[9] Transition states between different conformers were calculated using QST3 method. To understand the role of delocalization interactions in determining conformational preferences, Natural Bond Orbital (NBO) analysis was performed at the same level of theory. Atoms-in-molecules (AIM) analysis was performed to locate bond and ring critical points related to intramolecular interactions present in different conformers of DMSi.

7.3 Results and discussions

Two minima are found in the potential energy landscape of dimethoxy silanone, cis-cis and cis-trans. Cis-cis was found to be the ground state conformer whereas the higher energy conformer cis-trans was located 1.04 kcal/mol above the cis-cis form. Trans-trans geometry was optimized to be a first order saddle point. This geometry is also considered for discussion in order to compare with the near-trans-near-trans conformer of DMC. The optimized structures are shown in Fig. 7.1. Transition state calculation of the structure connecting the cis-trans to cis-cis comformers yielded a barrier for interconversion of 3.76 kcal/mol. The relative energies corrected for zero point energies and the dipole moments of each form are given in Table 7.1.

Table 7.2 gives some important geometrical parameters for the cis-cis, cis-trans and the trans-trans geometry. It should be mentioned that the geometrical parameters for the cis-cis conformer agree well with earlier calculation done by Khabashesku et al.[9] As can be seen from the Table 7.2, Si-O bond lengths in both the conformers of DMSi were calculated to be 1.625, 1.620 and 1.635 Å, which show a reasonable agreement with that of methylsilylether (1.640±0.003 Å)[12] and methyltrimethoxysilane (1.632±0.004 Å)[13] obtained from electron diffraction study. The calculated Si-O-C angles for the cis-cis and cis-trans conformers was 123.9° and 129.2° agree well with the experimentally obtained value of 120.6±0.9° and 123.6±0.5° respectively.

Table 7.3 compares the calculated vibrational frequencies with those obtained by matrix isolation infrared experiment[9]. It should be mentioned that the earlier DFT calculations with 6-31G* and 6-311G** basis sets by Khabashesku et al. considered only the cis-cis form, whose vibrational frequencies are also given in Table 7.3. As shown in the table, the experimental features at 888, 1102, 1174, 1199 and 1471 cm^{-1} cannot unambiguously assign particularly to the different vibrational modes of one conformer. However the only

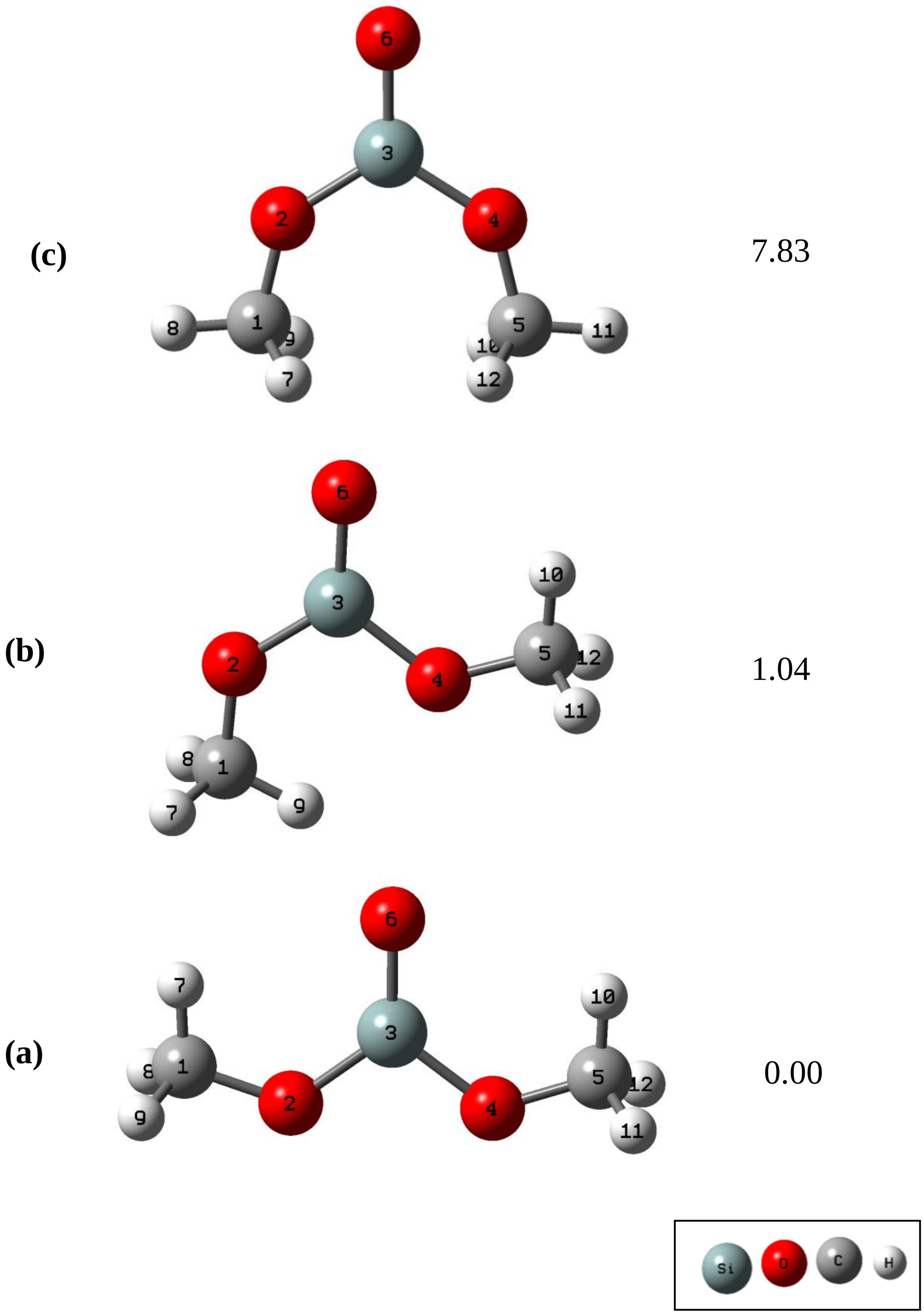

Fig. 7.1 – Computed structures at B3LYP/6-31++G** level of different conformers of dimethoxy silanone. (a) cis-cis, (b) cis-trans, (c) trans-trans (Trans-trans is a first order saddle point). The energy, in kcal/mol, of each structure relative to the ground state conformer, is given against each structure.

Table 7.1 – Relative energies (kcal/mol), and dipole moment (D) of the different conformers of DMSi, computed at B3LYP/6-31++G level of theory.**

Conformer	**Relative energy[a] (kcal/mol)**	**Dipole moment (D)**
Cis-cis	0.00	2.14
Cis-trans	1.04	5.01
Trans-trans[b]	7.83	7.34
TS1[c]	4.80	3.89

[a] Energies corrected for ZPE.
[b] Trans-trans geometry is a first order saddle point.
[c] Transition state connecting cis-cis and cis-trans conformer of DMSi.

Table 7.2 – Important geometrical parameters, bond lengths (Å), bond angles (°) and torsional angles (°) of the conformers of DMSi, computed at the B3LYP/6-31++G level.**

Parameters	Cis-cis	Cis-trans	Trans-trans (Saddle point)
C1-O2	1.440	1.436	1.427
O2-Si3	1.625	1.620	1.628
Si3-O4	1.625	1.635	1.627
Si3-O6	1.533	1.530	1.528
O4-C5	1.440	1.441	1.427
C1-O2-Si3	123.9	129.2	135.8
O2-Si3-O4	105.1	107.2	114.0
O2-Si3-O6	127.4	126.6	123.0
O4-Si3-O6	127.4	126.1	123.0
Si3-O4-C5	123.9	124.3	135.9
C1-O2-Si3-O6	-0.1	179.7	178.8
C1-O2-Si3-O4	179.9	-0.4	-1.2
C5-O4-Si3-O6	0.0	-0.4	178.5
C5-O4-Si3-O2	-180.0	179.7	-1.4

[a] Torsional angle ABCD implies the angle between two planes ABC and BCD.

Table 7.3 – Calculated and experimental vibrational wavenumbers of DMSi.

Calculated wavenumbers				**Experimental wavenumbers**[b]	**PED (%) and assignment**[b]
B3LYP/6-31++G** [a]		**B3LYP/ 6-31G*** [b]	**B3LYP/ 6-311G****[b]		
Cis-cis	**Cis-trans**	**Cis-cis**	**Cis-cis**		
712(46)[c]	690.0(15)	724(39)	716(41)		87 Si-O sym str
846(25)	831(106)	862(27)	848(25)	888(w)	62 Si-O asym str; 38 C-O asym str
1103(665)	1097(203)	1119(654)	1108(654)	1102(vs)	74 C-O asym str; 23 Si-O asym str
1105(11)	1120(298)	1123(8)	1112(7)		93 C-O sym str
1180(0)	1182(0.7)	1194(0)	1180(0)		93 CH$_3$ rock ip
1184(0.6)	1182(0.2)	1198(0.4)	1184(0.1)		93 CH$_3$ rock op
1199(15)	1198(5)	1216(8)	1199(7)	1174(w)	75 CH$_3$ sym ip rock; 10 Si=O str
1215(125)	1213(76)	1231(118)	1213(138)	1199(s)	80 CH3 asym rock in-plane
1267(156)	1280(304)	1292(115)	1284(135)	1247(m)	95 Si=O str
1486(0.3)	1485(0.6)	1508(4)	1484(0.2)		100 CH3 asym deform
1491(0.4)	1488(0)	1514(0.1)	1490(0.1)		100 CH3 asym deform
1506(0.1)	1505(7)	1530(1)	1501(1)		95 CH3 asym scissor deform
1506(8)	1506(6)	1531(9)	1501(13)	1471(w)	95 CH3 asym scissor deform
1506(4)	1507(9)	1532(0)	1502(0)		87 CH3 asym scissor deform
1507(14)	1508(1)	1533(6)	1502(9)		87 CH3 asym scissor deform

[a] This work.
[b] Ref. 9.
[c] IR intensities (km/mol) are given in parentheses.

experimental feature at 1247 cm^{-1} can unambiguously assign to the Si=O stretching of cis-cis conformer and hence the other features discussed above are assigned to the different vibrational modes of the cis-cis conformer as shown in Table 7.3.

7.3.1 Natural bond orbital analysis

The delocalization interactions and the second order perturbation energies (E2) obtained for the conformers using natural bond orbital analysis are listed in Table 7.4. Vicinal delocalization interactions involving SiO_3 group were found to be very similar to those involving CO_3 group in DMC (Chapter 4). However, the delocalization energies in DMSi are smaller compared to that in DMC. The magnitude of delocalization interactions involving lone pair of methoxy oxygens and the π*Si3-O6 are found to be largest and nearly the same in all the conformers and hence these interaction may not contribute much towards the conformational stability. However, this interaction probably determines the barrier for interconversion between the two conformers. The next higher delocalization energies in the conformers is the interactions between lone pair of O6 with σ*O2-Si3 and σ*Si3-O4. These interactions contribute very less to the conformational stability as these values are found to decrease from cis-cis to trans-trans (very small change in E2 values as shown in Table 7.4). The hyperconjugative interaction between the lone pair of methoxy oxygens and σ*Si3-O6 are probably more important in the conformational stability. The second order perturbation energy (E2) value of $n^1O2 \rightarrow \sigma^*Si3\text{-}O6$ interaction are found to be 7.67, 0.57 kcal/mol and 0.95 kcal/mol for the cis-cis, cis-trans conformers and trans-trans geometry. Similarly, the E2 values for the $n^1O4 \rightarrow \sigma^*Si3\text{-}O6$ interaction are respectively 7.67, 7.07 and 0.97 kcal/mol. The interactions $n^1O2 \rightarrow \sigma^*Si3\text{-}O4$ and $n^1O4 \rightarrow \sigma^*Si3\text{-}O2$ were found to less important towards the conformational stability as the E2 values are found to increase from cis-cis to trans-trans. We have also carried out computations by deleting these interactions separately in each conformer to see the changes in energies. Table 7.5 gives the deletion energies and

Table 7.4 – Second order perturbation energies (E_2) (kcal/mol) of some important delocalization interactions in different conformers of DMSi.

Donor NBO	**Acceptor NBO**	**Second order perturbation energy (E_2)**		
		Cis-cis	**Cis-trans**	**Trans-trans (Saddle point)**
Geminal interactions				
σO2-Si3	σ*Si3-O4	2.89	2.44	4.56
σO2-Si3	σ*Si3-O6	1.41	1.63	1.69
σSi3-O4	σ*O2-Si3	2.89	5.20	4.56
σSi3-O4	σ*Si3-O6	1.40	1.24	1.69
σSi3-O6	σ*O2-Si3	2.26	0.50	0.69
σSi3-O6	σ*Si3-O4	2.26	2.72	0.68
Vicinal interactions				
n^1O2	σ*O2-Si3	-[a]	0.64	1.17
n^1O2	σ*Si3-O4	1.99	5.46	6.60
n^1O2	σ*Si3-O6	7.67	0.57	0.95
n^2O2	π*Si3-O6	18.17	17.94	17.89
n^1O4	σ*O2-Si3	1.99	2.94	6.62
n^1O4	σ*Si3-O4	-	-	1.17
n^1O4	σ*Si3-O6	7.67	7.07	0.97
n^2O4	π*Si3-O6	18.18	17.67	17.91
n^1O6	σ*O2-Si3	2.73	4.13	3.02
n^1O6	σ*Si3-O4	2.73	2.11	3.04
n^1O6	σ*Si3-O6	1.06	1.02	0.97
n^2O6	Ry*(1)Si3	7.70	8.03	8.66
n^2O6	σ*O2-Si3	13.61	11.78	12.78
n^2O6	σ*Si3-O4	13.61	14.54	12.79

[a] Values are less than threshold value 0.5 kcal/mol.

Table 7.5 – Interactions deleted, deletion energies, changes in energies due to deletion of some important interactions of different conformers of DMSi.

Conformer	Interaction deleted		Deletion energy (Hartree)	Change in energy (kcal/mol)	Relative change in deletion energy (%)
Cis-cis	1	n^2O2→ π*Si3-O6 n^2O4→ π*Si3-O6	-594.947466221	86.9	0.023
	2	n^2O6→ σ*O2-Si3 n^2O6→ σ*Si3-O4	-594.964858669	76.0	0.020
	3	n^1O2→ σ*Si3-O6 n^1O4→ σ*Si3-O6	-595.018271245	42.5	0.011
	4	n^1O2→ σ*Si3-O4 n^1O4→ σ*O2-Si3	-595.069491044	10.4	0.003
Cis-trans	1	n^2O2→ π*Si3-O6 n^2O4→ π*Si3-O6	-594.947189561	86.1	0.023
	2	n^2O6→ σ*O2-Si3 n^2O6→ σ*Si3-O4	-594.967483044	73.4	0.020
	3	n^1O2→ σ*Si3-O6 n^1O4→ σ*Si3-O6	-595.050744194	21.1	0.006
	4	n^1O2→ σ*Si3-O4 n^1O4→ σ*O2-Si3	-595.049933831	21.6	0.006
Trans-trans (Saddle point)	1	n^2O2→ π*Si3-O6 n^2O4→ π*Si3-O6	-594.939079253	84.0	0.022
	2	n^2O6→ σ*O2-Si3 n^2O6→ σ*Si3-O4	-594.965084974	67.7	0.018
	3	n^1O2→ σ*Si3-O6 n^1O4→ σ*Si3-O6	-595.061142329	7.4	0.002
	4	n^1O2→ σ*Si3-O4 n^1O4→ σ*O2-Si3	-595.012225552	38.1	0.010

change in energies due to deletion of each pair of interactions for different conformers. As can be seen from the table the energy values reflect the importance of each interaction towards the stability of conformers as discussed above.

Table 7.6 gives electron occupancies of some of the important NBOs. From the table, it is clear that among all vacancy orbitals the π*Si3-O6 orbital has the maximum occupancy (~0.17e), which emphasizes the role of interactions involving the π* orbital towards the molecular stability.

The interactions discussed above are all vicinal type delocalization. In the silanone, we also observed a few geminal type interactions between σ and σ* orbitals involving the SiO_3 group, which were not observed in the case of carbonates. These interactions are listed in Table 7.4. Table 7.6 shows, the electron occupancies of the three σSi-O bonding orbitals are less than a Lewis orbital (2e), which clearly indicate the involvement of geminal interactions in this molecule.

To understand the role of vicinal and geminal interactions in conformational stability, all the vicinal and geminal interactions of cis-cis and cis-trans conformer and the trans-trans form of DMSi were deleted. The deletion energies and the change in energies due to deletion are listed in Table 7.7. Changes in energy due to deletion of all interactions by deleting all acceptor orbitals are also listed in the same table. Similar to carbonates, vicinal interactions were found to dominate over geminal interactions in DMSi. Further, the change in energy due to deletion of geminal interactions are also found to be less compared to those of DMC (Chapter 4, Table 4.7) and contribute less to the stability of conformers of DMSi. The change in energies due to deletion of all vicinal and all geminal interactions are more in cis-cis than cis-trans conformers, which emphasize their role towards the greater stability of former conformer.

We have studied the polarity of Si=O bond in DMSi using the NBO analysis. The

Table 7.6 – Electron occupancies of some important NBOs in different conformers of DMSi.

NBO	**Occupancy**		
	Cis-cis	**Cis-trans**	**Trans-trans (Saddle point)**
n^1O2	1.95453	1.95376	1.94760
n^2O2	1.87583	1.87596	1.88276
n^1O4	1.95451	1.95614	1.94747
n^2O4	1.87583	1.87984	1.88272
n^1O6	1.97366	1.97359	1.97358
n^2O6	1.85492	1.85374	1.85833
σO2-Si3	1.97845	1.97776	1.97425
σSi3-O4	1.97846	1.97612	1.97431
σSi3-O6	1.97937	1.98207	1.98398
πSi3-O6	1.99713	1.99741	1.99786
σ*O2-Si3	0.09266	0.08621	0.10812
σ*Si3-O4	0.09265	0.11050	0.10810
σ*Si3-O6	0.05592	0.03647	0.02018
π*Si3-O6	0.17281	0.16950	0.15897

Table 7.7 – Energies of different conformers of DMSi after deletion of all geminal, all vicinal and all delocalization interactions.

Conformer	Interactions deleted	Deletion energy (Hartree)	Change in energy(kcal/mol)	Relative change in deletion energy (%)
Cis-cis	Geminal	-595.009287820	48.1	0.013
	Vicinal	-594.365967585	451.8	0.121
	All	-594.274300714	509.3	0.136
Cis-trans	Geminal	-595.012870550	44.9	0.012
	Vicinal	-594.371145904	447.6	0.120
	All	-594.276669908	506.8	0.136
Trans-trans (Saddle point)	Geminal	-595.001129063	45.0	0.012
	Vicinal	-594.340908054	459.4	0.123
	All	-594.250598206	516.0	0.138

NBO analysis showed, Si3=O6 consists of one σ and one π orbital and these orbitals are very strongly polarized towards oxygen atom with ~80% of σ-NBO density and ~87% π-NBO density reside on oxygen atom. The high polarity of this bond was also observed based on the charges found on the Si3 and O6 atom from natural population analysis. It has been found that the charge on Si3 is ~2.3 e and on O6 is ~ -1.2 e, which shows a charge separation of ~3.5 e between the two atoms indicating Si3=O6 is a highly polarized bond. Eping et al. also performed similar calculations for a silanoicsilyl ester and observed the Si=O group to be a highly polarized bond.[11]

7.4 Comparison of DMSi with DMC

In DMSi, Si atom occupies the central position and shows tetravalence. This leads to similar conformational behaviour as in DMC. The restricted rotation around the Si3-O2 and O4-Si3 bond arise due to strong n→π* interaction, which determines the position of methyl group to be either cis or trans with respect to Si=O. This leads to cis-cis and cis-trans conformations of DMSi which is similar to DMC. The trans-trans form was found to be a saddle point in case of DMSi, whereas the same conformer is a minimum in DMC. Fig. 7.2 shows an energy correlation diagram of the different conformers of DMSi and DMC. The energy difference between the cis-cis and cis-trans conformer is smaller (1.0 kcal/mol) with DMSi when compared with DMC (2.9 kcal/mol), which indicates the greater stability of ground state conformer in DMC due to stronger delocalization interactions in DMC compared to DMSi. A similar observation was made in an earlier work from our lab, when dimethoxysilanes were compared with the analogous carbon compounds.[14]

The difference between the cis-cis conformers of DMSi and DMC is that, one of the cis-methyl hydrogen in DMSi is in the eclipsed position to Si=O group (H7-C1-O2-Si3 = 0.0°, Fig. 7.1a), whereas the same hydrogen is in the gauche orientation in DMC (H7-C1-O2-C3=60.6°, Fig. 4.1a). In DMC, gauche orientation of methyl hydrogen is preferred because it

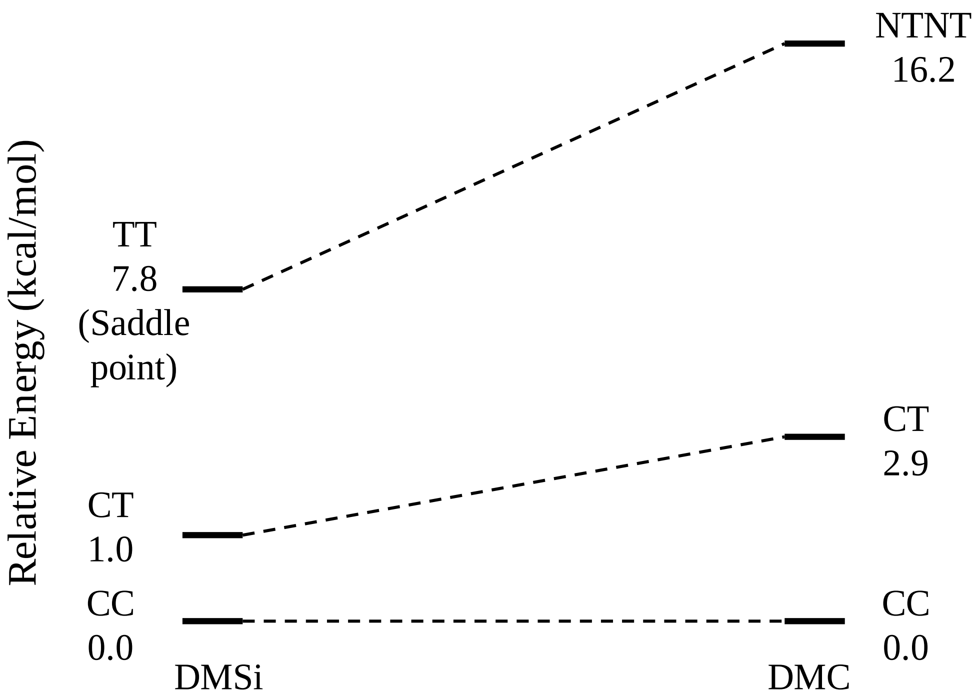

Fig. 7.2 – Diagram showing the correlation between the conformers of DMSi and DMC. The energies of each conformer, relative to the ground state conformers of the corresponding molecules, are mentioned along side.

probably removes the steric interaction between H7 and C3, whereas in DMSi even though there is a steric interaction is present in the eclipsed hydrogen but there could be a possible hydrogen-bonded interaction exist between hydrogen (H7) and oxygen (O6) which may stabilize this geometry. To find out whether hydrogen-bonded interaction exist between H7 and O6 we searched for (3,-1) bond critical point using AIM calculation and could not locate any bond critical points. To look for whether electronic interactions plays a role in stabilizing a particular orientation of methyl hydrogen in DMC and DMSi, first we have optimized the frozen geometry structure in DMSi, where H7 and H10 were in gauche positions (60.0°) with Si=O. Frequency calculation on this optimized geometry showed it was a second order saddle point. We then deleted the delocalization interactions involving hydrogen atoms (gauche position) in the cis-cis configuration in DMSi. The interactions involving all the H-atoms with $E2 \geq 0.5$ kcal/mol (the threshold value in NBO output), are deleted to calculate the effect of these delocalization towards the gauche configuration. Similar, deletion procedure was also carried out for eclipsed structure. It was found that the change in energy due to these deletions is greater in case of gauche form (77.0 kcal/mol) than for the eclipsed form (75.3 kcal/mol), which explains gauche configuration is more stabilized due to the electronic interaction than the eclipsed one but this is not the case and the eclipsed form is the stable conformer. Hence involvement of delocalization in stability of eclipsed form is also ruled out. We could not arrive any conclusion in DMSi, why eclipsed form is preferred over gauche in cis-cis conformer.

The magnitude of delocalization interaction energy (E2) involving Si-atom in DMSi is less when compared to C-atom in DMC. This is further confirmed by the changes in energy observed due to deletion of these delocalization interactions, which are listed in Table 7.5 for DMSi and Table 4.5 for DMC. The electron occupancies in different acceptor orbitals in DMC (Table 4.6) are much higher when compared to DMSi (Table 7.6), except for the σ*C3-

O6 where it is less than σ*Si3-O6, and shows the delocalization interactions are stronger in case C-system when compared to Si-system. Similar results were observed for methoxysilane compounds in comparison to their carbon analogous, where anomeric interactions are found to be stronger in C-systems than Si-systems.[14] From Tables 7.6 and 4.6 it can also be observed that, the electron occupancies of the σ orbitals involving SiO_3 group in DMSi are less compared to those of DMC (σ orbitals involving CO_3 group), which indicates the geminal interactions involving the σ orbitals observed in the Si-system are either not present in DMC or less than the threshold value (0.5 kcal/mol) of NBO output.

7.5 Comparison of DMSi, DMC with TMP

As described in chapter 1, conformations of TMP were well studied in our group using matrix isolation infrared spectroscopy and *ab initio* calculations.[15-17]

TMP exists in three conformations, C_3 ($G^{\pm}G^{\pm}G^{\pm}$), C_1 ($TG^{\pm}G^{\pm}$), C_s ($TG^{+}G^{-}$). The relative energies (corrected for zero point energy) of each conformer calculated at B3LYP/6-31++G** level of theory are 0.00, 0.87, 2.07 kcal/mol respectively. The computed structures are shown in Fig. 7.3. Grein reported that electrostatic and electronic effects dominate over steric interaction in stabilizing different conformers of TMP and phosphoric acid,[18] further the importance of electronic effect on conformational preferences of TMP is discussed here. Ruben et al. through NBO analysis, have shown that anomeric effect plays a major role in destabilizing the "high energy" phosphate bonds (P-O) during the process of hydrolysis.[19]

Importance of geminal interactions in conformational stability of TMP were also noticed when all geminal interactions were deleted for each conformer using NBO analysis.[17] Table 7.8 shows the changes in energy due to deletion of all geminal, vicinal and delocalization interactions for each conformer of TMP (values are taken from Ref. 17). The decreasing trend of geminal interactions in these conformers from higher to lower energy

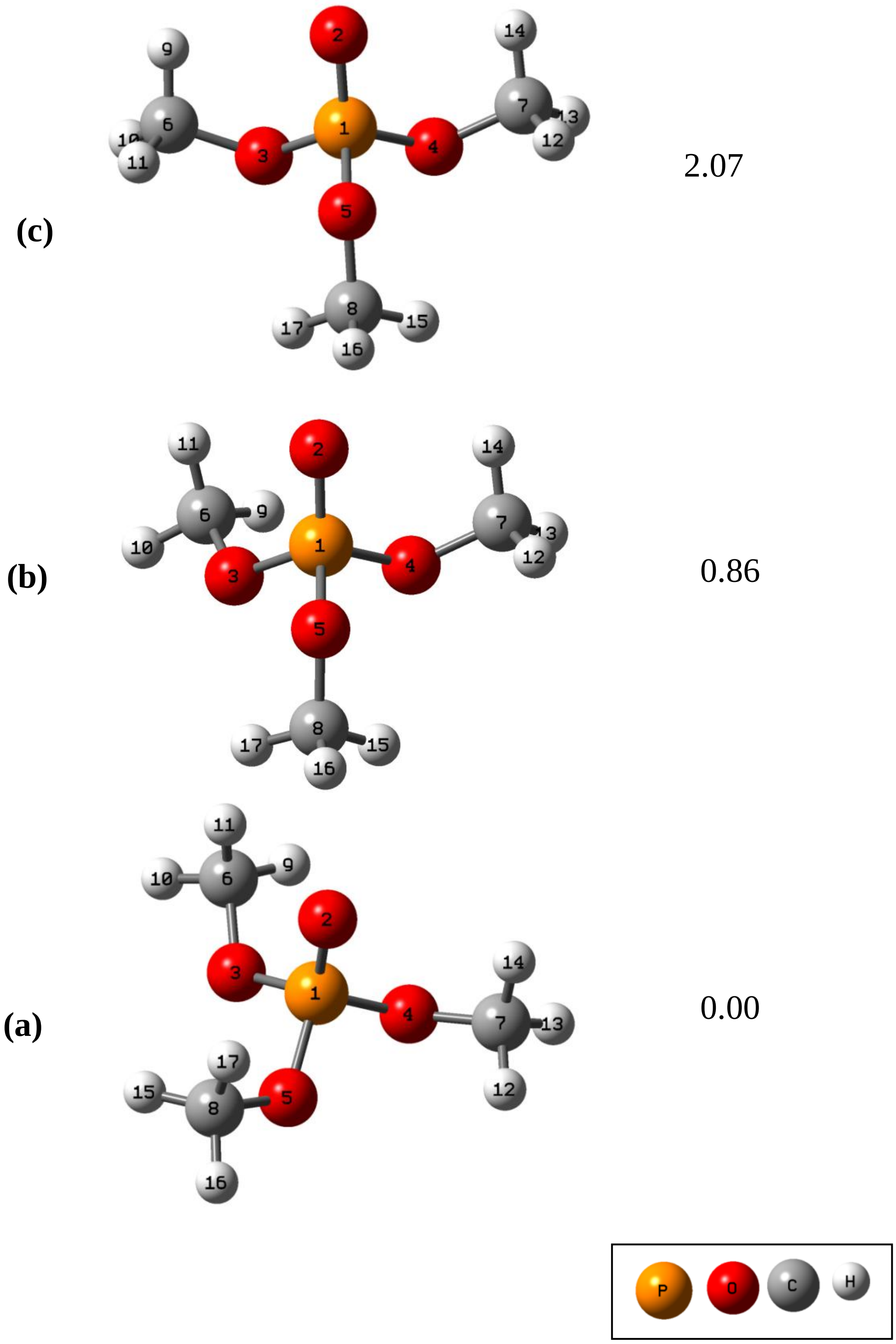

Fig. 7.3 – Computed structures at B3LYP/6-31++G** level of different conformers of trimethyl phosphate. (a) C_3 ($G^{\pm}G^{\pm}G^{\pm}$), (b) C_1 ($TG^{\pm}G^{\pm}$) and (c) C_s ($TG^{+}G^{-}$). The energy, in kcal/mol, of each structure relative to the ground state conformer, is given against each structure.

Table 7.8 – Energies of different conformers of TMP after deletion of all geminal, all vicinal and all delocalization interactions.

Conformer	Interactions deleted	Deletion energy (Hartree)	Change in energy (kcal/mol)	Relative change in deletion energy (%)
C_3 ($G^{\pm}G^{\pm}G^{\pm}$)	Geminal	-761.403463115	425.5	0.089
	Vicinal	-761.317762918	479.3	0.100
	All	-760.619912013	917.2	0.192
C_1 ($TG^{\pm}G^{\pm}$)	Geminal	-761.631221364	281.7	0.059
	Vicinal	-761.144842010	586.9	0.123
	All	-760.668804521	885.6	0.185
C_s ($TG^{+}G^{-}$)	Geminal	-761.654796116	265.5	0.056
	Vicinal	-761.155704064	578.6	0.121
	All	-760.705189320	861.4	0.180

clearly shows its importance in conformational preferences. Further, vicinal interactions are also found to contribute in stabilizing the conformers of TMP. It should be mentioned that in DMC and DMSi the vicinal interactions are found to dominate over geminal interactions. Table 7.9 shows some important geminal and vicinal interactions involving PO_4 group in each conformer of TMP. NBO analysis shows in C_3 conformer of TMP, P1-O2 bond has one σ bond and two π bonds. As mentioned before,[17] π and π^* delocalization interactions are found to participate in a greater extent in each conformer. Table 7.9 also shows, the C_3 conformer contains six geminal delocalization interactions involving P1-O3, P1-O4 and P1-O5 in a cyclic manner, three are in clockwise and other three in anti clockwise manner, which is similar to benzene molecule, where six vicinal conjugative interactions are found in cycles.[20] Another three interactions found in a cyclic manner both in C_3 and C_1 conformers, which involve the vicinal interactions between lone pair of methoxy oxygen and the σ^* orbitals of P-O(CH_3). Probably, these cyclic delocalization interactions may be giving extra stability to different conformers in TMP. It should be pointed out that the cyclic interactions do play a major role in deciding the conformational preferences in trimethoxymethane.[21]

The presence of geminal interactions was further evidenced by a larger decrease in electron occupancies of the σ and π bonding orbitals from that of a Lewis orbital (2e) as shown in Table 7.10 for different conformers of TMP.

An observation in conformational behaviour of trimethyl phosphite (TMPhite) showed that participation of d orbitals in bonding invokes geminal interactions in the system.[17] Participation of d orbital in different conformers of TMP, DMSi and DMC are compared here. Table 7.11 shows the percentage of d orbitals of the central atoms involved in bonding of some important NBOs of TMP, DMSi and DMC. As can be seen from the table, the participation of d orbitals of phosphorous in TMP in formation of those NBOs is higher when compared to that of silicon in DMSi. This explains clearly the greater role of geminal

Table 7.9 – Second order perturbation energies E_2 (kcal/mol) of a few delocalization interactions in different conformers of TMP.

Donor NBO	Acceptor NBO	Second order perturbation energy (E_2)		
		C_3 ($G^{\pm}G^{\pm}G^{\pm}$)	C_1 ($TG^{\pm}G^{\pm}$)	C_s ($TG^{+}G^{-}$)
Geminal interactions				
σP1-O2	π^1*P1-O2	-[a]	22.80	-
σP1-O2	σ*P1-O3	2.81	17.65	2.78
σP1-O2	σ*P1-O4	2.80	1.90	2.68
σP1-O2	σ*P1-O5	2.72	1.88	1.58
π^1P1-O2	σ*P1-O2	-	11.67	-
π^1P1-O2	π^1*P1-O2	3.41	0.86	3.96
π^1P1-O2	σ*P1-O3	13.40	16.06	21.10
π^1P1-O2	σ*P1-O4	1.26	1.39	21.11
π^1P1-O2	σ*P1-O5	22.95	18.00	-
π^2P1-O2	π^2*P1-O2	3.41	-	-
π^2P1-O2	σ*P1-O3	11.67	-	-
π^2P1-O2	σ*P1-O4	23.80	-	-
π^2P1-O2	σ*P1-O5	2.14	-	-
σP1-O3	σ*P1-O2	1.45	14.99	1.25
σP1-O3	π^1*P1-O2	36.55	38.29	54.05
σP1-O3	π^2*P1-O2	36.25	-	-
σP1-O3	σ*P1-O3	3.33	1.78	1.56
σP1-O3	σ*P1-O4	15.37	4.48	28.49
σP1-O3	σ*P1-O5	17.83	28.20	4.44
σP1-O4	σ*P1-O2	1.45	1.20	1.19
σP1-O4	π^1*P1-O2	4.78	1.75	54.03
σP1-O4	π^2*P1-O2	68.05	-	-
σP1-O4	σ*P1-O3	17.79	5.88	28.48
σP1-O4	σ*P1-O4	3.34	0.67	1.55
σP1-O4	σ*P1-O5	15.40	2.45	4.39
σP1-O5	σ*P1-O2	1.40	1.19	2.21
σP1-O5	π^1*P1-O2	67.88	47.54	-
σP1-O5	π^2*P1-O2	4.97	-	-
σP1-O5	σ*P1-O3	15.39	23.11	3.33
σP1-O5	σ*P1-O4	17.80	2.09	3.30
σP1-O5	σ*P1-O5	3.33	0.82	0.72
σ*P1-O2	π^1*P1-O2	-	16.27	-
σ*P1-O2	σ*P1-O3	-	57.25	-
σ*P1-O2	σ*P1-O5	-	22.82	-
π^1*P1-O2	σ*P1-O3	72.83	131.63	546.10
π^1*P1-O2	σ*P1-O4	5.29	-	560.35
π^1*P1-O2	σ*P1-O5	117.43	-	-
π^2*P1-O2	σ*P1-O3	57.69	-	-
π^2*P1-O2	σ*P1-O4	125.37	-	-

Continuation of Table 7.9………

π^{2}*P1-O2	σ*P1-O5	12.96	-	-
σ*P1-O5	σ*P1-O3		120.54	-
Vicinal interactions				
n^{1}O2	σ*P1-O3	0.94	0.92	1.03
n^{1}O2	σ*P1-O4	0.94	0.86	1.03
n^{1}O2	σ*P1-O5	0.94	1.66	1.12
n^{2}O2	σ*P1-O3	-	3.04	4.65
n^{2}O2	σ*P1-O4	-	25.93	4.68
n^{2}O2	σ*P1-O5	-	5.54	23.21
n^{1}O3	σ*P1-O2	5.16	1.96	6.04
n^{1}O3	π^{1}*P1-O2	-	3.34	0.78
n^{1}O3	π^{2}*P1-O2	3.46	-	-
n^{1}O3	σ*P1-O4	-	0.77	2.73
n^{1}O3	σ*P1-O5	2.48	4.54	-
n^{2}O3	σ*P1-O2	4.42	6.53	3.16
n^{2}O3	π^{2}*P1-O2	5.35	-	-
n^{2}O3	σ*P1-O4	4.29	9.31	1.46
n^{2}O3	σ*P1-O5	-	-	12.10
n^{1}O4	σ*P1-O2	5.15	3.56	6.05
n^{1}O4	π^{1}*P1-O2	1.91	2.45	0.75
n^{1}O4	π^{2}*P1-O2	1.78	-	-
n^{1}O4	σ*P1-O3	2.46	1.81	2.73
n^{2}O4	σ*P1-O2	4.44	4.61	3.17
n^{2}O4	π^{1}*P1-O2	4.68	1.29	-
n^{2}O4	π^{2}*P1-O2	0.75	-	-
n^{2}O4	σ*P1-O3	-	0.74	1.45
n^{2}O4	σ*P1-O5	4.29	7.67	12.10
n^{1}O5	σ*P1-O2	5.14	9.97	1.77
n^{1}O5	π^{2}*P1-O2	3.41	-	-
n^{1}O5	σ*P1-O3	-	-	1.57
n^{1}O5	σ*P1-O4	2.48	2.13	1.57
n^{2}O5	σ*P1-O2	4.48	-	6.25
n^{2}O5	π^{1}*P1-O2	3.38	1.55	-
n^{2}O5	π^{2}*P1-O2	2.05	-	-
n^{2}O5	σ*P1-O3	4.28	4.24	3.92
n^{2}O5	σ*P1-O4	-	9.34	3.93

[a]Values are less than threshold value 0.5 kcal/mol or these interactions are not present in the corresponding conformer.

Table 7.10 – Electron occupancies of some important NBOs in different conformers of TMP.

NBO	Occupancy		
	C_3 ($G^{\pm}G^{\pm}G^{\pm}$)	C_1 ($TG^{\pm}G^{\pm}$)	C_s ($TG^{+}G^{-}$)
n^1O2	1.97739	1.97781	1.97785
n^2O2	-[a]	1.80912	1.80871
n^1O3	1.95168	1.95121	1.95054
n^2O3	1.90466	1.90764	1.90885
n^1O4	1.95166	1.95452	1.95054
n^2O4	1.90466	1.90732	1.90886
n^1O5	1.95168	1.95239	1.95357
n^2O5	1.90470	1.90274	1.90330
σP1-O2	1.97729	1.95153	1.97896
σP1-O3	1.89191	1.91225	1.90955
σP1-O4	1.89186	1.97017	1.90966
σP1-O5	1.89190	1.92663	1.97115
π^1P1-O2	1.94753	1.93615	1.94325
π^2P1-O2	1.94753	-	-
σ*P1-O2	0.10753	0.10544	0.08371
σ*P1-O3	0.10202	0.12053	0.12624
σ*P1-O4	0.10200	0.20199	0.12638
σ*P1-O5	0.10199	0.12554	0.19651
π^{1*}P1-O2	0.14594	0.13978	0.14501
π^{2*}P1-O2	0.14582	-	-

[a] The particular NBOs are not present in the corresponding conformers.

Table 7.11 – Percent of d character of the central atoms in some of the NBOs involved in important delocalization interactions in different conformers of TMP, DMSi and DMC.

TMP NBO	% of d character of phosphorous in TMP		
	C_3 ($G^{\pm}G^{\pm}G^{\pm}$)	C_1 ($TG^{\pm}G^{\pm}$)	C_s ($TG^{+}G^{-}$)
σP1-O2	1.70	11.02	1.50
σP1-O3	33.72	27.16	26.33
σP1-O4	33.73	3.08	26.27
σP1-O5	33.72	21.06	2.90
π^1P1-O2	46.06	40.12	47.05
π^2P1-O2	46.08	-[a]	-
	% of d character of silicon in DMSi		
DMSi NBO	Cis-cis	Cis-trans	Trans-trans (Saddle point)
σO2-Si3	2.06	2.23	2.74
σSi3-O4	2.06	2.48	2.74
σSi3-O6	1.25	4.00	3.85
πSi3-O6	4.02	1.00	0.79
	% of d character of carbon in DMC		
DMC NBO	Cis-cis	Cis-trans	Near-trans-near-trans
σO2-C3	0.23	0.24	0.25
σC3-O4	0.23	0.25	0.25
σC3-O6	0.14	0.29	0.13
πC3-O6	0.31	0.12	0.26

[a] The particular NBOs are not present in the corresponding conformers.

interactions in TMP than that of DMSi. In DMC, as carbon atom does not use 3d orbitals for bond formation, the participations of d orbitals in DMC are negligible.

To further examine the role of d orbital the electron occupancies in different natural atomic d orbitals of central atoms in TMP, DMSi and DMC are analyzed and shown in Table 7.12. Electron occupancies of d orbitals are comparatively high for P in TMP than that of Si in DMSi and C in DMC. Further the natural electronic configuration of P, Si and central carbon atom in the ground state conformation of TMP, DMSi and DMC based on NAO analysis are [core]3s(0.74)3p(1.52)3d(0.11)5p(0.02), [core]3s(0.54)3p(1.07)3d(0.06)5p(0.01) and [core]2s(0.70)2p(2.22)3d(0.014)p(0.03) respectively. All these results clearly show the role of d orbitals participation in TMP for the geminal interactions, which in order stabilize the different conformers.

7.6 Conclusion

Conformations of DMSi were studied using B3LYP/6-31++G** method. Two conformers, cis-cis and cis-trans were found to be minima and the later being the higher energy conformer. The third conformer, trans-trans form was found to be a saddle point. In the cis-cis conformer, we observed the hydrogen atoms in the methyl group were eclipsed to Si=O in DMSi whereas in DMC it is gauche to C=O group. NBO analysis showed that vicinal interactions are dominating interactions in both DMSi and DMC. A few geminal interactions were observed in DMSi which were not present in DMC. Vicinal interactions involving the SiO_3 group in DMSi was found to be important in its conformational stabilities which is similar to the CO_3 group interactions in DMC, but the magnitude of second order perturbation energy values were smaller in DMSi than DMC.

Comparison of TMP, DMC and DMSi showed that participation of d orbital of phosphorous in TMP is higher than that of silicon and carbon in DMSi and DMC

Table 7.12 – Electron occupancies in different natural atomic d orbitals of central atoms in different conformers of TMP, DMSi and DMC.

P NAdO[a]	Electron occupancies of NAdO of P in TMP		
	C_3 ($G^{\pm}G^{\pm}G^{\pm}$)	C_1 ($TG^{\pm}G^{\pm}$)	C_s ($TG^{+}G^{-}$)
P1 d_{xy} Ry(3d)[b]	0.01664	0.02197	0.01943
P1 d_{xz} Ry(3d)	0.02655	0.02361	0.02655
P1 d_{yz} Ry(3d)	0.02655	0.02140	0.01763
P1 d_{x2-y2} Ry(3d)	0.01665	0.01701	0.02280
P1 d_{z2} Ry(3d)	0.02002	0.02259	0.01926
	Electron occupancies of NAdO of Si in DMSi		
Si NAdO	**Cis-cis**	**Cis-trans**	**Trans-trans (Saddle point)**
Si3 d_{xy} Ry(3d)	0.01942	0.01446	0.02142
Si3 d_{xz} Ry(3d)	0.00922	0.01084	0.01663
Si3 d_{yz} Ry(3d)	0.01690	0.01487	0.00811
Si3 d_{x2-y2} Ry(3d)	0.01024	0.01543	0.00906
Si3 d_{z2} Ry(3d)	0.00129	0.00130	0.00134
	Electron occupancies of NAdO of C in DMC		
C NAdO	**Cis-cis**	**Cis-trans**	**Near-trans-near-trans**
C3 d_{xy} Ry(3d)	0.00566	0.00335	0.00562
C3 d_{xz} Ry(3d)	0.00208	0.00245	0.00349
C3 d_{yz} Ry(3d)	0.00330	0.00277	0.00109
C3 d_{x2-y2} Ry(3d)	0.00274	0.00519	0.00320
C3 d_{z2} Ry(3d)	0.00046	0.00043	0.00079

[a] NAdO- Natural Atomic d Orbital.

[b] Ry-Rydberg orbital.

respectively, which is the cause of more geminal interactions in TMP. In TMP both geminal and vicinal interactions were involved in stabilizing the different conformers, whereas vicinal interactions play a major role in DMC and DMSi.

References

---

[1] R. West, M. J. Fink, J. Michl, Science, 1981, *214*, 1343.

[2] Y. Wang, Y. Xie, P. Wei, R. B. King, H. F. Schaefer, P. V. R. Schleyer, G. H. Robinson, Science, 2008, *321*, 1069.

[3] A. Sekiguchi, R. Kinjo, M. Ichinohe, Science, 2004, *305*, 1755.

[4] H. Bürger, Angew. Chem. Int. Ed., 1973, *12*, 474.

[5] J. Ma, S. Inagaki, J. Phys. Chem. A, 2000, *104*, 8989.

[6] J. Kapp, M. Remko, P. V. R. Schleyer, J. Am. Chem. Soc., 1996, *118*, 5745.

[7] R. Withnall, L. Andrews, J. Am. Chem. Soc., 1985, *107,* 2567.

[8] V. N. Khabashesku, K. N. Kudin, J. L. Margrave, L. Fredin, J. Organomet. Chem., 2000, *595*, 248.

[9] V. N. Khabashesku, Z. A. Kerzina, K. N. Kudin, O. M. Nefedov, J. Organomet. Chem., 1998, *566*, 45.

[10] S. Yao, Y. Xiong, M. Brym, M. Driess, J. Am. Chem. Soc., 2007, *129*, 7268.

[11] J. D. Epping, S. Yao, M. Karni, Y. Apeloig, M. Driess, J. Am. Chem. Soc., 2010, *132*, 5443.

[12] C. Glidewell, D. W. H. Rankin, A. G. Robiette, G. M. Scheldrick, B. Beagley, J. M. Freeman, J. Mol. Struct., 1970, *5*, 417.

[13] É. Gergö, I. Hargittai, G. Schultz, J. Organomet. Chem., 1976, *112*, 29.

[14] V. Kavitha, Ph. D. Thesis, Madras University, 2007.

[15] V. Vidya, K. Sankaran, K. S. Viswanathan, Chem. Phys. Lett., 1996, *258*, 113.

[16] L. George, K. S. Viswanathan, S. Singh, J. Phys. Chem. A, 1997, *101*, 2459.

[17] N. Ramanathan, K. Sundararajan, B. P. Kar, K. S. Viswanathan, J. Phys. Chem. A, 2011, *115*, 10059.

[18] F. Grein, J. Mol. Struct. Theochem, 2001, *536*, 87.

---

[19] E. A. Ruben, J. A. Plumley, M. S. Chapman, J. D. Evanseck, J. Am. Chem. Soc., 2008, *130*, 3349.

[20] F. Weinhold, C. Landis, Valency and Bonding – A natural bond orbital donor-acceptor perspective. Cambridge university press, 2005.

[21] V. Venkatesan, K. S. Viswanathan, J. Mol. Struct., 2010, *973,* 89.

CHAPTER 8

SUMMARY AND CONCLUSIONS

This thesis gives a detailed account of our studies on the conformations of molecules containing π- systems. Stilbene, a π- system and three n-π systems, dimethyl carbonate (DMC), diethyl carbonate (DEC), diphenyl carbonate (DPC) have been studied for their conformations, using matrix isolation infrared spectroscopy and *ab initio* calculations. Further, the conformations of dimethoxy silanone (DMSi) (n-π system), the silicon analogue of DMC, have also been studied, though only by using theoretical calculations and compared with the conformations of DMC and trimethyl phosphate (TMP). Natural bond orbital (NBO) analysis was performed on different conformations of the above molecules to find out the role of delocalization interactions and steric effect in conformational stability.

Non-planar trans-stilbene (NPTS) was formed by photoirradiation of cis-stilbene in inert gas matrixes at ~10 K and the IR spectra were recorded. The non-planarity of trans-stilbene arises due to the possible rotation of phenyl rings. On annealing, the features due to NPTS were found to decrease in intensity, whereas those of planar trans-stilbene gained in intensity. This clearly shows that the non-planar form is converting to a more stable planar form on annealing. Earlier studies on vibrational spectra of trans-stilbene in solution and melt, using Raman spectroscopy, have identified only one feature at 960 cm^{-1} for NPTS, whereas in our present work we have made a detailed assignment on the vibrational features of NPTS.

Our computation showed DMC can exist in three different conformations, cis-cis, cis-trans and near-trans-near-trans in increasing order of energy. Both ground state and first higher energy conformer were trapped in inert gas matrixes and studied through IR spectroscopy. In order to delineate the features due to higher energy conformer, an effusive hot nozzle source maintained at different temperatures and a supersonic jet source were used to alter the population of different conformers in gas phase, prior to deposition of the matrix mixture, on cold KBr window. As the band widths of observed vibrational features were less in our matrix isolation infrared experiments, we were able to assign many features due to the cis-trans conformer, which were not observed by Bohets and van der Vaken. NBO analysis showed n→π* interactions were the strongest delocalization interactions in DMC and were mainly responsible for its planar framework. Vicinal interactions were found to be the dominating interactions in DMC, which decides the conformational preferences in the molecule. A comparison with dimethoxymethane (DMM) showed, due to absence of C=O group in DMM, n→σ* interactions (anomeric effect) decide the non-planar framework and conformational preferences in this molecule. The ground state conformer in DMC was found to have a very similar structural configuration with the highest energy conformer of DMM, which emphasizes the role of the carbonyl group and the associated n→π* delocalization in DMC. A comparison of DMC with methylformate was also made in terms of theoretical computations, which showed that due to competitive conjugation, the rotational barrier between the cis and trans orientation of methyl group is less in DMC. The competitive conjugation is occurred in DMC as the π*(C=O) orbital is shared by two n→π* delocalization interactions, whereas the only one n→π* delocalization present in methylformate uses the π* orbital.

Diethyl carbonate DEC is the next higher member of DMC. Conformations of DEC were found to arise due to the different orientation of anomeric and terminal carbon atoms. For each orientation of anomeric carbon atoms, the different orientations of terminal carbon atoms form a cluster of conformers. In a given cluster of conformers, the conformer where the terminal carbon atoms orient to a trans positions were found to be the lowest energy conformer. A study of DEM, DEE and TEP, showed this trend to be a common feature. DEC was co-deposited with Ar and N_2 gas and IR spectra were recorded. The vibrational features observed were assigned primarily to the lowest energy conformer cc(tt). Five features of relatively low intensity were tentatively assigned to the higher energy conformers of cis-cis cluster of DEC, cc($tg^{\pm}$), cc($g^{\pm}g^{\mp}$) and cc($g^{\pm}g^{\pm}$) (ordered in increasing energy). DFT calculations showed low barriers of inter conversion between the conformers and it is likely that during the deposition of the sample and annealing process this small barrier can be surmounted. NBO analysis showed that $n \rightarrow \pi^*$ interactions plays similar role as in DMC and the vicinal interactions are found to be the dominating interactions. However, it is not the delocalization interactions, but the steric effect, which directs the orientation of terminal carbon atoms and hence the conformational preferences in different clusters.

The next system we have studied is the Diphenyl carbonate (DPC) system. DPC was calculated to have three conformers. They are cis-cis (anti), cis-cis (syn) and cis-trans in order of increasing energy. Cis-cis (anti) and cis-cis (syn) conformers were arisen due to rotation of phenyl rings whereas rotation around the $PhO\text{–}C_{carbonyl}$ gives rise to cis-trans conformer. In our experiment, we could trap and assign features only to the ground state conformer in N_2 matrix. NBO analysis revealed that the vicinal interactions are the dominating interactions in DPC. It should be mentioned that the phenyl rings in the ground state conformer of DPC is slightly twisted away from the plane of the carbonyl group and we found through NBO analysis the reason for this is due to the steric repulsion between one of the ortho carbon atoms of phenyl rings and the carbonyl group. Earlier studies on DPC predicted that the steric interaction between one of the ortho hydrogen atoms and the carbonyl oxygen; whereas the NBO analysis and AIM theory showed to be an attractive interaction.

DMSi was found to have similar conformational behaviour as in DMC. The two forms, cis-cis and cis-trans were optimized to be minima whereas the trans-trans form was found to be a first order saddle point in the conformational landscape of DMSi. NBO analysis showed the vicinal interactions are the dominating interactions; however, a few geminal interactions were found to operate in SiO_3 group of DMSi which were not observed in CO_3 group of DMC and other carbonates. In TMP, a large amount of geminal interactions were found to operate in PO_4 group in combination with vicinal interactions. It was observed that participation of d orbitals of centralized atom (phosphorous) in bonding leads to geminal interactions, and it plays a major role in deciding the conformational preferences in TMP.

From the study of conformations of above molecules we can conclude the following points. Phenyl rings rotations in trans-stilbene leads to planar and non-planar conformers in trans-stilbene. The same phenyl rotation also gives rise to the cis-cis (anti) and cis-cis (syn) conformers in DPC. In organic carbonates, the cis and trans orientation of alkyl and aryl groups arise due to the rotations around the RO–C bonds. Due to the partial double bond character of RO–C bond, conformation interconversions have somewhat large barriers. In DMSi, conformational preferences were found to be similar to those of DMC. A natural bond orbital analysis of DMC, DMSi and TMP showed a greater participation of *d* orbital of phosphorous in bonding, which resulted in strong geminal and vicinal delocalization interactions, and in turn, determined the conformational preferences in the phosphate.

In combination to conformation study of the above compounds, we have also studied the 1:1 DMC-H_2O and DEC-H_2O complexes. These studies were performed in order to assign the new features, which we observed on annealing. Only the ground state conformers of DMC and DEC water complexes were considered and the computed frequencies for these adducts were corroborated with experiments. In both cases, computation showed two types complexes; one where water was H-bonded to the carbonyl oxygen (carbonyl complexes) and in the other water was attached to alkoxy oxygen (alkoxy complexes). Calculation of interaction energies and charge density topology study using atoms-in-molecules (AIM) theory for the individual complexes, showed the carbonyl complexes to be the stronger than alkoxy complexes. We could observe only the carbonyl complexes in our inert gas matrixes.

8.1 Scope for future work

The work described in this thesis pertaining to conformations of π systems with atoms C, Si and O, can be further extended to other π systems, such as pyridine, thiophene, pyrole, furan and with different substitutions. These studies will have relevance to many biological systems with π systems; for example, amides can be studied to understand the biological phenomena related to conformational changes such as protein folding. Photoirradiation of these molecules followed by trapping the products in a matrix isolation experiments, may throw light on shallow local minima formed in photoreaction pathway for these molecules. Effect of competitive conjugation can be studied in various π systems containing S, N, F, Cl heteroatoms. Studies on cation-π interactions can also be undertaken, which has significant relevance in ion transport mechanisms in biology. The role of various delocalization interactions in molecules containing heteroatoms can be studied as these interactions can have varying degrees of importance with different heteroatom systems. For example, this work showed that the n→π* delocalization interaction was found to be smaller in case of Si system (DMSi) compared with C system (DMC). There exists therefore a vast scope for further study of conformations and reasons for conformational preferences in π systems.

PUBLICATIONS

List of publications relevant to thesis

a. Journals

1. **Matrix Isolation FTIR Studies of Non-Planar Trans-Stilbene,** Bishnu Prasad Kar, N. Ramanathan, K. Sundararajan, K. S. Viswanathan, *Journal of Molecular Structure*, 2011, *994*, 364-370.
2. **Conformations of Dimethyl Carbonate and its Complexes with Water: A Matrix Isolation Infrared and *ab initio* Study,** Bishnu Prasad Kar, N. Ramanathan, K. Sundararajan, K. S. Viswanathan, *Journal of Molecular Structure*, 2012, *1024,* 84-93.
3. **Conformations of Diethyl Carbonate: A Matrix Isolation Infrared and *ab initio* Study,** Bishnu Prasad Kar, N. Ramanathan, K. Sundararajan, K. S. Viswanathan. (manuscript in preparation).
4. **Conformations of Diphenyl Carbonate: A Matrix Isolation Infrared and *ab initio* Study.** (manuscript in preparation).

b. Conference presentations

1. **Non-planar trans-stilbene trapped in inert gas solids,** Bishnu Prasad Kar, K. S. Viswanathan, Poster presentation, Discussion Meeting on Spectroscopy and Dynamics of Molecules and Clusters, Goa, India, February 18-21, 2010.
2. **Conformations of dimethyl carbonate and its complexes with water: A matrix isolation and *ab initio* study,** Bishnu Prasad Kar, K. Sundararajan, N. Ramanathan, K. S. Viswanathan, Poster presentation, Discussion Meeting on Spectroscopy and Dynamics of Molecules and Clusters, Uttarakhand, India, February 18-20, 2011.
3. **Conformations of dimethyl carbonate: A Matrix isolation infrared and *ab initio* study,** Bishnu Prasad Kar, N. Ramanathan, K. Sundararajan, K. S. Viswanathan, Oral

presentation, Chemistry Research Scholar's Meet, Indira Gandhi Centre for Atomic Research, Kalpakkam, India, July 14-15, 2011.

4. **Conformations of diethyl carbonate: A Matrix isolation infrared and *ab initio* study,** Bishnu Prasad Kar, N. Ramanathan, K. Sundararajan, K. S. Viswanathan, Poster presentation, International Conference on Vistas in Chemistry, Indira Gandhi Centre for Atomic Research, Kalpakkam, India, October 11-13, 2011.
5. **Conformations of diphenyl carbonate: A Matrix isolation infrared and *ab initio* study,** Bishnu Prasad Kar, N. Ramanathan, K. Sundararajan, K. S. Viswanathan, Poster presentation, Discussion Meeting on Spectroscopy and Dynamics of Molecules and Clusters, Bengaluru, India, February 17-19, 2012.

List of other journal publications

1. **Hydrogen Bonded Complexes of Acetylene and Boric Acid: A Matrix Isolation Infrared and *ab initio* Study,** K. Sundararajan, N. Ramanathan, Bishnu Prasad Kar, K. S. Viswanathan, *Journal of Molecular Structure*, 2011, *991*, 35-41.
2. **Conformations of Trimethyl Phosphite: A Matrix Isolation Infrared and *ab initio* Study,** N. Ramanathan, K. Sundararajan, Bishnu Prasad Kar, K. S. Viswanathan, *Journal of Physical Chemistry A*, 2011, *115*, 10059–10068.
3. **A Matrix Isolation Infrared and ab initio study of the Trimethyl phosphite-Hydrogen Chloride Interaction: Hydrogen bonding versus nucleophilic substitution,** N. Ramanathan, Bishnu Prasad Kar, K. Sundararajan, K. S. Viswanathan, *Journal Physical Chemistry A*, 2012, *116*, 12014–12023.